SIMULATION WITH MINIMUM EQUIPMENT OF RANDOM VIBRATION INDUCED BY COMPLEX EXCITATION

A Dissertation

Presented to

the Faculty of the Department of Mechanical Engineering

University of Houston

In Partial Fulfillment

of the Requirements for the Degree of

Doctor of Philosophy

---

by

Otto Emil Crenwelge, Jr.

May, 1970

To

My Brother, Joe

God Bless and Keep You

ACKNOWLEDGMENTS

The author wishes to express his sincere appreciation to the following:

Dr. D. Muster, his advisor, who provided encouragement, assistance, and financial support to the author throughout his graduate study program;

Mr. W. D. Dorland, Mr. A. D. Gist, Mr. J. L. Fisher, Mr. G. E. Griffith, Mr. J. N. Kotanchik, and Dr. J. L. Youngblood of the National Aeronautics and Space Administration Manned Spacecraft Center for their respective roles in the loan of random test equipment and in the approval of the author's request for digital computer data analysis; Mr. J. McBryde of Lockheed Electronics for the incorporation of the cross-spectral density into the digital program, and Mr. D. Jones of Lockheed for digiting the data and running the program;

Mr. B. Smith and Mr. J. Baklik for fabrication of the test structures; Mr. C. Hatfield for procurement of the electronic equipment; and the Mechanical Engineering Department secretaries for their cheerful assistance;

the Office of Naval Research, whose grant furnished partial financial assistance;

the Aluminum Company of America for donation of two aluminum ingots which will be used in follow-up work on shells at a later date;

and most importantly, Penny, his wife, and Kris and Lori, his daughters, whose encouragement and faith never ceases.

SIMULATION WITH MINIMUM EQUIPMENT OF RANDOM VIBRATION INDUCED BY COMPLEX EXCITATION

An Abstract of a Dissertation

Presented to

the Faculty of the Department of Mechanical Engineering

University of Houston

In Partial Fulfillment

of the Requirements for the Degree of

Doctor of Philosophy

---

by

Otto Emil Crenwelge, Jr.

May, 1970

ABSTRACT

Complete simulation of random response induced in service by complex, ergodic, Gaussian excitation requires the exact reproduction of the response spectral densities at all points of the system and the cross-spectral densities between each pair of points. This in turn requires exact reproduction of the service loading. If a less-than-complete exact simulation of the response spectra at and between n system locations is acceptable, this can be accomplished using n discrete random forces. For certain types of systems previous theorization has shown that one discrete random force can be used to produce simulation which is accurate in the neighborhood of the resonance frequencies and approximate in the vicinity between resonance peaks. These systems must have light damping and widely spaced resonances so that modal coupling does not exist. The discrete random simulation force must have the appropriately shaped spectrum and must be properly located so that all modes will be excited. For systems of this type the theory shows that reproduction of the response spectral density at any one point assures reproduction of the spectral and cross-spectral densities at and between all other points.

In order to assess the practicability of using one electromechanical shaker to simulate random structural vibration which had been induced by complex excitation environments, an experimental study was conducted on two, lightly damped, far-coupled structures having widely separated resonances in their lower frequency range, i.e., a cantilever beam and a simply-supported rectangular plate. The complex, random excitation environment was provided for the beam by two mechanical shakers and for the plate by acoustic noise. One properly located shaker, providing an appropriately shaped input force spectrum, was used to reproduce practicably the narrow-band response spectra and cross-spectra for two measurement locations on each structure. Comparisons made between experimentally and theoretically determined frequency response functions show exceptional agreement. The effects of attaching shakers directly to the structures are discussed. From the results it is concluded that reproduction of the response spectral density at any one point on structures of this type assures reproduction with the same degree of accuracy of the spectra at all other points and the cross-spectra between points.

TABLE OF CONTENTS

LIST OF SYMBOLS

A	cross sectional area of beam, in.^{2}
A_r	magnitude of normal coordinate for rth mode, in.
B	data reduction bandwidth
D	flexural rigidity of plate, lb-in.
$D_r(x,y,z)$	deflection shape of rth normal mode at structural location (x,y,z)
D_{r_A}, D_{r_1}	deflection shape of rth normal mode at location of force F_A and accelerometer A_1, respectively
E	modulus of elasticity, psi
E_r	generalized force of rth normal mode, lb.
F_{A_o}	magnitude of sinusoidal point force, lb.
$H_{1A}(if)$	complex frequency response function giving acceleration at location (1) due to a unit force input at location (A), g/lb.
I	moment of inertia of beam cross section about centroidal axis, in.^{4}
M	bending moment, in-lb.; or total mass of structure, lb-sec^2/in.
M_r	generalized mass of rth mode, lb-sec^2/in.
Q	quality factor measuring amplification at resonance
$S_{12}(f), S_{AB}(f), S_{1A}(f)$	cross-spectral density between accelerations at points 1 and 2, g^2/Hz; forces at points A and B, lb^2/Hz; and acceleration at point 1 and force at point 2, g-lb/Hz; respectively.
$S_{11}(f)$, $S_{AA}(f)$	spectral densities of acceleration and force at points 1 and A, respectively, g^2/Hz and lb^2/Hz

T	length of time slice of random record to be analyzed, sec.
$W_r(x,y)$	deflection shape of rth normal plate mode at location (x,y)
$Y_r(x)$	deflection shape of rth normal beam mode at location x
a	plate length in x direction, in.
b	plate length in y direction, in.; or mass stiffness ratio for beam, sec^2/in.
c	mass per unit area of plate, lb-sec^2/in.^{3}
$d(x,y,z,t)$	displacement at structural location (x,y,z), in.
$d_1(t)$	displacement at point (1) on structure, in.
$\ddot{d}_1(t)$	acceleration at point (1) on structure, g
$\ddot{d}_{1_o}$	magnitude of acceleration at point (1) on structure, g
e	2.72
f	frequency, Hz
f_r	resonance frequency, Hz
g	acceleration of gravity, 386.4 in/sec.^{2}
h	thickness of plate, in.
i	$\sqrt{-1}$
L	length of beam, in.
m	mass, lb-sec^2/in.; or number of half-waves in plate x direction
n	number of half-waves in plate y direction
t	time, sec.
$w(x,y,t)$	lateral displacement at plate location (x,y), in.
x	distance measured from clamped end of beam, in.; or distance along x direction for plate, in.
y	distance along y direction for plate, in.
$y(x,t)$	lateral displacement at beam location (x), in.

α_r	beam boundary condition constant for rth mode
β_r	rth mode shape argument constant, in.$^{-1}$
γ	specific weight, lb/in.^{3}
δ	logarithmic decrement
ϵ	normalized standard error for spectral density values
$\epsilon_r(t)$	normal coordinate for rth mode
ζ_r	viscous damping coefficient for rth mode
η_r	structural damping coefficient for rth mode
θ_{1A}	phase of cross-spectral density between acceleration at point 1 and force at point A
ν	Poisson's ratio for beam material
ϕ_{1A}	phase of complex frequency response function between acceleration at point 1 and force at point A
ω	circular frequency, rad/sec.

Subscripts

A,B,C,	refers to locations of point forces F_A, F_B, F_C
r	refers to rth normal mode or resonance
α,β	refers to pressure loadings at points α and β
1,2	refers to locations of measured accelerations A_1 and A_2

Superscripts

s	refers to service response
t	refers to simulation test response
*	denotes complex conjugate

LIST OF TABLES

LIST OF FIGURES

Chapter 1

INTRODUCTION

Laboratory environmental simulation tests may be divided into two categories, as suggested by Lyon [1]:[1] direct environmental simulations and substitute environmental simulations. In the direct simulations an aerodynamic environment is usually simulated by a wind tunnel environment, an acoustic environment by a sound field, and a vibration environment by mechanical shakers. In the substitute simulations a sound field or mechanical shakers replace service aerodynamic excitation, and shakers replace service acoustic excitation. These tests all have as their goal the best possible reproduction of the service vibration levels on a system that can be obtained within the time and cost limits of the program.

An excellent direct environmental simulation test would be possible if the service loading on the system could be duplicated exactly; however, for many structures and equipments subjected to severe random loadings in service, reproduction of service loads is not possible because of size limitations of test facilities and/or the inherent difficulties involved in the exact reproduction of the complex loadings. An example of one such service load is the aerodynamic fluctuating

---

[1]Numbers in brackets refer to entries in the Bibliography.

pressure environment of spacecraft at transonic and low supersonic conditions. This environment is produced by interactions between boundary layer turbulence, separated flows, oscillating shock waves, and protuberance wakes.

Attempts at direct simulation of the above aerodynamic loads in wind tunnels must necessarily employ aeroelastic scale models because of the relatively small size of tunnels. One such attempt has been made for the Apollo boilerplate service module [2]. Results of this study indicate that aeroelastic models may provide a promising alternative to full-scale testing of spacecraft, especially as the sizes of spacecraft increase in the future.

It has recently become possible to test large portions of space vehicles with a sound field which closely simulates the lift-off acoustic environment caused by rocket engine noise [3], [4], [5]. This advance was made possible by the development of large acoustic test facilities, such as the NASA Spacecraft Acoustic Laboratory (SAL), which enable the generation of either a reverberant field or a progressive wave field. For tests employing the progressive wave technique, control can be exercised upon the pressure magnitude over the length of the vehicle section and the circumferential pressure correlation; however, the pressure correlation and the variation of pressure spectra as a function of longitudinal position cannot be controlled.

To date, none of the tests conducted at the SAL facility can be considered direct environmental simulations;

however, the results of two substitute environmental simulation tests have been reported [4], [5]. One test attempted to reproduce an envelope of flight vibration data at each of three locations on the Apollo spacecraft-lunar module-adapter [5]. The envelopes consisted of data obtained at flight conditions having exceedingly different excitation environments. The test data compare favorably with the service envelopes when data are reduced on a one-third-octave band basis. This wide frequency bandwidth, however, tends to obscure the narrow band response characteristics of lightly-damped structures, which is a very important consideration, particularly if equipments which respond in a narrow frequency band are mounted within the structure.

The other test reported [4] was a substitute environmental simulation of the aerodynamic loading on the Apollo service module at a low supersonic condition. Vibration data obtained at a large number of locations on the surface of the shell structure were space-averaged, with comparison being made between the flight and test averages on a one-third-octave band basis. Attempts at comparison of narrow-band acceleration spectral densities from flight and test have been unsuccessful to date.

A major impetus for the development of large acoustic facilities such as the one just discussed is the desire for a more realistic simulation of the service excitation environment; however, the pressure correlations of a sound field will never closely duplicate those of an aerodynamic environment.

In addition, the use of acoustic facilities have probably not effected a better reproduction of the service vibration levels than could have been obtained using mechanical shakers [6]. The major advantage of acoustic excitation for large and complex structures is that the sound field offers greater spatial homogeneity than do mechanical shakers.

Mechanical vibrators are more efficient sources of excitation than a sound field [1], [6], in that a structure absorbs much more of the power produced by a shaker. In addition, vibration test facilities are usually more readily available than acoustic test facilities.

However, the use of shakers has its disadvantages also. On large, close-coupled, complex structures, when using one shaker, there is response attenuation along the structural transmission paths at the higher frequencies. There is also a localized inhomogeneity in the vicinity of the shaker attachment point due to its direct field. If a large number of shakers is used to make the over-all vibration field more homogeneous or to simulate service motions or forces at multiple equipment mounting points, control problems are encountered because each shaker is strongly influenced by the others [7], [8]. Problems of this type are often simplified by some form of averaging technique [9], [10], [11], [12] whereby the system is tested to some average input force level or average response level which does not yield a truly realistic simulation of the service vibration response. In addition, attachment of the shakers to the structure changes the mechanical impedances at the attachment points. In many instances fixtures are used to accept the mechanical energy from the shaker and redistribute it over the system under test, which is mounted within the fixture. Fixtures also change the dynamics of the system unless the fixture closely approximates the structure to which the system is attached in service. Eldred [3] considers the amount of service structure necessary to be tested with the system of interest in a proposed "criteria for structural sufficiency." Elaborate electronic equalizer systems have been developed for negating the changes in system dynamics introduced by the fixtures or shakers themselves [7], [8], [13], [14], [15], [16], but the system dynamics are still not the same as that of the original system.

The replacement of reverberant acoustic excitation by mechanical shakers has been discussed [6], [17], [18], [19], for structures which are complex, close-coupled, and have many modes within each frequency band so that the vibration field may be assumed reverberant. For a structure of this type, its characteristic dimension must be greater than five to ten times the bending wavelength of the modes of interest [3]. The mean responses of the modes within each frequency band are considered approximately equal, and data are analyzed on a wide-band basis. The theory associated with this method does not consider the response of the structure in single selected modes; it looks at average response over many modes and over many points on the structure. The inexactness of reproduction inherent in this method is great at low frequencies where there are not many modes in a frequency band, i.e., modes are widely separated, since it has been found that the spatial variation of response is inversely proportional to the number of modes contributing to the response in the frequency band [19].

As can be seen, considerably more effort has been expended in the development of substitute environmental simulation techniques than in the development of direct environmental simulation techniques. This is because it is usually easier in practice to attempt the reproduction of the actual responses experienced in service, than it is to attempt reproduction of the actual service loads. However, the reproduction of previously recorded motions is not a simple matter. Most of the work discussed so far has attempted to simplify the problem by reproducing a spatial average of the structural motions rather than the motion at each instrumented point on the structure. Comparisons are usually made on a wide-band basis; therefore, the narrow-band response characteristics of lightly damped structures have been obscured.

Complete simulation of previously recorded motions requires exact matching of the response spectral densities of all points on a structure in all planes, as well as matching of the cross-spectral densities between each pair of points. In general, if mechanical shakers are used, the minimum number required is equal to the number of points at which exact response simulation is required [20]. However, for structures with small damping and widely separated resonances, Robson [20] and Robson and Roberts [21] have shown that a single, properly placed shaker with the appropriately shaped input force spectrum will, in principle, give good simulation of both the spectra and cross-spectra of the response. Robson does not consider the practical effects of shaker attachment, such as the modification of structure dynamics, in his analyses.

For lightly damped structures where resonances are not widely separated and it becomes necessary to consider the contributions of n modes at any frequency, a close approximate simulation can, in principle, be achieved by ensuring that the response spectral densities at any n points and their cross-spectral densities are matched at all frequencies [21]. This requires applying n forces and controlling their spectral and cross-spectral densities, which would be difficult to achieve. However, if n is a sufficiently small number, and it is necessary to consider n modes only in a few frequency bands throughout the frequency range of interest, then the problem is simplified considerably. Since this is often the case with practical structures, it appears that the methods of simulation testing proposed by Robson and Roberts may have merit for large and complex structures. This method would then have direct application to random vibration testing of spacecraft structures and equipment, in that random response could be closely simulated on the structure without a close reproduction of the flight aerodynamic or acoustic environment.

In order to assess the practicability of using one shaker to simulate the random vibration of structures which have been excited in service by complex excitation environments, an experimental study was conducted on two far-coupled structures having small damping and widely separated resonances, i.e., a cantilever beam and a simply-supported rectangular plate. The complex service excitation environment for the cantilever beam was provided by two mechanical shakers, while that for the plate was provided by acoustic noise. One properly placed shaker, with an appropriately shaped input force spectrum, was used to produce narrow-band simulations of the response spectra and cross spectra at two measurement locations on each structure. Discrepancies existing in the experimental simulations are explained. Comparisons are also made between experimentally and theoretically determined complex frequency response functions for each structure.

Chapter 2

THEORY

2.1 Free Vibration of Structures

2.1.1 Lateral Vibration of a Cantilever Beam

The following assumptions are made in the analysis:

1. The beam material is homogeneous, isotropic, and elastic;

2. The beam is straight and of uniform cross-section;

3. The beam is long compared to its cross-sectional dimensions, so that transverse shear deformation and rotatory inertia may be neglected; and

4. The deflections and deflection gradients are small so that linear theory is applicable.

For a beam of this type, called the Bernoulli-Euler beam, the well-known flexure equation [23], [24], [25], [26], [27]

$$M = EI \frac{d^2y}{dx^2} \tag{2.1}$$

may be used to obtain the equation of motion for a beam of constant EI undergoing lateral vibration

$$\frac{\partial^4 y}{\partial x^4} + b^2 \frac{\partial^2 y}{\partial t^2} = 0 \tag{2.2}$$

where

$$b^2 = \gamma A/(gEI) \tag{2.3}$$

Assuming a solution of the form

$$y(x,t) = \sum_r Y_r(x) A_r e^{i\omega_r t} \tag{2.4}$$

equation (2.2) becomes

$$\frac{d^4 Y_r}{dx^4} - b^2 \omega_r^2 Y_r = 0 \tag{2.5}$$

The solution of this equation yields, for the rth mode of vibration

$$Y_r = A \cosh\beta_r x + B \sinh \beta_r x + C \cos\beta_r x + D \sin\beta_r x \tag{2.6}$$

where

$$\beta_r^4 = (b\omega_r)^2 \tag{2.7}$$

From equation (2.7) the undamped natural frequencies are given by

$$f_r = \frac{(\beta_r L)^2}{2\pi L^2} \sqrt{\frac{gEI}{\gamma A}} \tag{2.8}$$

For a cantilever beam the boundary conditions are

$$Y_r(0) = \frac{dY_r(0)}{dx} = 0 \tag{2.9}$$

and

$$\frac{d^2 Y_r(L)}{dx^2} = \frac{d^3 Y_r(L)}{dx^3} = 0 \tag{2.10}$$

Using these equations, (2.6) becomes

$$Y_r = \cosh \beta_r x - \cos \beta_r x - \alpha_r(\sinh \beta_r x - \sin \beta_r x) \tag{2.11}$$

where

$$\alpha_r = \frac{\sinh \beta_r L - \sin \beta_r L}{\cosh \beta_r L + \cos \beta_r L} = \frac{\cosh \beta_r L + \cos \beta_r L}{\sinh \beta_r L + \sin \beta_r L} \qquad (2.12)$$

which yields the frequency equation

$$\cosh \beta_r L \quad \cos \beta_r L = -1 \qquad (2.13)$$

Equations (2.12) and (2.13) are satisfied for the following values of α_r and $\beta_r L$ [28]:

r	1	2	3	4	5
α_r	0.734	1.018	0.999	1.000	1.000
$\beta_r L$	1.875	4.694	7.855	10.996	14.137

Values of the mode shapes, $Y_r(x)$, are tabulated in [28] where they have been normalized so that

$$\int_0^L Y_r^2(x)dx = L \qquad (2.14)$$

Therefore, the generalized mass of the rth mode is

$$M_r = \int_V Y_r^2(x)dm = \int_0^L \frac{\gamma A}{g} Y_r^2(x)dx$$

or

$$M_r = \frac{\gamma A}{g} L = M \qquad (2.15)$$

where M is the total mass of the uniform beam.

2.1.2 Lateral Vibration of a Simply-Supported Plate

The following assumptions are made in the analysis:

1. The plate material is homogeneous, isotropic, and elastic;

2. The plate is flat, rectangular, and of uniform thickness;

3. The plate thickness is small compared to its other dimensions so that stresses and strains in the direction perpendicular to the plate middle surface are negligible;

4. Transverse shear and rotatory inertia are neglected;

5. Plate deflections and deflection gradients are small so that linear theory is applicable; and

6. Extension and shear of the plate middle surface are neglected, i.e., pure bending is assumed.

For a plate of this type with constant EI, the differential equation of lateral vibration is [25], [26]:

$$D\nabla^4 w + c\ddot{w} = 0 \tag{2.16}$$

where

$$D = Eh^3/[12(1-\nu^2)] \tag{2.17}$$

and

$$c = \gamma h/g \tag{2.18}$$

Assuming a solution of the form

$$w(x,y,t) = \sum_r W_r(x,y)A_r e^{i\omega_r t} \tag{2.19}$$

equation (2.16) becomes

$$D\nabla^4 W_r - c\omega_r^2 W_r = 0 \tag{2.20}$$

For a simply-supported plate the boundary conditions are

$$W_r(0,y) = W_r(a,y) = W_r(x,0) = W_r(x,b) = 0 \tag{2.21}$$

and

$$\frac{\partial^2 W_r(0,y)}{\partial x^2} = \frac{\partial^2 W_r(a,y)}{\partial x^2} = \frac{\partial^2 W_r(x,0)}{\partial y^2} = \frac{\partial^2 W_r(x,b)}{\partial y^2} = 0 \tag{2.22}$$

The following assumed modal deflection shapes satisfy eqs. (2.21) and (2.22) for any integral values of m and n

$$W_r = W_{mn} = \sin\frac{m\pi x}{a}\sin\frac{n\pi y}{b} \tag{2.23}$$

Solving eq. (2.20) for the undamped natural frequencies, $f_r = \omega_r/2\pi$

$$f_r = \frac{\pi}{2}\sqrt{\frac{gD}{\gamma h}}\left(\frac{m^2}{a^2} + \frac{n^2}{b^2}\right) \tag{2.24}$$

The generalized mass of the rth mode is

$$M_r = \int_v W_r^2(x,y)\,dm = \int_0^a\int_0^b \left(\frac{\gamma h}{g}\right)W_r^2(x,y)\,dx\,dy$$

or

$$M_r = \frac{\gamma abh}{4g} = \frac{M}{4} \tag{2.25}$$

where M is the total mass of the plate.

2.2 Structural Damping

Two convenient methods used to measure the damping present in a system are called the logarithmic decrement and the bandwidth method [29]. Both of these descriptions of damping are derived from the linear, single-degree-of-freedom system of a viscous damper in parallel with a spring; however, these concepts are commonly applied to linear, multiple-degree-of-freedom systems by assuming that the damping can be accounted for separately in each normal mode and that there is no coupling between the modes due to damping.

The logarithmic decrement is defined as [23]

$$\delta = \frac{1}{n} \ln \frac{x_o}{x_n} \tag{2.26}$$

where x_n is the amplitude of oscillation after n cycles have elapsed from the measurement of x_o, and is a measure of the vibration decay rate of a system. It can be shown that

$$\delta = 2\pi\zeta/(1 - \zeta^2)^{\frac{1}{2}} \tag{2.27}$$

which gives

$$\delta \cong 2\pi\zeta \tag{2.28}$$

for small damping. The structural damping coefficient, or loss factor, is defined as [23], [25]

$$\eta = 2\zeta f/f_r \tag{2.29}$$

at resonance

$$\eta_r = 2\zeta_r = \frac{\delta}{\pi} \tag{2.30}$$

For values of Q between 10 and 100 [29], it is possible to obtain reasonable results by using the bandwidth method. It can be shown that

$$\eta_r = \frac{1}{Q} = \frac{f_2 - f_1}{f_r} \tag{2.31}$$

where f_2 and f_1 are the frequencies measured above and below f_r, respectively, for which the amplitude of vibration has decreased to $1/\sqrt{2}$ times the resonance amplitude for the same input force.

2.3 Response of a Structure to a Sinusoidal Point Force

It is assumed in the following that:

1. The structural material is homogeneous, isotropic, and elastic;

2. Structural displacements and displacement gradients are small, so that linear theory is applicable;

3. Structural displacements are one dimensional;

4. Structural damping is small and there is no coupling between normal modes due to damping, so that damping can be accounted for separately in each mode;

5. The modal damping force is proportional to displacement and in phase with the velocity; and

6. The force applied at a single point on the structure is sinusoidal and in the same direction as the displacement of the structure.

Then the displacement at any point on the structure may be expressed in terms of the normal modes of the structure as

$$d(x,y,z,t) = \sum_r D_r(x,y,z)\,\epsilon_r(t) \tag{2.32}$$

where $D_r(x,y,z)$ represents the displacement shape of the rth normal mode of the structure, and $\epsilon_r(t)$ is the normal coordinate for the rth mode.

Inserting the kinetic energy, potential energy, dissipation function, and generalized force into Lagrange's equations [20], it is possible to obtain the uncoupled equation of motion for the rth normal mode

$$\ddot{\epsilon}_r + \omega_r^2(1 + i\eta_r)\,\epsilon_r = \frac{E_r}{M_r} \tag{2.33}$$

where the generalized force and mass, E_r and M_r, are, respectively.

$$E_r = D_r(x_A, y_A, z_A) F_{A_o} e^{i\omega t} \tag{2.34}$$

and

$$M_r = \int_V D_r^2(x,y,z)\,dm \tag{2.35}$$

The steady-state solution of (2.33) is of the form $\epsilon_r = \epsilon_{r_o} e^{i\omega t}$, so that $\ddot{\epsilon}_r = -\omega^2\epsilon$, and

$$\epsilon_r = \frac{D_{r_A} F_{A_o} e^{i\omega t}}{M_r(\omega_r^2 - \omega^2 + i\eta_r\omega_r^2)} \tag{2.36}$$

Substituting (2.36) into (2.32) for the displacement at point (1) on the structure

$$d_1(t) = F_{A_o} e^{i\omega t} \sum_r \frac{D_{r_1} D_{r_A}}{M_r} \frac{\frac{1}{\omega_r^2}\left[1 - \left(\frac{\omega}{\omega_r}\right)^2 - i\eta_r\right]}{\left\{\left[1 - \left(\frac{\omega}{\omega_r}\right)^2\right]^2 + \eta_r^2\right\}} \tag{2.37}$$

The acceleration at point (1) in g units is then

$$\ddot{d}_1(t) = F_{A_o} e^{i\omega t} \sum_r \frac{-D_{r_1} D_{r_A}}{g M_r} \frac{(f/f_r)^2 \left\{[1 - (f/f_r)^2] - i\eta_r\right\}}{\left\{[1 - (f/f_r)^2]^2 + \eta_r^2\right\}} \tag{2.38}$$

or

$$\ddot{d}_1(t) = \ddot{d}_{1_o}e^{i\omega t} = H_{1A}(if)F_{A_o}e^{i\omega t} \tag{2.39}$$

so that the complex frequency response function which describes the acceleration at location (1) due to a unit force input at location (A) is given by

$$H_{1A}(if) = \sum_r \lambda_{r_{1A}}(U_r - iV_r) \tag{2.40}$$

where

$$\lambda_{r_{1A}} = \frac{-D_{r_1}D_{r_A}}{gM_r} \tag{2.41}$$

$$U_r = \frac{(f/f_r)^2[1-(f/f_r)^2]}{\{[1-(f/f_r)^2]^2+\eta_r^2\}} \tag{2.42}$$

and

$$V_r = \frac{(f/f_r)^2\eta_r}{\{[1-(f/f_r)^2]^2+\eta_r^2\}} \tag{2.43}$$

Equation (2.40) may also be written as

$$H_{1A}(if) = \sum_r \frac{-D_{r_1}D_{r_A}(f/f_r)^2e^{-i\phi_r}}{gM_r\ \{[1-(f/f_r)^2]^2+\eta_r^2\}^{\frac{1}{2}}} \tag{2.44}$$

where

$$\tan\phi_r(f) = \frac{\eta_r}{[1-(f/f_r)^2]} \tag{2.45}$$

The product $H_{1A}^*H_{2B}$ is given as

$$H_{1A}^*H_{2B} = \sum_r \lambda_{r_{1A}}(U_r+iV_r)\sum_r \lambda_{r_{2B}}(U_r-iV_r) \tag{2.46}$$

or

$$H_{1A}^{*}H_{2B} = \sum_r \lambda_{r_{1A}} U_r \sum_r \lambda_{r_{2B}} U_r + \sum_r \lambda_{r_{1A}} V_r \sum_r \lambda_{r_{2B}} V_r$$
$$-i \left(\sum_r \lambda_{r_{1A}} U_r \sum_r \lambda_{r_{2B}} V_r - \sum_r \lambda_{r_{1A}} V_r \sum_r \lambda_{r_{2B}} U_r \right) \qquad (2.47)$$

which is, in general, complex unless $\lambda_{r_{1A}} = \lambda_{r_{2B}}$.

In general, eq. (2.46) cannot be simplified further; however, if the damping, η_r, is small and the resonance frequencies are widely separated, so that no modal coupling exists, eqs. (2.46) and (2.47) may be approximated at frequencies near resonance by neglecting cross-product terms $U_r U_s \ll U_r^2$, $V_r V_s \ll V_r^2$, $U_r V_s \ll U_r V_r$. Therefore,

$$H_{1A}^{*}H_{2B} = \sum_r \lambda_{r_{1A}} \lambda_{r_{2B}} (U_r^2 + V_r^2) \qquad (2.48)$$

Between resonance frequencies, eq. (2.48) will not provide a good approximation to $H_{1A}^{*}H_{2B}$, but this inadequacy can be permitted, since response in these regions does not significantly contribute to the mean square response quantities for the beam.

Further approximation is possible when only one term predominates at frequencies near resonance. Then

$$(H_{1A}^{*}H_{2B})_r = \lambda_{r_{1A}} \lambda_{r_{2B}} (U_r^2 + V_r^2) \qquad (2.49)$$

for $\eta_r \ll 1$, $f_{r-1} \ll f_r \ll f_{r+1}$, and $f \cong f_r$. We could further approximate by using eq. (2.49) in the frequency range $\frac{f_{r-1} + f_r}{2} < f < \frac{f_r + f_{r+1}}{2}$.

The square of the modulus of the frequency response function, which will be compared later with experimental values, is from (2.47)

$$\left|H_{1A}(if)\right|^2 = H_{1A}^{*}H_{1A} = \left(\sum_r \lambda_{r_{1A}} U_r\right)^2 + \left(\sum_r \lambda_{r_{1A}} V_r\right)^2 \qquad (2.50)$$

or

$$\left|H_{1A}(if)\right|^2 = \sum_r \frac{D_{r_1}^{2} D_{r_A}^{2}}{g^2 M_r^2} \frac{(f/f_r)^4}{\{[1-(f/f_r)^2] + \eta_r^2\}}$$

$$+ \sum_r \sum_{s \neq r} \frac{D_{r_1} D_{s_1} D_{r_A} D_{s_A}}{g^2 M_r M_s}$$

$$\cdot \frac{(f^2/f_r f_s)^2 \, \{[1-(f/f_r)^2][1-(f/f_s)^2] + \eta_r \eta_s\}}{\{[1-(f/f_r)^2]^2 + \eta_r^2\}\{[1-(f/f_s)^2]^2 + \eta_s^2\}} \qquad (2.51)$$

For the cantilever beam the D_r are given by eq. (2.11) as $Y_r(x)$, while for the simple-supported plate, $D_r = W_r(x,y)$ of eq. (2.23).

Following the reasoning used in obtaining eq. (2.48) for structures with light damping and widely separated resonances

$$\left|H_{1A}(if)\right|^2 = \sum_r \lambda_{r_{1A}}^2 (U_r^2 + V_r^2) \qquad (2.52)$$

or

$$\left|H_{1A}(if)\right|^2 = \sum_r \frac{D_{r_1}^{2} D_{r_A}^{2}}{g^2 M_r^2} \frac{(f/f_r)^4}{\{[1-(f/f_r)^2]^2 + \eta_r^2\}} \qquad (2.53)$$

Again, if one term predominates at frequencies near resonance, we may make the approximation

$$\left|H_{1A}(if)\right|_r^2 = \lambda_{r_{1A}}^2 (U_r^2 + V_r^2) \tag{2.54}$$

or

$$\left| H_{1A}(if)\right|_r^2 = \frac{D_{r_1}^2 D_{r_A}^2}{g^2 M_r^2} \frac{(f/f_r)^4}{\{[1-(f/f_r)^2]^2 + \eta_r^2\}} \tag{2.55}$$

with the constraints that $\eta_r \ll 1$, $f_{r-1} \ll f_r \ll f_{r+1}$, and $f \cong f_r$.

In the regions away from resonance a much better approximation to $\left|H_{1A}(if)\right|^2$ for $\eta_r \ll 1$ is

$$\left|H_{1A}(if)\right|^2 = \sum_r \frac{D_{r_1}^2 D_{r_A}^2}{g^2 M_r^2} \frac{(f/f_r)^4}{[1-(f/f_r)^2]^2}$$

$$+\sum_r \sum_{s \neq r} \frac{D_{r_1} D_{s_1} D_{r_A} D_{s_A}}{g^2 M_r M_s} \frac{(f^2/f_r f_s)^2}{[1-(f/f_r)^2][1-(f/f_s)^2]} \tag{2.56}$$

2.4 Response of a Structure to a Random Excitation

In addition to the assumptions made in Section 2.3 for the structure, it is assumed here that each random record of excitation or response is self-stationary. Verification of this condition for a single sample record effectively justifies an assumption of stationarity and ergodicity for the random process from which the sample record is obtained [30]. Temporal averages over short time intervals of a single record may then replace ensemble averages. If the excitation of a linear system is stationary (or ergodic), then the response will also be stationary (or ergodic) [31]. For definitions of the above terms, please see Appendix 1.

In general the acceleration cross-spectral density between points (1) and (2) on a structure excited by a distributed random pressure loading is given as

$$S_{12}(f) = \int_A \int_A H_{1\alpha}^*(if) H_{2\beta}(if) S_{\alpha\beta}(f) dA_\alpha dA_\beta \qquad (2.57)$$

When making use of the frequency response function as defined by eqs. (2.40)-(2.43)

$$S_{12}(f) = \sum_r \sum_s \frac{D_{r_1} D_{s_2}}{g^2 M_r M_s}$$

$$\cdot \frac{(f^2/f_r f_s)^2 \{[1-(f/f_r)^2]+i\eta_r\} \{[1-(f/f_s)^2]-i\eta_s\}}{\{[1-(f/f_r)^2]^2+\eta_r^2\} \{[1-(f/f_s)^2]^2+\eta_s^2\}}$$

$$\cdot \int_A \int_A D_{r_\alpha} D_{r_\beta} S_{\alpha\beta}(f) dA_\alpha dA_\beta \qquad (2.58)$$

The acceleration spectral density at point (1) on the structure becomes

$$S_{11}(f) = \int_A \int_A H_{1\alpha}^*(if) H_{1\beta}(if) S_{\alpha\beta}(f) dA_\alpha dA_\beta \qquad (2.59)$$

where $S_{\alpha\beta}(f)$ is the pressure cross-spectral density between points α and β on the structure.

The acceleration cross-spectral density for a structure excited by multiple random point forces is given by

$$S_{12}(f) = \sum_A \sum_B H_{1A}^*(if) H_{2B}(if) S_{AB}(f) \qquad (2.60)$$

or

$$S_{12}(f) = \sum_r \sum_s \frac{D_{r_1} D_{s_2}}{g^2 M_r M_s}$$

$$\cdot \frac{(f^2/f_r f_s)^2 \{[1-(f/f_r)^2]+i\eta_r\} \{[1-(f/f_s)^2]-i\eta_s\}}{\{[1-(f/f_r)^2]^2+\eta_r^2\} \{[1-(f/f_s)^2]^2+\eta_s^2\}}$$

. . . . .

. . . .
$$\cdot \sum_A \sum_B D_{r_A} D_{s_B} S_{AB}(f) \tag{2.61}$$

and the acceleration spectral density at point (1) is given by

$$S_{11}(f) = \sum_A \sum_B H_{1A}^{*}(if) H_{1B} S_{AB}(f) \tag{2.62}$$

For two random point forces (F_A and F_B) acting on a structure

$$S_{12}(f) = H_{1A}^{*} H_{2A} S_{AA} + H_{1A}^{*} H_{2B} S_{AB}$$
$$+ H_{1B}^{*} H_{2A} S_{BA} + H_{1B}^{*} H_{2B} S_{BB} \tag{2.63}$$

and

$$S_{11}(f) = \left|H_{1A}\right|^2 S_{AA} + H_{1A}^{*} H_{1B} S_{AB}$$
$$+ H_{1B}^{*} H_{1A} S_{BA} + \left|H_{1B}\right|^2 S_{BB} \tag{2.64}$$

For one random point force acting on a structure the acceleration cross-spectral density between points (1) and (2) becomes

$$S_{12}(f) = H_{1A}^{*} H_{2A} S_{AA} \tag{2.65}$$

or

$$S_{12}(f) = \sum_r \sum_s \frac{D_{r_1} D_{s_2} D_{r_A} D_{s_A}}{g^2 M_r M_s}$$

$$\cdot \frac{(f^2/f_r f_s)^2 \left\{[1-(f/f_r)^2]+i\eta_r\right\} \left\{[1-(f/f_s)^2]-i\eta_s\right\}}{\left\{[1-(f/f_r)^2]^2+\eta_r^2\right\} \left\{[1-(f/f_s)^2]^2+\eta_s^2\right\}} \cdot S_{AA} \tag{2.66}$$

and the acceleration spectral density at point (1) is

$$S_{11}(f) = \left|H_{1A}(if)\right|^2 S_{AA}(f) \tag{2.67}$$

where $\left|H_{1A}(if)\right|^2$ is given by eq. (2.50).

For one random point force acting on a structure the cross-spectral density between excitation and response is given by

$$S_{A1}(f) = H_{1A}(if)S_{AA}(f) \tag{2.68}$$

or

$$S_{A1}\ e^{-i\theta_{A1}} = H_{1A}\ e^{-i\phi_{1A}}S_{AA} \tag{2.69}$$

Therefore

$$\left|S_{A1}\right| = \left|H_{1A}\right| S_{AA} \tag{2.70}$$

and

$$\phi_{1A} = \theta_{A1} \tag{2.71}$$

But

$$S_{1A} = S_{A1}^{*} \tag{2.72}$$

Therefore

$$S_{1A} = H_{1A}^{*}S_{AA} \tag{2.73}$$

From (2.73)

$$\left|S_{1A}\right| = \left|H_{1A}\right| S_{AA} \tag{2.74}$$

and

$$\phi_{1A} = -\theta_{1A} \tag{2.75}$$

From eqs. (2.67)-(2.75), a complete description of $H_{1A}(if)$ may be obtained if the force spectral density and the acceleration-force cross-spectral density are known.

For two random point forces which may be correlated, F_A and F_B, acting on a structure, Bendat [30] gives the cross spectral densities between the two excitation points and a response point as

$$S_{A1}(f) = H_{1A}S_{AA} + H_{1B}S_{AB} \tag{2.76}$$

$$S_{B1}(f) = H_{1A}S_{BA} + H_{1B}S_{BB} \tag{2.77}$$

The complex frequency response functions are then

$$H_{1A}(if) = \frac{S_{A1}\left[1 - \dfrac{S_{AB}S_{B1}}{S_{BB}S_{A1}}\right]}{S_{AA}[1 - \gamma_{AB}^2]} \tag{2.78}$$

$$H_{1B}(if) = \frac{S_{B1}\left[1 - \dfrac{S_{BA}S_{A1}}{S_{AA}S_{B1}}\right]}{S_{BB}[1 - \gamma_{AB}^2]} \tag{2.79}$$

where

$$\gamma_{AB}^2(f) = \frac{|S_{AB}(f)|^2}{S_{AA}(f)S_{BB}(f)} \tag{2.80}$$

is the coherence function. If F_A and F_B are uncorrelated, ${\gamma_{AB}}^2(f) = S_{AB}(f) = S_{BA}(f) = 0$, and we have $H_{1A}(if)$ and $H_{2A}(if)$ given by eq. (2.68). If $\gamma_{AB}^2(f) = 1$, complete linear dependence between F_A and F_B is implied. Therefore, we could consider a linear system acting between them, and F_A actually could be considered as taking two different paths to arrive at point (1). For this case a single frequency response function, $H(if)$, will relate F_A to A_1 [30]

$$S_{A1} = H(if)S_{AA} \tag{2.81}$$

where

$$H(if) = H_{1A}(if) + H_{1B}H_{AB} \tag{2.82}$$

2.5 Simulation of the Structural Vibration Induced by Complex Random Excitation Environments

In addition to the assumption of self-stationarity for all random records (ergodicity for all random processes) which was made in Section 2.4, it is further assumed that each individual time history record of excitation or response is Gaussian. It can be shown that, if a linear system experiences Gaussian excitation, the response is Gaussian also [20], [30], [31]. For an ergodic Gaussian process, a knowledge of the spectral density of a sample record enables a unique determination of the probability density of the random process. Similarly, if weak ergodicity exists between two Gaussian processes (weak ergodicity implies strong ergodicity for Gaussian processes), then a knowledge of the cross-spectral densities between sample records of the two processes enables a unique determination of the joint probability distribution between the two processes. Similarly, strong ergodicity enables a determination of all higher order probability functions. With this in mind, simulation of random ergodic Gaussian response processes requires only that the spectral densities and cross-spectral densities of all simulated accelerations match those obtained under service excitation.

Robson and Roberts [21] have shown that if the response spectra and cross spectra, obtained in service at every point on a linear, elastic structure under Gaussian excitation, are to be matched exactly in a simulation test, the structure must be tested under its exact service environment. Therefore, the simulation loading must match exactly the spectral and cross-spectral densities of the service loading at every point on the structure. Complete simulation is defined here as the exact matching of response spectral and cross-spectral densities at every point on the structure. If it is possible to accept a less-than-complete simulation, such that the response spectral and cross-spectral densities are exactly matched at a finite number of points only, simulation becomes more practicable, although still not simple. Robson [21] has shown that if the response spectral densities at n structural locations and the response cross-spectral density magnitudes and phases between each pair of points are to be matched exactly (the exact matching of n^2 quantities), n force inputs are necessary, and n^2 adjustable quantities must be at our control (the force spectral densities and cross-spectral density magnitudes and phases).

If it is possible to settle for a less than exact response simulation at every point and between every pair of points on a structure, a close approximate simulation may be obtained for some structures, at least in principle, with relative ease [20].

Consider a structure which is excited in service by two self-stationary random forces, F_A and F_B, which may have any degree of correlation, so that eqs. (2.63) and (2.64) describe the acceleration cross-spectral density between any two points and the acceleration spectral density at any point on the structure for motion in one direction. The service response spectral and cross-spectral densities for any two points are then

$$S_{11}^{s} = H_{1A}^{*}H_{1A}S_{AA} + H_{1A}^{*}H_{1B}S_{AB} + H_{1B}^{*}H_{1A}S_{BA} + H_{1B}^{*}H_{1B}S_{BB} \quad (2.83)$$

$$S_{22}^{s} = H_{2A}^{*}H_{2A}S_{AA} + H_{2A}^{*}H_{2B}S_{AB} + H_{2B}^{*}H_{2A}S_{BA} + H_{2B}^{*}H_{2B}S_{BB} \quad (2.84)$$

and

$$S_{12}^{s} = H_{1A}^{*}H_{2A}S_{AA} + H_{1A}^{*}H_{2B}S_{AB} + H_{1B}^{*}H_{2A}S_{BA} + H_{1B}^{*}H_{2B}S_{BB} \quad (2.85)$$

If we desire to simulate these response quantities using one input force, F_C, the simulated quantities

$$S_{11}^{t} = H_{1C}^{*}H_{1C}S_{CC} \quad (2.86)$$

$$S_{22}^{t} = H_{2C}^{*}H_{2C}S_{CC} \quad (2.87)$$

and

$$S_{12}^{t} = H_{1C}^{*}H_{2C}S_{CC} \quad (2.88)$$

must be made equal to the quantities obtained in service. If we adjust the spectrum of S_{CC} so that

$$S_{11}^{t} = S_{11}^{s} \quad (2.89)$$

then

$$S_{CC} = \frac{H_{1A}^{*}H_{1A}S_{AA} + H_{1A}^{*}H_{1B}S_{AB} + H_{1B}^{*}H_{1A}S_{BA} + H_{1B}^{*}H_{1B}S_{BB}}{H_{1C}^{*}H_{1C}} \quad (2.90)$$

and we have obtained exact simulation at point (1); however, at point (2) and between points (1) and (2), we now have the requirements that

$$S_{22}^{t} = H_{2C}^{*}H_{2C}\left[\frac{H_{1A}^{*}H_{1A}S_{AA}+H_{1A}^{*}H_{1B}S_{AB}+H_{1B}^{*}H_{1A}S_{BA}+H_{1B}^{*}H_{1B}S_{BB}}{H_{1C}^{*}H_{1C}}\right] \qquad (2.91)$$

and

$$S_{12}^{t} = H_{1C}^{*}H_{2C}\left[\frac{H_{1A}^{*}H_{1A}S_{AA}+H_{1A}^{*}H_{1B}S_{AB}+H_{1B}^{*}H_{1A}S_{BA}+H_{1B}^{*}H_{1B}S_{BB}}{H_{1C}^{*}H_{1C}}\right] \qquad (2.92)$$

Therefore, the ratios between test and service spectra are

$$\frac{S_{11}^{t}}{S_{11}^{s}} = 1 \qquad (2.93)$$

$$\frac{S_{22}^{t}}{S_{22}^{s}} = \frac{H_{2C}^{*}H_{2C}}{H_{1C}^{*}H_{1C}}\,\frac{H_{1A}^{*}H_{1A}S_{AA}+H_{1A}^{*}H_{1B}S_{AB}+H_{1B}^{*}H_{1A}S_{BA}+H_{1B}^{*}H_{1B}S_{BB}}{H_{2A}^{*}H_{2A}S_{AA}+H_{2A}^{*}H_{2B}S_{AB}+H_{2B}^{*}H_{2A}S_{BA}+H_{2B}^{*}H_{2B}S_{BB}} \qquad (2.94)$$

and

$$\frac{S_{12}^{t}}{S_{12}^{s}} = \frac{H_{1C}^{*}H_{2C}}{H_{1C}^{*}H_{1C}}\,\frac{H_{1A}^{*}H_{1A}S_{AA}+H_{1A}^{*}H_{1B}S_{AB}+H_{1B}^{*}H_{1A}S_{BA}+H_{1B}^{*}H_{1B}S_{BB}}{H_{1A}^{*}H_{2A}S_{AA}+H_{1A}^{*}H_{2B}S_{AB}+H_{1B}^{*}H_{2A}S_{BA}+H_{1B}^{*}H_{2B}S_{BB}} \qquad (2.95)$$

In general, there is no reason why the expressions of eqs. (2.94) and (2.95) should equal unity and thereby provide exact simulation, i.e., this requires that terms of the form

$$\frac{H_{1C}^{*}H_{2C}}{H_{1C}^{*}H_{1C}}\,\frac{H_{1A}^{*}H_{1A}}{H_{1A}^{*}H_{2A}} = \frac{H_{2C}^{*}H_{2C}}{H_{1C}^{*}H_{1C}}\,\frac{H_{1A}^{*}H_{1A}}{H_{2A}^{*}H_{2A}} = \;.\;.\;.\;.\; = 1 \qquad (2.96)$$

which, if the expressions of eqs. (2.46) and (2.50) are used, is clearly not so. However, for structures with light damping and widely separated resonances, where only the rth term of the frequency response function dominates in the vicinity of the rth resonance, we can use eqs. (2.49) and (2.54), so that the first term of eq. (2.96) becomes

$$\frac{H_{1C}^{*}H_{2C}}{H_{1C}^{*}H_{1C}}\,\frac{H_{1A}^{*}H_{1A}}{H_{1A}^{*}H_{2A}} = \frac{D_{r_1}D_{r_C}D_{r_2}D_{r_C}}{D_{r_1}^{2}D_{r_C}^{2}}\cdot\frac{D_{r_1}^{2}D_{r_A}^{2}}{D_{r_1}D_{r_A}D_{r_2}D_{r_A}} = 1 \qquad (2.97)$$

and similarly for the remainder of the terms in eq. (2.96). Therefore, for structures with $\eta_r \ll 1$ and $f_{r-1} \ll f_r \ll f_{r+1}$, we have obtained accurate simulation of the response spectral and cross-spectral densities at every point on the structure at frequencies near to the resonance frequencies ($f \cong f_r$) by using only one simulation force and simulating the response spectral density at any one point. Our simulation for $f_r \ll f \ll f_{r+1}$ is only approximate; however, this can usually be tolerated since response in these regions does not contribute appreciably to the mean square response of the structure.

For a cantilever beam the above degree of simulation will be obtained if the simulation force spectral density, $S_{CC}(f)$, is adjusted as given in eq. (2.90).

Similarly, if the spectral density of one simulation force is adjusted according to

$$S_{CC} = \frac{\int_A \int_A H_{1\alpha}(if)H_{1\beta}(if)S_{\alpha\beta}(f)\,dA_\alpha\,dA_\beta}{\left|H_{1C}(if)\right|^{2}} \qquad (2.98)$$

as obtained using equations (2.49), (2.54), and (2.57), it is possible, in principle, to simulate with the above degree of accuracy the response spectral and cross-spectral densities at every point on a simply-supported plate by simulating the response spectral density at only one point. The service response in this case was originally induced by a fluctuating pressure field.

In the above development, it was assumed that the dynamics of the structure were not affected by physically connecting the shaker to the structure. In practice this is not the case; however, reasonable, approximate simulations are still possible using this method, as will be shown. It was also assumed that the simulation force spectrum could be accurately shaped, that the shaker input point and the response measurement points do not lie on nodes of the vibration modes, and that all modes of interest have response components in the direction of the applied force.

The conditions of low damping and widely spaced resonances, which make it possible to consider the response contribution of only one mode at each frequency, usually will be realized only in the lower end of the frequency range for practical structures. In the higher end of the frequency range, however, some overlapping of resonance peaks is to be expected, even for structures with low damping. Therefore, the validity of the above simulation procedure is greatly extended if it is based on the assumption that n modes must be considered at each frequency. Robson and Roberts [21] have shown that simulation can be achieved for this case by ensuring that the response spectral densities at any n points and the cross spectral density magnitudes and phases between each pair of points (n^2 quantities) are matched at all frequencies. This requires the application of n forces and complete control of their n^2 spectral and cross-spectral densities, which may become an insurmountable problem as n becomes large. However, if n is a small number, and it is necessary to consider n modes only in a few frequency bands throughout the frequency range of interest, it appears that one shaker could accomplish simulation over the frequency range outside of the few narrow bands having multi-modal response. In these narrow bands, then, n-1 auxiliary shakers could be used to provide the necessary simulation, thereby reducing the complexity of the problem considerably. This method of vibration simulation testing using a small number of mechanical shakers would then have wide application to practical structures.

Chapter 3

EXPERIMENTAL INVESTIGATIONS

3.1 Structures Tested

The structures tested, a cantilever beam and a simply-supported rectangluar plate, are shown in Figure 3.1 with the electronic equipment and instrumentation used in the various tests. The structures were mounted on a concrete seismic mass which provided isolation from building vibration above 10 Hz.

3.1.1 Cantilever Beam

The cantilever beam, along with the excitation equipment and measurement instrumentation is shown in Figure 3.2. It was machined from a $1\frac{1}{4}$-inch diameter, 6061 aluminum alloy rod which had been imbedded by shrink fitting in an aluminum block weighing 34 pounds. The block was then bolted to the seismic mass. The beam was 10 inches long, 1 inch wide, and $\frac{1}{2}$-inch thick. Microminiature accelerometers were located at distances of 5.5 and 9.5 inches from the clamped end of the beam. The shakers were attached to the beam through force transducers at distances of three and seven inches from the clamped end. Beam material properties are: $E = 9.9 \times 10^6$ psi and $\gamma = 0.098$ lb/in^3.

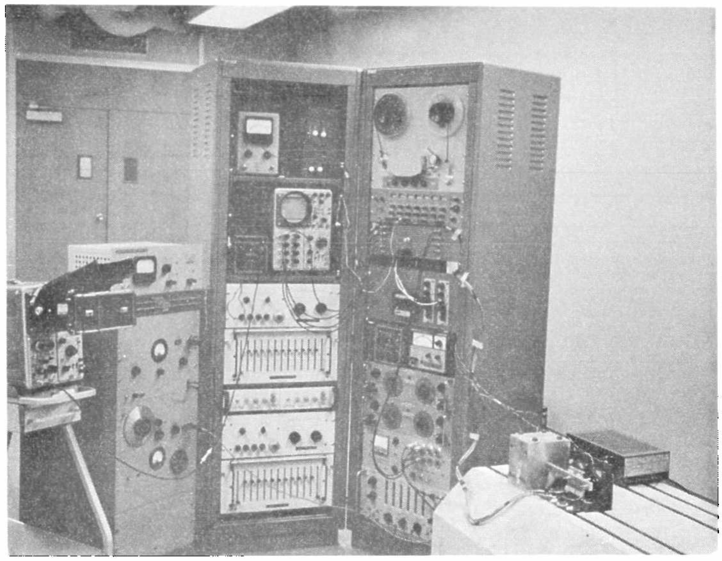

(a)

Cantilever Beam

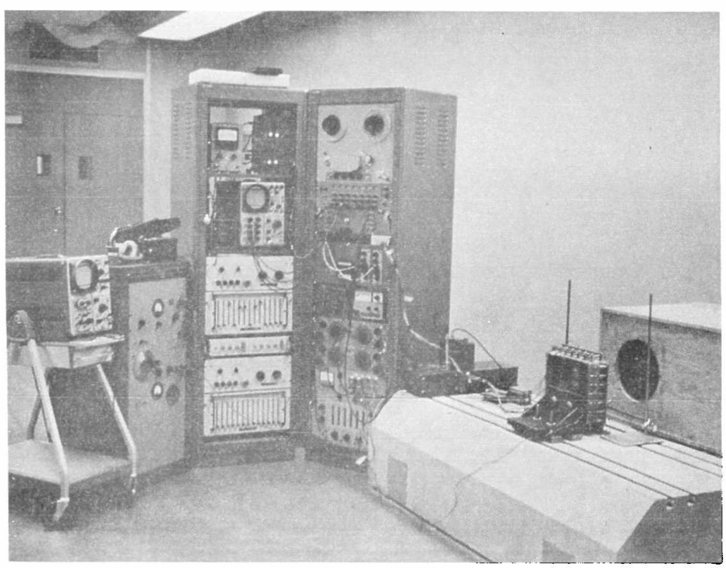

(b)

Simply-Supported Flat Plate

Fig. 3.1 Experimental Apparatus

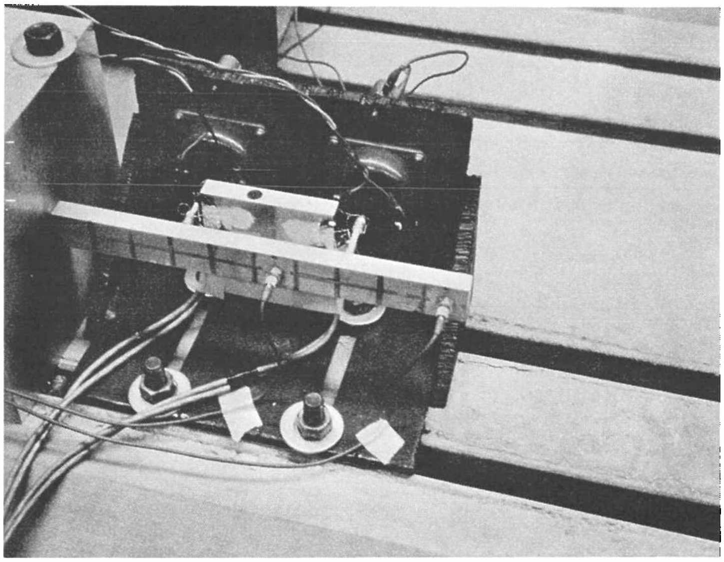

(a)

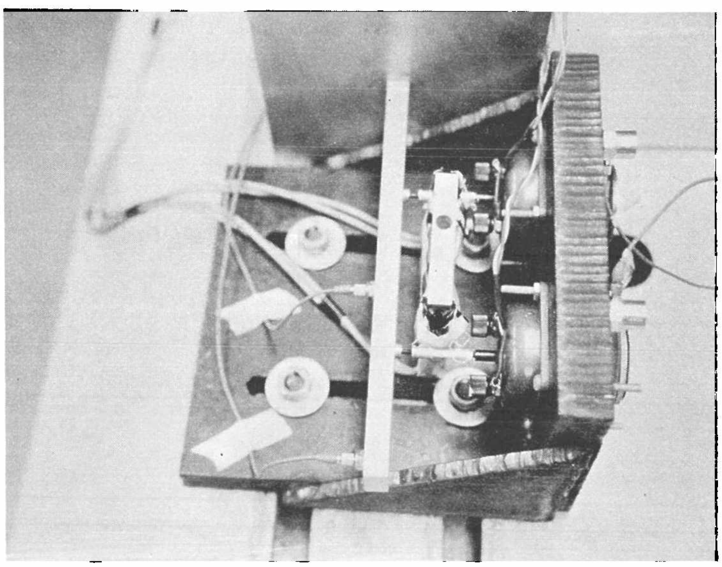

(b)

Fig. 3.2 Cantilever Beam

3.1.2 Simply-Supported Plate

The simply-supported rectangular plate, together with its excitation equipment and measurement instrumentation, is shown in Figure 3.3. The simply-supported boundary conditions were obtained by mounting the plate between knife-edges which had been machined on the support frame (Figure 3.4). The thickness of the plate was reduced from 1/8-inch to 1/16-inch at the edges in order to reduce the effects of moments applied to the plate edges by the knife-edge supports. The plate support structure was bolted to the seismic mass in the vertical position. A sketch showing plate dimensions and exact locations of the accelerometers and the shaker attachment point is presented in Figure 3.4. The material properties of the 2024 aluminum alloy used are: $E = 10.5 \times 10^6$ psi, $\gamma = 0.10$ lb/in^3, and $\nu = 0.313$.

3.2 Measurement Instrumentation and Shaker Support Structure

Force transducers, which acted as the connecting links between the small electromagnetic shakers and the structures, were constructed from $\frac{1}{4}$-inch aluminum rod as shown in Figure 3.5. Each transducer was instrumented with two small (0.031-inch x 0.031-inch) strain gages. The gages were located on opposite sides of the transducer and connected in opposite arms of the bridge circuit (Figure 3.5), so that the effects of transducer bending were cancelled and the transducer axial strain signal was doubled. Each end of the transducer was fitted with a short, No. 6 ANC, all-thread screw.

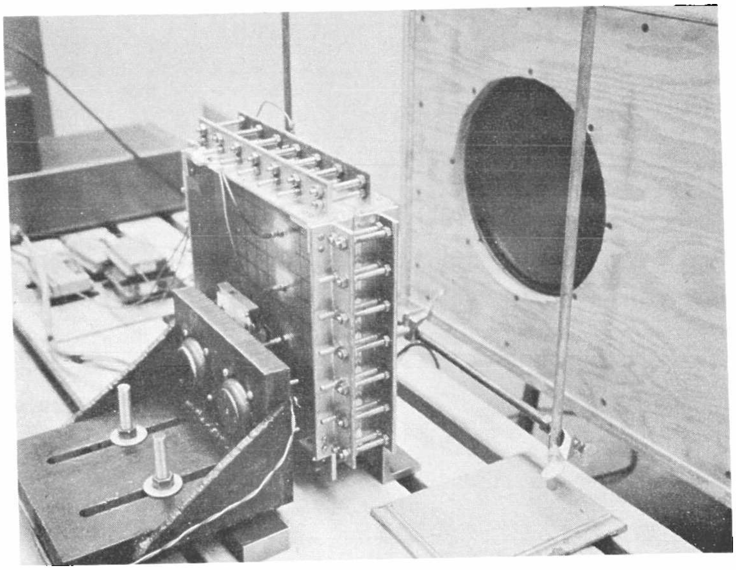

(a)

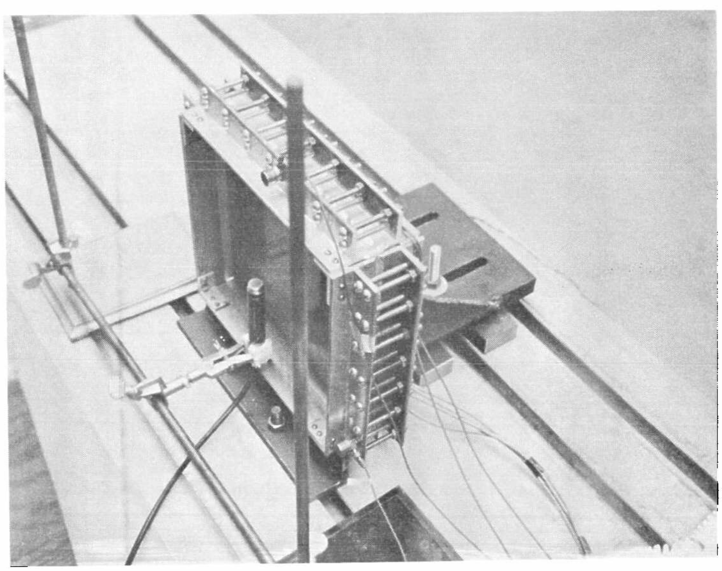

(b)

Fig. 3.3 Simply-Supported Rectangular Plate

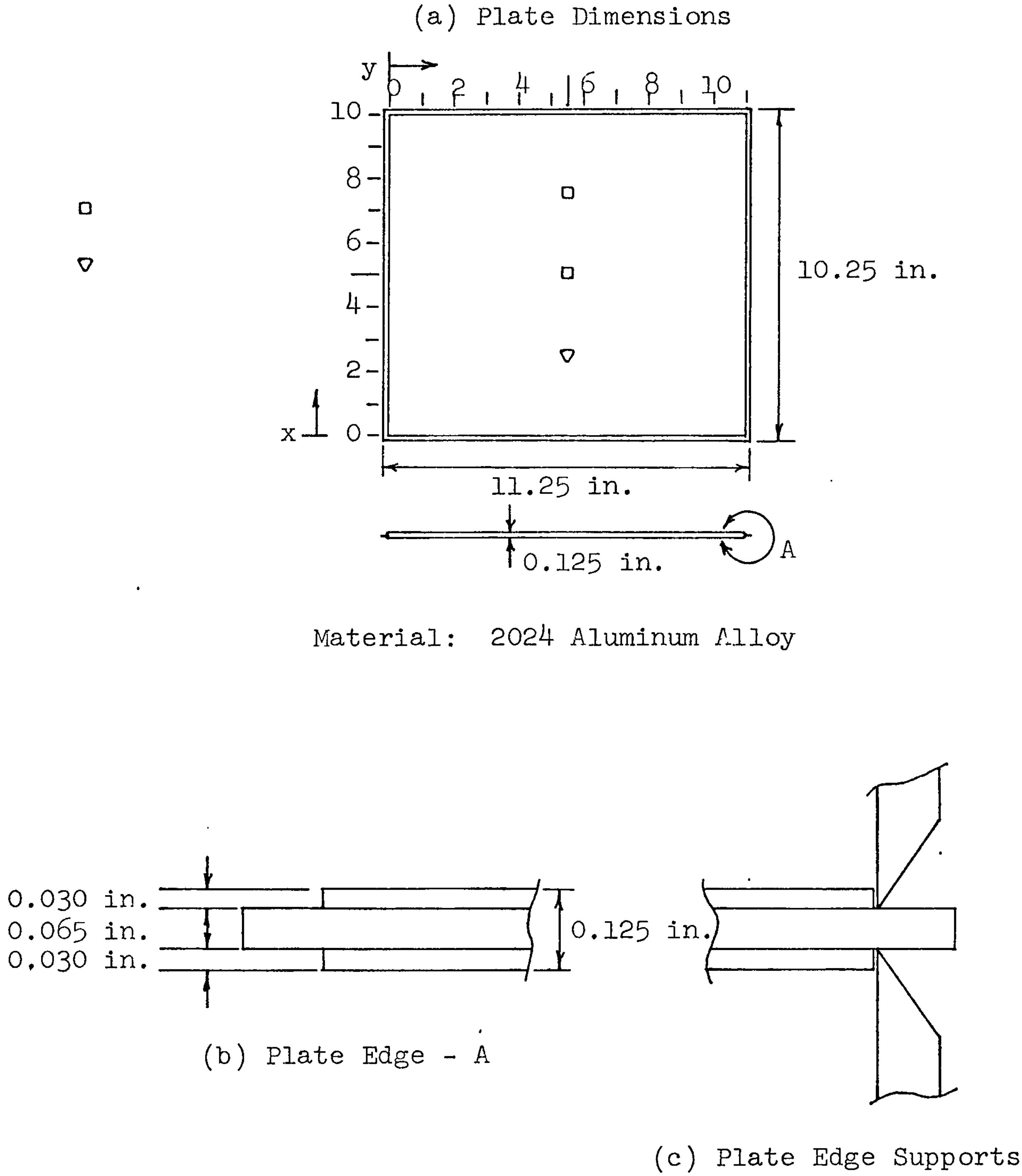

Fig. 3.4 Simply-Supported Rectangular Plate

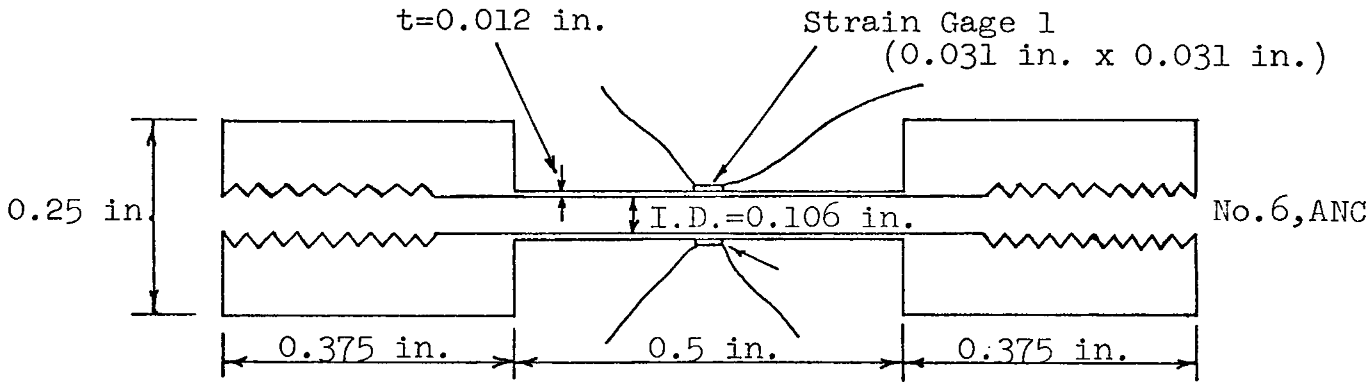

(a) Force Transducer

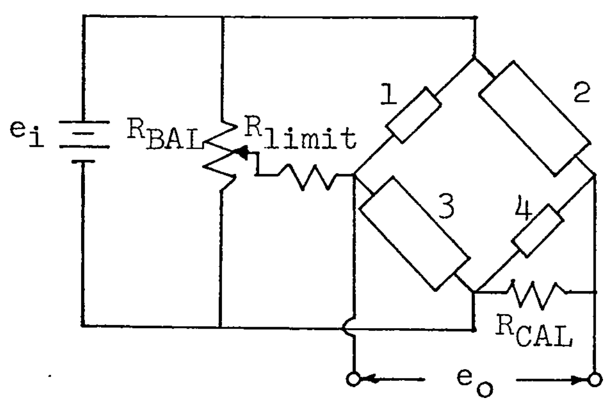

Gages 2 and 3 are dummy gages mounted on an aluminum block near the transducer. They complete the bridge and provide temperature compensation.

(b) Bridge Circuit

Fig. 3.5 Force Measuring Instrumentation

The transducer was attached to the structure by a lightweight threaded adapter, which had been cemented to the structure. The opposite end was attached to the shaker through its threaded connection. Total weight of the transducer, including the screws and adapter, was 3.3 grams. The first resonance frequency of the transducer in longitudinal vibration was calculated to be approximately 4000 Hz, while that of the transducer shaker moving mass system was calculated as approximately 2900 Hz. Each force transducer was calibrated statically at 0.30 V/lbf for a bridge excitation of 1.5 Vdc, after amplifying 10^4 times for recording purposes.

Micro-miniature accelerometers, which were attached with cement, were used to measure the vibration response at two locations on each structure. Each accelerometer weighed 2.8 grams. Each accelerometer signal, after amplifying 10 times, was calibrated at 57.5 V/g. In addition, two accelerometers were installed on the back of the shaker support structures in order to measure the frequencies of large response for these structures, since they were tied to the test structure through the force links. Two accelerometers were also installed on a flange of the plate edge support to measure its frequencies of significant response.

A microphone was used to obtain an estimate of the random acoustic pressure which provided the complex excitation environment for the simply supported rectangular plate, as shown in Figure 3.3b, page 36.

The shaker support structure was constructed from 1-inch steel plate as shown in Figure 3.2b, page 34. The frequencies of significant response of this structure, when it is coupled to the beam by two shakers, are presented in Table 3.1. Table 3.2 gives these frequencies for the support structure when it is coupled to the plate with one shaker. The frequencies of significant response in the edge support flanges of the simply-supported rectangular plate are presented in Table 3.3 for the clean plate and the plate with one shaker attached to it.

3.3 Research Tests

Tests were conducted to determine the basic structural information about mode shapes, resonance frequencies, and damping of the beam and the plate for use in the theoretical analyses and the simulation tests.

3.3.1 Cantilever Beam

In Test 1a the first five resonance frequencies of the cantilever beam were determined by exciting the beam with the electromagnetic shakers. The accelerometers and shakers were located so that they did not lie on nodes of the modes of vibration. Table 3.4 gives the values of frequency for both shakers attached to the beam with either F_A or F_B excited and for F_A only attached to the beam. In addition to variations in frequency depending upon which shaker was excited, small variations in measured resonance frequencies were obtained between the two accelerometer measurements;

Table 3.1 Frequencies of Significant Response in 1-inch Shaker Support Structure with Both Shakers Attached to Beam.

Frequency, Hz	
F_A Excited	F_B Excited
354	
707	707
1340	1340
1650	1650
3688	3686
4223	4221
4392	4372
4531	
4682	4668

Table 3.2 Frequencies of Significant Response in 1-inch Shaker Support Structure with One Shaker Attached to Plate

Frequency, Hz	
Acoustically Excited	Shaker Excited
331	331
986	985
1245	1220
1259	
2453	2454
2535	2538
2542	
2593	2594
3081	3062

Table 3.3 Frequencies of Significant Response in Plate Edge-Support Flanges

Frequency, Hz		
Clean Plate Acoustically Excited	One Shaker Attached Acoustically Excited	Shaker Excited
221	53	
221	219	219
593		
657	659	658
	910	948
986	979	976
1026	1019	1018
	1135	1134
1160		1170
1211	1203	1199
		1365
1499		
	1621	1621
1717		1710
1744		
	1776	1778
1840		
		1910
		1956
2109	2134	
	2177	2178
2193		
	2250	
2345		
		2405
	2412	2413
2458	2470	
	2477	2475
2503		2519
2594	2591	2587
2656		2607
	2768	2771

Table 3.4 Resonance Frequencies of Cantilever Beam

Mode Number r	Resonance Frequency, f_r, Hz				
	Theory	Experiment			
		Two Shakers Attached			
	Clean Beam	F_A Excited	F_B Excited	One Shaker Attached	Clean Beam Electromagnet Excitation
1	161	149	149	149	163
2	1008	906	907	928	974
3	2815	2362	2365	2540	2684
4	5510	5188	5203	5174	5142
5	9140	8104	8133	8126	8258

however, these were considered negligible. The second and third mode resonance frequencies are seen to be raised by approximately 2% and 8%, respectively, while the 4th mode frequency drops less than 1%, when the shaker F_B is detached from the beam. The large shift in the third resonance frequency indicates that the effect of the second attached shaker and support structure on this beam mode is particularly important. When compared with the values obtained from Bernoulli-Euler beam theory, the resonant frequencies are low by 5-14% for the various modes with either two or one shaker attached. In Test 1b the clean beam (no shakers or accelerometers attached) was excited with a small electromagnet. The magnetic circuit was completed by using a small piece of steel attached to the beam at a distance of 7 inches from the clamped end. A crystal pickup was placed on the beam to observe response, and this provided the only inertia loading on the beam. Resonance frequencies from this test are also shown in Table 3.4. When comparisons are made with theory, it is seen that the experimental values are generally lower than theory by as much as 3-10%, with disagreement increasing with frequency.

In Test 2a, the mode shapes of the first five beam resonances, with both shakers attached and only F_A excited, were mapped using the attached accelerometers on all modes and, in addition, a crystal pickup on modes 4 and 5. The crystal pickup could not be used on the large displacement, lower frequency modes (1-3), since the force required to maintain it in constant contact with the beam distorted the mode shape greatly near the free end of the beam. As is shown in Figure 3.6, the experimental mode shapes are identical to the theoretical shapes, which were determined from the Bernoulli-Euler theory with no mass or stiffness attachments to the uniform beam, i.e., a clean beam. It is therefore concluded that the theoretical mode shapes may be used in calculations of the complex frequency response function for comparison with the experimentally determined values.

In Test 2b, the damping of the cantilever beam in its first five modes was determined by impulsing the beam with a soft, blunt object and recording the filtered response decay data of the accelerometers and one of the force transducers, as shown in Figure 3.7.

The logarithmic decrement, δ, was determined from eq. (2.26) and the structural damping or loss factor, η_r, for the rth mode from eq. (2.30). Values of η_r are given in Table 3.5 for the beam with both shakers attached, with only one shaker, F_A, attached, and for the clean uniform beam with only one accelerometer, A_2, attached. As is seen, the damping increases by less than a factor of two when the second shaker is connected to the beam; however, the attachment of one shaker to the clean beam increases damping values by 1.5 to 20 times.

It may therefore be concluded that the attachment of shakers to a structure can modify its dynamic characteristics considerably. In the case of the beam, the resonance

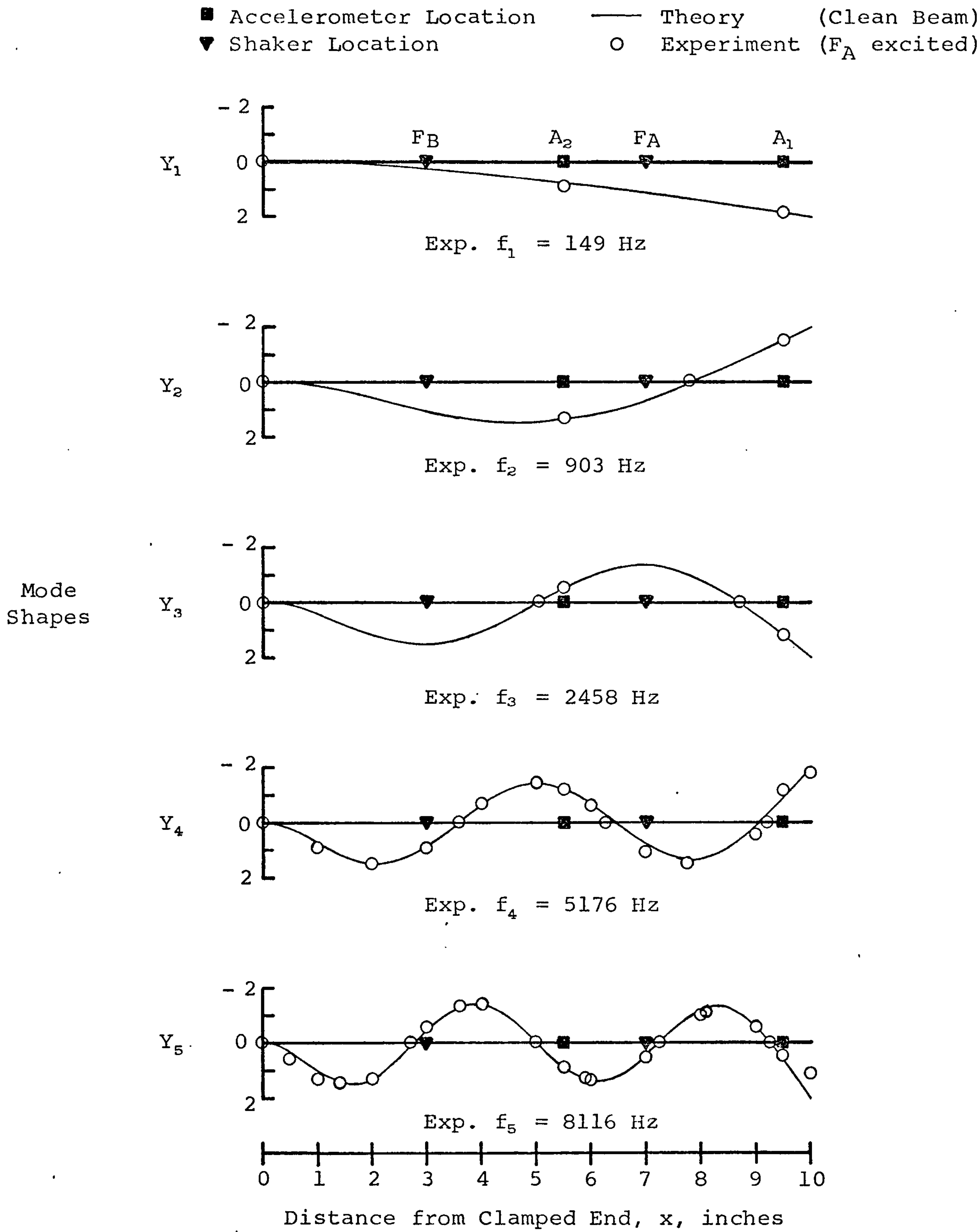

Fig. 3.6 Comparison of Theoretical and Experimental Mode Shapes for First Five Resonances of Cantilever Beam

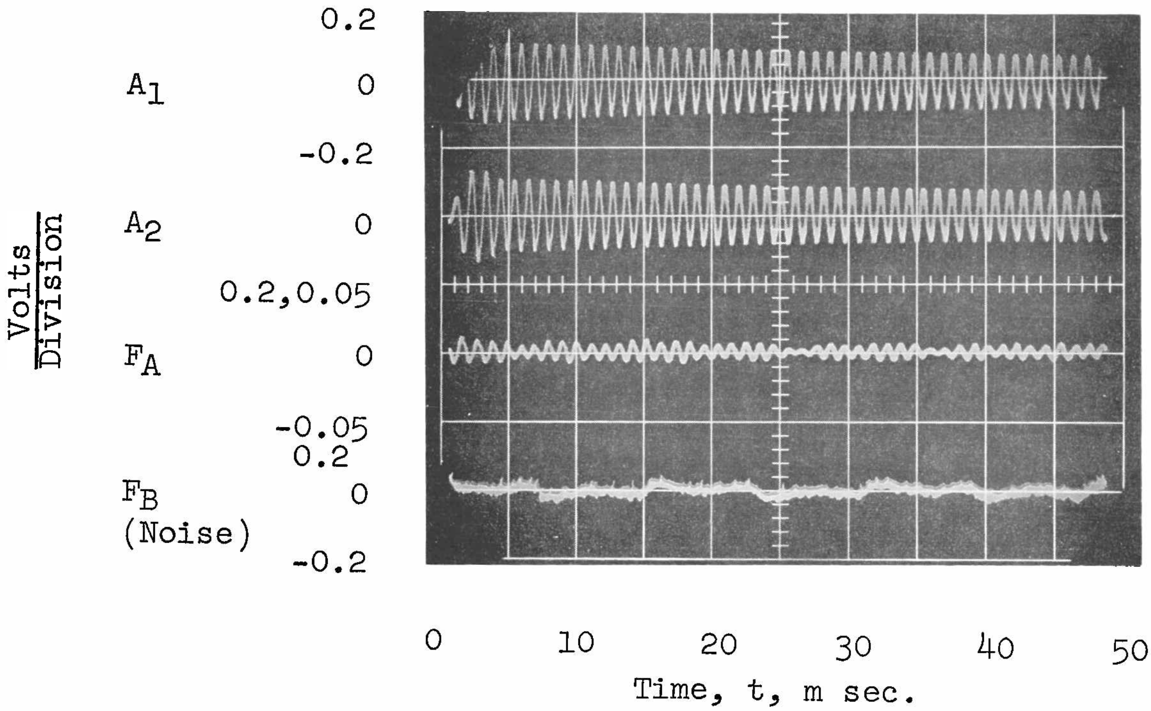

(a) Filter f = 910 Hz

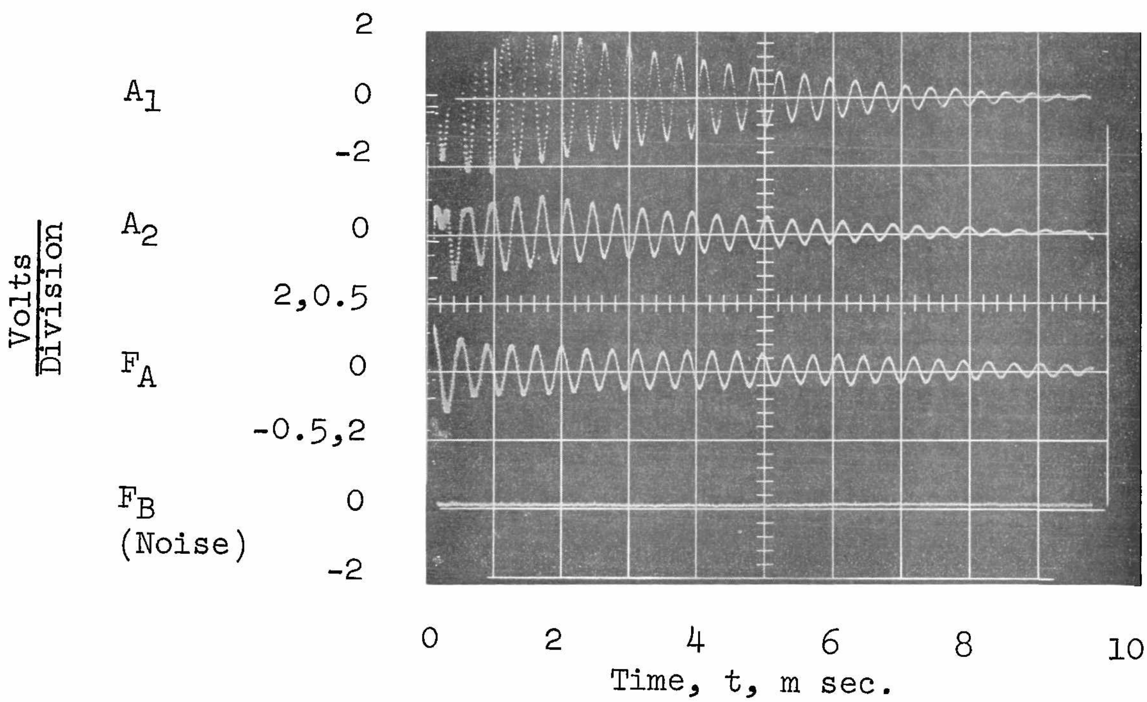

(b) Filter f = 2500 Hz

Fig. 3.7 Cantilever Beam Vibration Decay

Table 3.5 Damping of Cantilever Beam[1]

Mode Number r	Structural Damping Coefficient, η_r						
	Both Shakers Attached			One Shaker Attached			Both Shakers Disconnected
							A_1 Disconnected
	A_1	A_2	F_A	A_1	A_2	F_A	A_2
1	.00763 .00768	.00815 .00787	.00755 .00697	.00796 .00701	.0079 .00787	.00647 .00621	.000372
2	.00586 .00528	.0057 .00605		.00342	.00348		.00229
3	.0398	.0528		.0386 .0303	.03098 .0285	.01472	.0079
4	.0656	.0459		.0301	.02992	.01338	.00704
5	.0229	.0217		.0215	.02218		.00676

[1]Damping was determined by impulsing beam with a soft, blunt object and recording the decay in amplitude for logarithmic decrement determination.

frequencies and damping were changed considerably by the attachment of shakers to a clean beam, while the effect on the modal deflection shapes was negligible. However, it appears that the attachment of additional shakers after the first has a much smaller effect on frequencies and damping.

3.3.2 Simply-Supported Plate

In Test 5a, the resonance frequencies of the simply-supported plate were determined by exciting the clean plate (no shaker attached) with harmonic acoustic excitation, exciting the plate with simulation shaker attached by acoustic excitation, and exciting the plate with the simulation shaker F_A. Table 3.6 gives the values of resonance frequency for the first five odd-odd modes and for the first two even-odd modes. The resonances of the first four odd-even modes, the first three even-even modes, and the remaining two even-odd modes which lay in the 0-3000 Hz frequency range were not identified, since the two accelerometers were located on node lines for these particular modes. The accelerometers were positioned on the plate in this manner so that, with the one exception of the one-third-octave band from 1123-1414 Hz, only one resonance would be detected in each of the one-third-octave filter bandwidths in the 350-2800 Hz range of interest. This was done because it would have been impossible to obtain a good simulation in the random tests with more than one mode appearing within a one-third octave frequency band of the spectrum shaping filters. Table 3.7 gives the first 16

Table 3.6 Resonance Frequencies of Simply-Supported Rectangular Plate

Mode Number	Half-Wave Numbers		Resonance Frequency, f_r, Hz			
			Theory	Experiment		
r	m	n	Clean Plate	Acoust.Excit. Clean Plate	Acoust.Excit. Shaker Conn.	Shaker Excitation
1	1	1	220	221	219	219
3	2	1	580	594	582	580
5	1	3	1013	1024 982	1019 977	1019 976
6	3	1	1180	1209	1202 1133 1168	1202 1130 1166
7	2	3	1373	1402	1364	1365
10	3	3	1975	1988	1955	1956
14	1	5	2600	2674	2593	2638

Table 3.7 Spectrum-Shaping-Filter Bandwidth Envelope of Theoretical Resonance Frequencies for Simply-Supported Plate

Filter		Odd-Odd Modes			Even-Odd Modes			Odd-Even Modes			Even-Even Modes		
Center Frequency	Band-width	m	n	f_r (Hz)	m	n	f_r (Hz)	m	n	f_r (Hz)	m	n	f_r (Hz)
None		1*	1	220									
400	354 445												
500	445 561							1	2	517			
630	561 707				2**	1	580						
800	707 891										2	2	876
1000	891 1123	1*	3	1013									
1250	1123 1414	3*	1	1180	2**	3	1373						
1600	1414 1782							3 1	2 4	1477 1708			
2000	1782 2245	3*	3	1975	4	1	2020				2	4	2070
2500	2245 2828	1*	5	2600	4	3	2813	3	4	2665	4	2	2318
3150	2828 3564	5* 3*	1 5	3098 3560	2**	5	2958	5	2	3398	4	4	3504
4000	3564 4490	5*	3	3890	4 6**	5 1	4400 4415	1	6	3690	2	6	4050
5000	4490 5657	1* 5*	7 5	4975 5480	6** 2**	3 7	5220 5340	5 3	4 6	4575 4650	6 4	2 6	4720 5490

* Modes for which response was possible at A_1 and A_2 locations.
** Modes for which response was possible at A_2 location only.

theoretical resonance frequencies and the filter frequency bands in which they lie.

From Table 3.6 the resonance frequencies measured when the clean plate was excited acoustically are seen to be only slightly higher (generally less than 2%) than the theoretically determined values. It is seen that the attachment of a shaker to the plate has a slight lowering effect on the resonance frequencies. In the vicinity of the fourteenth resonance frequency (2400-2800 Hz), it was possible to excite the mode with $m = 1$ half-wave in the x direction and $n = 5$ half-waves in the y direction at approximately six different frequencies. An examination of Tables 3.2 and 3.3, pages 42 and 43, shows that the 1-inch shaker support structure, when connected to the plate, and the plate edge support flange responded significantly in the 2400-2800 Hz range. Since the calculated resonance frequency of the force transducer/shaker-moving-mass combination was approximately 2900 Hz, it appears that there are a number of subsystem responses which may affect the plate dynamics in the vicinity of this resonance.

In addition, the plate responds at approximately 980 Hz in mode $m = 1$, $n = 3$. It is seen from Tables 3.2 and 3.3 that both the shaker support and plate support respond at this frequency also. It is believed that this response, prior to reaching the resonance frequency of 1020 Hz for this mode, may be caused by a resonance in the plate supports, since plate response is noted at this frequency even for the clean plate. The plate, with shaker attached, also responds at frequencies of approximately 1130 and 1170 Hz in mode $m = 3$, $n = 1$, whose resonance frequency is approximately 1200 Hz. This is believed caused by the significant involvement of the plate-edge support structure at these frequencies, as shown in Table 3.3, page 43.

In Test 6a, the mode shapes of the six resonances of Table 3.6, page 51, were mapped for the clean plate using harmonic acoustic excitation, and for the plate with shaker attached using the shaker for excitation. For the test using acoustic excitation, the modes were mapped completely using a piezoelectric crystal probe. In the shaker excited tests, only the mode nodal locations were mapped. Examples comparing the mode nodal locations of the two test cases with theory are given in Figure 3.8. There is slight distortion of modal displacement shapes from the assumed simply-supported functions in some of the modes. This is caused by the addition of the shaker and/or the two accelerometers to the clean plate. However, the distortion is not excessive, and it is concluded that the theoretical mode shapes may be used in calculations of complex frequency response functions.

In Test 6b, the structural damping of the plate was determined by either the logarithmic decrement or the bandwidth method. In the tests which made use of the logarithmic decrement, the plate was either impulsed with a soft, blunt object and the response decay recorded, or it was excited harmonically to a steady-state condition with acoustic or

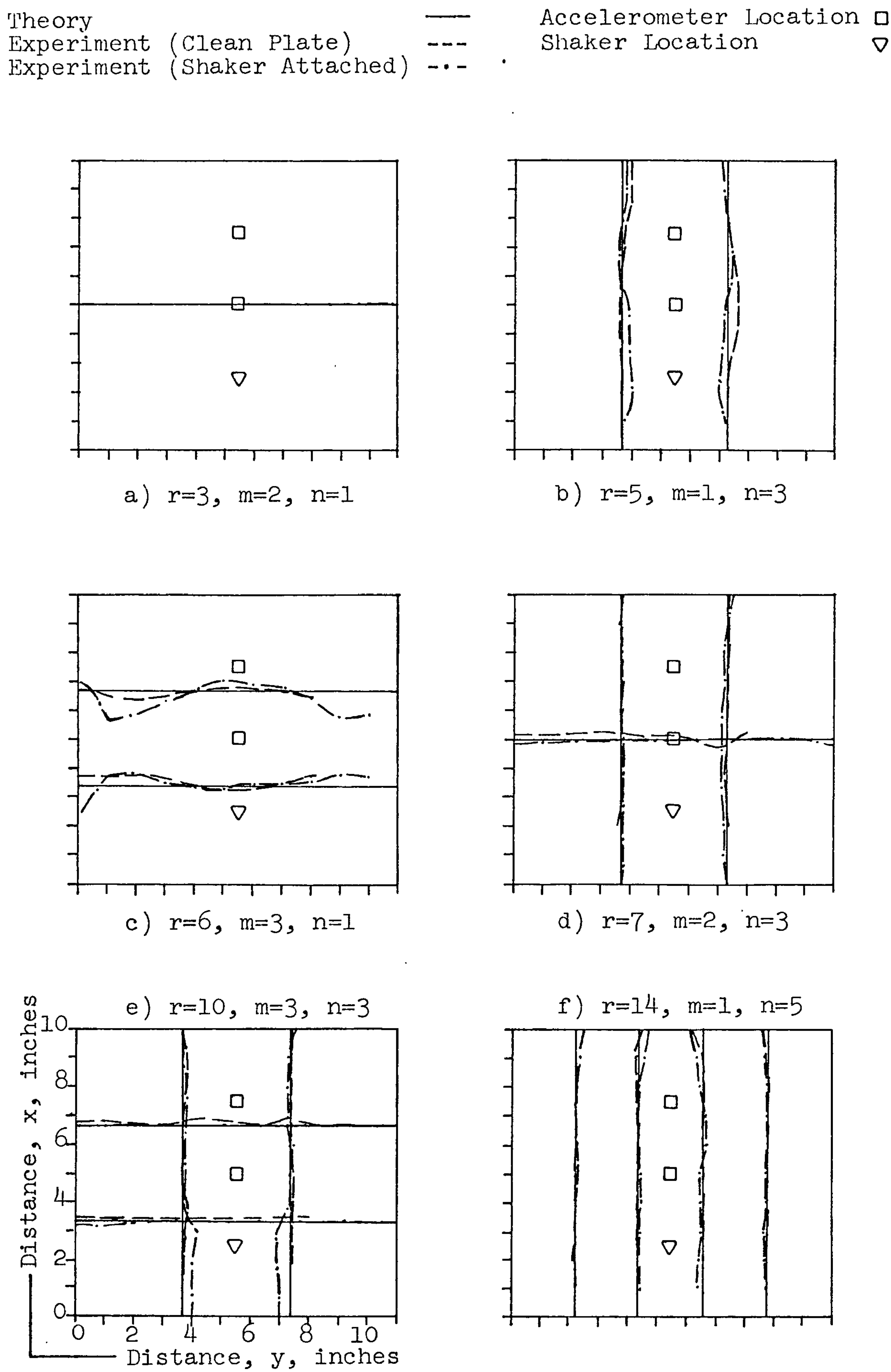

Fig. 3.8 Node Lines for Mode Shapes of Simply-Supported Plate.

shaker excitation, which was then rapidly turned off, allowing a measurement of the response decay. Damping values for the clean plate were determined for comparison with those obtained for one shaker attached to the plate. In the tests making use of the bandwidth method, one shaker was attached to the plate, and the plate was either excited with a sinusoidal acoustic pressure or with a sinusoidal shaker force. The resonance frequency and the half-power point frequencies were then measured for each resonance peak. In Table 3.8 it is seen that that damping value for any one mode may vary from test to test by as much as a factor of 4. In general, with one shaker attached to the plate, the test which impulsed the beam with a blunt object was taken to provide the best estimate of modal damping values, η_r.

It is seen from Table 3.8 that the damping values for the clean plate are roughly one-half of those for the plate with one shaker attached.

Therefore, the effects of attaching the shaker to the clean plate were not as great as for the beam, i.e., the values of resonance frequency and damping were not affected nearly so much; however, the shaker and accelerometers did tend to distort the plate mode shapes somewhat.

3.4 Random Vibration Tests Using Complex Excitation Environments

3.4.1 Cantilever Beam

The complex excitation environment for the cantilever beam was provided by two shakers, F_A and F_B, attached as

Table 3.8 Damping of Simply-Supported Rectangular Plate

Structural Damping Coefficient, η_r							
				Bandwidth Method			
Mode Number	Resonance Frequency (Hz)	Number of Half-Waves		Shaker Connected Acoustically Excited		Shaker Excited	
r	f_r	m	n	A_1	A_2	A_1	A_2
1	219	1	1	.00776	.00776	.0087	.00824
3	580	2	1		.01115		.0308
5	1019 982	1	3	.00389 .00713	.00485 .00814	.00584 .00815	.00584 .00815
6	1202 1167 1133	3	1	.00913	.01827	.01163 .01375 .0212	.0174 .01109 .01322
7	1365	2	3		.00512		.011
10	1956	3	3	.00716	.00767	.00767	.00717
14	2638	1	5	.033	.0411	.0766	.0437

Table 3.8 (Continued)

				Structural Damping Coefficient, η_r							
				Logarithmic Decrement Method							
Mode Number	Resonance Frequency (Hz)	No. of Half-Waves		Shaker Connected Impulse Excited		Shaker Connected Acoustically Excited		Shaker Excited		Clean Plate Impulse Excited	
r	f_r	m	n	A_1	A_2	A_1	A_2	A_1	A_2	A_1	A_2
1	219	1	1	.00484	.00481	.00669	.00627	.00596	.00494	.00378	.00418
3	580	2	1		.01987		.00481				.0071
5	1019 982	1	3	.0078 .00653	.00115 .00701	.00297 .00325	.00221 .00173	.00516 .00685	.00589 .00567	.00275 .00325	.00385 .00312
6	1202 1167 1133	3	1	.00857	.0085					.0048	.00294
7	1365	2	3								
10	1956	3	3			.00121	.00107				
14	2638	1	5								

shown in Figure 3.2, page 42, at distances of 7 inches and 3 inches, respectively, from the clamped end of the 10-inch long beam. Beam accelerations were measured by two accelerometers, A_1 and A_2, located at distances of 9.5 inches and 5.5 inches, respectively, from the clamped end.

In Tests 3d and 3e, the shakers were mounted on the 1-inch steel support structure with both shakers being excited in Test 3d. In Test 3e, only shaker F_A was excited; however, since shaker link F_B was attached to the beam and to the shaker suspension system, it did provide a large narrow-band random force input at this location.

Random data from the two accelerometers and the two force transducers were recorded on magnetic tape for a period of one minute during each test. After the random tests, the tapes were supplied with noise floors for each data channel, so that noise components could be identified later in the reduced data. Significant noise components did show up at multiples of 60 Hz in the frequency range of the force data below 500 Hz. In addition, each data channel was provided with a known force or acceleration calibration signal.

After tape recording, over-all rms values of the random signals were measured on a random noise voltmeter. Photographs of the rms spectral content of each signal were then taken from a memory oscilloscope equipped with a spectrum analyzer unit, so that the spectral content of the beam vibration could be simulated in later tests. Oscilloscope spectrum analysis of each signal was first conducted over the total frequency range of interest, 400-7000 Hz. This range contained the second, third, and fourth beam modes. Narrow-band rms spectrum analysis was then conducted over the small frequency range of each resonance noted in the wide-band analysis. Examples of oscilloscope spectrum analysis are shown in Figures 3.9-3.12.

The magnetic tapes were then digitized by the NASA-MSC Computation and Analysis Division and data reductions were performed digitally, as explained in Appendix A4. Data were reduced in the form of digitized signal, autocorrelation, normalized probability density, spectral density, and rms spectrum for each measurement; and co-spectral density, quadrature-spectral density, cross-spectral density modulus and phase, coherence function, and transfer function between each pair of measurements. Examples of reduced data are given in Figs. A3.1a-A3.1m, pages 127 through 139. The data displayed all the characteristics attributed to wide and narrow-band, approximately Gaussian data. The most important data reductions were the acceleration auto- and cross-spectral densities for accelerometers A_1 and A_2, which were compared with the same data from the vibration simulation tests to ascertain the degree of successful simulation. Data reduction was conducted using a 24-Hz narrow-band filter and a 1.6-second time slice of the digitized data. This yields a normalized standard error [30], according to

$$\epsilon = 1/(BT)^{\frac{1}{2}}$$

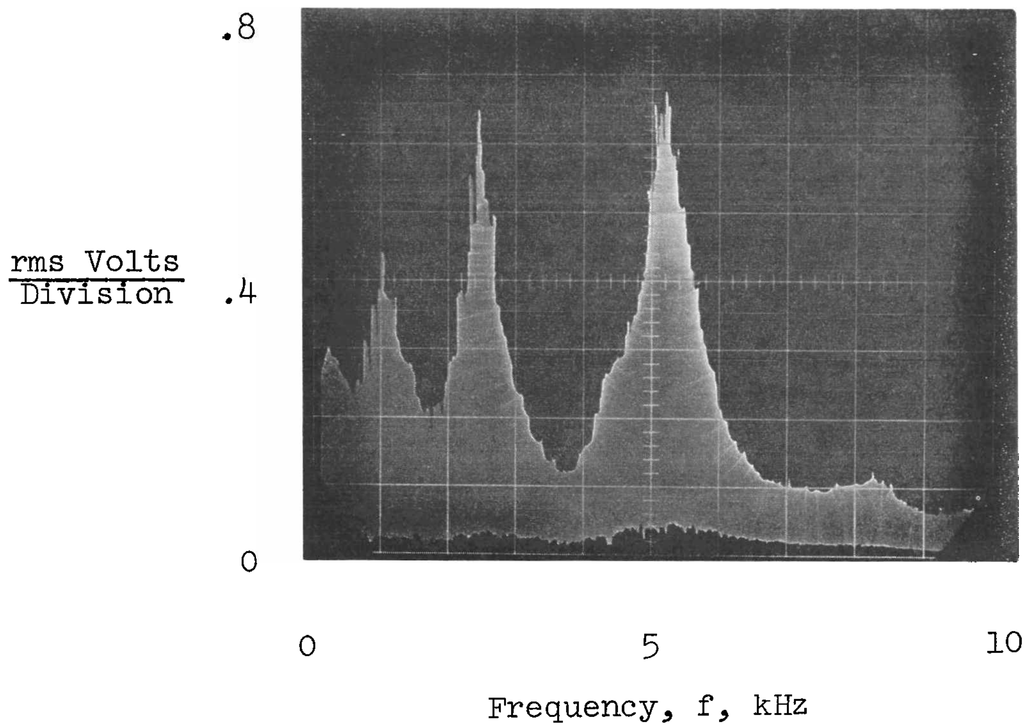

Time Base:
5 sec/Div.
Resolution:
Coupled

(a) Complex Excitation Test 3e

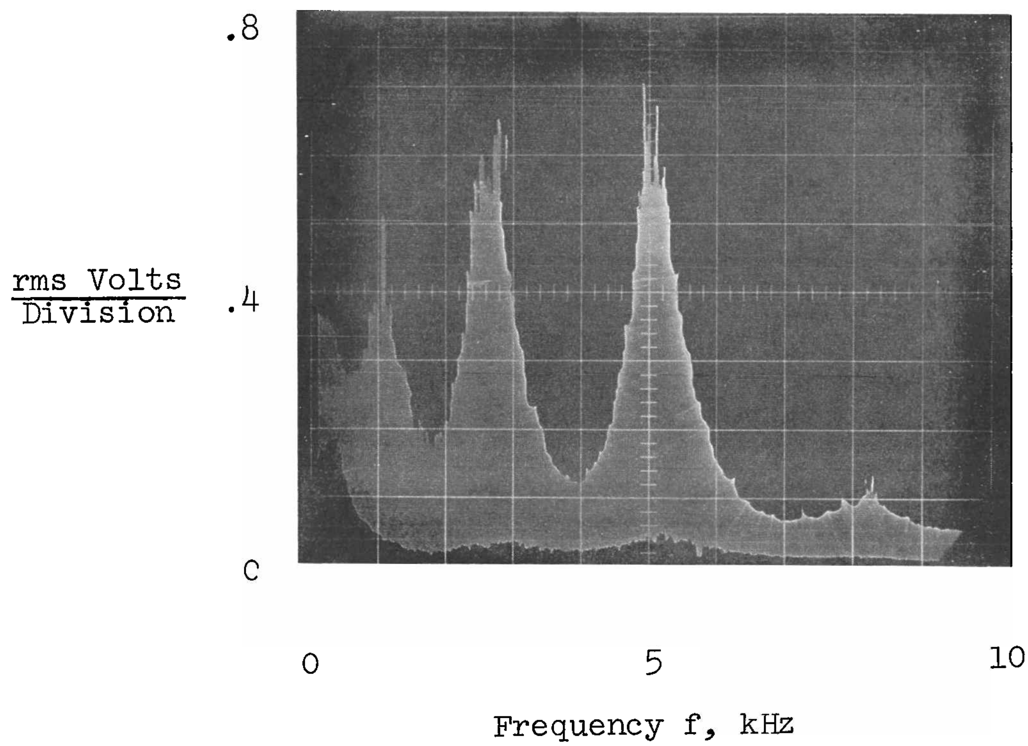

Time Base:
5 sec/Div.
Resolution:
Coupled

(b) Simulation Test 4e

Fig. 3.9 rms Spectrum of Cantilever Beam Tip Acceleration A_1--Second, Third, and Fourth Resonances.

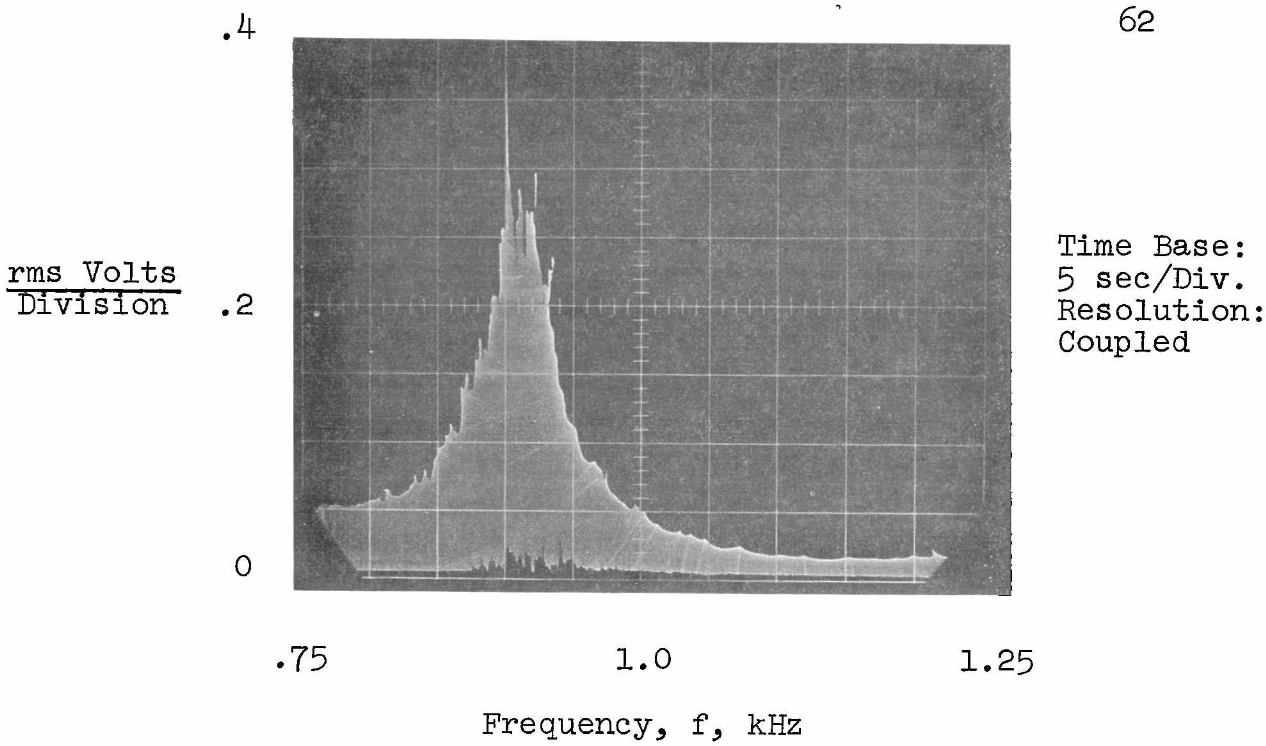

(a) Complex Excitation Test 3e

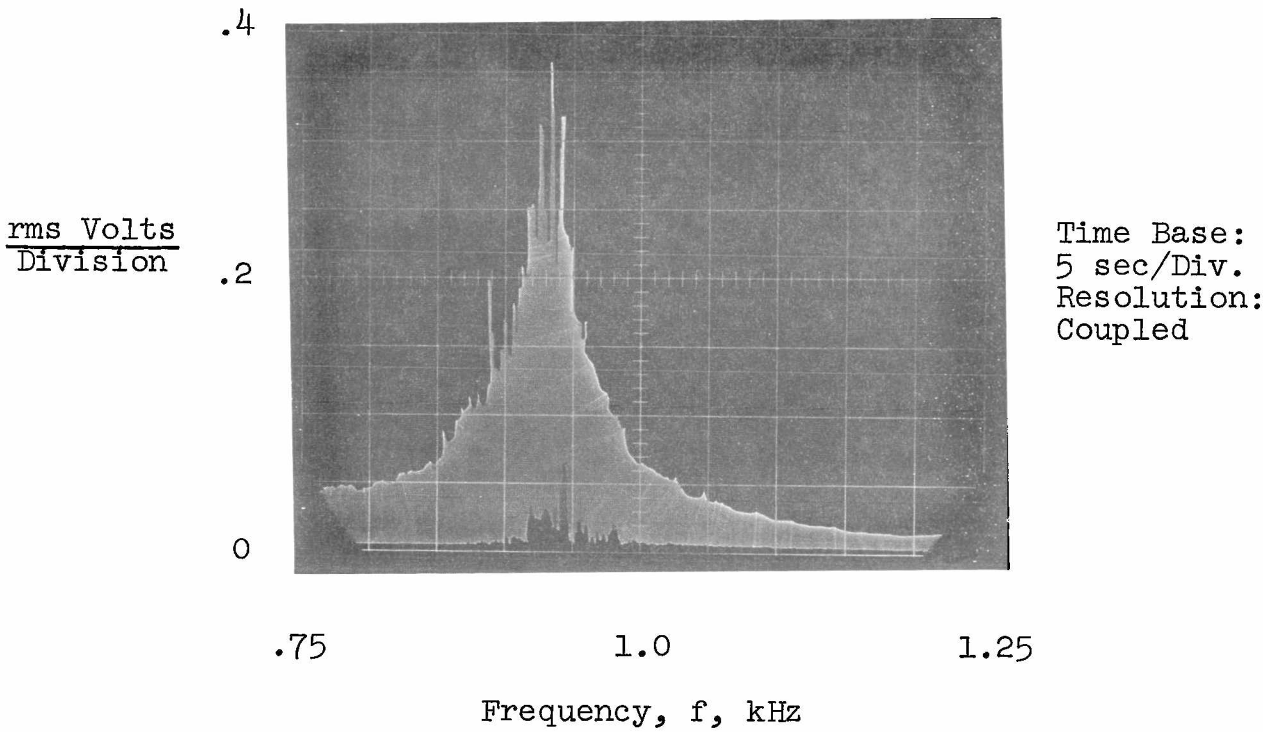

(b) Simulation Test 4e

Fig. 3.10 rms Spectrum of Cantilever Beam Tip Acceleration A_1--Second Resonance.

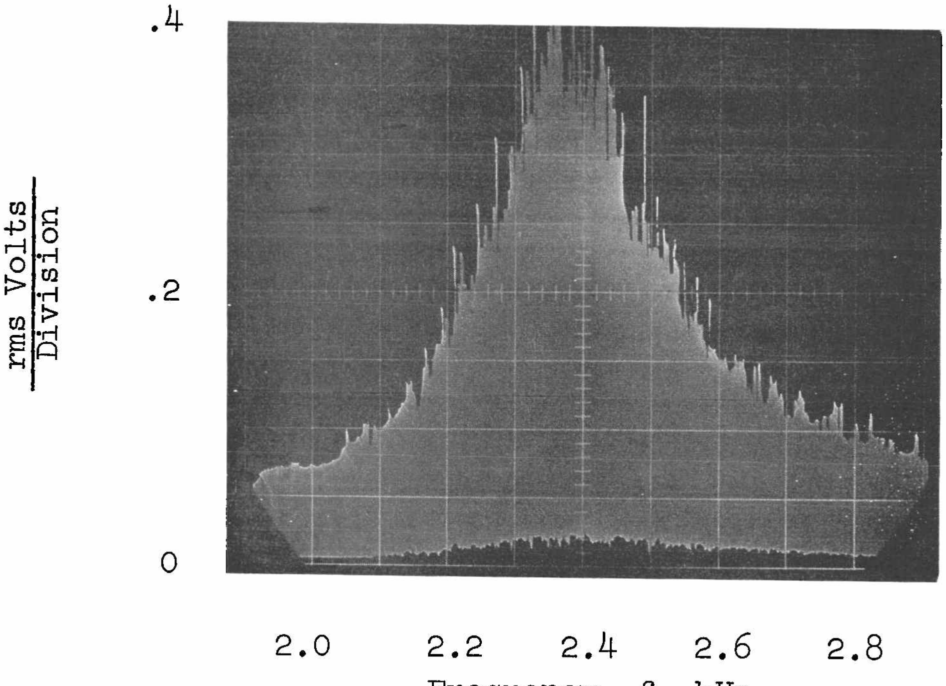

Settings
Time Base:
5 sec/Div.
Resolution:
Coupled

(a) Complex Excitation Test 3e

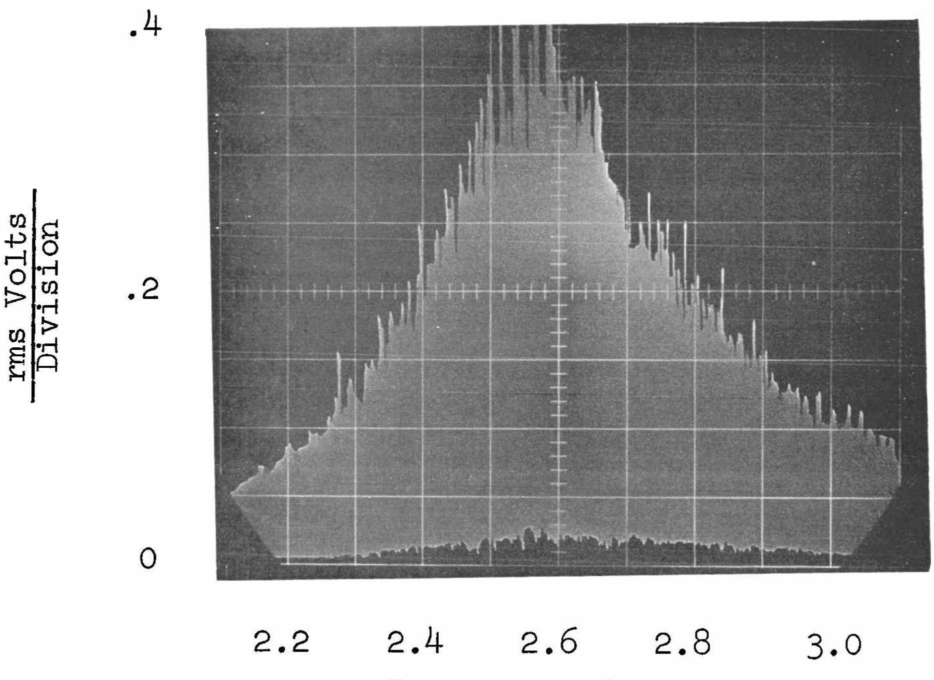

Settings:
Time Base:
5 sec/Div.
Resolution:
Coupled

(b) Simulation Test 4e

Fig. 3.11 rms Spectrum of Cantilever Beam Tip Acceleration A_1--Third Resonance

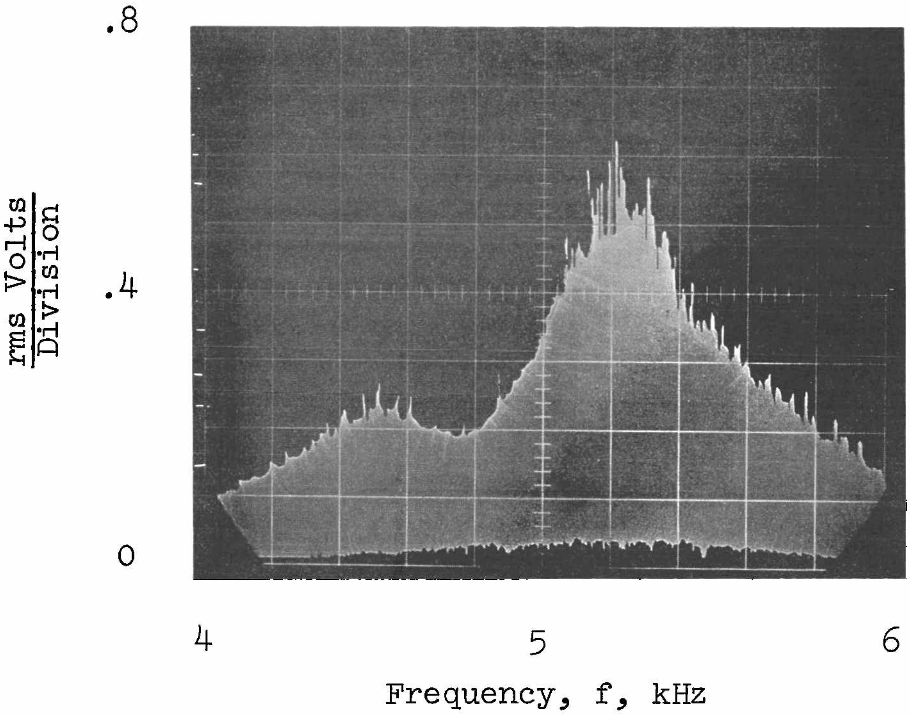

Settings
Time Base:
5 sec/Div.
Resolution:
Coupled

(a) Complex Excitation Test 3e

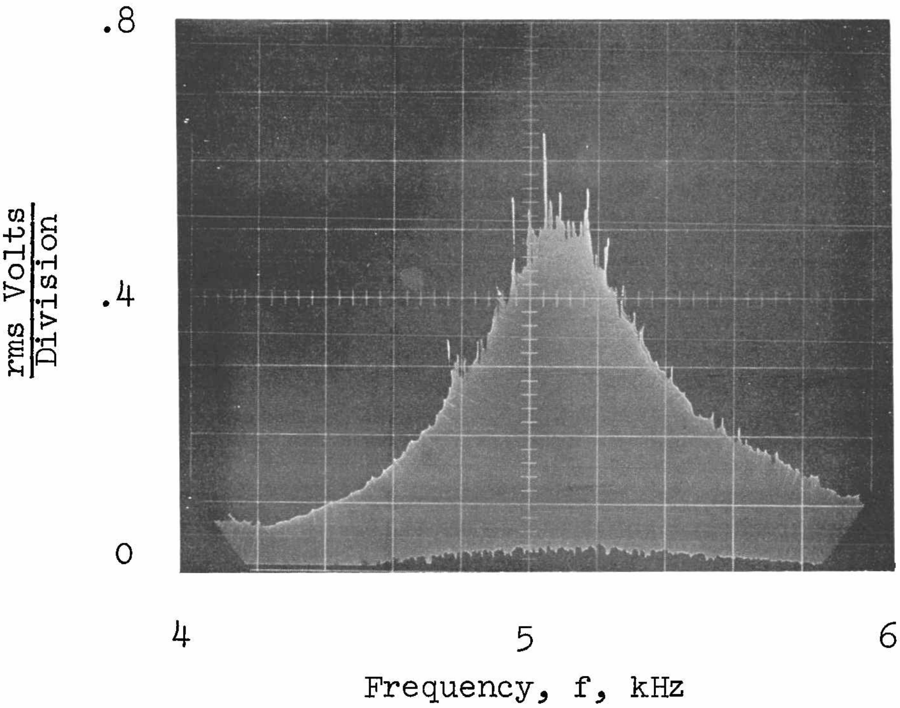

Settings
Time Base:
5 sec/Div.
Resolution:
Coupled

(b) Simulation Test 4e

Fig. 3.12 rms Spectrum of Cantilever Beam Tip Acceleration A_1 - Fourth Resonance of 16% for the spectral density estimates; however, since all data were very nearly Gaussian (see Figs. A3.1b and A3.1c, pages 128 and 129), the actual error present in the reduced data should be much smaller than this. At any rate, even if maximum error did exist, it should still be possible to ascertain if a satisfactory simulation did or could, in fact, be obtained.

A schematic diagram of the equipment used in the complex excitation tests is given in Figure 3.13, while Figure 3.1a, page 33, is a photograph of all equipment used. A list of all equipment used in the tests is provided in Appendix 2.

3.4.2 Simply-Supported Plate

The complex excitation environment for the plate was acoustic noise with an over-all sound pressure level of 131 db, provided by a speaker located with respect to the plate as shown in Figures 3.1b and 3.3a, pages 33 and 36. Plate accelerations were measured by two accelerometers, A_1 and A_2, located at the center-plate position ($x = 5.0$ in., $y = 5.5$ in.) and the quarter-plate position ($x = 7.5$ in., $y = 5.5$ in.) as shown in Figures 3.3a and 3.4, pages 36 and 37.

Two tests were conducted. In Test 7a, the plate had no shaker attached, while in Test 7b, one shaker, mounted on the 1-inch support structure, was attached at the quarter-plate position ($x = 2.5$ in., $y = 5.5$ in.). Although not excited electrically, shaker F_A did provide a large narrow

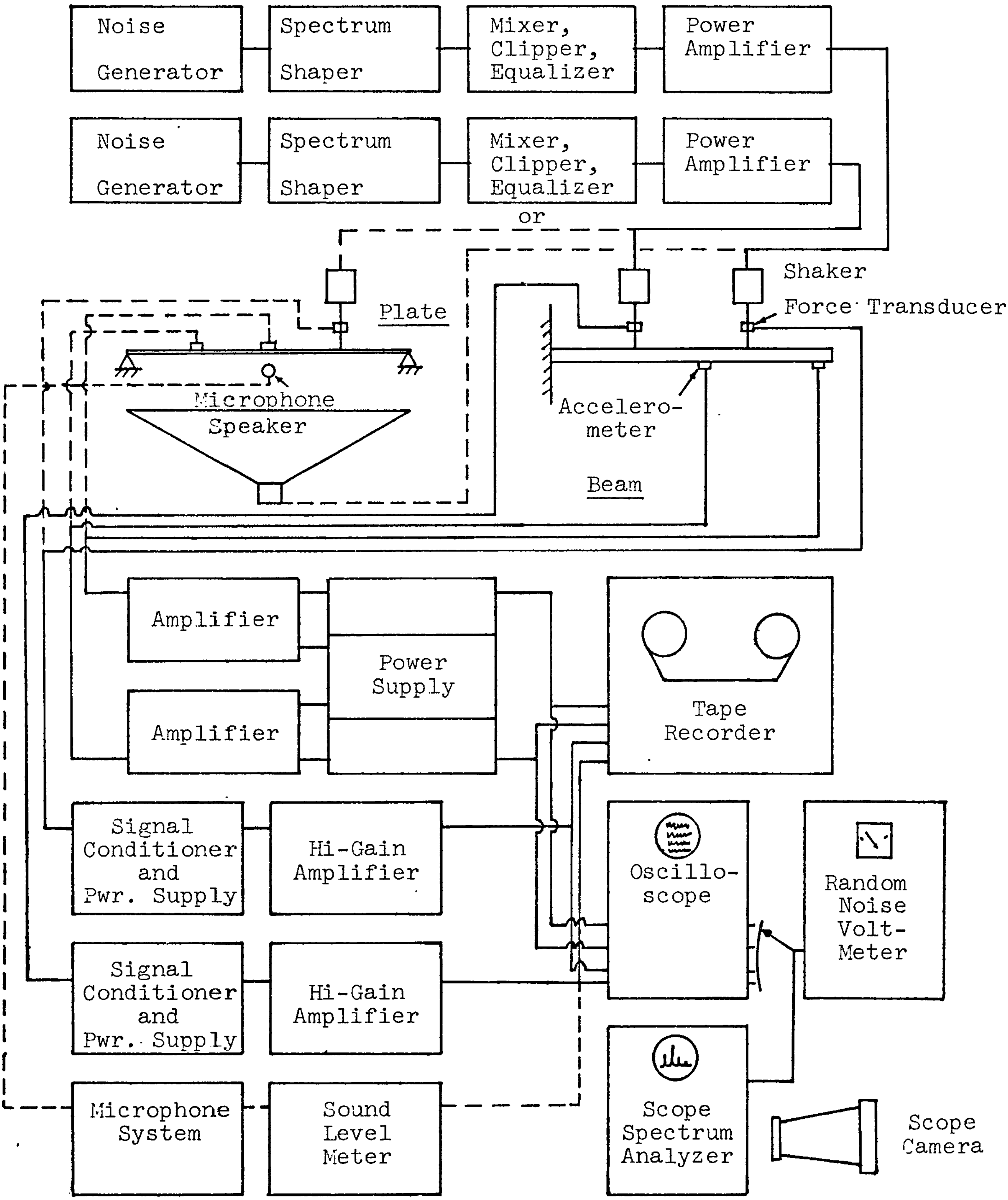

Fig. 3.13 Schematic of Equipment Used in Random Vibration Tests.

band random force input at this location by virtue of the connection of the force transducer F_A between the plate and the shaker suspension system.

Random data from the two accelerometers, the microphone, and the force transducer were recorded on magnetic tape for a period of one minute during each test. The procedure followed in tape recording, over-all rms and rms spectrum determination, and data reduction is the same as for the cantilever beam, except that the frequency range of interest in the plate tests was 400-3000 Hz, and the data reduction was conducted using a 12 Hz narrow-band filter and a 3.2-second time slice. Figure 3.1b, page 33, is a photograph of all equipment used.

Because of accelerometer locations, responses of only the m(odd), n(odd) modes were measured by A_1, and responses of the same odd-odd modes plus two even-odd modes were measured by A_2. No even-even or odd-even modal responses were seen by either accelerometer.

3.5 Vibration Simulation Tests

3.5.1 Cantilever Beam

The narrow-band auto- and cross-spectral densities of the beam accelerations at locations A_1 and A_2 for Tests 3c and 3d were simulated using one shaker, F_A, located at a distance of 7 inches from the clamped end of the beam. In order to achieve good simulation, the force spectrum was shaped using a spectral density equalizer consisting of thirteen, one-third-octave band, variable gain filters with the center frequencies and bandwidths given in Table 3.7, page 52.

Tests 4c and 4d were conducted by adjusting the equalizer filters until the best possible simulation of beam acceleration had been obtained on the oscilloscope analyzer at every resonance within the frequency range of interest. In Figures 3.9-3.12, pages 61 through 64, a comparison is shown between the rms acceleration spectra of a complex excitation test and a simulation test. Data from accelerometers A_1 and A_2 and force gage F_A were then recorded on magnetic tape and reduced digitally in the manner described for the complex excitation tests, so that comparisons could be made in a more exact manner.

3.5.2 Simply-Supported Plate

The narrow-band auto- and cross-spectral densities of plate accelerations at locations A_1 and A_2 for Tests 7a and 7b were simulated using one shaker, F_A, located at $x = 2.5$ in., $y = 5.5$ in. in Tests 8a and 8b, respectively. The procedure for data reduction is the same as for the cantilever beam.

Chapter 4

RESULTS AND DISCUSSION

4.1 Cantilever Beam

4.1.1 Research Tests

Table 4.1 summarizes the experimental findings of Chapter 3 for the second through the fourth modes of the cantilever beam. These are the resonance frequencies, structural damping coefficients, and mode shapes which were used to further an understanding of the experimental random response data and also in the computation of the square of the theoretical frequency response modulus (eq. 2.50) between beam accelerations and the simulation force.

The experimentally determined mode shapes are shown in Fig. 3.6, page 47, to be identical with the displacement shapes given by the Bernoulli-Euler beam theory, even with two shakers and two accelerometers attached; therefore, the theoretical values were used in the above-mentioned computations. However, since the addition of shakers to the clean beam has a significant effect on the resonance frequencies and structural damping, it is necessary to use the experimentally obtained values of Table 4.1 to gain insight into discrepancies between the complex excitation response and the simulated response.

Table 4.1 Resonance Frequencies, Damping, and Mode Shapes of Cantilever Beam Used in Analysis of Random Vibration Data.

Mode Number r	Experimental Resonance Frequency f_r, Hz		Experimental Structural Damping Coefficient η_r		Theoretical Mode Shape Constants	
	2 Shakers Attached	1 Shaker Attached	2 Shakers Attached	1 Shaker Attached	a_r	$\beta_r L$
2	906	928	.00572	.00345	1.018	4.694
3	2362	2540	.04630	.03210	0.999	7.855
4	5188	5174	.05580	.03000	1.000	10.996

Mode Shape: $Y_r = \cosh \beta_r x - \cos \beta_r x - a_r(\sinh \beta_r x - \sin \beta_r x)$

$L = 10$ inches

4.1.2 Comparison of Simulated Response with That Induced by the Complex Excitation Environment

Since each experimental random pressure, force, and acceleration time history was essentially self-stationary in the tests conducted, it is assumed that each record was obtained from an ergodic (and therefore stationary) random process. Therefore, temporal averages over short time intervals of a single record may replace ensemble averages. In addition, each beam input force and output acceleration record was essentially Gaussian (see Figures A3.1b and A3.1c, pages 128 and 129). This, of course, verifies the assumptions of linearity in response for the beam undergoing small deflections, since it is known that the response of a linear system subjected to a stationary, ergodic, or Gaussian input is stationary, ergodic, or Gaussian, respectively. Because of the reasons given in Section 2.5, simulation of strongly ergodic, Gaussian, structural response processes requires only that the spectral densities and cross-spectral densities of all simulated motions match those obtained under service excitation.

Comparisons of the spectral and cross-spectral densities of beam tip and mid-length accelerations, A_1 and A_2, during complex excitation tests with the same quantities obtained during the simulation tests are presented in Figures 4.1 and 4.2. The complex excitation environment of the beam, as given by Figures 4.3 and 4.4, was provided by two mechanical shakers, while one mechanical shaker,

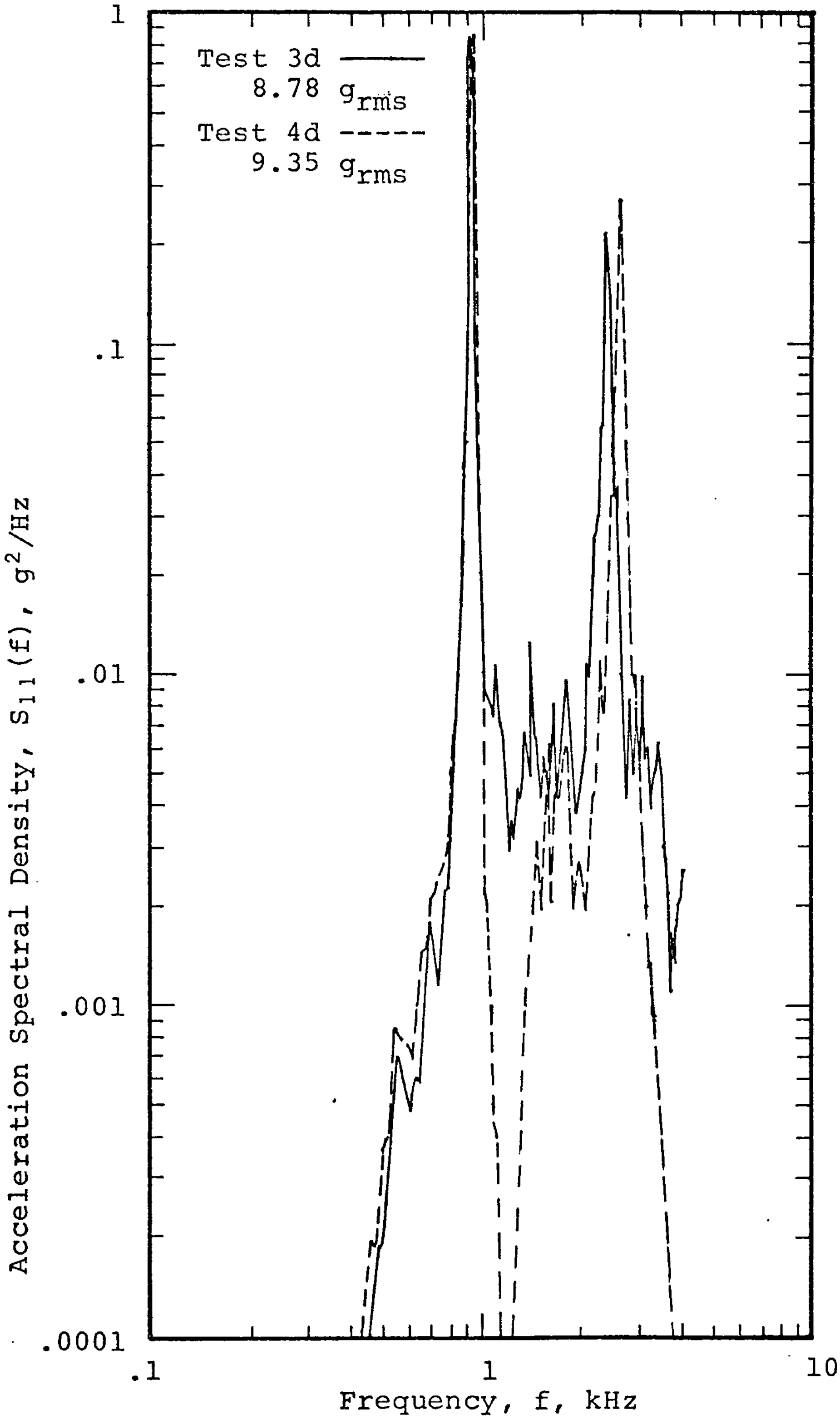

(a) Acceleration Spectral Density for Tip Accelerometer A_1

Fig. 4.1 Comparison of Complex Excitation Test 3d and Simulation Test 4d for Cantilever Beam

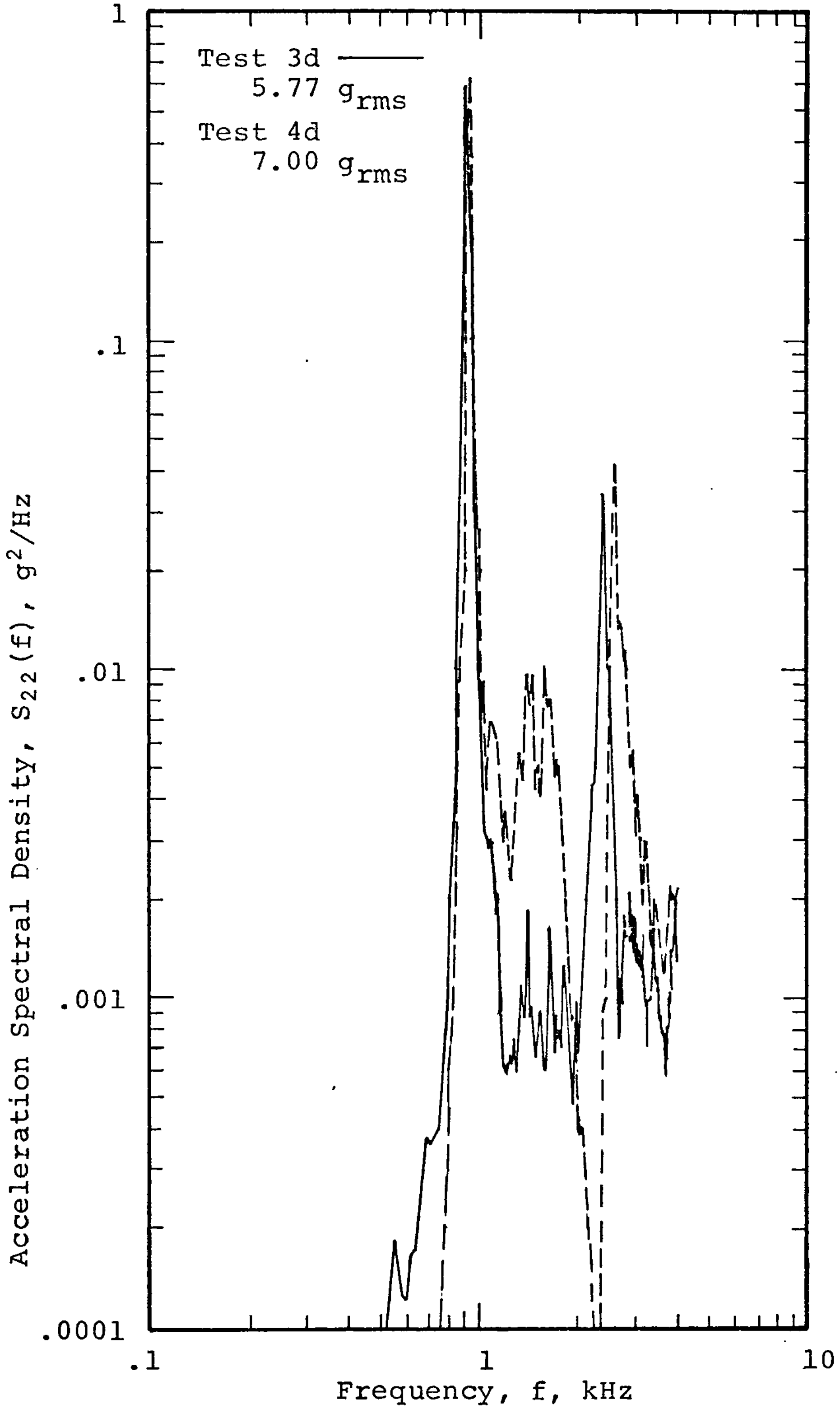

(b) Acceleration Spectral Density for Mid-length Accelerometer A_2

Fig. 4.1 (Continued)

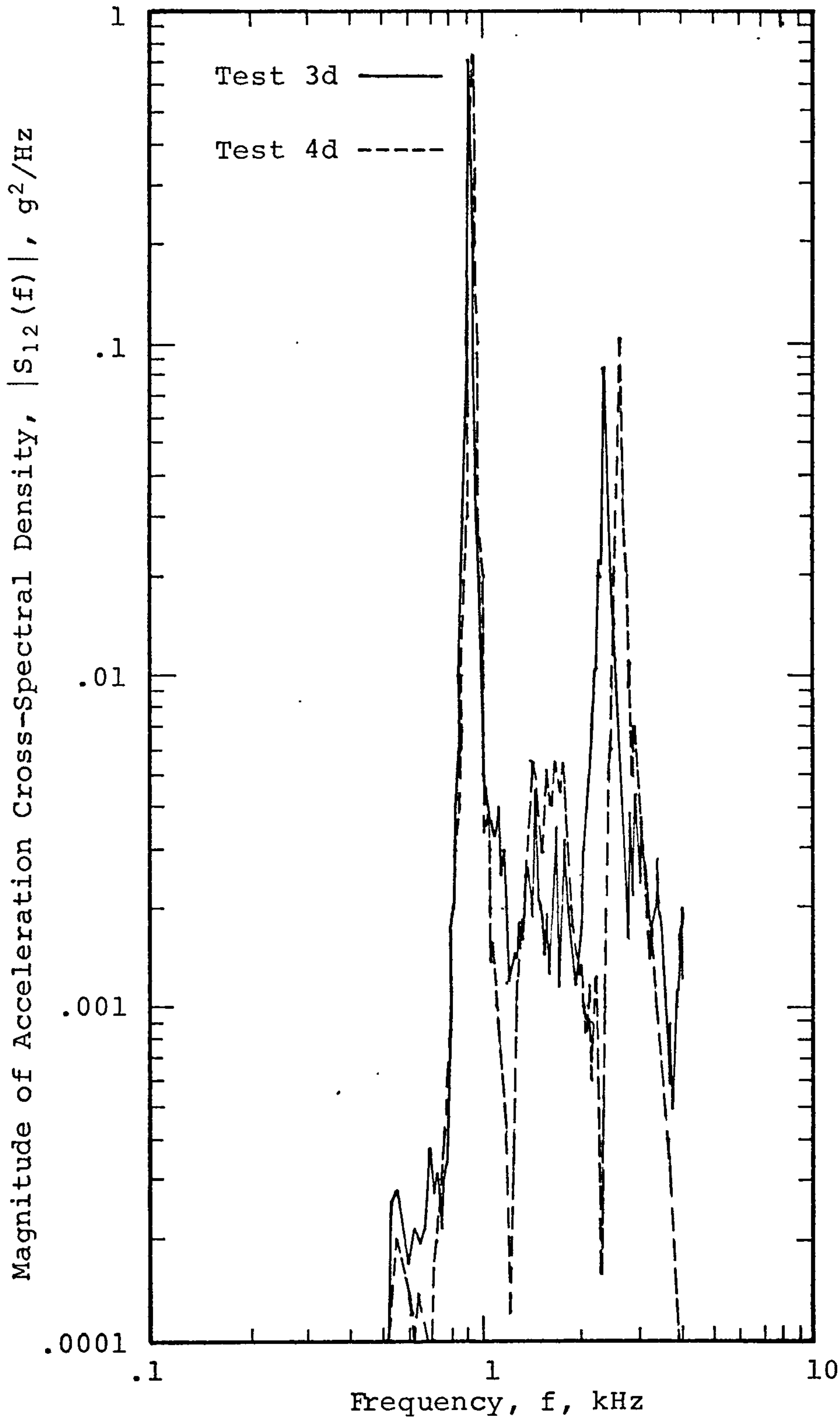

(c) Acceleration Cross-Spectral Density Magnitude for Accelerometers A_1 and A_2

Fig. 4.1 (Continued)

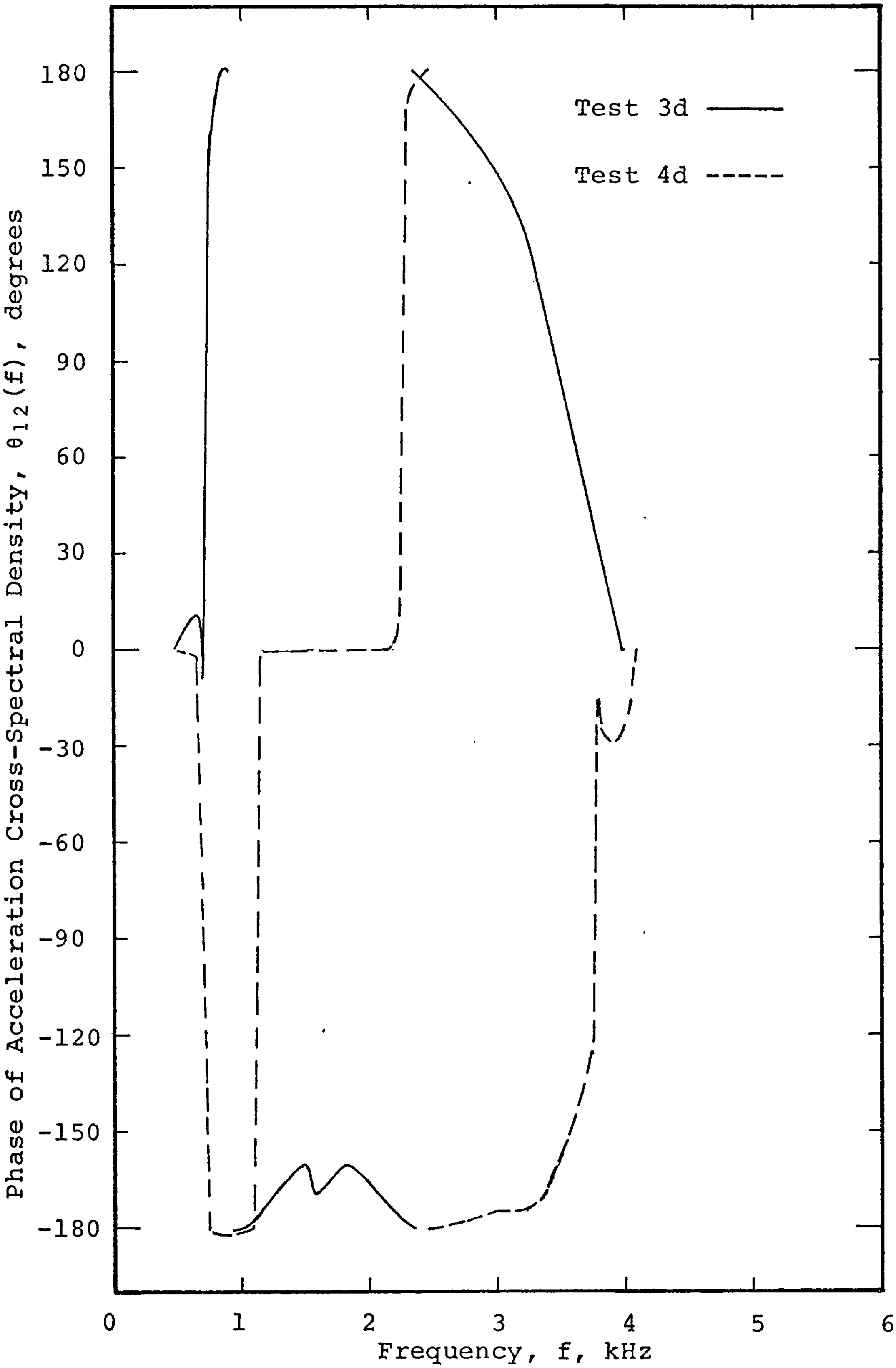

(d) Acceleration Cross-Spectral Density Phase for Accelerometers A_1 and A_2

Fig. 4.1 (Continued)

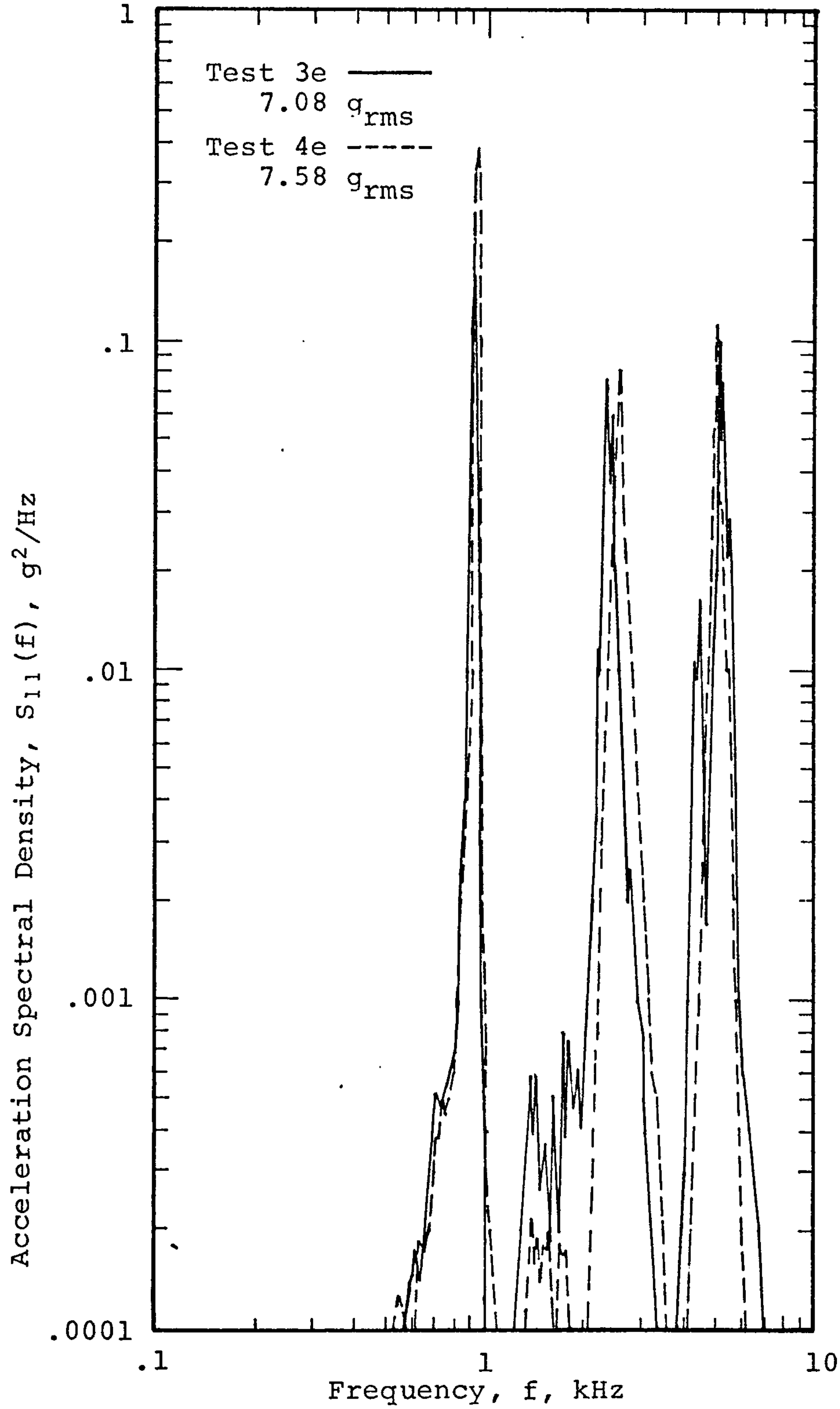

(a) Acceleration Spectral Density for Tip Accelerometer A_1

Fig. 4.2 Comparison of Complex Excitation Test 3e and Simulation Test 4e for Cantilever Beam

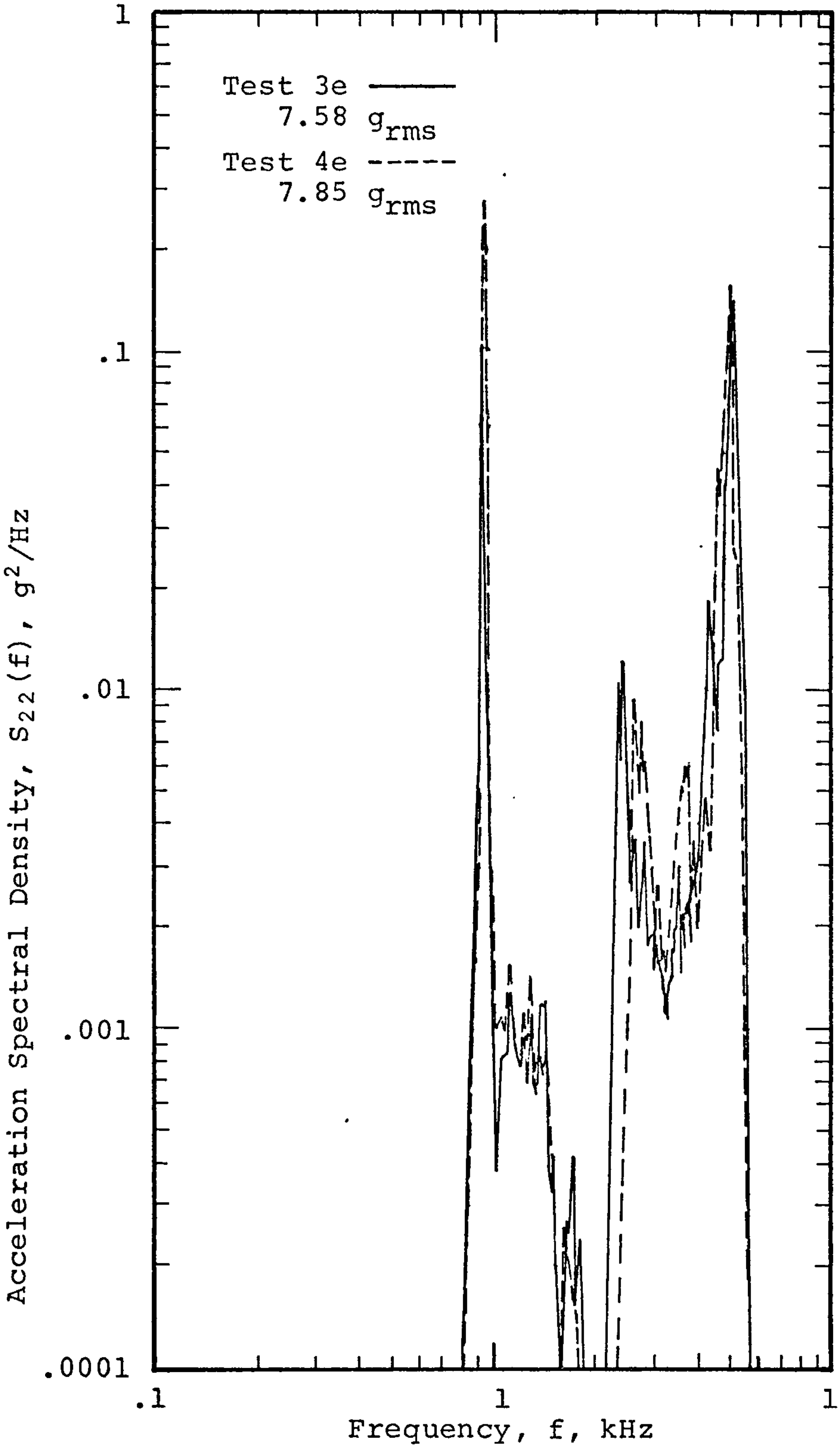

(b) Acceleration Spectral Density for Mid-length Accelerometer A_2

Fig. 4.2 (Continued)

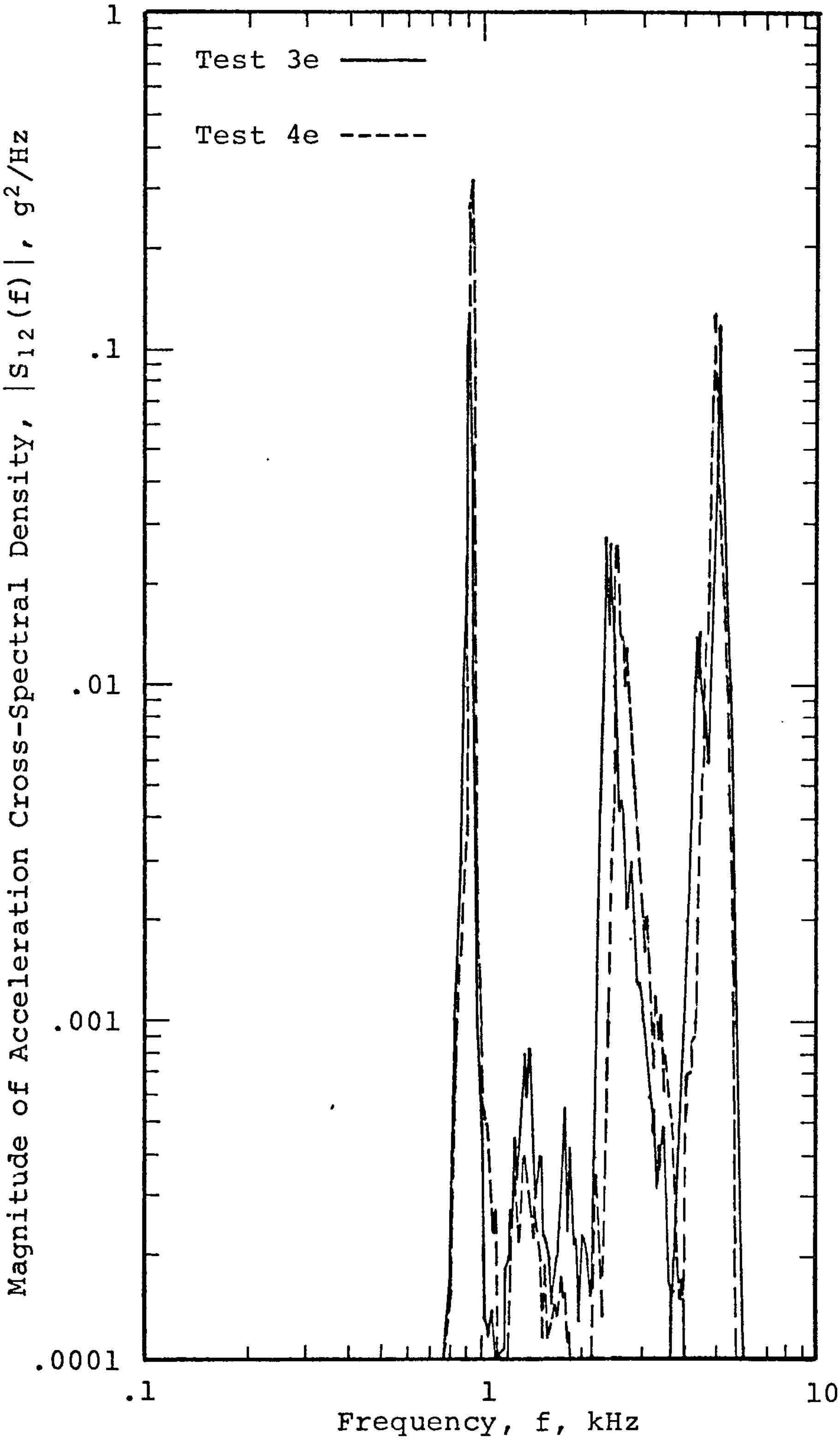

(c) Acceleration Cross-Spectral Density Magnitude for Accelerometers A_1 and A_2

Fig. 4.2 (Continued)

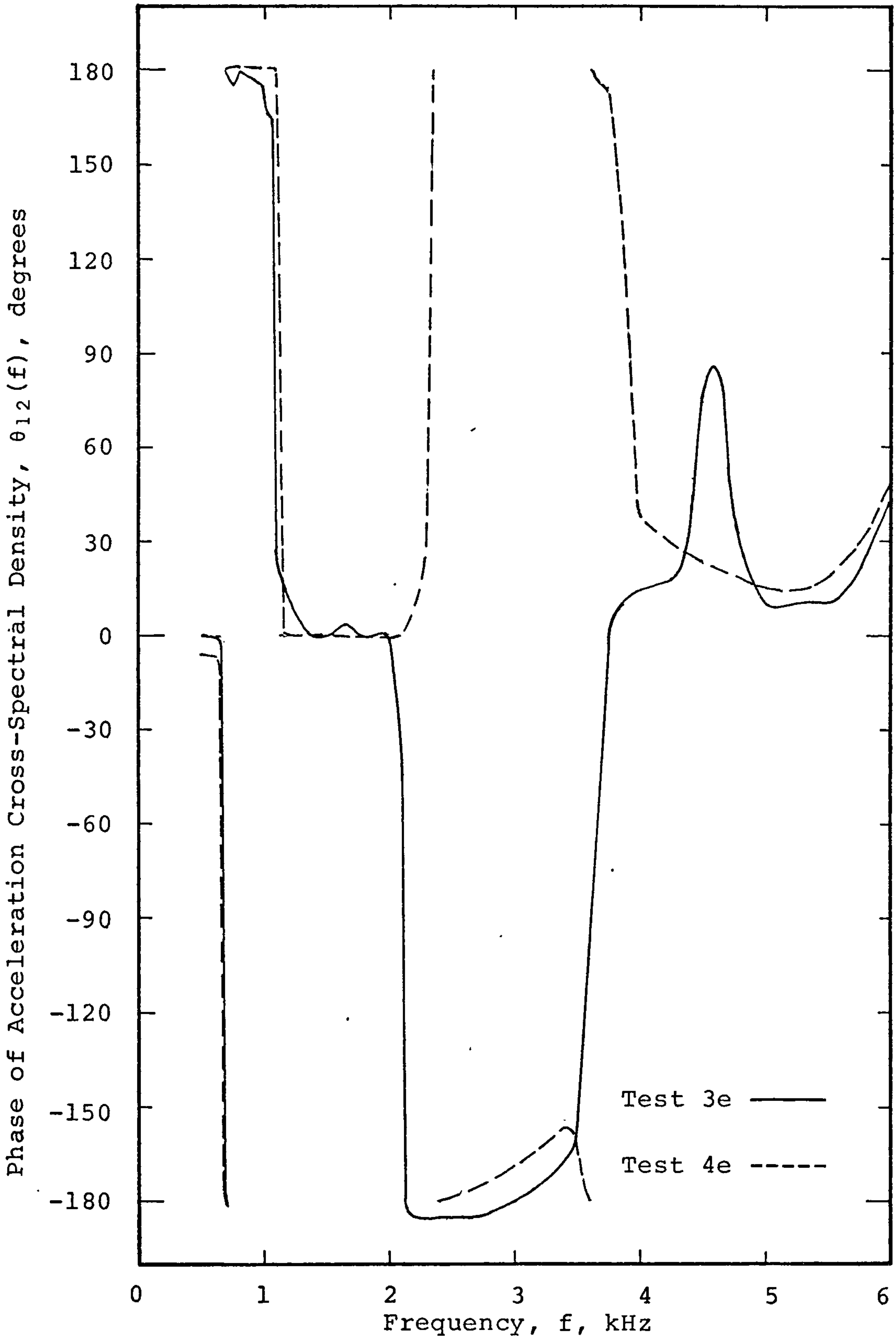

(d) Acceleration Cross-Spectral Density Phase for Accelerometers A_1 and A_2

Fig. 4.2 (Continued)

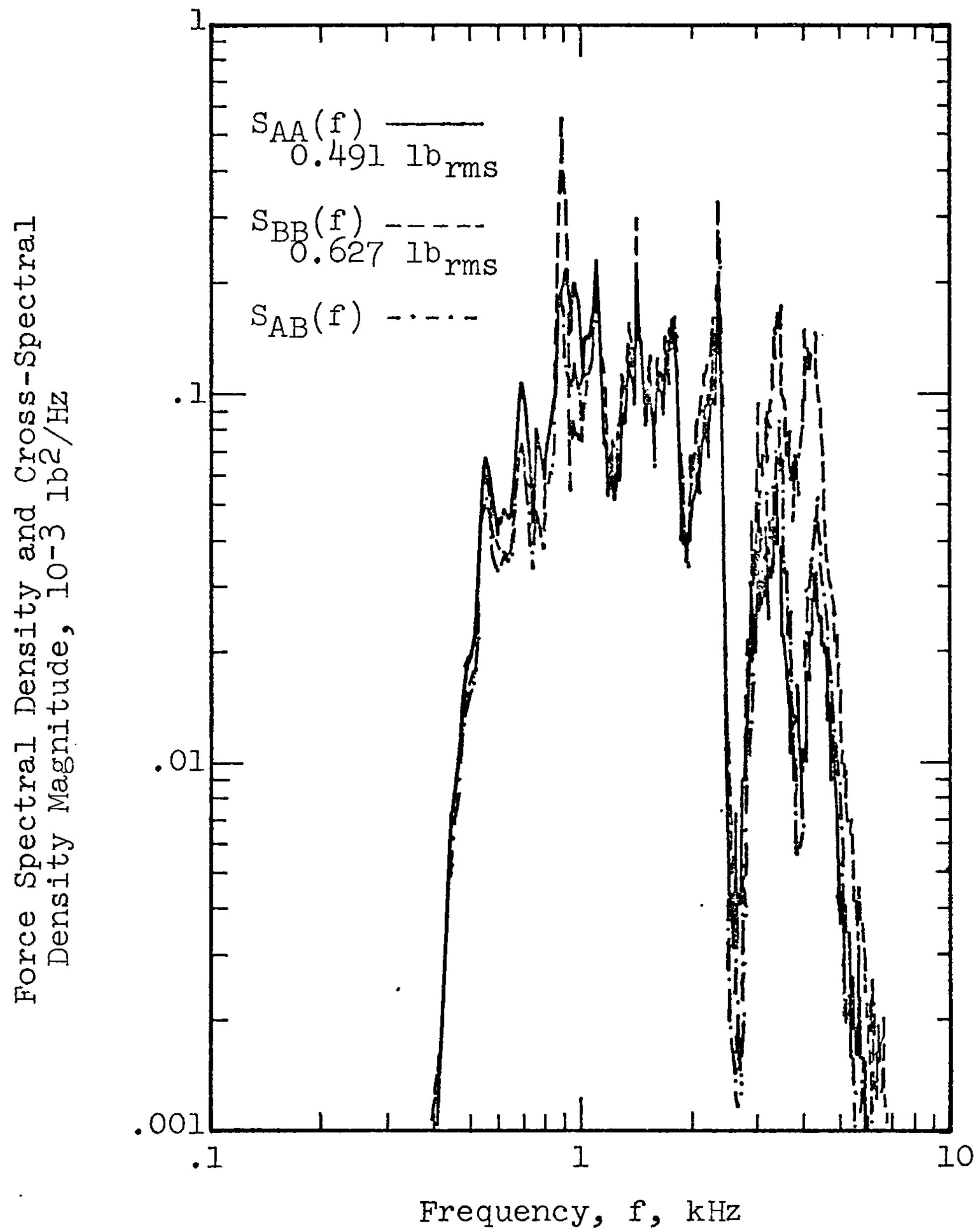

(a) Force Spectral Density and Cross-Spectral Density Magnitude

Fig. 4.3 Complex Excitation Environment of Test 3d.

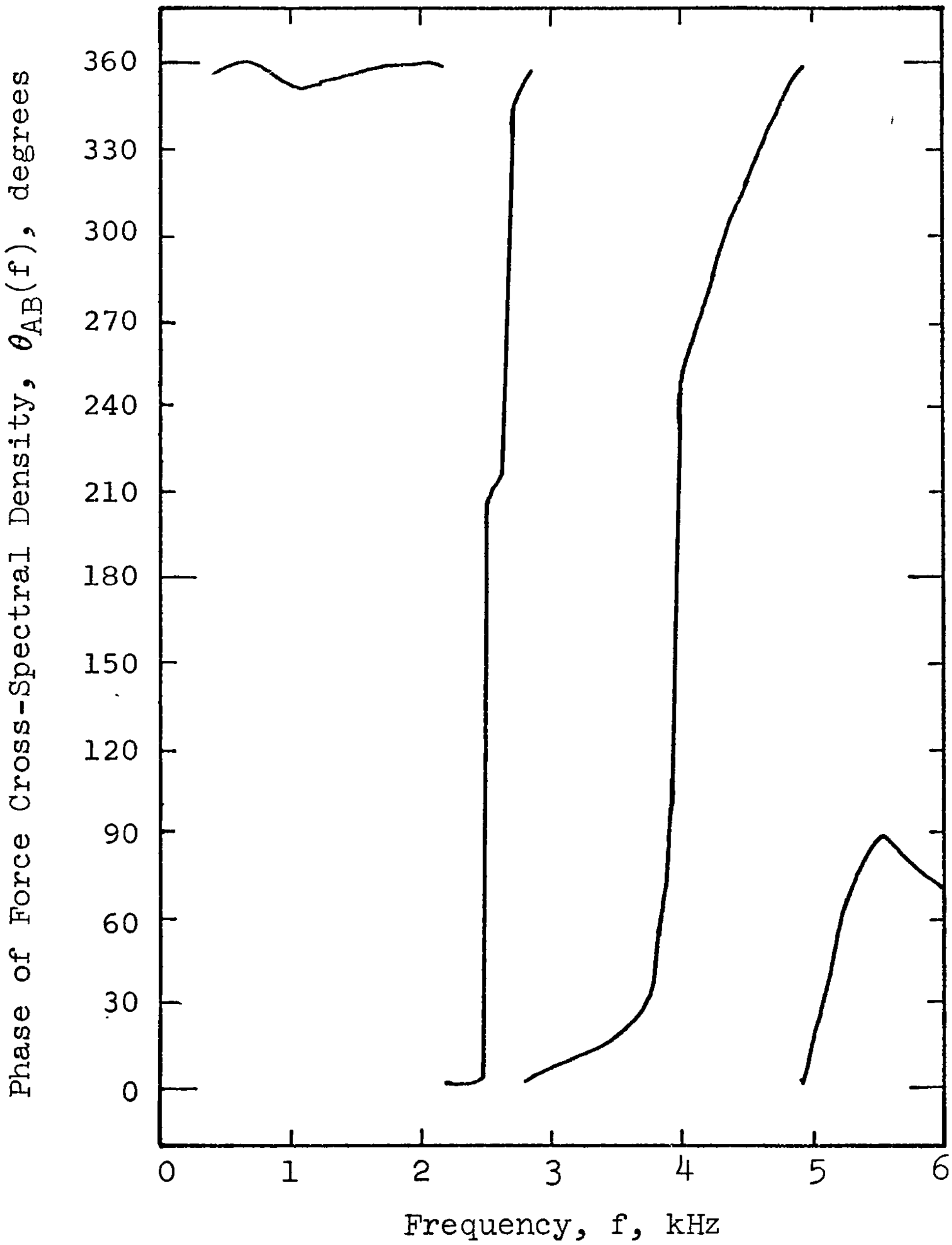

(b) Force Cross-Spectral Density Phase

Fig. 4.3 (Continued)

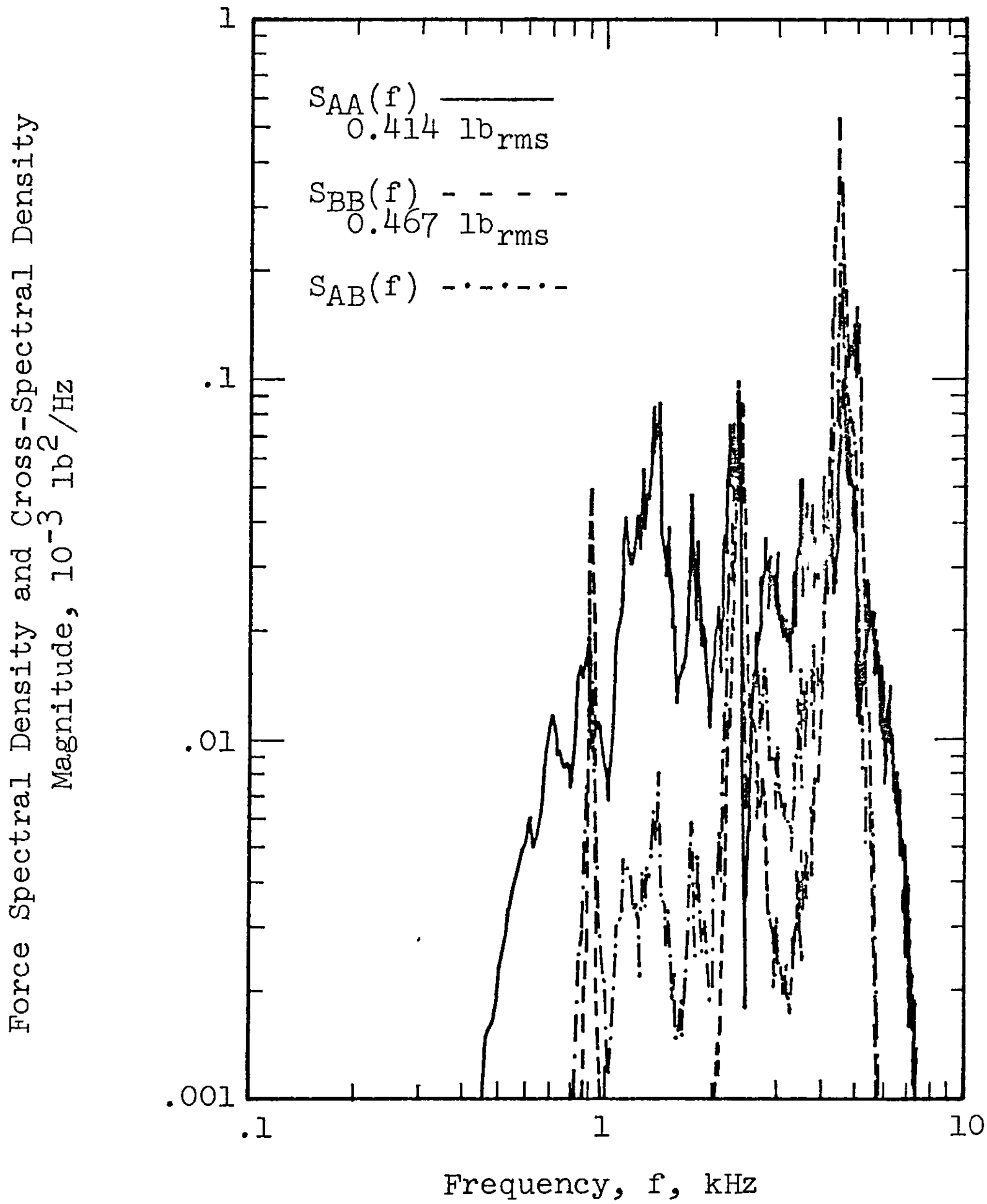

(a) Force Spectral Density and Cross-Spectral Density Magnitude

Fig. 4.4 Complex Excitation Environment of Test 3e.

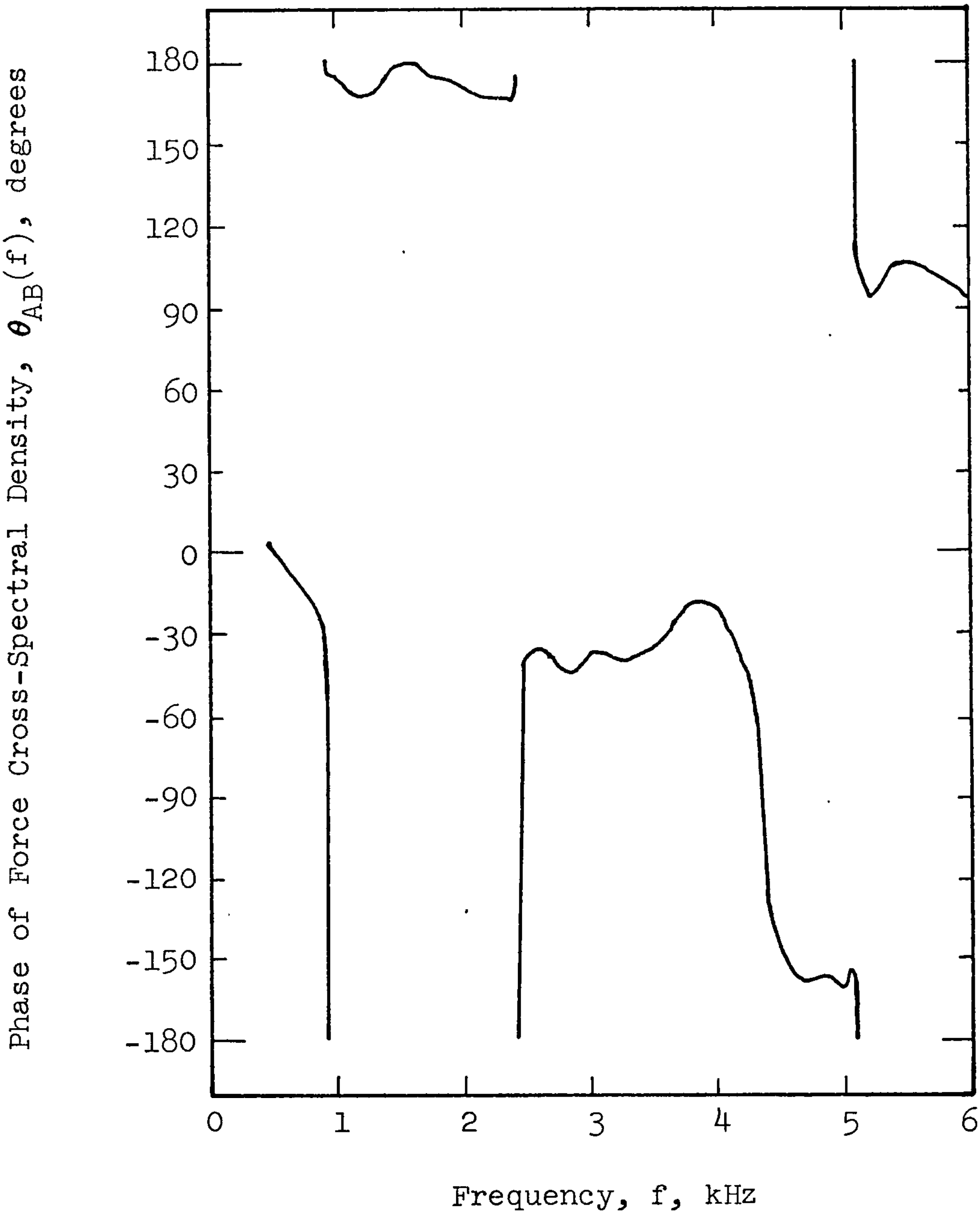

(b) Force Cross-Spectral Density Phase

Fig. 4.4 (Continued)

possessing the appropriately shaped input force spectrum as shown in Figure 4.5, provided the simulation excitation.

In Figure 4.1, pages 72 through 75, simulation was attempted for the second and third beam resonances. As is seen, the 900 Hz resonance peak value, bandwidth , and phase angle are simulated exactly, with the simulation frequency shifted slightly upward, as expected from the data of Table 4.1, page 70. For the third beam resonance at approximately 2500 Hz, the peak value, resonance bandwidth, and phase angle are simulated reasonably well; however, the resonance frequency has been shifted upward considerably, again as expected. This undesirably large frequency shift is by far the most predominant change in beam dynamics caused by detaching one of the two complex excitation test shakers from the beam.

In Figure 4.2, pages 77 through 79, Test 4e was an attempt to simulate the second, third, and fourth resonance responses of Test 3e. As is seen, the 900-Hz resonance width and phase angle were simulated exceptionally well; however, the peak value is somewhat high and the expected slight frequency shift is again noted. For the 2500-Hz resonance, the peak value and resonance width are simulated exceptionally well, while the phase angle simulation is within reason. The undesirable shift in resonance frequency is again noted. For the fourth beam resonance at approximately 5000 Hz, the resonance bandwidth, peak value, and phase angle are simulated exceptionally well; however, in

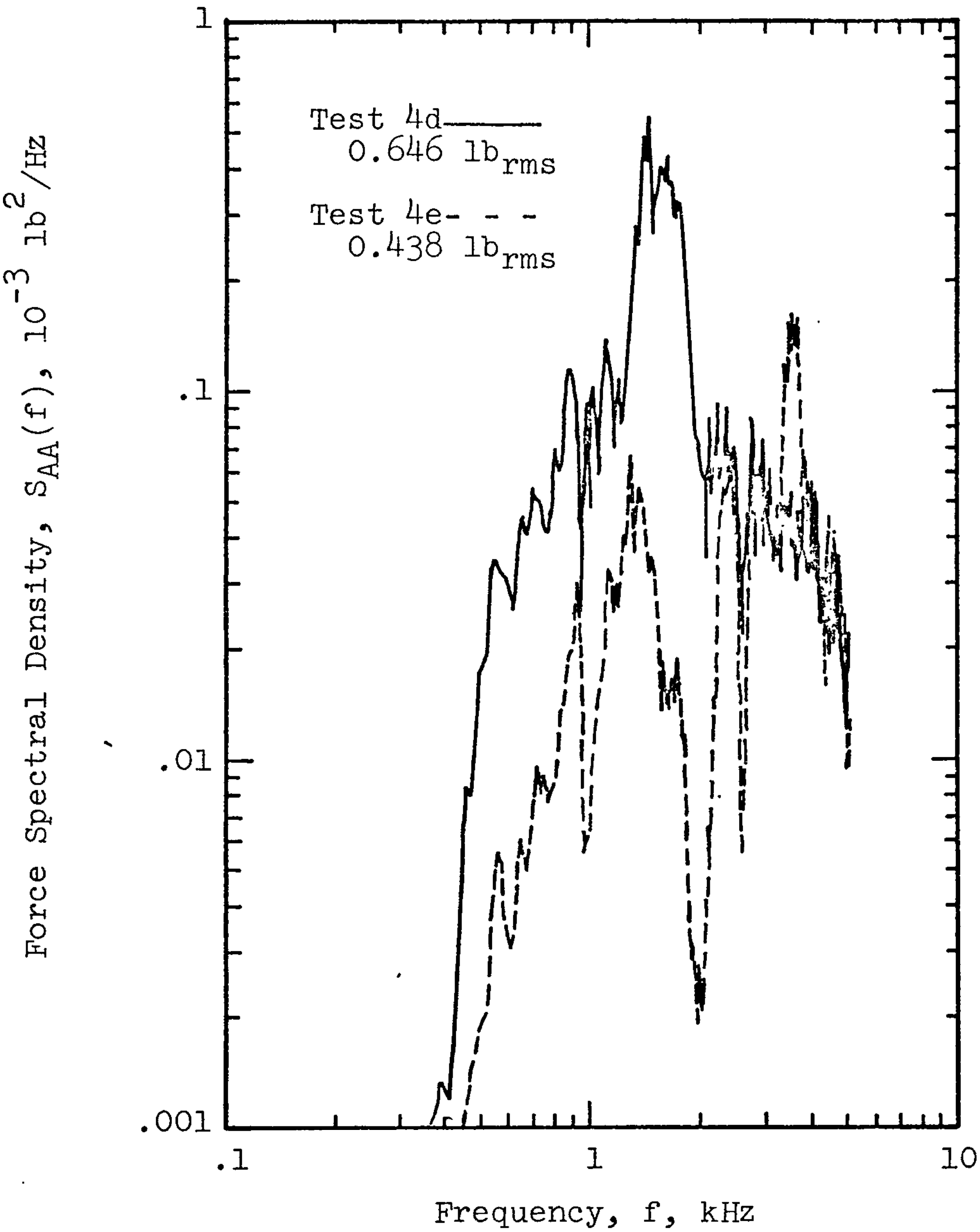

Fig. 4.5 Simulation Force Spectral Density of Tests 4d and 4e.

addition to the expected slight lowering of frequency when the F_B shaker was detached from the beam for the simulation test, it was impossible, using the large bandwidth, spectrum shaping filters, to simulate the undesirable response peak or the radical change in phase angle of Test 3e at approximately 4500 Hz without jeopardizing the simulation of beam fourth mode response. Using Table 3.1, page 40, it is seen that this undesirable effect is caused by beam/shaker-support-structure interaction, since the support structure undergoes significant response in this frequency range with both shakers attached. The large force input to the structure in the 4000-5000 Hz range can be seen in the force data of Tests 3d and 3e, Figures 4.3 and 4.4, pages 80 through 83, respectively.

We have thus far discussed the experimental attempts at reproducing the acceleration spectral and cross-spectral densities exactly in the regions near resonance for lightly damped systems. It is obvious that the attachment of the shakers to the clean beam has had an effect on the dynamics of the beam, so that it was impossible to obtain anything other than an approximate simulation in the frequency regions near a resonance; however, it is seen that adequate simulation of response in the near-resonance regions at one beam location ensures the same degree of simulation at any other beam location and between any pair of locations.

For the regions in between resonances, Test 4e provided exceptional simulation of the respective $S_{11}(f)$,

$S_{22}(f)$, and $S_{12}(f)$ quantities of Test 3e, while Test 4d provided adequate simulation for Test 3d; however, as is seen from Figures 4.1d and 4.2d, pages 75 and 79, the phase angles were not always simulated as well as would be desired, particularly in the frequency regions approaching, from both sides, the third resonance in the 2500 Hz range. There is no reason to expect, as was shown in Section 2.5, that simulation of the response spectral density in the between-resonance regions at one location on the structure insures simulation at every other location.

4.1.3 Comparison of Computed and Measured Frequency Response Functions

The simulation force spectral densities, $S_{AA}(f)$, for Tests 4d and 4e are shown in Figure 4.5, page 85. Using these values in eq. (2.67) with the values of simulated acceleration spectral density, $S_{11}(f)$ and $S_{22}(f)$ of Figures 4.1 and 4.2, pages 72 through 79, it is possible to calculate the experimental squared modulus of the frequency response functions, $H_{1A}(if)^2$ and $H_{2A}(if)^2$, for the beam. These values are compared in Figures 4.6 and 4.7 with the functions obtained using eq. (2.51) and the research test data of resonance frequencies, damping factors, and mode shapes from Table 4.1, page 70. In addition, data from two other simulation tests, Test 4a and 4b, which are discussed in Appendix 5, have been included in these figures.

It is seen that the computed values agree well with values from the random simulation test data concerning

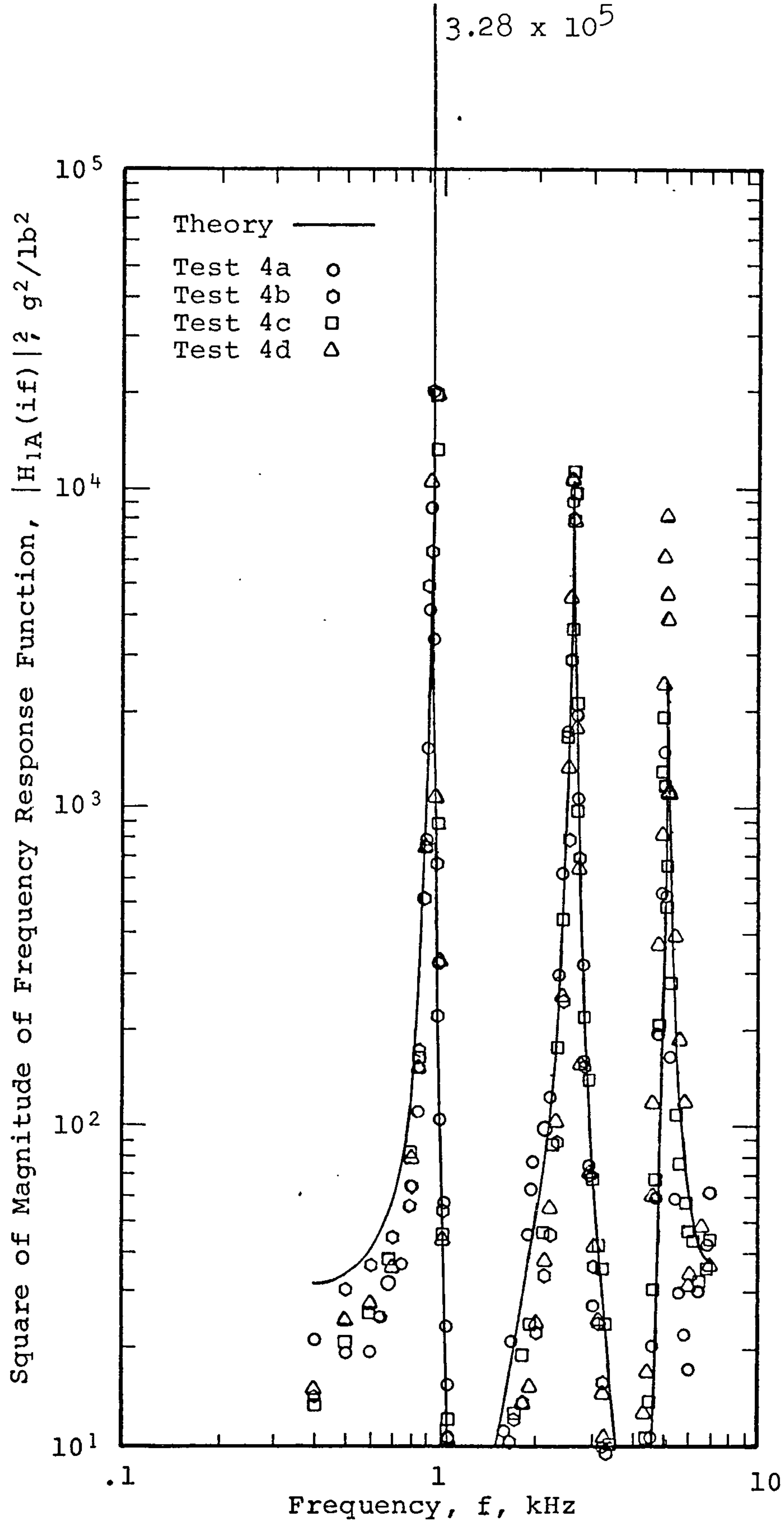

Fig. 4.6 Comparison of Square of Magnitude of Theoretical and Experimental Frequency Response Functions Between Tip Acceleration and Simulation Force on Cantilever Beam.

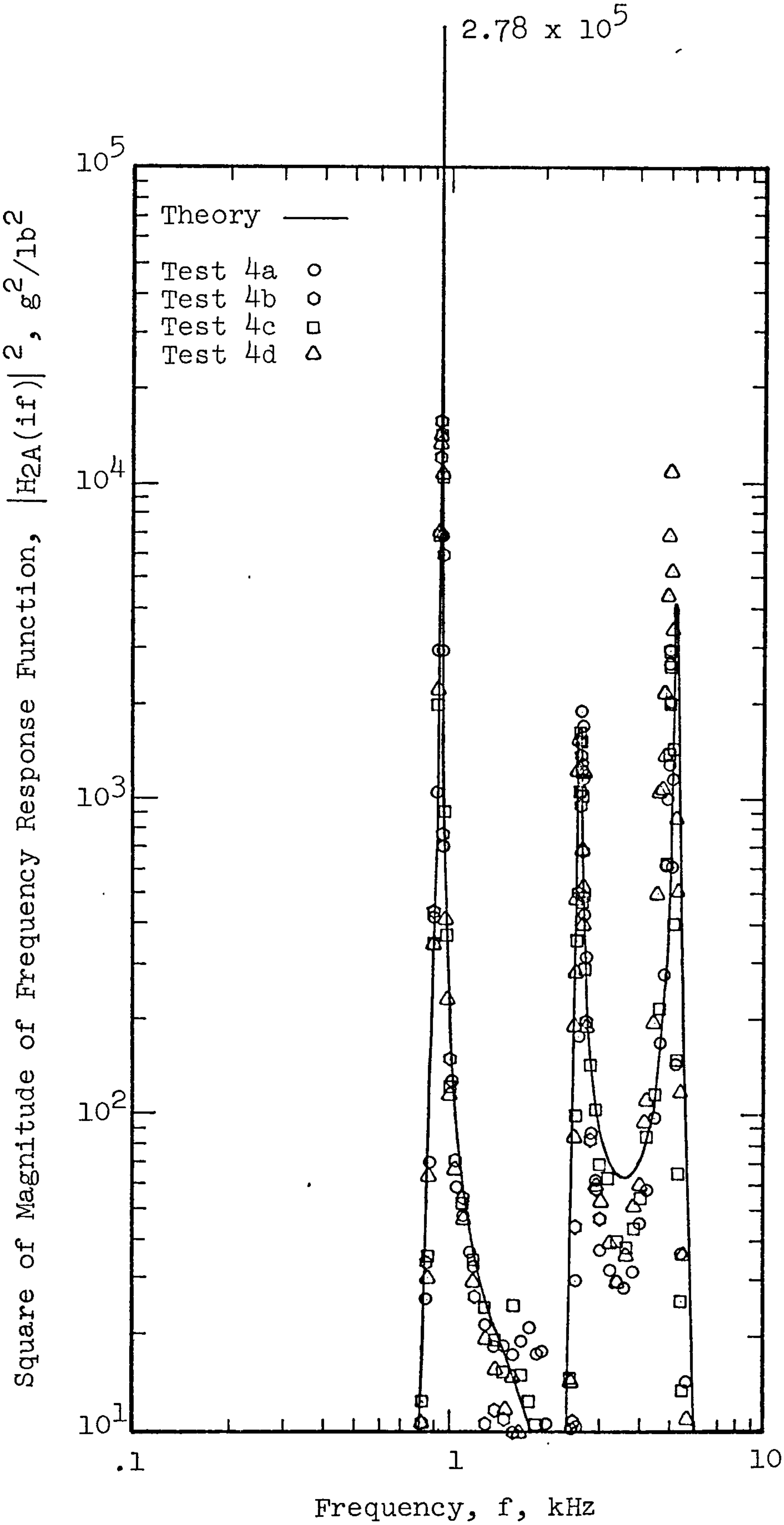

Fig. 4.7 Comparison of Square of Magnitude of Theoretical and Experimental Frequency Response Functions Between Mid-Length Acceleration and Simulation Force on Cantilever Beam.

resonance frequency and bandwidth for the second and third modes; however, although resonance 4 has excellent bandwidth simulation, the frequency obtained in the sinusoidal research tests with the shaker attached to the 1-inch support is evidently slightly high.

A comparison of peak values for the third mode at approximately 2500 Hz in Figures 4.6 and 4.7 shows excellent agreement; however, the computed peak value of this squared quantity for the 900-Hz mode is some sixteen times larger than the experimental value. This large disagreement is caused by the analyzer filter having much too wide a bandwidth for this extremely lightly-damped mode, as shown in Table 4.2; therefore, the experimental mean square level within the bandwidth divided by the filter bandwidth gave a much smaller spectral density level than actually occurred. The peak values of the experimental squared response functions compare excellently with the computed values for the fourth resonance, with one exception in which the experimental values are three times the theoretical values. The cause of this discrepancy is believed to be the beam/shaker-support interaction. In this particular case with two resonance frequencies, which both appear in the frequency response functions of Figures 4.6 and 4.7, so close together, a situation similar to the linear, two-degree-of-freedom (two mass-two spring) system may exist. If this is the case, the actual resonance of one spring-mass system (the beam) may become an antiresonance when coupled to the

Table 4.2 Comparison of Cantilever Beam Data Reduction Bandwidths with Recommended Values of [30]

Resonance Frequency f_r, Hz	Structural Damping η_r	Half-Power Point Band-width, Δf_{hp} Hz	Recommended* Bandwidth B, Hz	Data Reduction Band-width, Hz
928	.00345	3.2	.8	24
2540	.03210	81.6	20.4	24
5174	.03000	155.9	39.0	24

*$B < \Delta f_{h.p.}/4 = f_r \eta_r / 4$

other spring-mass system (the force-link/shaker/shaker-support-structure system), and be surrounded by the two resonance frequencies of the two-degree-of-freedom system.

In the regions between resonance peaks, the theory provides a good estimate of the frequency response functions, as seen from the figures.

Although the squared modulus of the frequency response functions are the only structural quantities necessary to predict the response spectral density of a structure to one discrete random input, eq. (2.67), the phase of the response functions are necessary for response cross-spectral density, eq. (2.65), and sinusoidal response predictions, eq. (2.39). It is for this reason that the experimentally determined phase angles of frequency response functions $H_{1A}(if)$ and $H_{2A}(if)$, $\phi_{1A}(f)$, and $\phi_{2A}(f)$, have been included in Figures 4.8 and 4.9, respectively. These quantities display the expected trends, i.e., the phase angles between force and acceleration are 90^o at resonance and antiresonance frequencies and either 0^o or 180^o at frequencies between resonance.

4.2 Simply-Supported Plate

4.2.1 Research Tests

Table 4.3 summarizes the experimental findings of Chapter 3 for the second through the fifth m(odd), n(odd) modes and the first and second m(even), n(odd) modes of the simply-supported plate. These are the resonance frequencies,

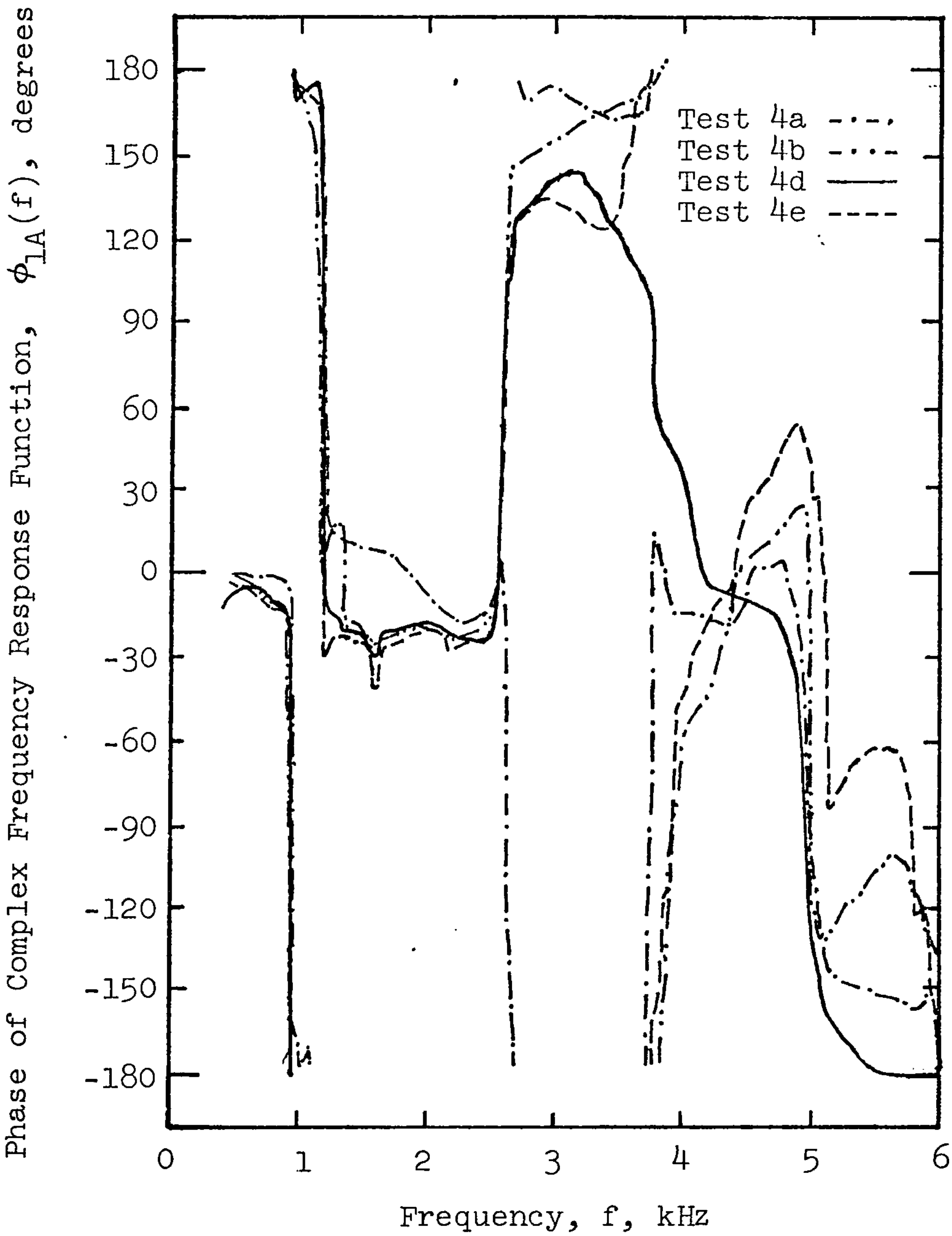

Fig. 4.8 Phase of Experimental Frequency Response Function Between Tip Acceleration and Simulation Force on Cantilever Beam.

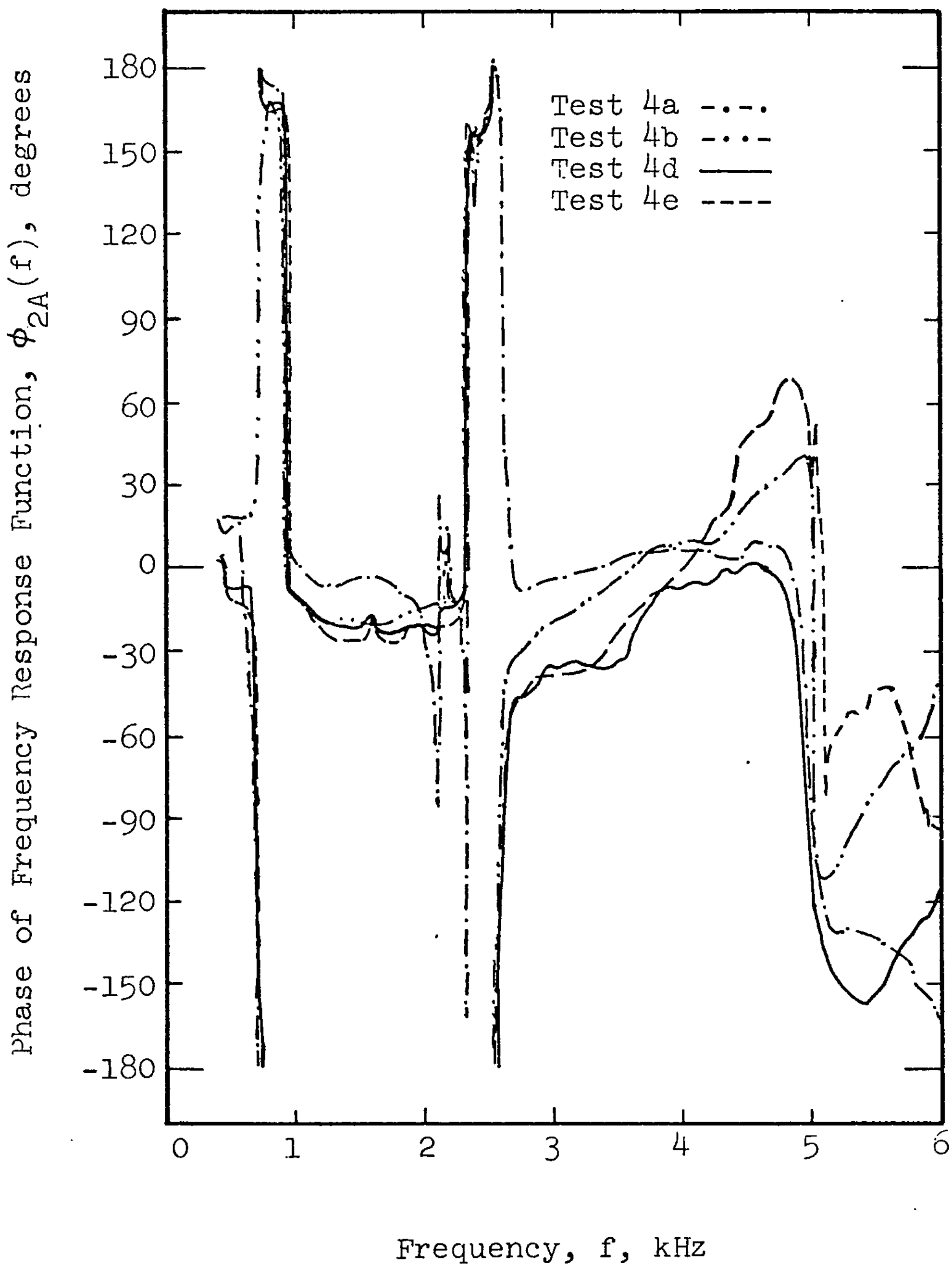

Fig. 4.9 Phase of Experimental Frequency Response Function Between Mid-Length Acceleration and Simulation Force on Cantilever Beam.

Table 4.3 Resonance Frequencies, Damping, and Mode Shapes of Simply-Supported Plate Used in Analysis of Random Vibration Data

Mode Number	Number of Half-Waves		Experimental Resonance Frequency f_r, Hz		Experimental Structural Damping Coefficient, η_r	
r	m	n	Clean Plate	One Shaker Attached	Clean Plate	One Shaker Attached
3	2	1	594	580	.00710	.01989
5	1	3	1024 982	1019 976	.00330	.00780
6	3	1	1209	1202 1130 1166	.00387	.00854
7	2	3	1402	1365		.00800*
10	3	3	1988	1956		.00742
14	1	5	2674	2638		.00750*

*Assumed value.

Mode shape: $W_r = W_{mn} = \sin \frac{m\pi x}{a} \sin \frac{n\pi y}{b}$

$a = 10$ inches, $b = 11$ inches.

structural damping factors, and mode shapes which were used in the same manner as for the beam.

The experimentally determined mode shapes are shown in Figure 3.8 to agree reasonably well with those assumed in eq. (2.23) for the simply-supported plate; therefore, the theoretical values were used in computations. The addition of a shaker to the plate tended to lower the clean plate resonance frequencies slightly and bring them closer to the theoretical values of Table 3.6, page 51; however, the plate edge-support-structure and the force-link/shaker/ shaker-support-structure interactions with the plate affected the plate dynamics in such a manner that it was possible to excite the modes 5, 6, and 14 at several frequencies near the predominant resonance frequency. The addition of the simulation shaker to the clean plate is seen to have increased the structural damping by a factor of approximately two. It was therefore deemed necessary to use the experimentally determined resonance frequencies and structural damping in order to understand any discrepancies between the complex excitation response and the simulated response.

4.2.2 Comparison of Simulated Response with That Induced by the Complex Excitation Environment

The same assumptions made in Section 4.1.2 for the random excitation and response time histories of the beam are made here for the plate.

Comparisons of the spectral and cross-spectral densities of center-plate and quarter-plate accelerations, A_1

and A_2, during Complex Excitation Test 7a with the same quantities obtained during the Simulation Test 8a are presented in Figure 4.10. The complex excitation environment of the plate was provided by acoustic noise of approximately 131 db over-all. A pressure spectral density of the noise, measured approximately two inches from the plate, is shown in Figure 4.11. One mechanical shaker, possessing the appropriately shaped input force spectrum, as shown in Figure 4.12, provided the simulation excitation.

First, consider the m(odd), n(odd) modes in Figure 4.10. An examination of the center- and quarter-plate acceleration spectral densities and cross-spectral density magnitudes and phases shows that the response in the vicinity of the mode r = 14 at approximately 2600 Hz is simulated excellently with regard to resonance frequency, bandwidth, and peak value, and reasonably for phase angle. The mode r = 10 at approximately 2000 Hz is simulated excellently also with respect to every quantity except peak values, where the simulated peaks are low by a factor of three. The mode r = 6 at 1200 Hz is simulated well with respect to every quantity except peak values, with the simulation again low by a factor of three. In addition, there is large response in this mode at 1130 and 1160 Hz. The mode r = 5 at 1020 Hz is well simulated with regard to every quantity; however, there is also undesirable response in this mode at approximately 980 Hz.

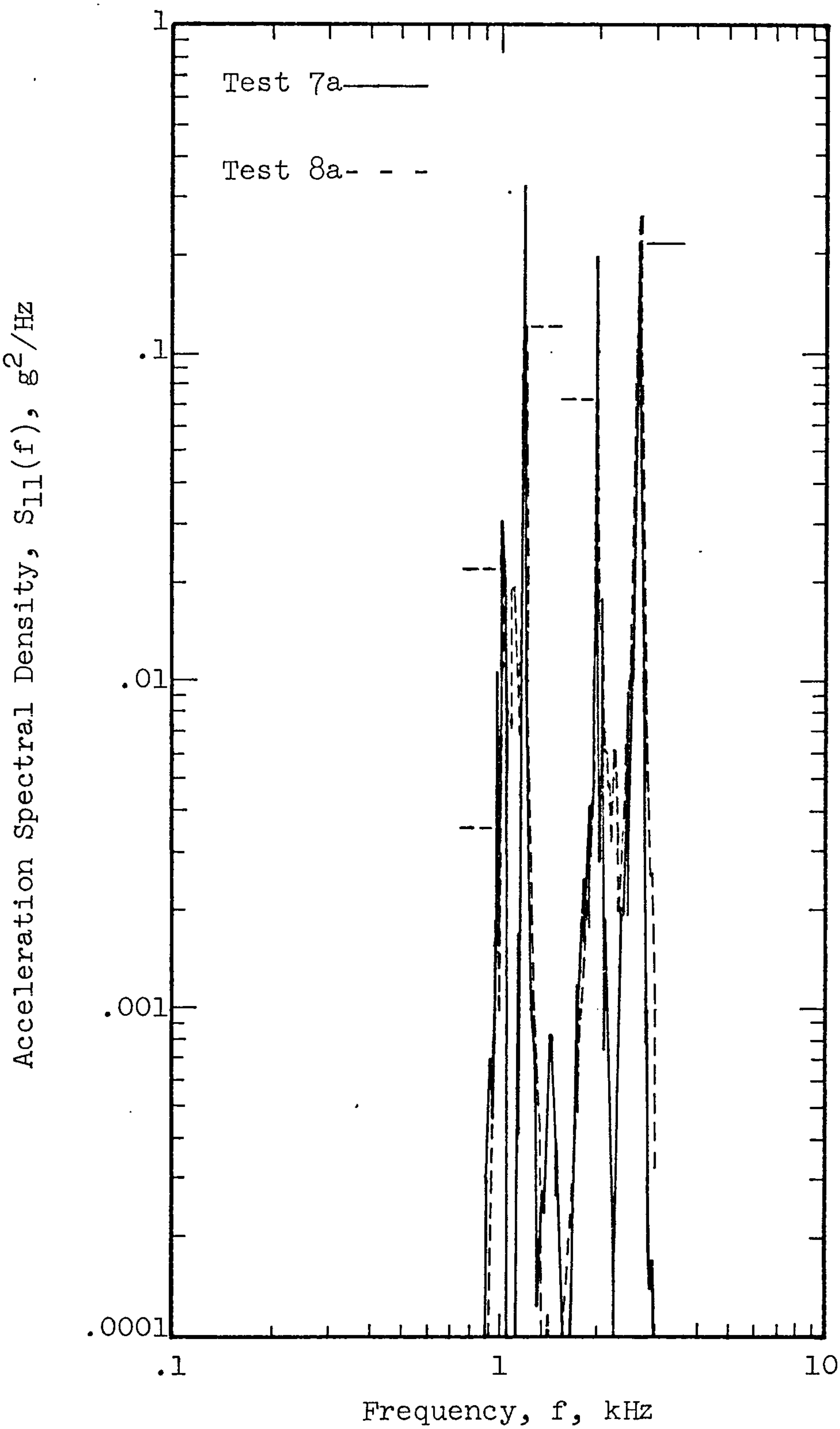

(a) Acceleration Spectral Density for Center-Plate Accelerometer A_1

Fig. 4.10 Comparison of Complex Excitation Test 7a and Simulation Test 8a for Simply-Supported Rectangular Plate.

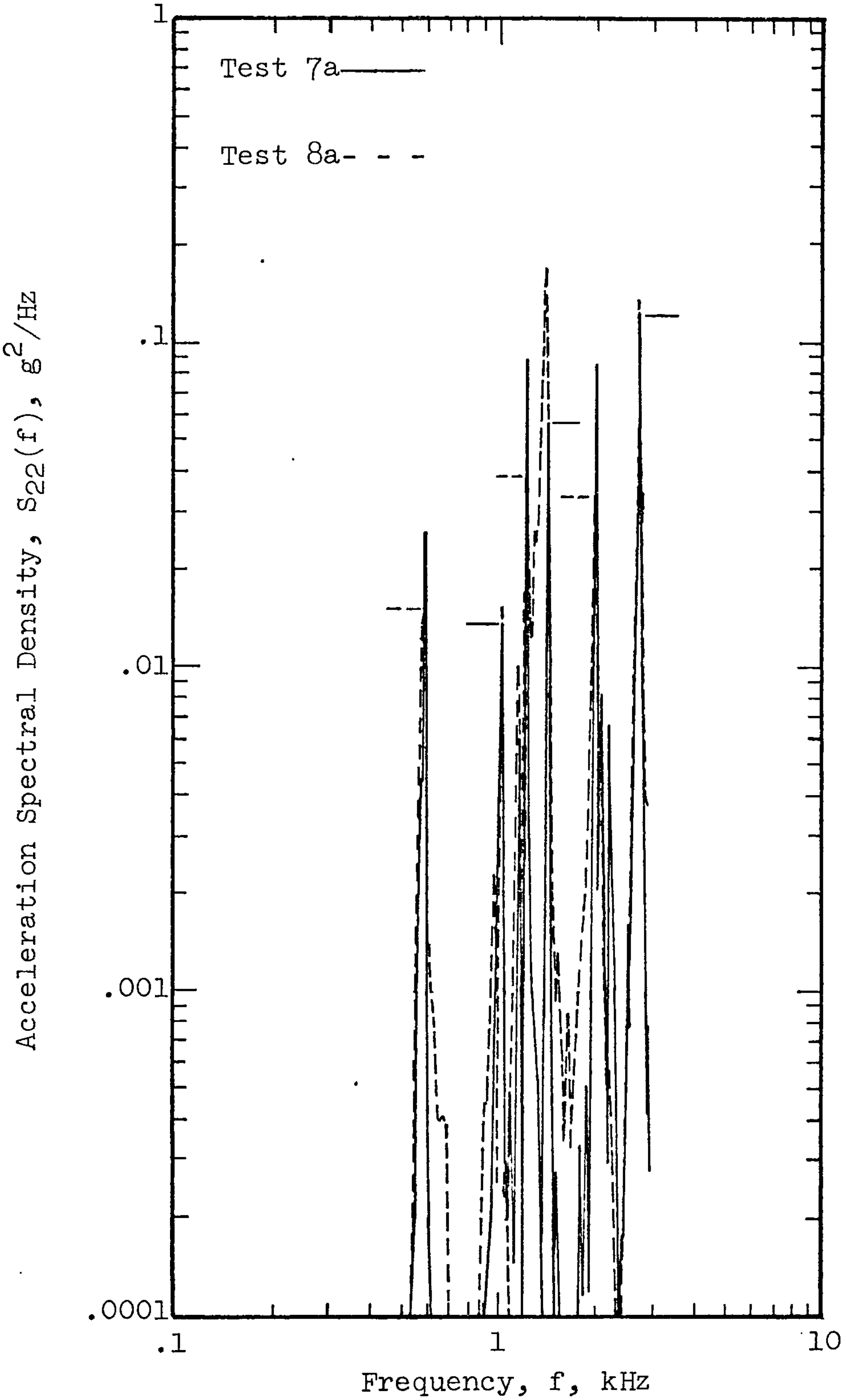

(b) Acceleration Spectral Density for Quarter-Plate Accelerometer A_2

Fig. 4.10 (Continued)

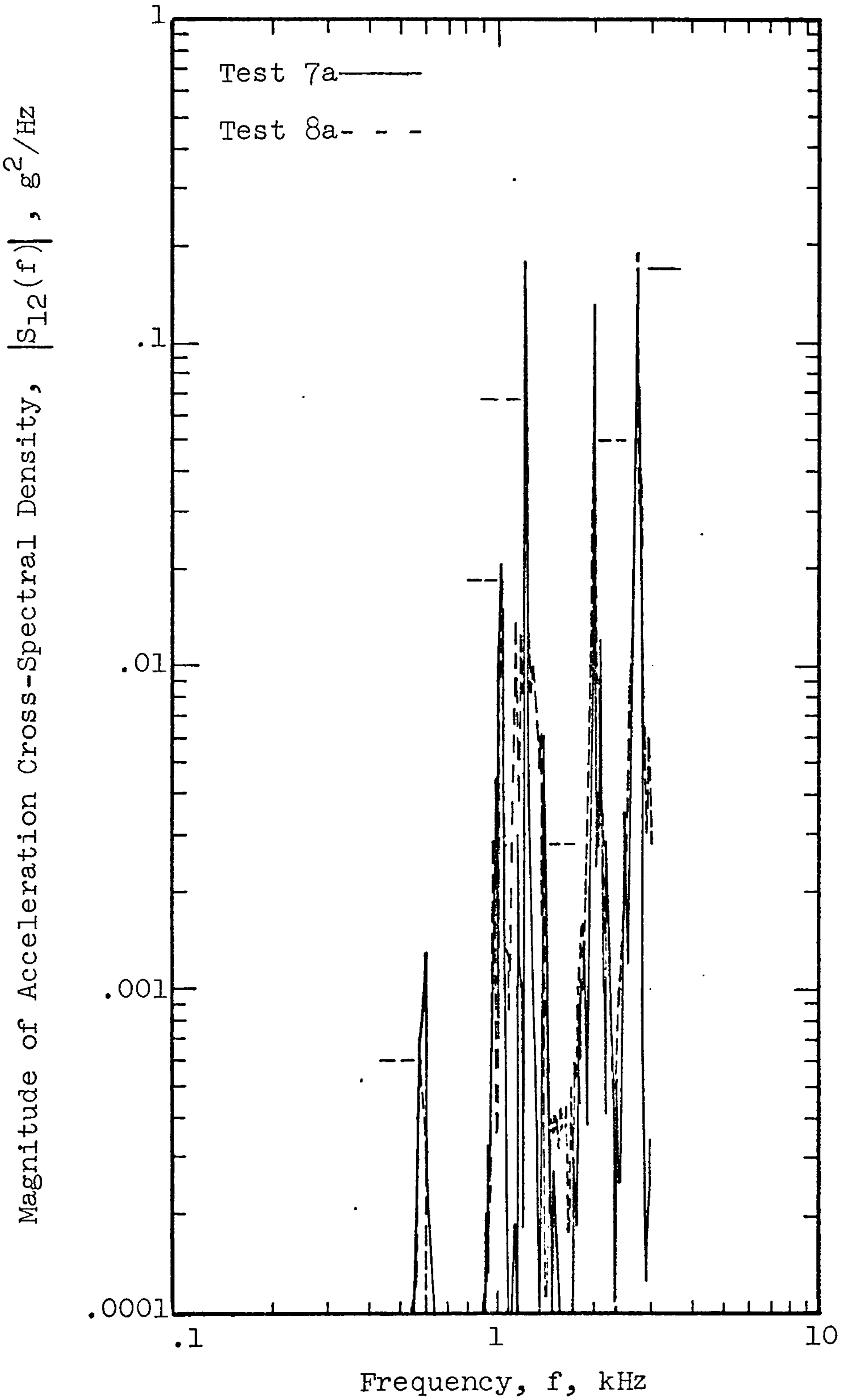

(c) Acceleration Cross-Spectral Density Magnitude for Accelerometers A_1 and A_2

Fig. 4.10 (Continued)

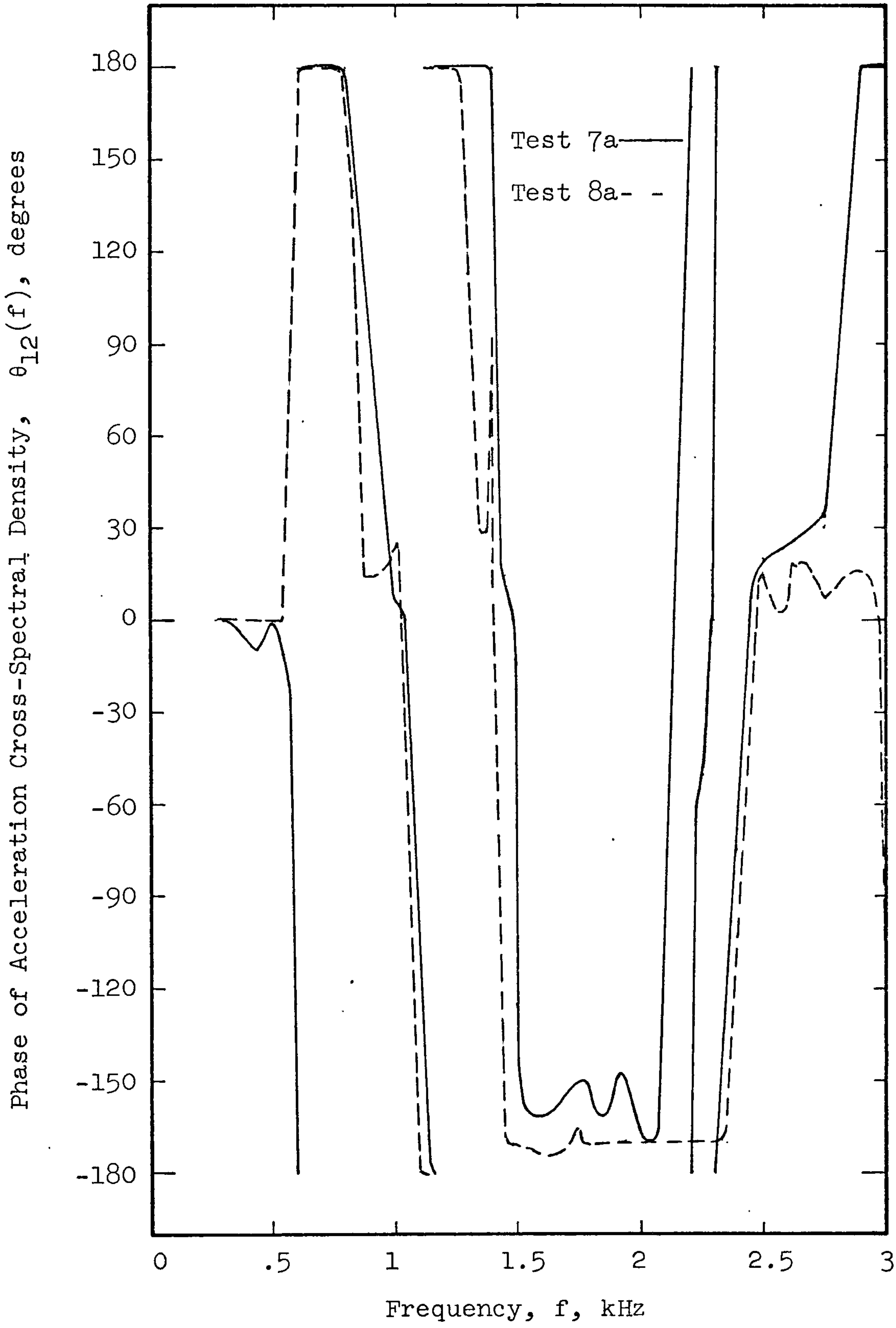

(d) Acceleration Cross-Spectral Density Phase for Accelerometers A_1 and A_2

Fig. 4.10 (Continued)

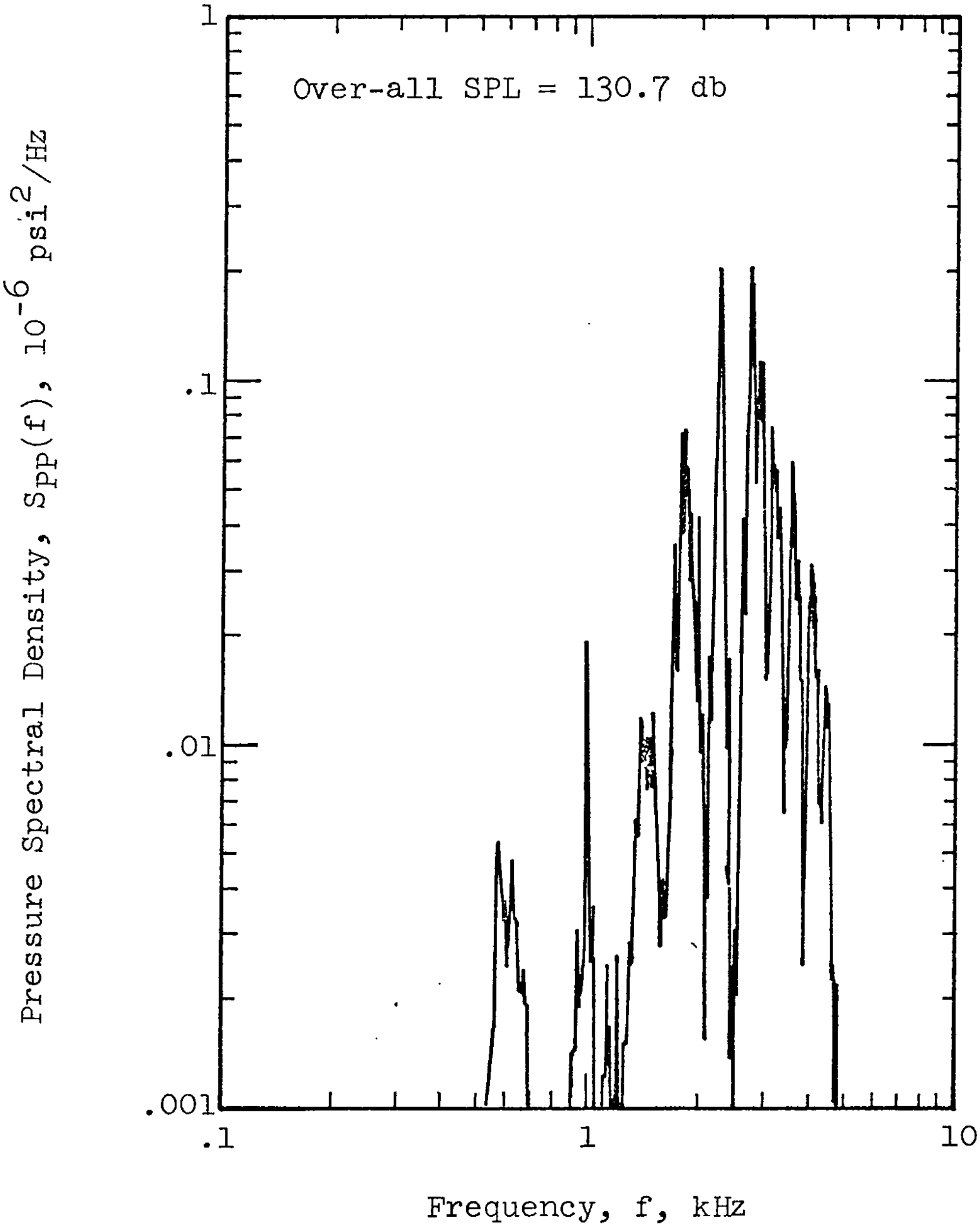

Fig. 4.11 Pressure Spectral Density for Complex Excitation Test 7a.

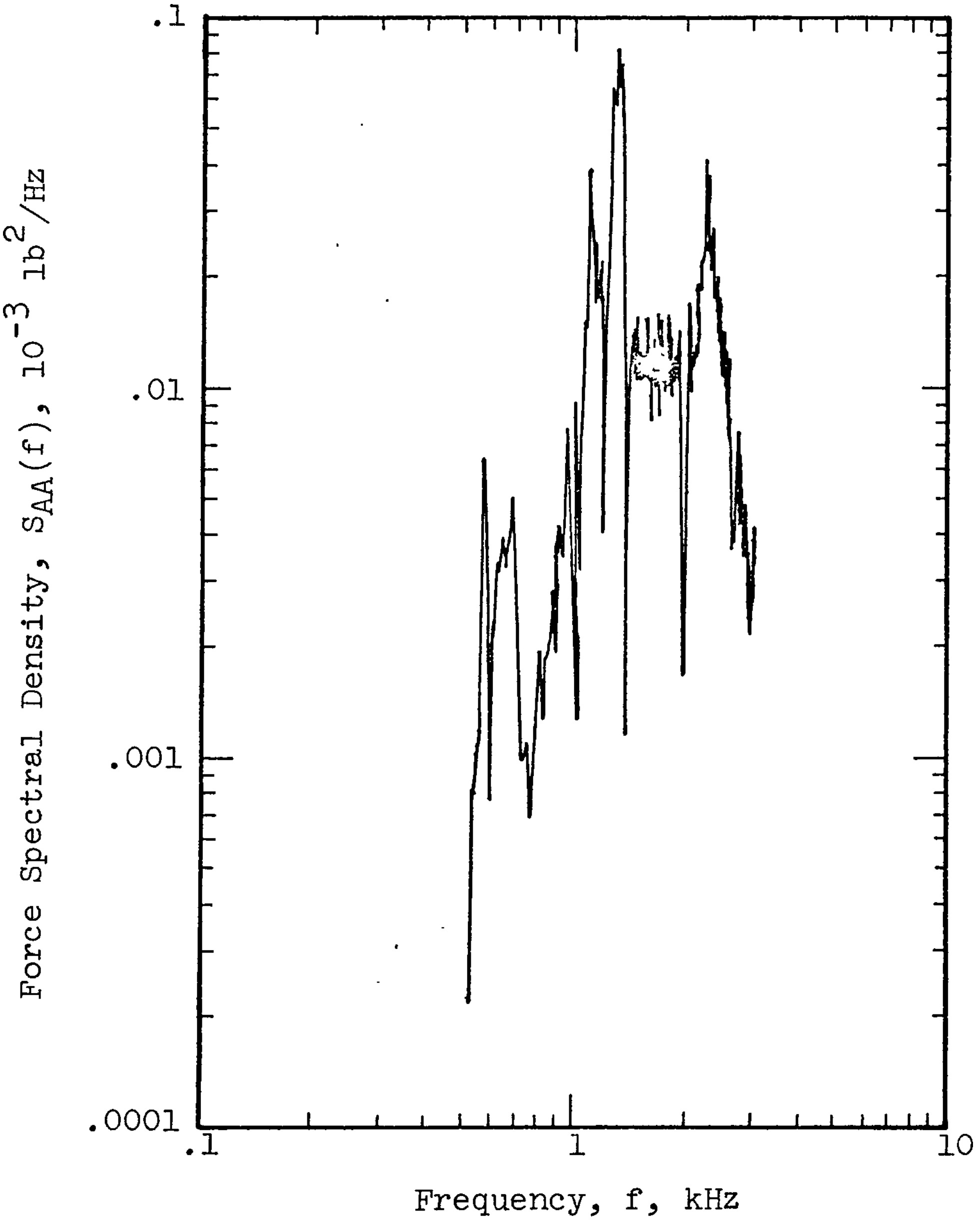

Fig. 4.12 Force Spectral Density for Simulation Test 8a.

Next, considering the m(even), n(odd) modes which do not appear at the center-plate A_1 location, it is seen that the mode r = 3 at approximately 580 Hz is simulated well with respect to phase angle and resonance bandwidth; however, the simulation peak value is low by approximately two, and the simulation resonance frequency is shifted to a slightly lower value, as expected from Table 4.3, page 95. For the mode r = 7 at approximately 1400 Hz, the phase angle is simulated at, but not in the near vicinity of, resonance ; and the frequency has lowered slightly as expected, the simulated resonance bandwidth is much too wide, and the simulated peak value is high by a factor of three.

It was impossible to negate the undesirable effects of mode r = 7 electronically by using the one-third-octave shaping filter, since mode r = 6 at 1200 Hz also lies within this filter bandwidth. Therefore, any lowering of peak value for r = 7 also jeopardizes the simulation of r = 6. It is seen that much narrower filter bandwidths are needed to properly simulate the response spectrum when resonances are not widely separated.

The unwanted response in mode r = 6 at frequencies of 1130 and 1160 Hz, which lie below its true resonance frequency of 1200 Hz, is believed to be caused by resonances in the plate edge-support-structure, since large response is shown at these frequencies in Table 3.3, page 43. The 1-inch shaker support does not respond significantly at these frequencies (see Table 3.2, page 42).

The unwanted response in mode $r = 5$ at 980 Hz, below its resonance frequency of 1020 Hz, is believed to be caused by interactions between the plate, plate-support, and shaker-support, since both the 1-inch shaker support (Table 3.2, page 42) and the plate edge supports (Table 3.3, page 43) respond significantly at this frequency. Between resonances, the response is generally simulated very well except at the frequencies already discussed.

4.2.3 Comparison of Computed and Measured Frequency Response Functions.

The simulation force spectral density, $S_{AA}(f)$, of Figure 4.12, page 103, was used with the values of simulated acceleration spectral density, $S_{11}(f)$ and $S_{22}(f)$ of Figure 4.10, pages 98 through 101, in eq. (2.67) to calculate the experimental squared modulus of the frequency response functions, $H_{1A}(if)$ ^{2} and $H_{2A}(if)$ ^{2}, for the plate. These results are compared in Figures 4.13 and 4.14 with the response functions obtained using eq. (2.51) and the research test resonance frequencies, damping factors, and mode shapes from Table 4.3, page 95. It is seen that the computed values agree well with the values from the simulation test with regard to resonance frequency and bandwidth; however, the computed peak values are generally more conservative than the experimentally obtained values. As with the beam, Table 4.4 shows that the data analyzer filter had a bandwidth which was two to six times as wide as recommended for these lightly damped modes; therefore, the experimental mean square level within the bandwidth divided

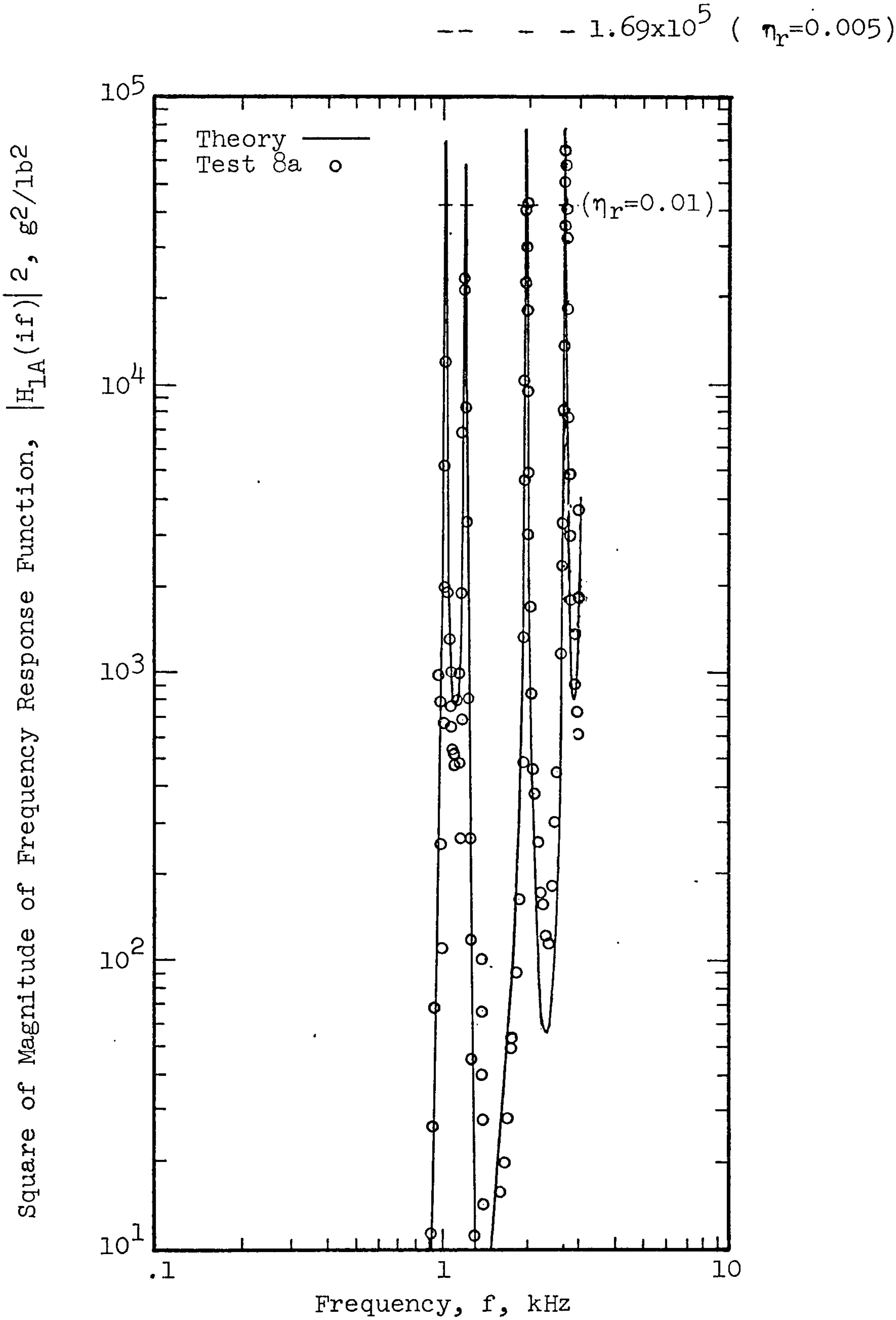

Fig. 4.13 Comparison of Square of Magnitude of Theoretical and Experimental Frequency Response Functions Between Center-Plate Acceleration and Simulation Force on Simply-Supported Rectangular Plate.

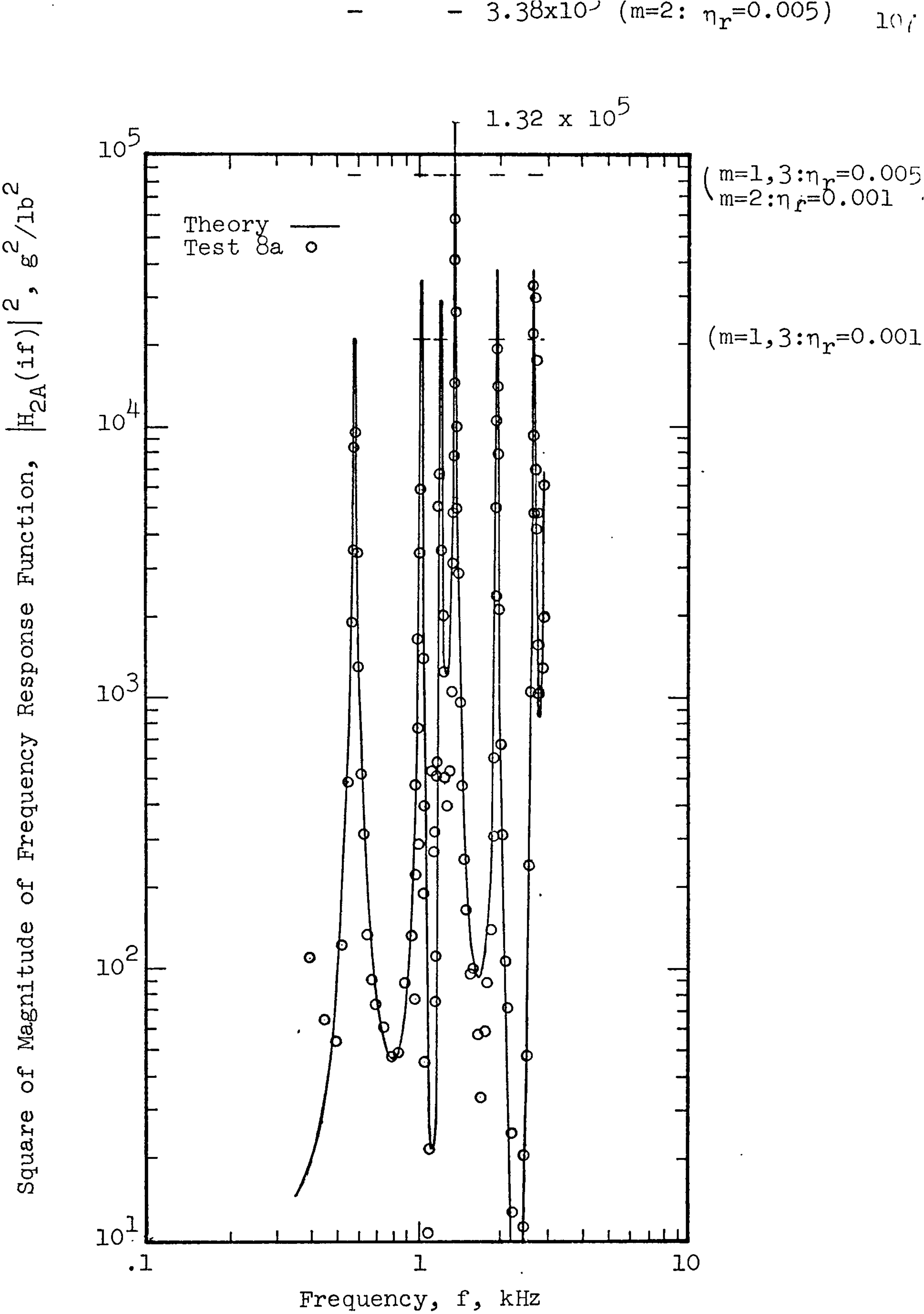

Fig. 4.14 Comparison of Square of Magnitude of Theoretical and Experimental Frequency Response Functions Between Quarter-Plate Acceleration and Simulation Force on Simply-Supported Rectangular Plate.

Table 4.4 Comparison of Simply-Supported Plate, Data Reduction Bandwidths with Recommended Values of [30]

Resonance Frequency f_r, Hz	Structural Damping η_r	Half-Power Point Band-width, Δf_{hp} Hz	Recommended* Bandwidth B, Hz	Data Reduction Bandwidth Hz
580	.01989	11.5	2.9	12
1019	.00780	7.9	2.0	12
1202	.00854	10.4	2.6	12
1365	.00800	10.9	2.7	12
1956	.00742	14.5	3.8	12
2638	.00750	19.8	5.0	12

*$B < \Delta f_{h.p.}/4 = f_r \eta_r / 4$

by the filter bandwidth gave a smaller spectral density level than actually occurred.

In the regions between resonance peaks the theory provides reasonable estimates of frequency response functions, as seen from the figures. The undesirable frequencies discussed earlier--980, 1130, and 1160 Hz--are also present in the experimental frequency response function data of Figures 4.13 and 4.14, pages 106 and 107.

The experimentally determined phase angles $\phi_{1A}(f)$ and $\phi_{2A}(f)$ of the complex frequency response functions $H_{1A}(if)$ and and $H_{2A}(if)$ are presented in Figures 4.15 and 4.16.

Another complex excitation test was run in which the complex excitation was again acoustic noise; however, in this test (Test 7b) the simulation shaker was attached to the beam, and, although not excited, it did provide a large, narrow-band force input to the plate. Data from Test 7b and its corresponding Simulation Test 8b are included in Appendix 4.

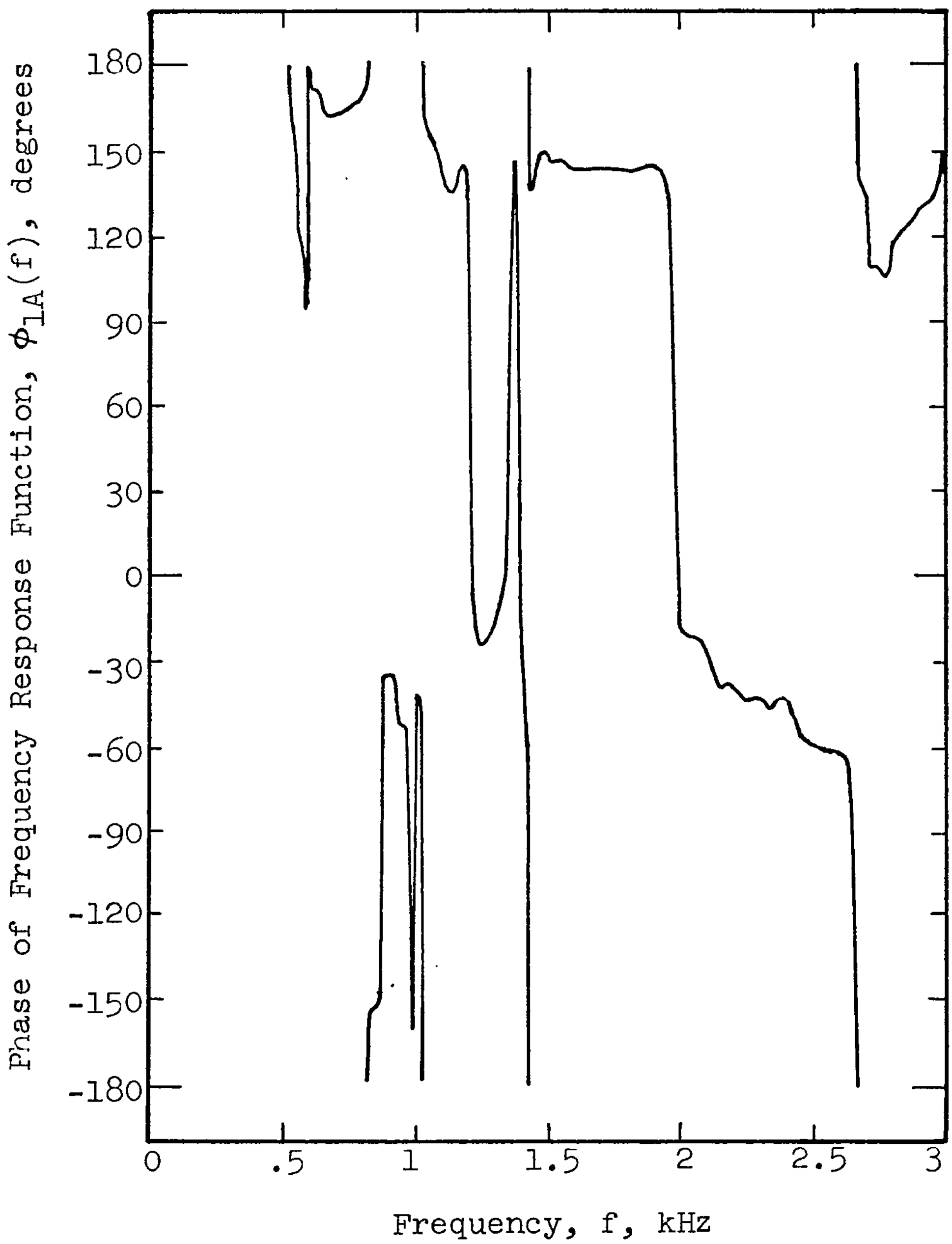

Fig. 4.15 Phase of Experimental Frequency Response Function Between Center-Plate Acceleration and Simulation Force on Simply-Supported Plate (Test 8a).

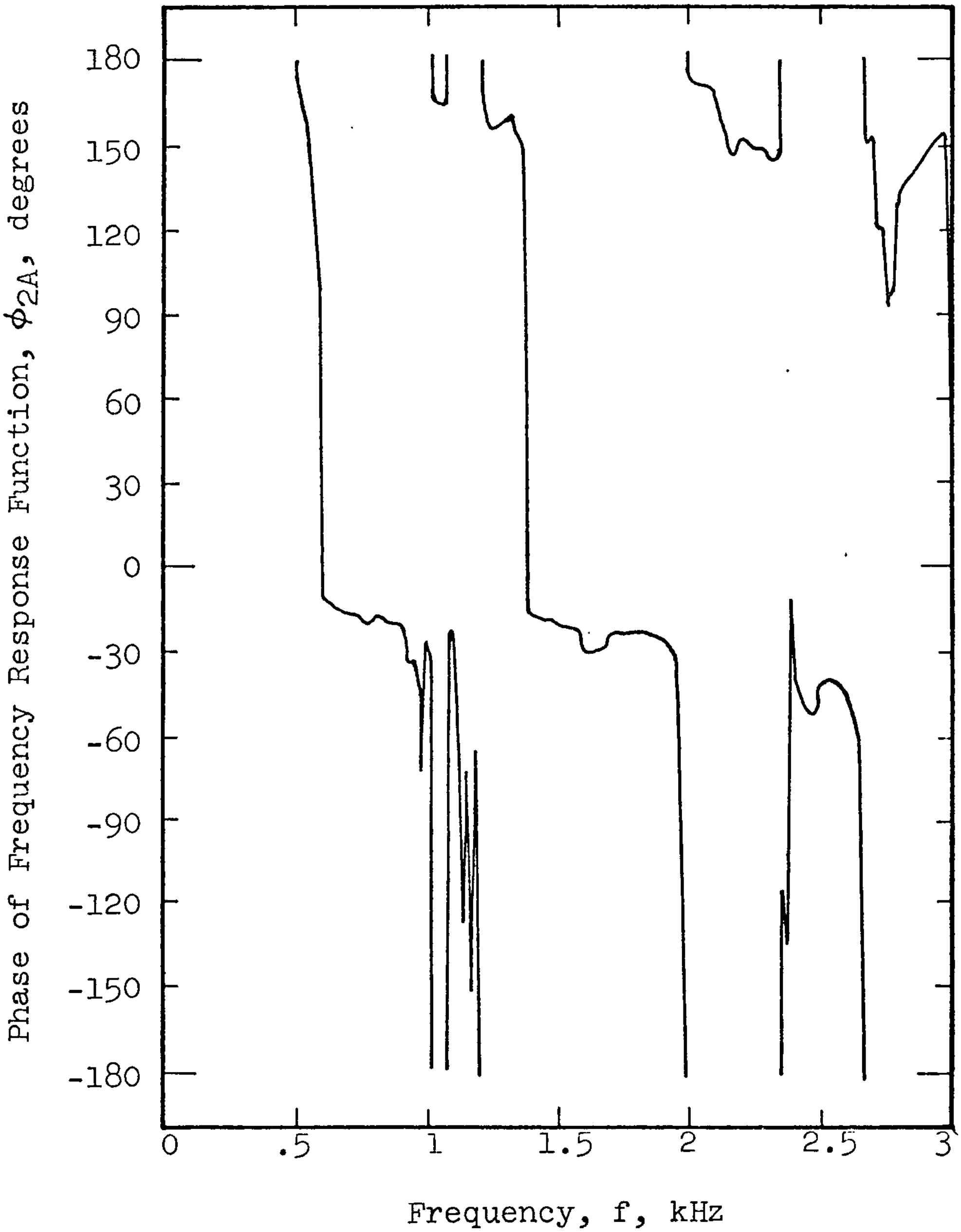

Fig. 4.16 Phase of Experimental Frequency Response Function Between Quarter-Plate Acceleration and Simulation Force on Simply-Supported Plate (Test 8a).

Chapter 5

CONCLUSIONS AND RECOMMENDATIONS

5.1 Conclusions

From the results obtained for the cantilever beam and the simply-supported plate, the following conclusions are made:

1. The random response of a linear, elastic structure to a complex, ergodic, Gaussian excitation environment may be adequately simulated using one mechanical shaker, provided the structure has light damping and widely separated resonances.

2. Simulation of structural response is complete, in the sense that the response spectral densities at every point and the cross-spectral densities between each pair of points are simulated with the same degree of accuracy, if the response spectral density at any one structural location is simulated adequately.

3. A complete simulation of structural response as suggested by Robson [20], [21], which is accurate in the vicinities of the resonance peaks and approximate in the frequency regions between resonance peaks, could be obtained if it were not for changes in structure dynamics caused by physically attaching the shaker to the structure.

4. When a light-weight mechanical shaker is attached to the structure, it appears that there is only slight distortion of the theoretical mode shapes; however, the damping may increase considerably, especially for extremely lightly damped structures, and the resonance frequencies may change substantially, particularly if the shaker connecting link, the shaker armature-flexure system, or the shaker support structure has resonances within the frequency range of interest.

5. Modifications to the shaker system of paragraph 4 may be necessary to reduce the undesirable effects on structure dynamics, or it may be possible to negate these effects by using either narrow-band, variable gain, filters or peak-notch filters.

6. The shaker used for simulation tests must be properly positioned so that (a) it does not lie on a node of a vibration mode, and (b) it supplies a component of force in each direction necessary to excite the modes of interest.

7. The spectrum shaping filters, used to shape the simulation force spectrum supplied by the shaker, should be of sufficiently narrow bandwidth so that no more than one resonance peak lies within the bandwidth of each filter. If large changes in damping are experienced when the shaker is attached to the clean structure, filter bandwidths will have to be narrower than the resonance bandwidth that is to be simulated.

8. The desired simulation force spectral density can be accurately calculated from a knowledge of the squared modulus of the complex frequency response function and the response spectral density to be simulated, using

$$S_{AA}(f) = \frac{S_{11}(f)}{|H_{1A}(if)|^2}$$

9. The complex frequency response function may be determined experimentally or, for the simple structures used here, by using a modified theoretical frequency response function which accounts for any changes in structure dynamics caused by the addition of the shaker to the structure.

5.2 Recommendations

Based upon the results of this study and the conclusions presented above, it is recommended that:

1. This method of vibration simulation testing should be attempted, using one shaker with a set of narrow-band spectrum shaping filters, on other simple beam, plate, and shell structures which have light damping and widely separated resonances in their lower frequency ranges.

2. The method proposed by Robson and Roberts [21] for simulating the response of the lightly damped, simple structures of paragraph 1 in their intermediate frequency ranges, where response in two (or n) modes must be considered at any frequency, should be attempted. This would require the complete control of two (or n) force spectral densities and their cross-spectral densities, and it should be ascertained whether simulation of the response spectral densities and cross-spectral densities between any two (or n) points does in fact assure complete simulation in the approximate sense of this paper. The problems associated with control of force spectra and cross-spectra become formidable as n increases; however, if n is small, and it is necessary to consider n modes in only a few frequency bands throughout the frequency range of interest (as on some practical structures), the control problems will be simplified.

3. In paragraph 2 above, the number of resonances, n, should be determined for which it is no longer practical to use this modal method of simulation testing. Above this value of n, for which the structure may be considered multi-modal and reverberant, rational simulation techniques should be developed [1] such as those which simulate the spatial average over the structure of the average vibrational energy over many modes in a frequency band.

4. The studies of paragraphs 1, 2, and 3 above be performed on structures which have larger damping. Robson theorizes that this would require n shakers to simulate exactly the response at and between n points; however, the simulation would not be complete in that the simulation is not assured at every other point on the structure.

5. The studies of paragraphs 1, 2, 3, and 4 above be performed on more complex structures such as stiffened plates and shells and coupled structures.

Appendix 1

DEFINITIONS

Random Process--an ensemble $\{x(t)\}$ of all records $x^{(1)}(t)$, $x^{(2)}(t), \ldots, x^{(j)}(t)$, $-\infty \leq t \leq \infty$, which were obtained at the same location on a system under identical test conditions.

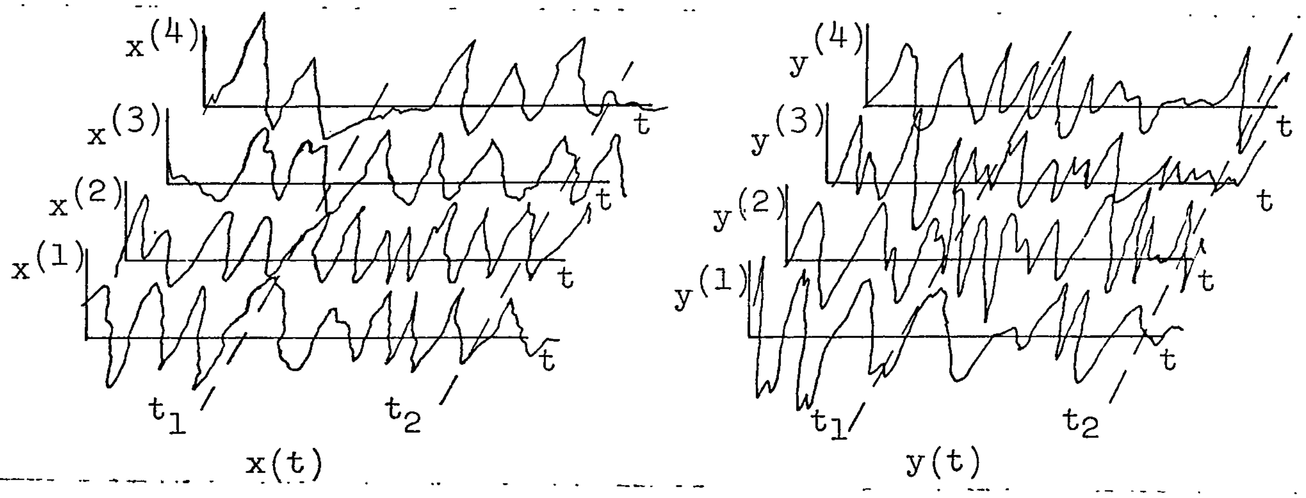

Stationary Random Process--a random process whose ensemble probability distributions, and all ensemble averages based upon them, are invariant under a shift of the time scale.

Ergodic Random Process--a stationary random process whose ensemble averages are equal to the corresponding temporal averages taken over any sample record $x^{(k)}(t)$ of the process.

Strongly Stationary Random Processes--two arbitrary random processes $\{x(t)\}$ and $\{y(t)\}$, whose individual and joint ensemble probability distributions of any order are independent of time translations.

Weakly Stationary Random Processes--two arbitrary random processes, $\{x(t)\}$ and $\{y(t)\}$, whose individual and joint, first and second order ensemble probability distribution are independent of time translations.

Strongly Ergodic Random Processes--two arbitrary, strongly stationary random processes, $\{x(t)\}$ and $\{y(t)\}$, whose individual and joint ensemble probability distributions of any order are equal to the corresponding individual and joint averages taken over any arbitrary pair of sample records, $x^{(k)}(t)$ and $y^{(k)}(t)$.

Weakly Ergodic Random Processes--two arbitrary, weakly stationary random processes, $\{x(t)\}$ and $\{y(t)\}$, whose individual and joint, first and second order probability distributions are equal to the corresponding individual and joint temporal averages taken over any arbitrary pair of sample records, $x^{(k)}(t)$ and $y^{(k)}(t)$.

Self-Stationary Random Record--a single random record $x^{(k)}(t)$ whose statistical properties computed over short time intervals do not vary significantly from one interval of the record to the next.

In the following equations it is assumed that the random processes under consideration are strongly ergodic so that ensemble averages may be replaced by temporal averages over any arbitrary pair of sample records. In addition, it is further assumed that each sample record is self-stationary so that the temporal averages of individual records may be taken over any short time interval of the record. When joint properties between two random records are being computed, the time intervals of each record must begin and end at identical times. The equations presented are the theoretical definitions of the various quantities which were computed digitally as illustrated in Appendix 3.

Probability Distribution--For a self-stationary random record the probability distribution is given by

$$P(x) = \frac{\sum \Delta t_{(X \leq x)}}{T} \tag{A1.1}$$

where T is the length of the time slice and $\sum \Delta t_{(X \leq x)}$ is the total amount of time for which the instantaneous value of the signal, X, is less than some fixed value, x, i.e.,

$$P(x) = P_r[X \leq x] \tag{A1.2}$$

Probability Density--the slope of the probability distribution curve

$$p(x) = \frac{dP(x)}{dx} \tag{A1.3}$$

Gaussian Probability Density--The probability density of instantaneous values, x, is Gaussian when

$$p(x) = \frac{1}{\sigma_X \sqrt{2\pi}} \exp. \left\{-[x-<x>]^2/2\sigma_X^2\right\} \tag{A1.4}$$

where the variance, σ_X^2, is given by

$$\sigma_x^2 = \langle [x(t) - \langle x(t)\rangle]^2 \rangle$$

$$= \lim_{T\to\infty} \frac{1}{T} \int_{-T/2}^{T/2} [x_T(t) - \langle x_T(t)\rangle]^2 dt$$

$$= \langle x^2(t)\rangle - \langle x(t)\rangle^2 \qquad \text{(A1.5)}$$

$\sigma_x = (\sigma_x^2)^{\frac{1}{2}}$ is called the standard deviation. If the mean value

$$\langle x(t)\rangle = \lim_{T\to\infty} \frac{1}{T} \int_{-T/2}^{T/2} x_T(t)dt \qquad \text{(A1.6)}$$

is zero, the variance becomes the mean square value and the standard deviation becomes the root mean square value.

<u>Autocorrelation</u>--The autocorrelation is given by

$$R_x(\tau) = \langle x(t)x(t+\tau)\rangle$$

$$= \lim_{T\to\infty} \frac{1}{T} \int_{-T/2}^{T/2} x_T(t)x_T(t+\tau)dt \qquad \text{(A1.7)}$$

where $x_T(t) = x(t)$ in the range $-T/2<t<T/2$ and $x_T(t) = 0$ at all other times. The autocorrelation is also expressible in terms of the Fourier transform, $A_T(if)$, of the truncated signal, $x_T(t)$, as

$$\int_{-\infty}^{\infty} R_x(\tau)\exp.\left\{-i2\pi f\tau\right\} d\tau = \int_{-\infty}^{\infty} \lim_{T\to\infty} R_{x_T}(\tau)\exp.\left\{-i2\pi f\tau\right\} d\tau$$

$$= \lim_{T\to\infty} \frac{1}{T} \left| A_T(if)\right|^2 \qquad \text{(A1.8)}$$

where

$$A_T(if) = \frac{1}{T}\int_{-T/2}^{T/2} x_T(t)\exp.\left\{-i2\pi ft\right\}dt \qquad (A1.9)$$

and

$$x_T(t) = \frac{1}{T}\int_{-T/2}^{T/2} A_T(if)\exp.\left\{i2\pi ft\right\}df \qquad (A1.10)$$

are Fourier transforms. This result is useful in determining the autocorrelation function using the Fast Fourier Transform technique, as mentioned in Appendix 3.

Spectral Density--The mean square value is given by

$$<x^2(t)> = \lim_{T\to\infty} <x_T^2(t)>.$$

$$= \int_0^\infty \lim_{T\to\infty} [\frac{2}{T} \left|A_T(if)\right|^2]df \qquad (A1.11)$$

and the spectral density is defined as

$$S_X(f) = \lim_{T\to\infty} [\frac{2}{T} \left|A_T(if)\right|^2] \qquad (A1.12)$$

Therefore, $S_X(f)$ can also be determined using the Fourier transform $A_T(if)$.

The spectral density and autocorrelation are inverse transforms, as given by the Wiener-Khintchine relations

$$S_X(f) = \int_{-\infty}^{\infty} 2R_X(\tau)\exp.\left\{-i2\pi f\tau\right\}d\tau \qquad (A1.13)$$

$$R_X(\tau) = \int_{-\infty}^{\infty} \tfrac{1}{2}S_X(f)\exp.\left\{i2\pi f\tau\right\}df \qquad (A1.14)$$

Cross-Spectral Density--The cross-spectral density between two random signals is given by

$$S_{xy}(f) = \lim_{T\to\infty} \frac{2}{T} A_T^*(if)B_T(if) \tag{A1.15}$$

where $A_T(if)$ and $B_T(if)$ are the Fourier transforms of the truncated signals $X_T(t)$ and $y_T(t)$, respectively. Also,

$$S_{xy}(f) = C_{xy}(f) - iQ_{xy}(f) \tag{A1.16}$$

where the co-power spectral density is

$$C_{xy}(f) = \tfrac{1}{2}[S_{xy}(f) + S_{yx}(f)] \tag{A1.17}$$

and the quad-power spectral density is

$$Q_{xy}(f) = \frac{i}{2}\,[S_{xy}(f) - S_{yx}(f)] \tag{A1.18}$$

since

$$S_{xy}(f) = S_{yx}^*(f) \tag{A1.19}$$

In addition, the cross-spectral density may be written

$$S_{xy}(f) = \left|S_{xy}(f)\right| \exp.\left\{-i\theta_{xy}(f)\right\} \tag{A1.20}$$

where

$$S_{xy}(f) = [C_{xy}^2(f) + Q_{xy}^2(f)]^{\frac{1}{2}} \tag{A1.21}$$

is the magnitude, and

$$\theta_{xy}(f) = \tan^{-1}\frac{Q_{xy}(f)}{C_{xy}(f)} \tag{A1.22}$$

is the phase.

<u>Coherence Function</u>--The coherence function is defined as

$$\gamma_{xy}^2(f) = \frac{|S_{xy}(f)|^2}{S_x(f)S_y(f)} \tag{A1.23}$$

where $0 \leq \gamma_{xy}^2(f) \leq 1$. For a single input to a constant parameter linear system, $\gamma = 1$ because of the relationships given by eqs. 2.67 and 2.73. If $0 < \gamma < 1$, either extraneous noise is present in the measurements, the system is not linear, and/or y(t) is an output due to other inputs as well as x(t) (see Figure A3.1(l), page 138).

<u>Frequency Response Function</u>--The complex frequency response function for a linear system subjected to one input is given by

$$H_{yx}(if) = \frac{S_{xy}(f)}{S_x(f)} \tag{A1.24}$$

with its magnitude given by

$$|H_{yx}(if)| = \left(\frac{S_y(f)}{S_x(f)}\right)^{\frac{1}{2}} \tag{A1.25}$$

or

$$|H_{yx}(if)| = \frac{|S_{xy}(f)|}{S_x(f)} \tag{A1.26}$$

Figure A3.1m, page 139, is representative of calculations using eq. A1.26; however, the results are not valid since there was more than one input to the beam in Test 3e. Therefore, eqs. 2.78 or 2.82 would have to be used to get meaningful results.

Appendix 2

EQUIPMENT LIST

Storage Oscilloscope, Tektronix, Type 564

Spectrum Analyzer Unit, Tektronix, Type 3L5

Time Base Unit, Tektronix, Type 2B67

Storage Oscilloscope, Tektronix, Type 564B

Four Trace Amplifier Unit, Tektronix, Type 3A74

Time Base Unit, Tektronix, Type 3B4

Oscilloscope Camera, Hewlett Packard, Model 196A

Film, Polaroid Land, Type 47

FM/Direct Recorder/Reproducer, Ampex, SP-300

6 Instrumentation Grade Magnetic Tapes, Ampex, Type 738-151111

Vacuum Tube Voltmeter, Hewlett Packard, Model 400 DR

DC Null Voltmeter, Hewlett Packard, Model 419A

Volt-Ohm-Milliammeter, Simpson, Model 260

Random Noise Voltmeter, Bruel & Kjaer, Type 2417

Electronic Counter, Hewlett Packard, Model 523 DR

Regulated DC Power Supply, Kepco, Model CK 36-1.5

2 Variable Band-Pass Filters, Krohn-Hite, Model 310 CR

Variable Band-Pass Filter, Spencer-Kennedy Labs., Model 302

2 Decade Amplifiers, H. H. Scott, Type 140B

Audio Oscillator, M B Electronics, Model N525

Electronic Amplifier and Power Supply, MB Electronics, Model P 13

2 Power Oscillator/Amplifiers, Ling, Model POA-1

2 Vibration Generators, Goodman, Type V 47/3

2 Noise Generator/Mixer-Clipper-Equalizers, Sine Engr., Model 1865/CE

2 Spectral Density Equalizers, Ling, Model ESD-26B

2 Random Noise Generators, General Radio, Type 1381

Electromagnet

Sound Level Meter, General Radio, Type 1551-C

Condenser Microphone System, General Radio, Type 1551-P1H

Sound Level Calibrator, General Radio, Type 1552-B

Loudspeaker, Muter Co., Jenson

Earmuffs, Wilson, Sound Barrier

DC Power Supply, Endevco, Model 2622

4 Subminiature AC Accelerometer Amplifiers, Endevco, Model 2607

2 Micro-Miniature Shear Accelerometers, Endevco, Model 2226C

2 Accelerometers, Endevco, Model 2242

Crystal Phonograph Cartridge, Rystal MR, No. PS-3

2 Bridge Signal Conditioners, BLH, Model 2530

2 Direct Coupled Data Amplifiers, DANA, Model 2615-V3

Amplifier Power Supply, DANA, Model 2602

2 Strain Gage Force Transducers

10 Strain Gages, Bean, Model BAE-13-031 DD-120S

10 Strain Gages, Bean, Model BAE-13-031 DD-120L

4 Strain Gages, Bean, Model BAE-13-250 BB-120

10 Strain Gages, BLH, Model FAE-03H-12SL 13L

Strain Gage Primary Application Kit, Bean

Various Strain Gage Application Tools, BLH

Contact Cement, Eastman 910

N-N Dimethylformamide, Eastman

Appendix 3

RANDOM DATA ANALYSIS

As described in Chapter 3, the random acceleration, force, and pressure data from tests on the cantilever beam and the simply-supported plate were recorded on magnetic tape. The data were then reproduced on an oscillograph record which was used for selecting a representative time slice of data for analysis purposes. The procedures for determining length of time slice, cut-off frequency, analyzer filter bandwidth, and standard error are found in [30], and are illustrated in the following.

If the time interval Δt between digital samples of the continuous analog data is h seconds, then the sampling rate is 1/h samples per seconds. Assuming at least two samples per cycle, the useful data will be from 0 to 1/2h Hz, since frequencies in the data which are higher than 1/2h Hz will be folded into the lower frequency range from 0 to 1/2h and confused with data in this lower range. The cutoff frequency

$$f_c = \frac{1}{2h} \tag{A3.1}$$

is known as the Nyquist frequency. For any frequency f in the range $0 \leq f \leq f_c$, the higher frequencies aliased with f are $2nf_c \pm f$ $(n = 1, 2, \ldots)$. If significant data exist in the analog record above the highest frequency of interest, it is a good rule to select f_c to be approximately two times the highest frequency of interest. It is also a good idea to filter the data prior to sampling so that information above the desired cutoff frequency is not present. Both of these methods were used to overcome the aliasing problem. Since the maximum frequency of interest was 6000 Hz for the beam and 3000 Hz for the plate, data were filtered above cutoff frequencies of 10,000 and 5,000 Hz, respectively, for the two structures.

The number of samples per second, $1/h$, for the beam and plate data was then 20,000 and 10,000, respectively, from eq. (A3.1). The limit imposed by the Univac 1108 computer for the total number of digitized samples in the time slice was 32,768. Therefore, the limit was set at 32,000 samples and the length of time slice, T, was computed from

$$T = 32{,}000\ h \tag{A3.2}$$

to be 1.6 seconds for the beam and 3.2 seconds for the plate.

In addition to the above, consideration must be given to the effect of the analyzer filter bandwidth on the resolution of narrow-band spectral density resonance peaks. A reasonable criterion [30] is that the filter bandwidth, B, be chosen such that

$$B \leq \tfrac{1}{4}\Delta f_{hp} \tag{A3.3}$$

where

$$\Delta f_{hp} = \eta_r f_r \tag{A3.4}$$

Also, the effects of filter bandwidth and time slice length on the normalized standard error, ϵ, for the spectral density estimate must be considered. ϵ may be approximated by

$$\epsilon \cong \frac{1}{(BT)^{\frac{1}{2}}} \tag{A3.5}$$

if bias error may be neglected, i.e., if the data resonance peaks are properly resolved through use of eq. (A3.3). Since B was chosen as 24 Hz for the beam and 12 Hz for the plate, $\epsilon = 0.16$ for both structures; however, for highly coherent signals, a much smaller error than this will actually occur, i.e., eq. (A3.5) presents an upper bound for ϵ.

The digitized random data were reduced according to the methods presented in reference [32], using the Fast Fourier Transform Technique for correlation and spectral density determination. The quantities determined in the data analysis were digitized signal, normalized probability density, autocorrelation, spectral density, and rms spectrum for each signal; and co-spectral density, quadrature-spectral density, cross-spectral density magnitude and phase, coherence function, and transfer function between each pair of signals. Examples of these quantities are given in Figure A3.1.

In Figures A3.1b and A3.1c are shown probability density functions for output acceleration and input force, respectively. These functions are approximately Gaussian and illustrate the fact that a Gaussian input to a linear system yields a Gaussian output.

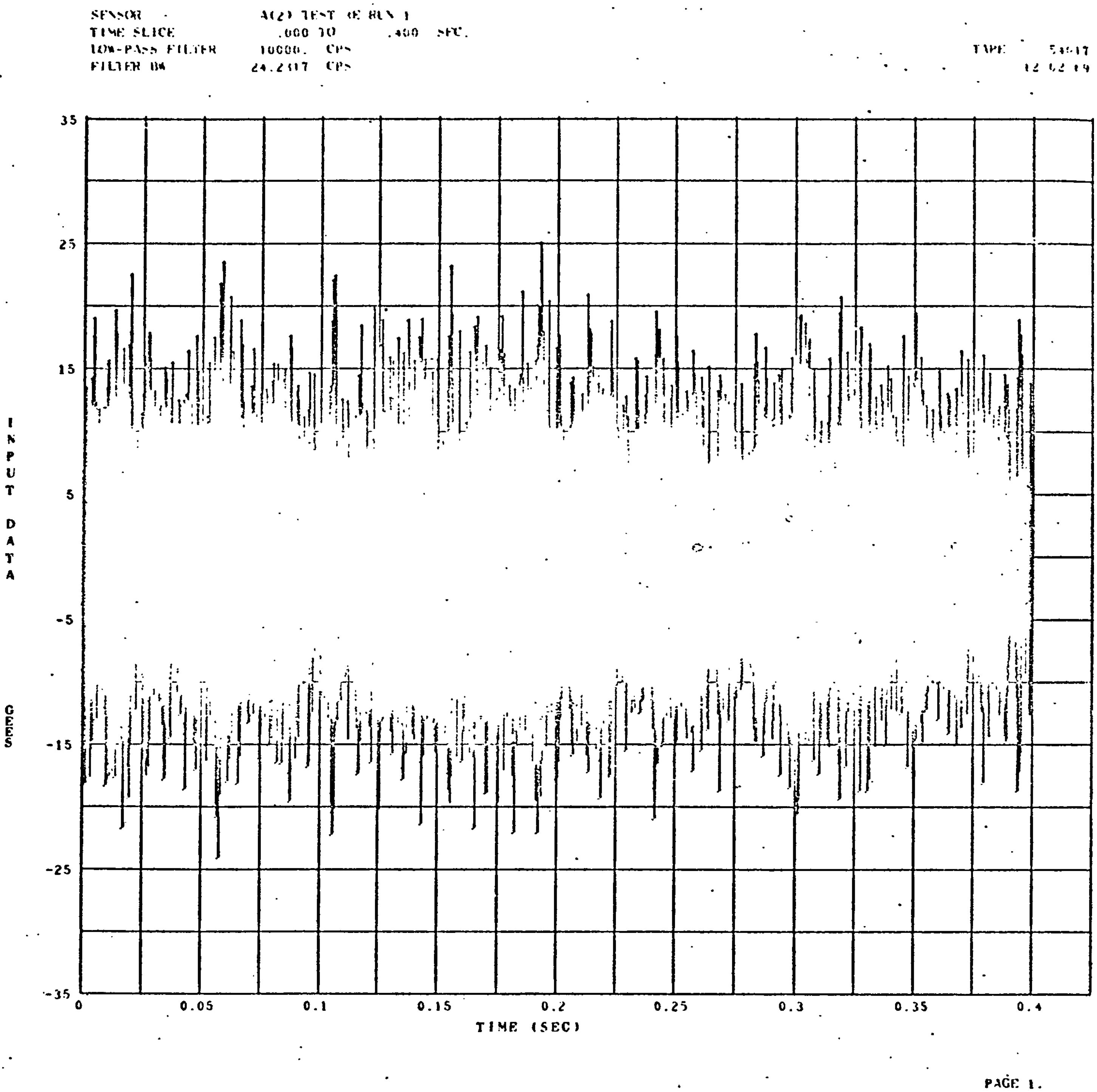

(a) Digitized Random Acceleration Signal

Fig. A3.1 Examples of Digitally Reduced Data

SENSOR A(2) TEST 3E RUN 1 TAPE 54611
TIME SLICE .000 TO 1.600 SEC. 12 02 63
CHI-SQUARE= 196.655= 2.5 PERCENT= 44.4607 5 PERCENT-- 41.3372 2= DEGREES OF FREEDOM
N= 31762 RANGE= -27.14239 TO 25.25594 MEAN= .013107 RMS= 7.575466 SKEW= -.014874 KURT.= 2.6614-5.
COEFFICIENT OF VARIATION= 336.4672-1.

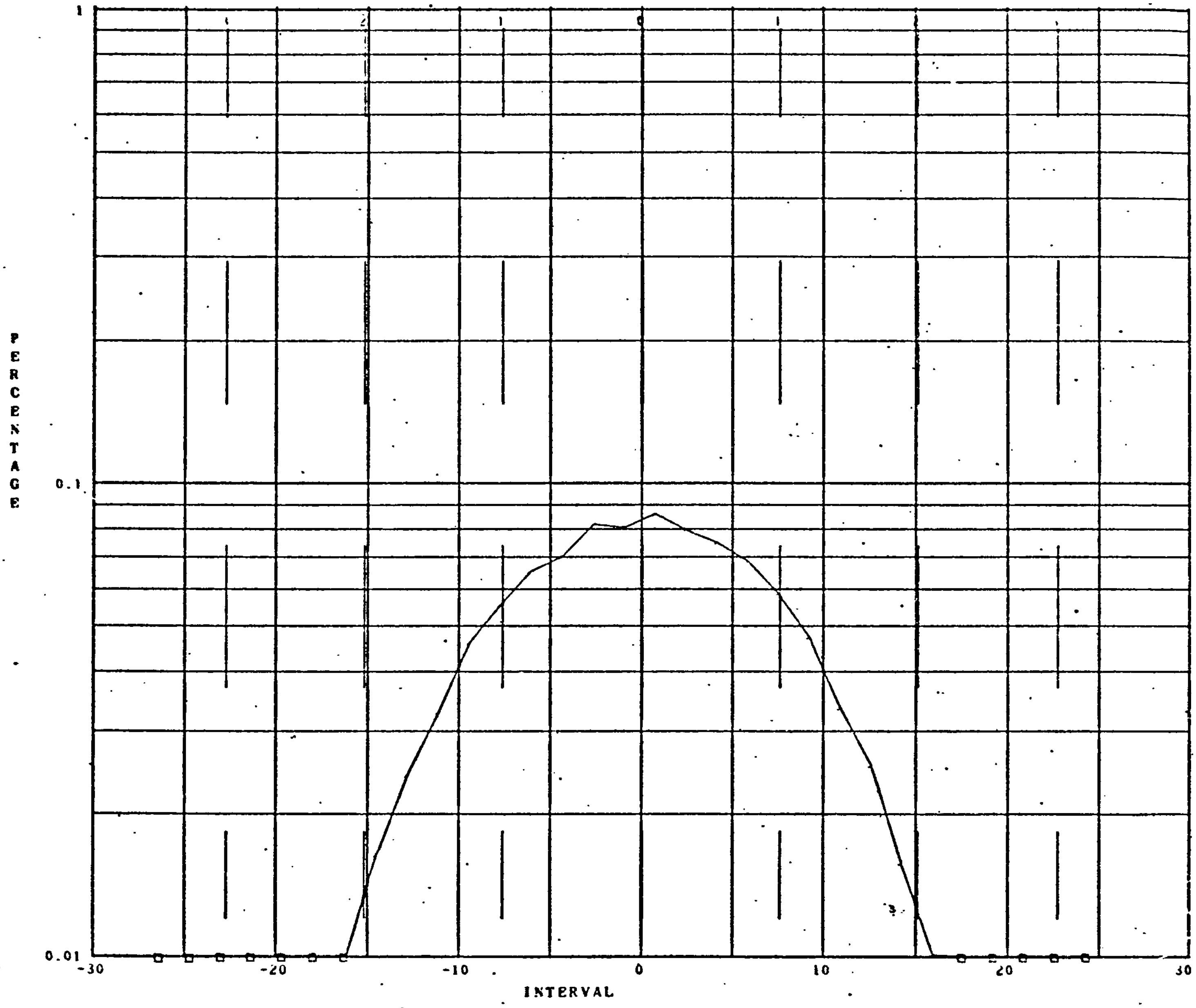

(b) Normalized Probability Density of Acceleration

Fig. A3.1 (Continued)

SENSOR F(A) TEST 3E RUN 1 TAPE 54U15
TIME SLICE .000 TO 1.600 SEC. 12/02-19
CHI-SQUARE- 114.4507 2.5 PERCENT- 44.4607 5 PERCENT-- 41.3172 2= DEGREES OF FREEDOM
N= 31762 RANGE= -1.53579 TO 1.49327 MEAN= .007217 RMS= .413364 SKEW= -.073016 KURT.= 2.-39400
COEFFICIENT OF VARIATION= 56.672122

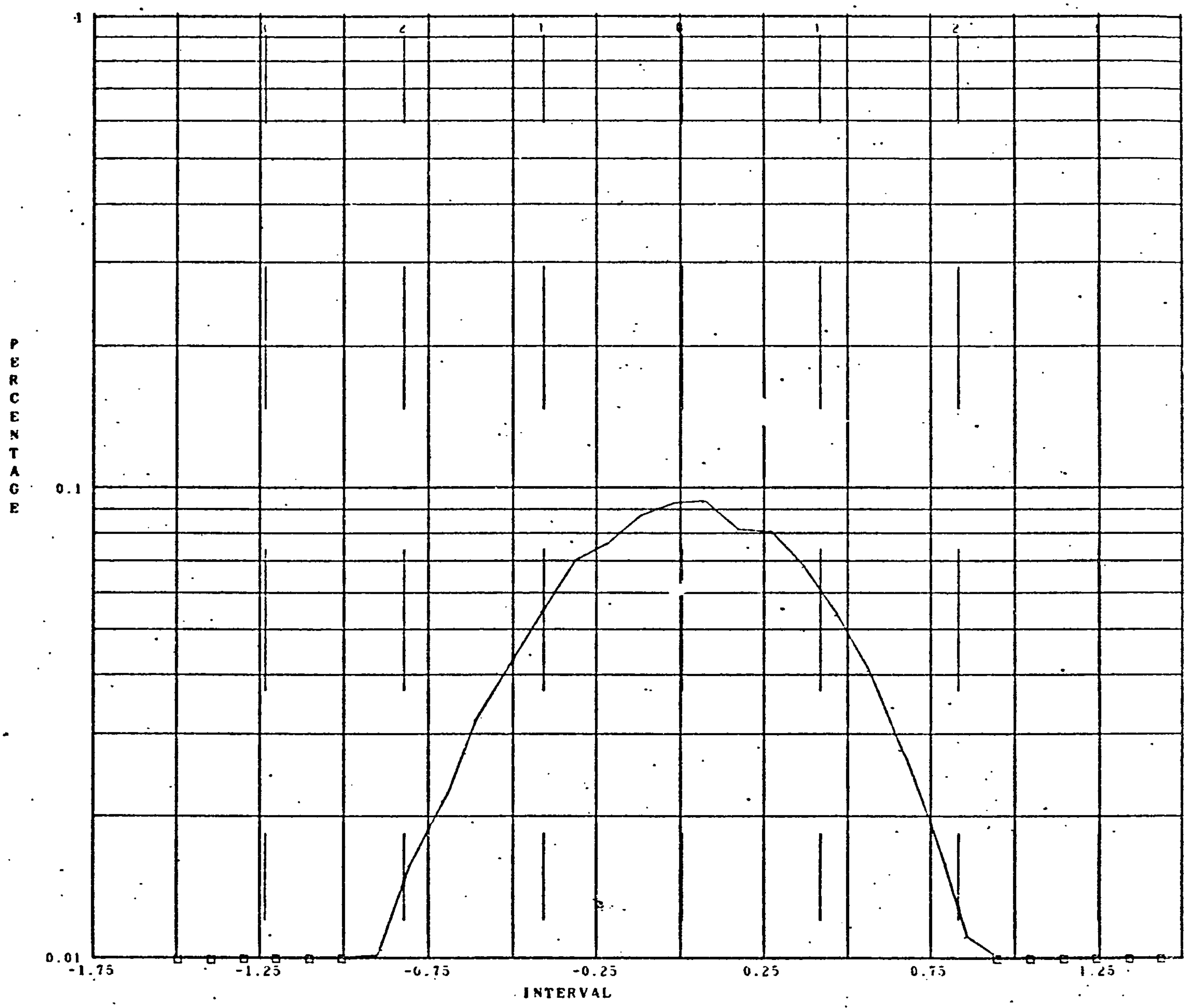

PAGE 5.

(c) Normalized Probability Density of Force

Fig. A3.1 (Continued)

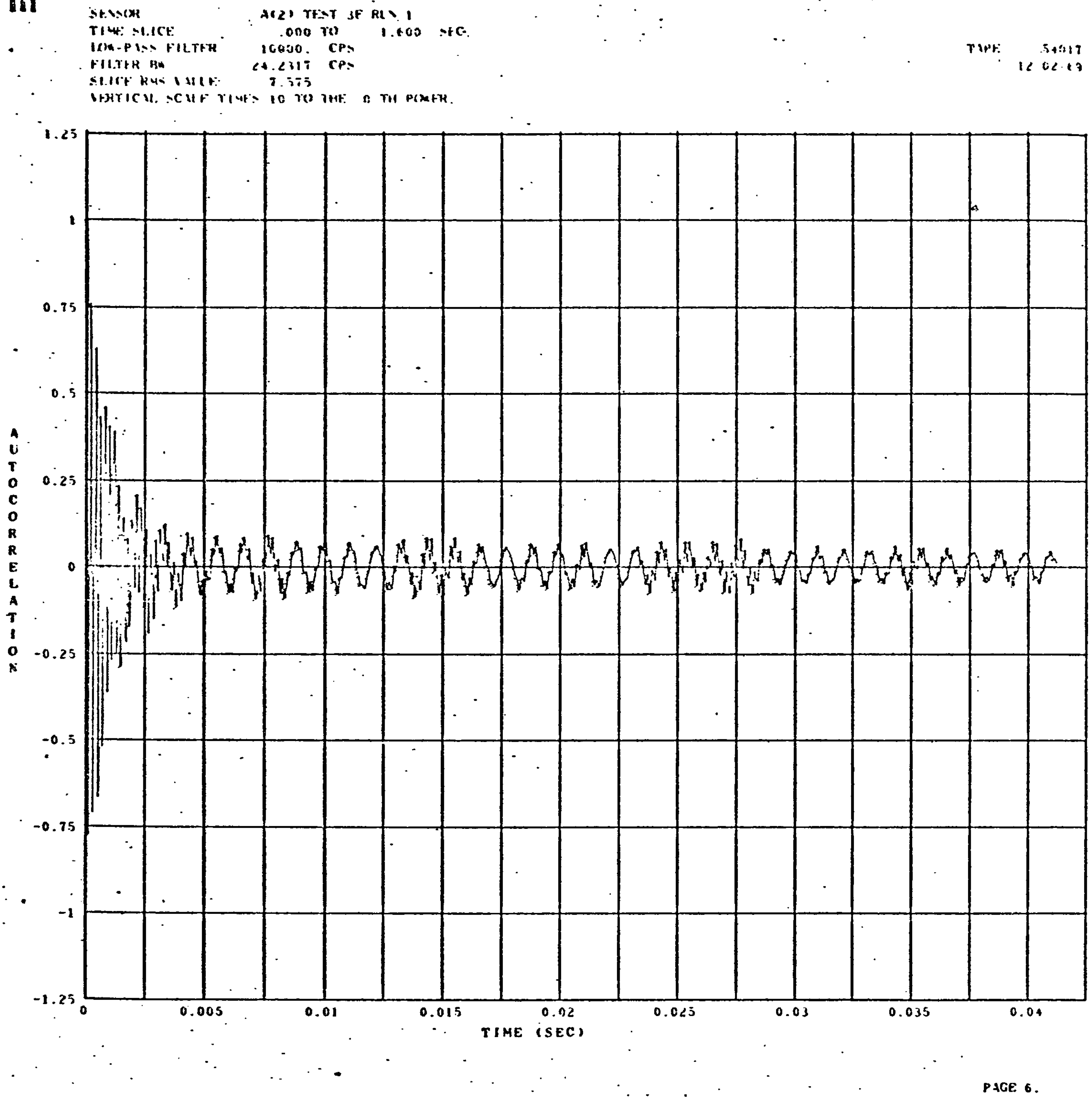

(d) Acceleration Autocorrelation

Fig. A3.1 (Continued)

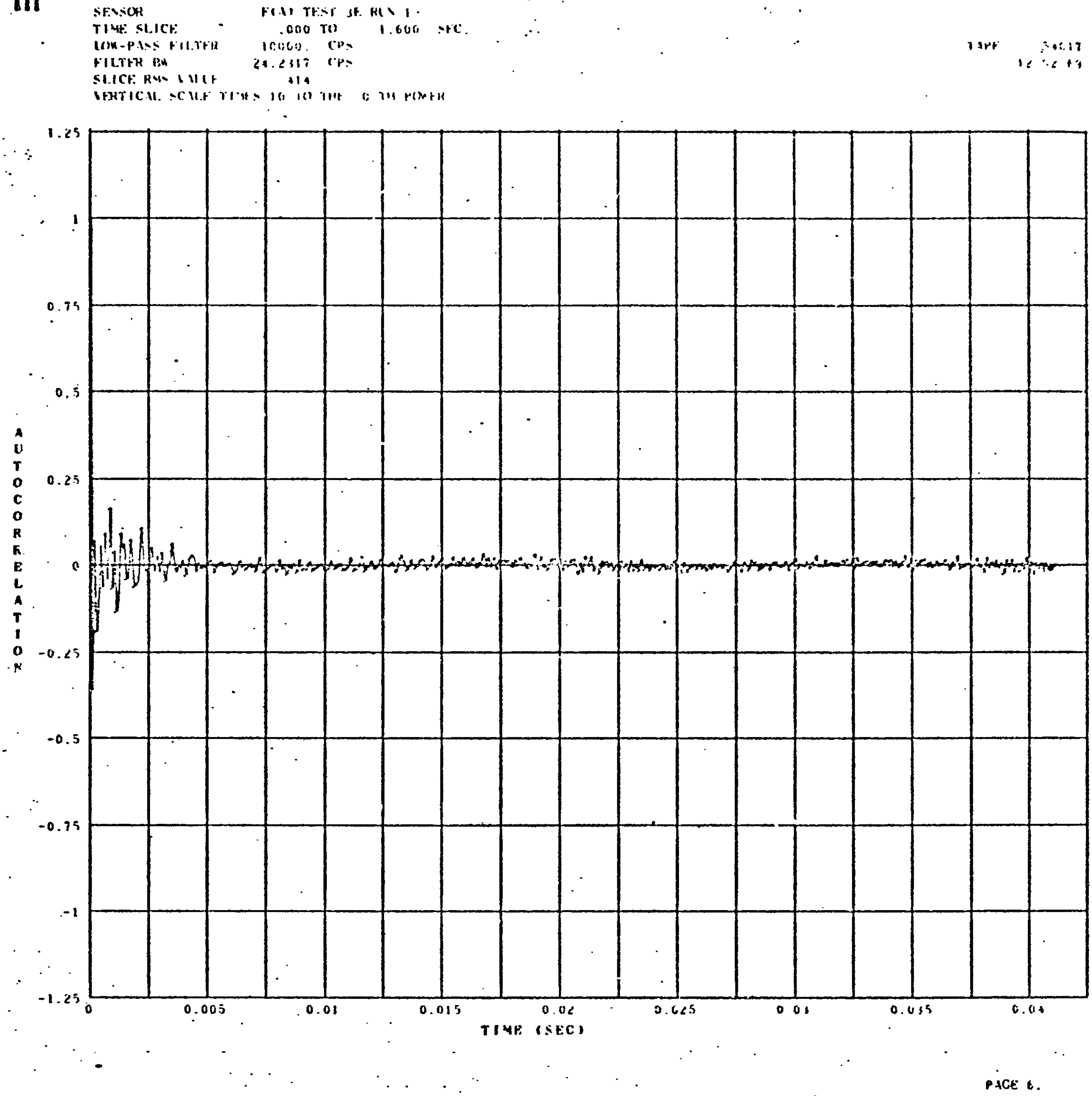

(e) Force Autocorrelation

Fig. A3.1 (Continued)

SENSOR A(2) TEST 3E RUN 1
TIME SLICE .000 TO 1.600 SEC.
LOW-PASS FILTER 10000. CPS
FILTER BW 24.2417 CPS
SLICE RMS VALUE 7.575
VERTICAL SCALE TIMES 10 TO THE 0 TH POWER.

TAPE 54017
12/02 69

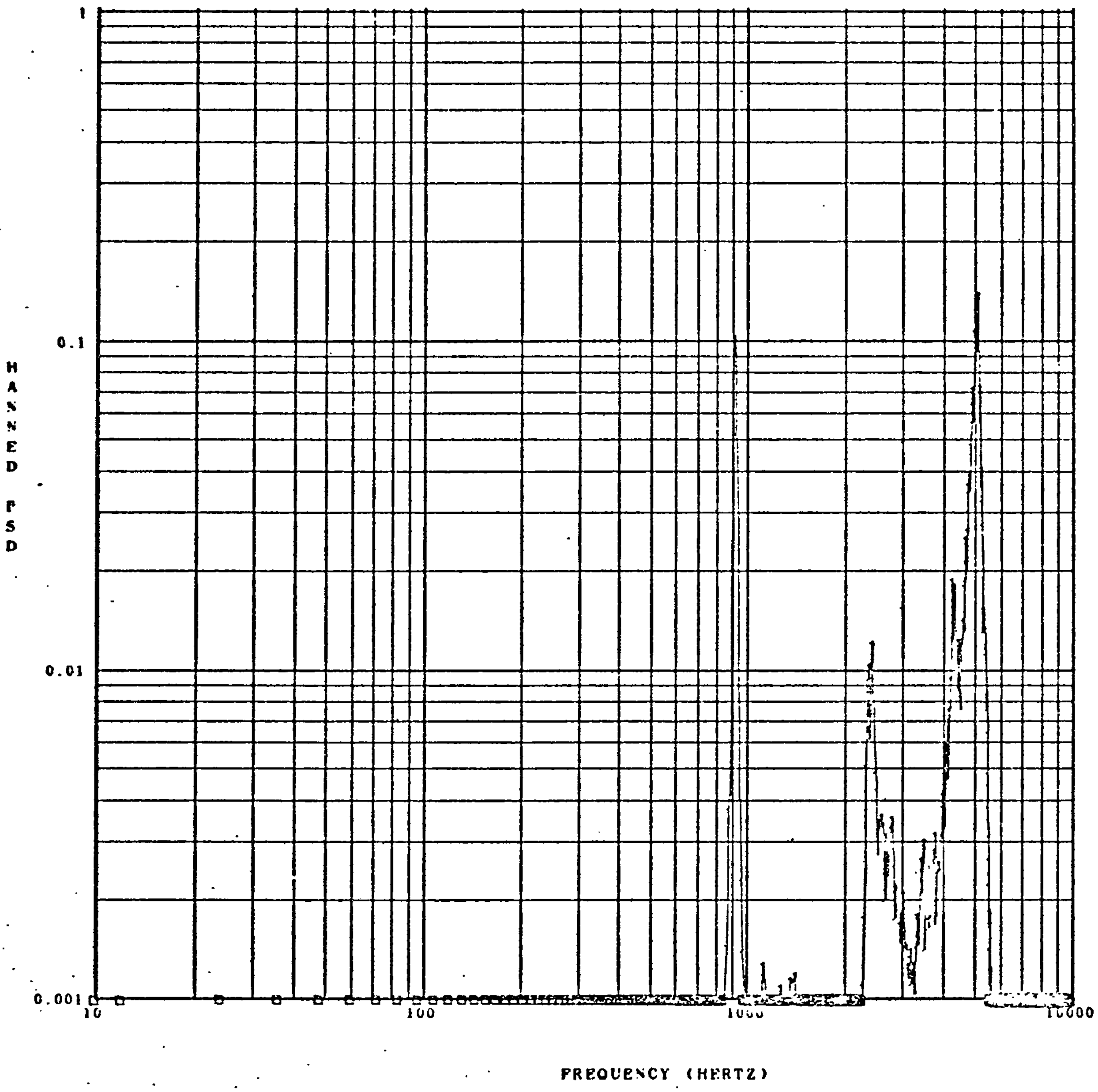

PAGE 7.

(f) Acceleration Spectral Density

Fig. A3.1 (Continued)

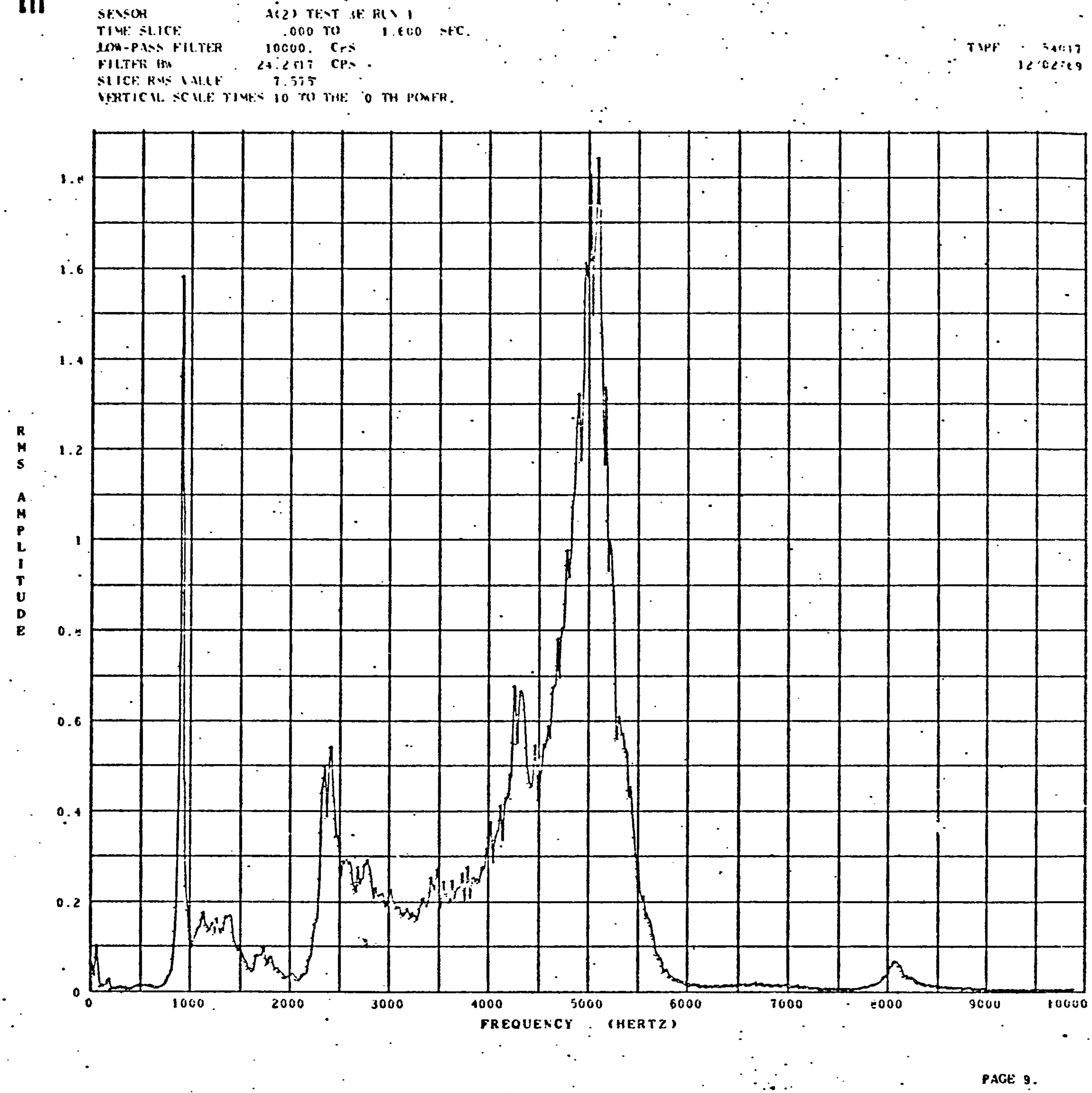

(g) Acceleration rms Spectrum

Fig. A3.1 (Continued)

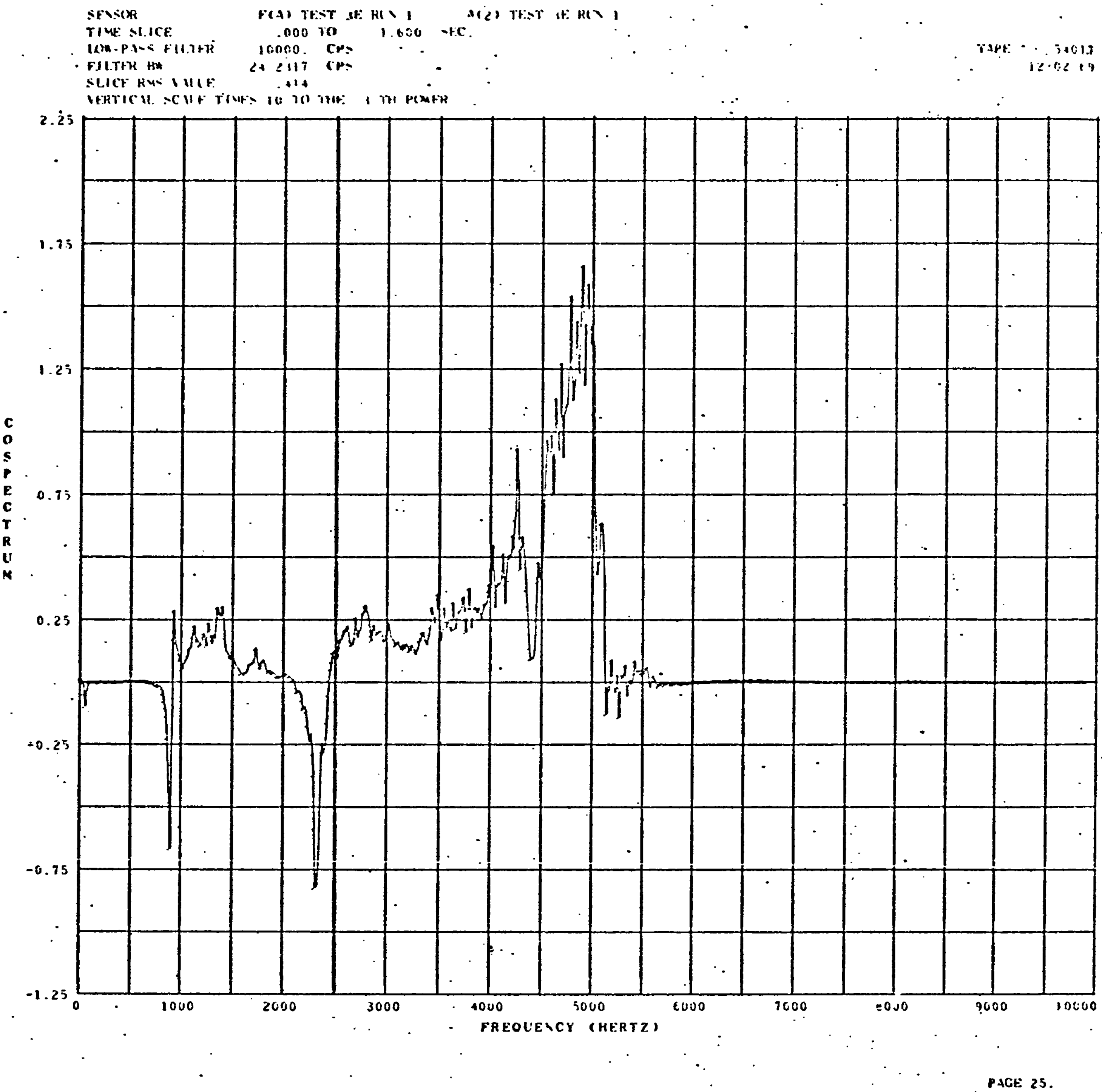

(h) Co-Spectral Density Between Acceleration and Force

Fig. A3.1 (Continued)

SENSOR F(A) TEST 3E RUN 1 A(2) TEST 3E RUN 1
TIME SLICE .000 TO 1.600 SEC.
LOW-PASS FILTER 10000. CPS
FILTER BW 24.2317 CPS
SLICE RMS VALUE .414
VERTICAL SCALE TIMES 10 TO THE 3 TH POWER.

TAPE 54017
12-02-69

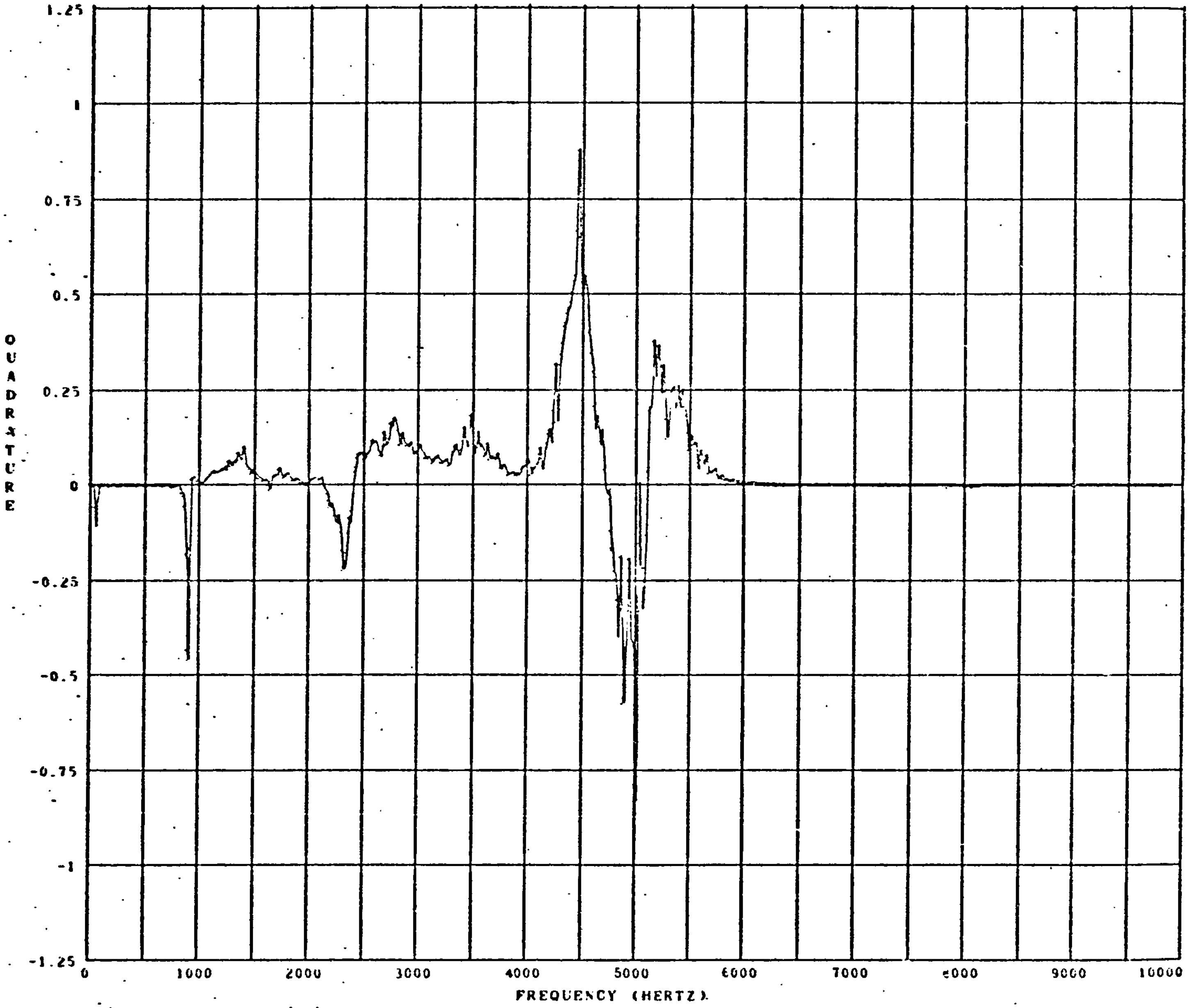

PAGE 26.

(i) Quadrature-Spectral Density Between Acceleration and Force

Fig. A3.1 (Continued)

SENSOR F(X) TEST 3E RUN 1 A(2) TEST 3E RUN 1
TIME SLICE .000 TO 1.600 SEC.
LOW-PASS FILTER 10000. CPS TAPE 54017
FILTER B= 24.2317 CPS 12-02-69
SLICE RMS VALUE .414

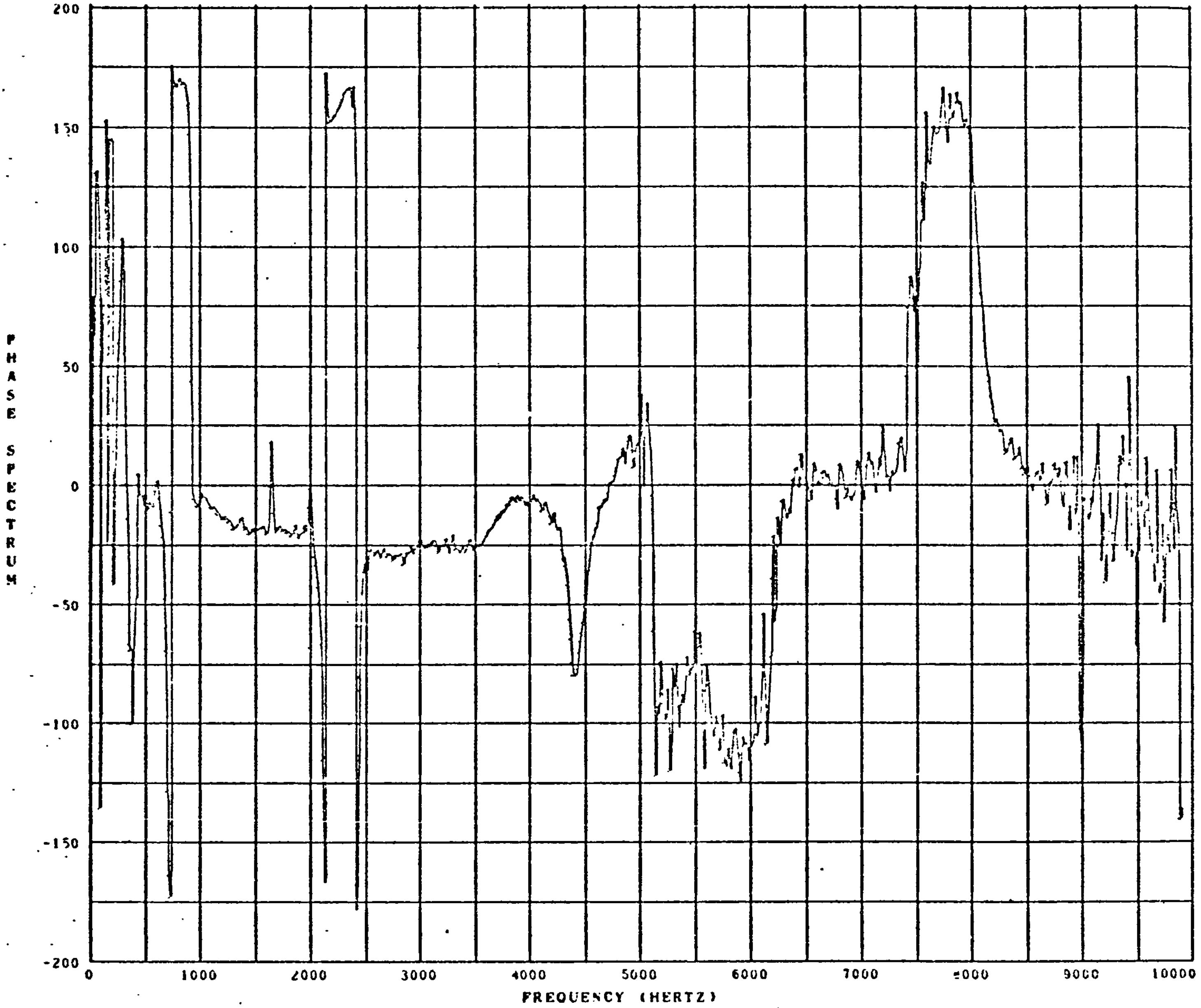

PAGE 27.

(j) Phase of Cross-Spectral Density Between Acceleration and Force

Fig. A3.1 (Continued)

SENSOR F(A) TEST 3F RUN 1 A(Z) TEST 3F RUN 1
TIME SLICE .000 TO 1.600 SEC.
LOW-PASS FILTER 10000. CPS
FILTER BW 24.2417 CPS
SLICE RMS VALUE .414
VERTICAL SCALE TIMES 10 TO THE 3 TH POWER.

TAPE 54617
12/02/69

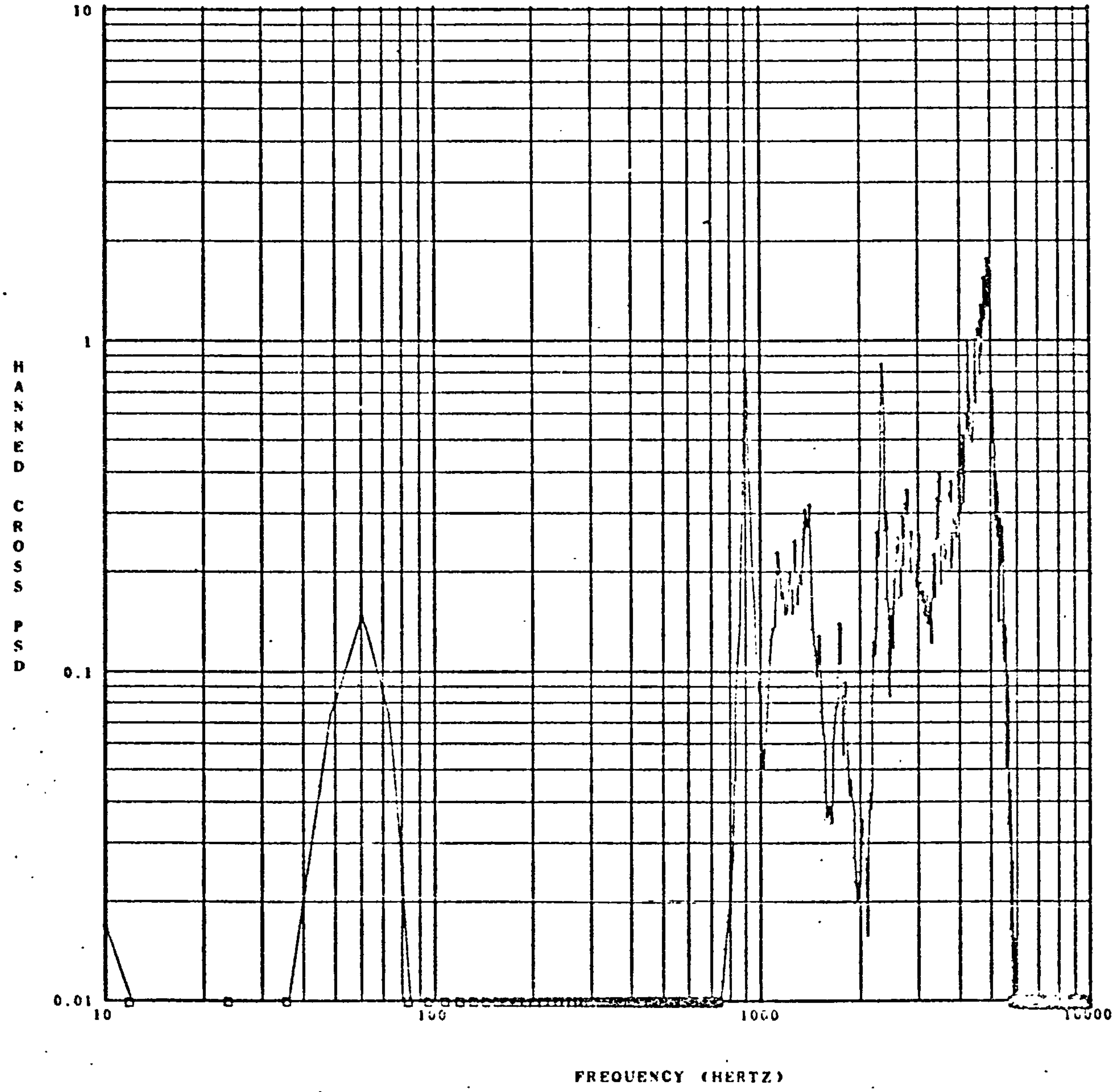

PAGE 28.

(k) Magnitude of Cross-Spectral Density Between Acceleration and Force

Fig. A3.1 (Continued)

SENSOR F(1) TEST 3E RUN 1 A(2) TEST 3E RUN 1
TIME SLICE .000 TO 1.600 SEC.
LOW-PASS FILTER 10000. CPS
FILTER BW 24.2317 CPS
SLICE RMS VALUE .414
VERTICAL SCALE TIMES 10 TO THE 0 TH POWER.

TAPE 54017
12:02

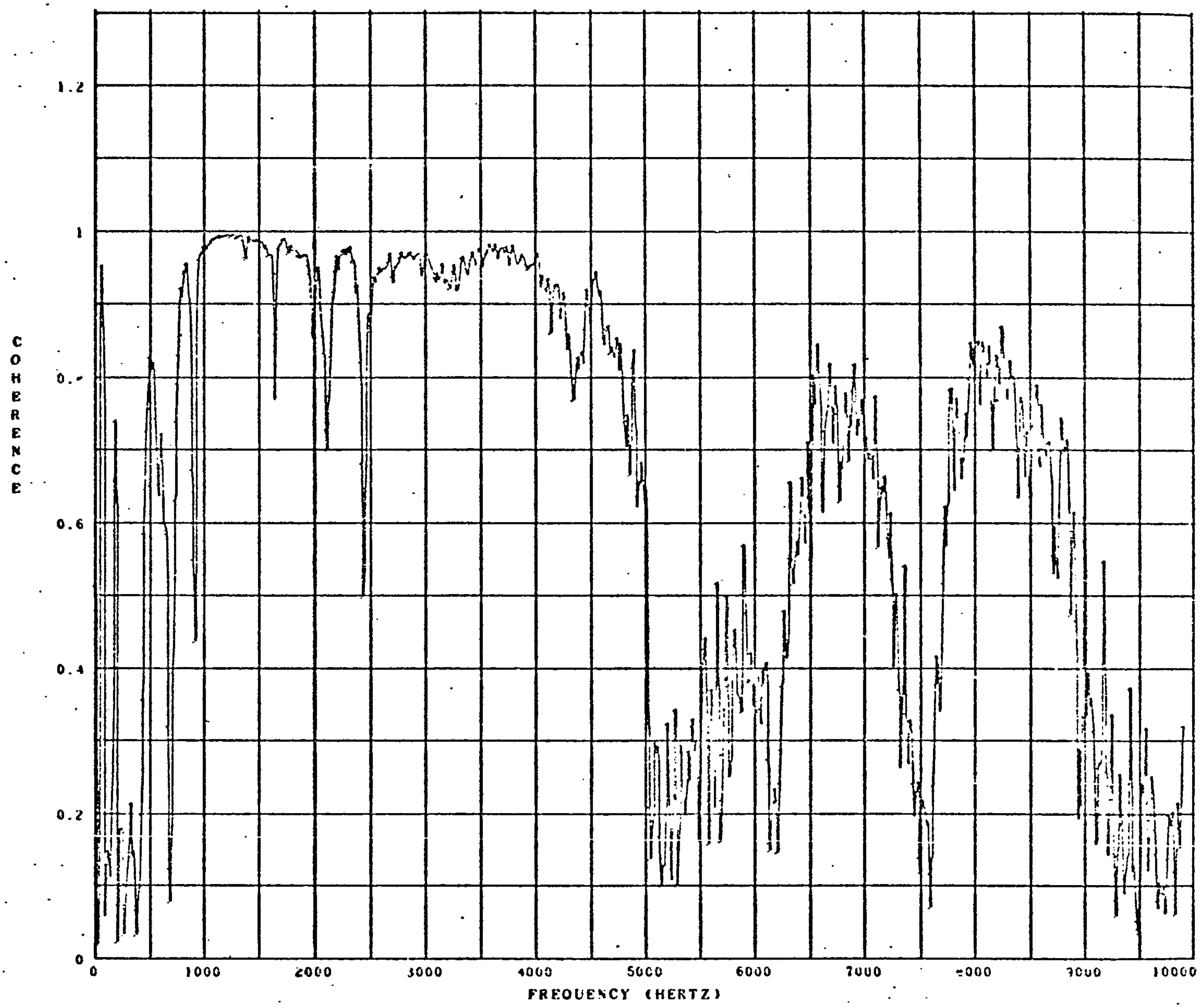

PAGE 30.

(1) Coherence Between Acceleration and Force

Fig. A3.1 (Continued)

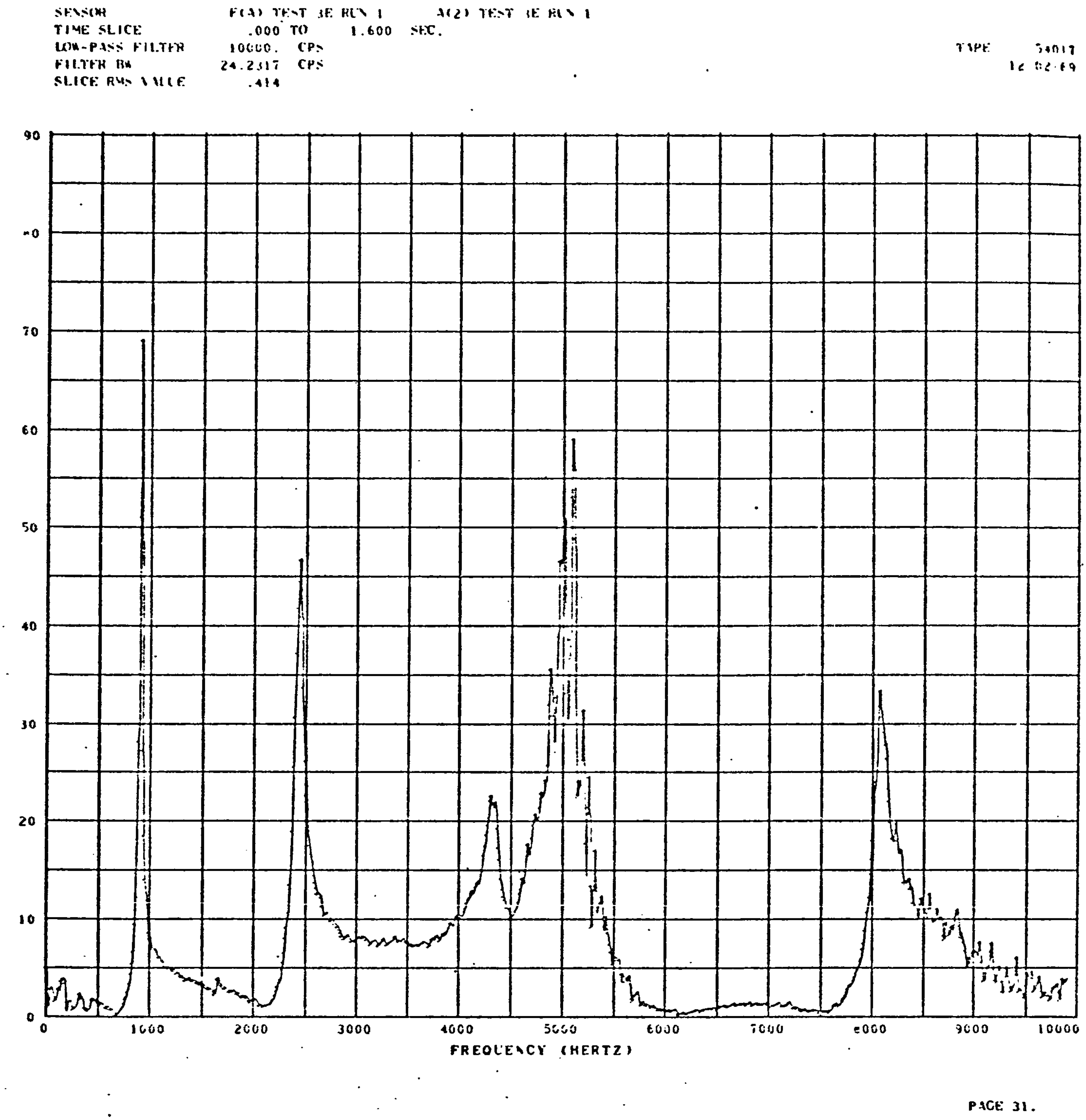

(m) Transfer Function Between Acceleration and Force

Fig. A3.1 (Continued)

Autocorrelation functions for the above acceleration and force are shown in Figures A3.1d and A3.1e, pages 130 and 131, respectively. The force autocorrelation exhibits the characteristics of wide-band random data with high frequency spectral content, in that the correlation dies out fast. The acceleration autocorrelation exhibits the characteristics of narrow-band random data, in that the signal is correlated for a much longer period of time. Note also that the acceleration higher frequency content (approximately 5000 Hz) dies out faster than the low-frequency content (approximately 900 Hz). This is because the 900 Hz resonance has a much narrower band-width than the higher resonance frequency, i.e., this resonance is more lightly damped, as was shown in Figure 4.2, page 76. Note also that the essential differences between narrow-band acceleration and wide-band force were illustrated in the spectral density plots of Figures 4.2b and 4.4a, pages 77 and 82.

Equations and definitions for the quantities are to be found in Appendix 1.

Appendix 4

SIMPLY-SUPPORTED PLATE TESTS 7b AND 8b

Presented in this appendix are the data from Complex Excitation Test 7b and Simulation Test 8b for the simply-supported rectangular plate. These tests were conducted in the manner of Tests 7a and 8a of Chapter 3, except that in Test 7b the shaker was attached to the plate. Although not excited electrically, the shaker did provide a large narrow-band force input, as shown in Fig. A4.5, by virtue of its connection to the plate and the shaker support structure.

SENSOR 1 A(1) TEST 7B RUN 1 REQ DJ 468
TIME SLICE .000 TO 3.200 SEC.
LOW-PASS FILTER 5000. CPS
FILTER BW 12.1769 CPS
SLICE RMS VALUE 3.646
VERTICAL SCALE TIMES 10 TO THE 0 TH POWER.

TAPE 56*63
01/19/70

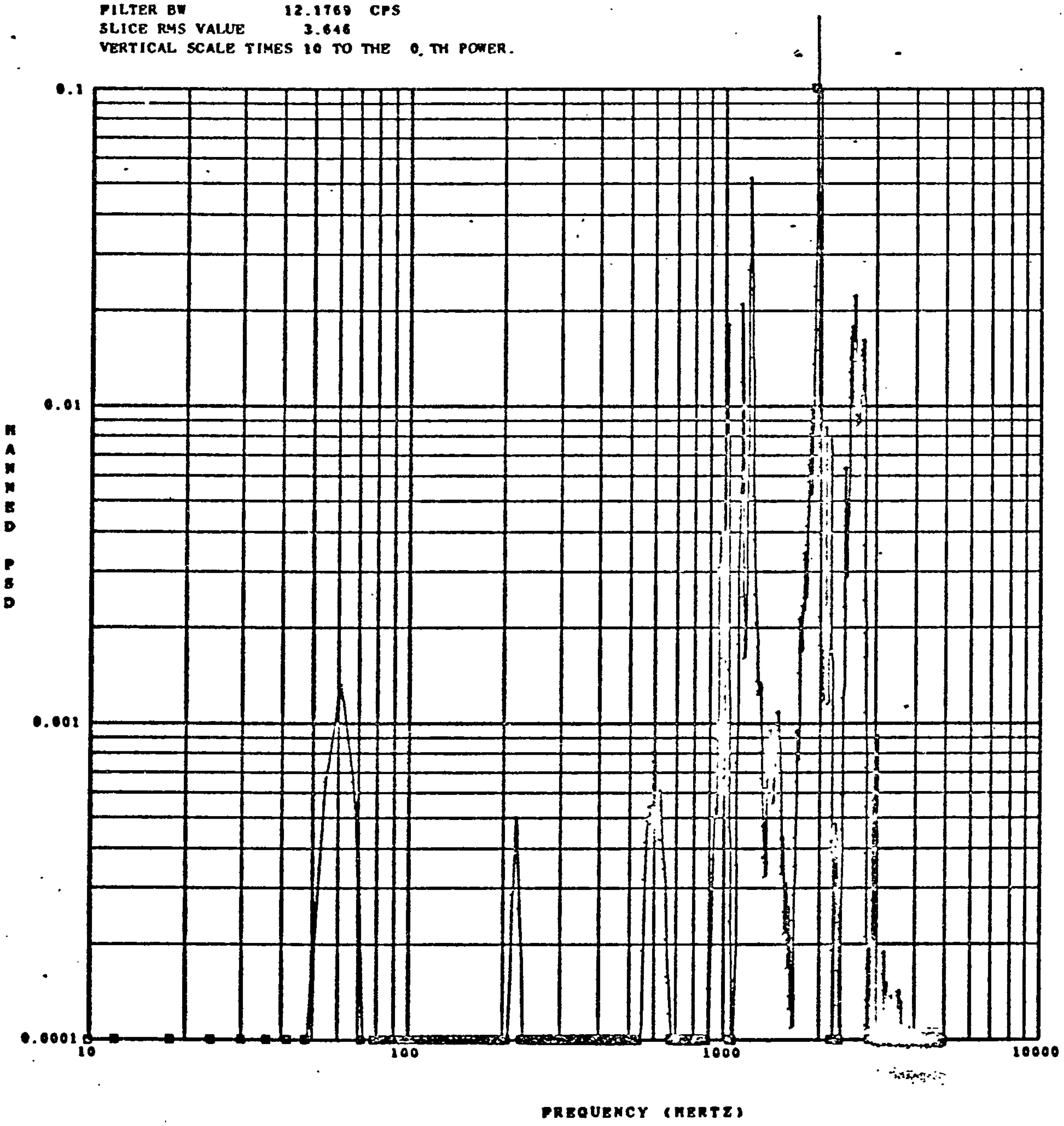

PAGE 9.

(a) Test 7b

Fig. A4.1 Spectral Density of Center-Plate Acceleration A_1 on Simply-Supported Plate

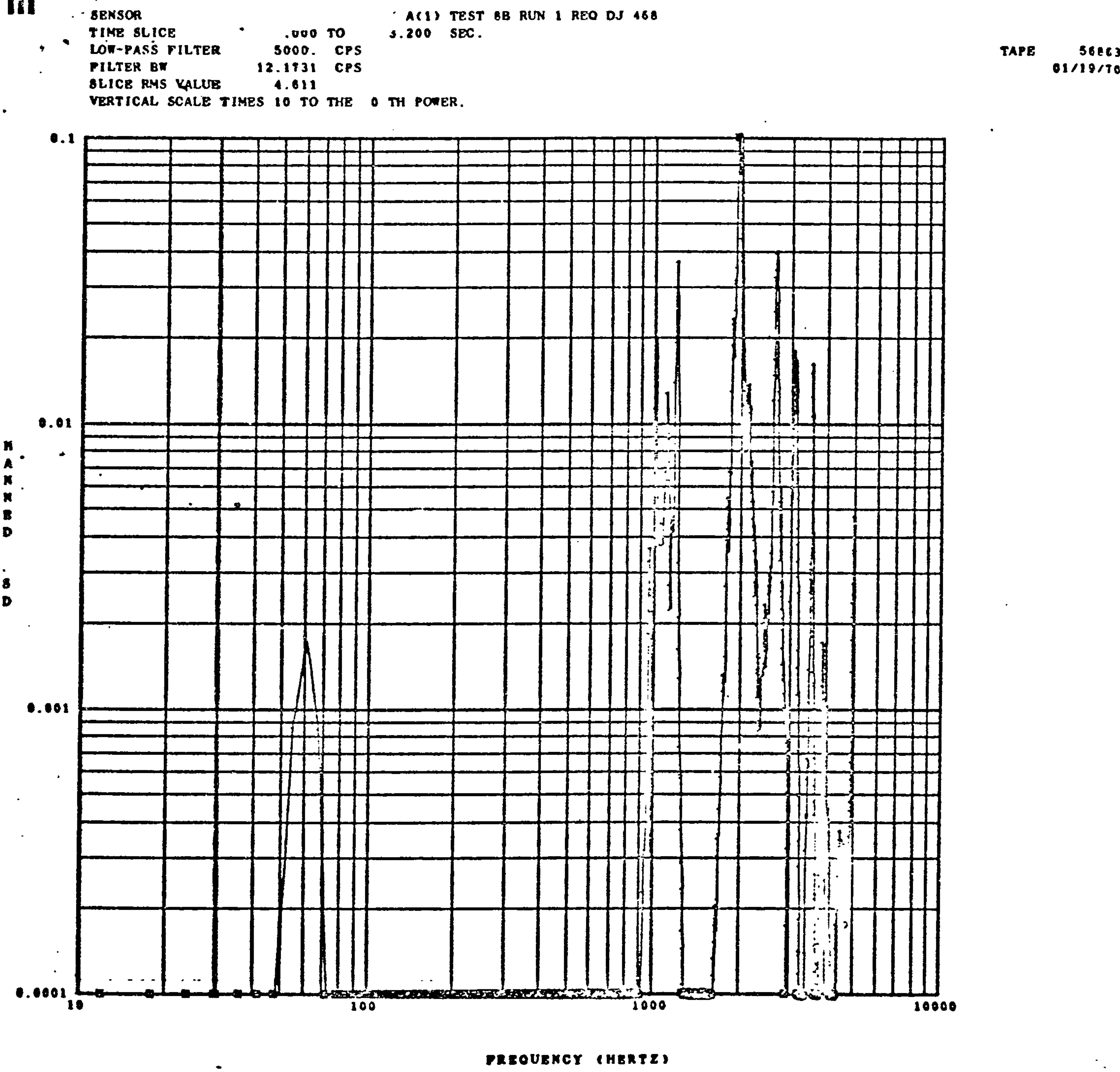

(b) Test 8b

Fig. A4.1 (Continued)

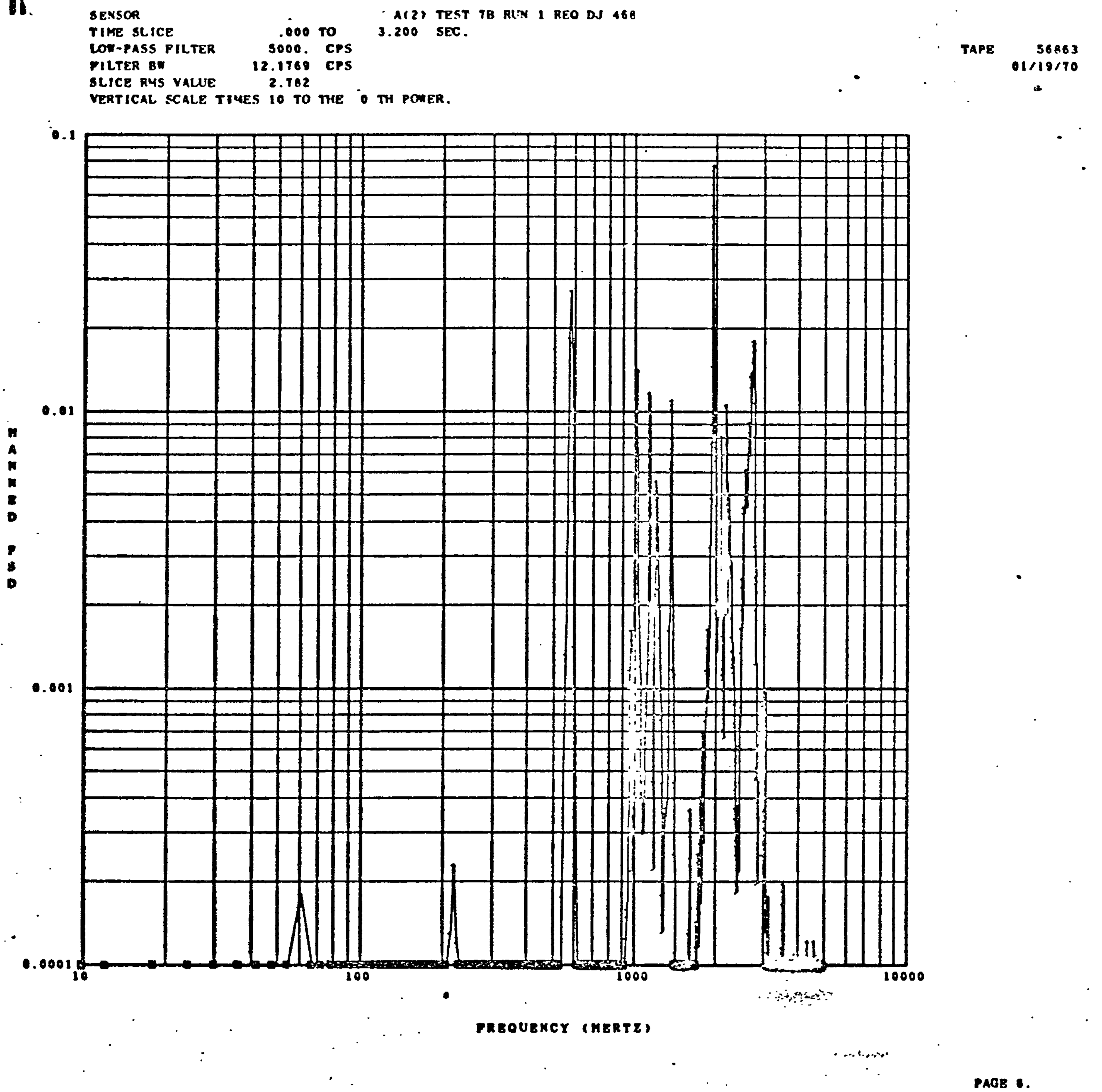

(a) Test 7b

Fig. A4.2 Spectral Density of Quarter-Plate Acceleration A_2 on Simply-Supported Plate

SENSOR A(2) TEST 8B RUN 1 REQ DJ 468
TIME SLICE .000 TO 3.200 SEC.
LOW-PASS FILTER 5000. CPS
FILTER BW 12.1731 CPS
SLICE RMS VALUE 4.009
VERTICAL SCALE TIMES 10 TO THE 0 TH POWER.

TAPE 56[illegible]
01/19/[illegible]

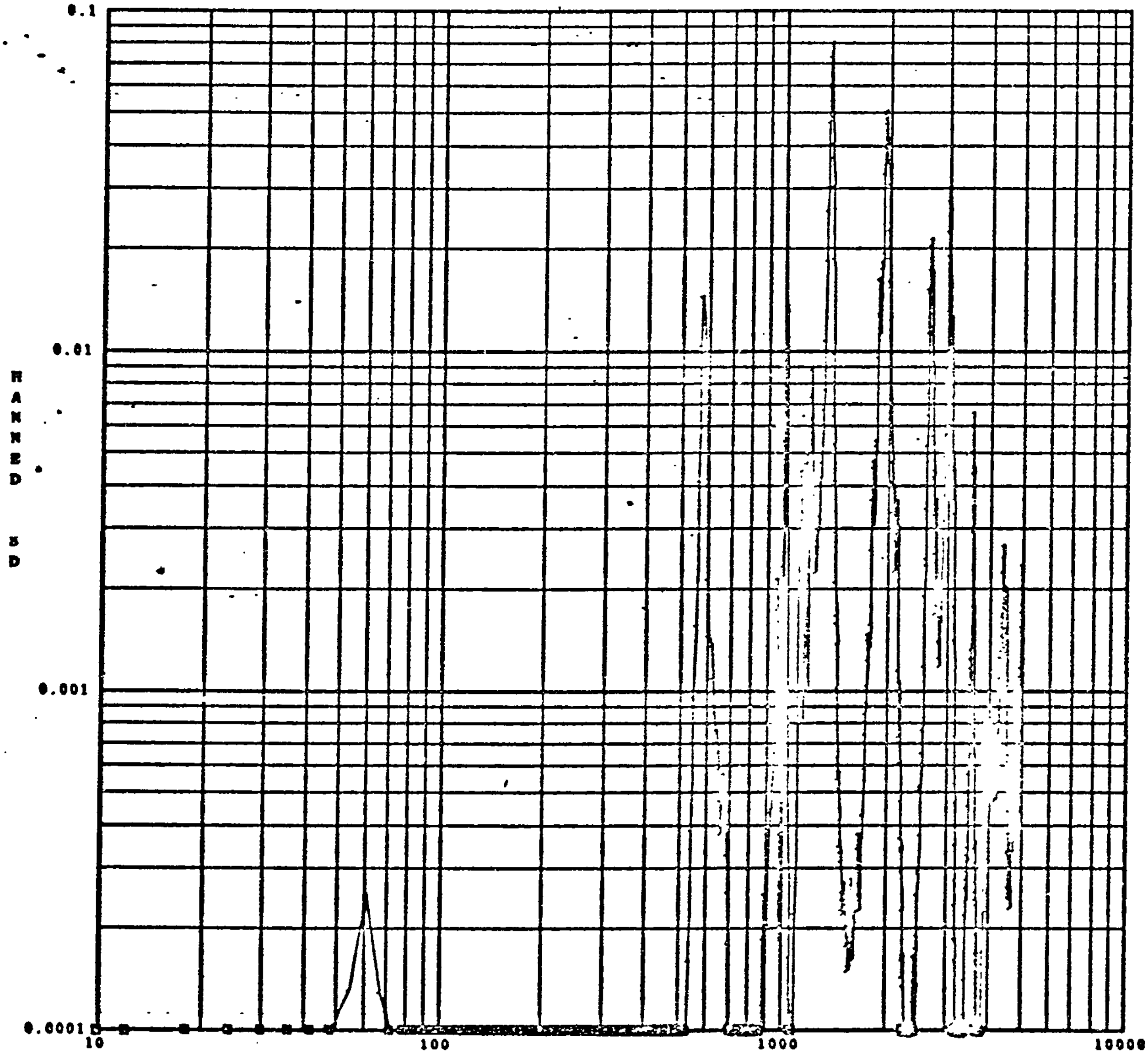

PAGE 8.

(b) Test 8b

Fig. A4.2 (Continued)

SENSOR A(1) TESCANTILEVER BEAM A(2) TES
TIME SLICE .000 TO 3.200 SEC.
LOW-PASS FILTER 5000. CPS
FILTER BW 12.1769 CPS
SLICE RMS VALUE 3.646
VERTICAL SCALE TIMES 10 TO THE 0 TH POWER.

TAPE 56863
01/19/70

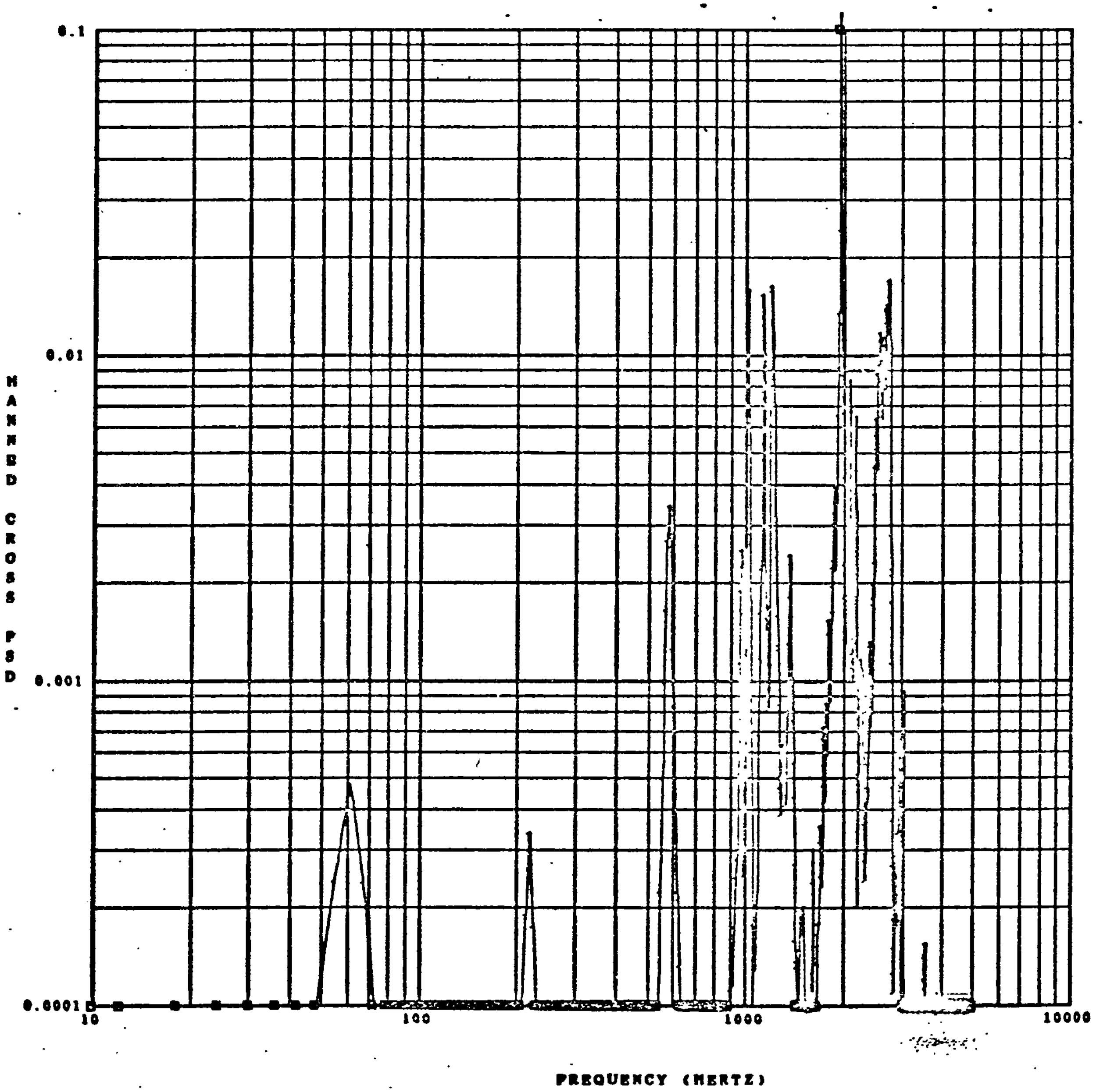

PAGE 45.

(a) Test 7b

Fig. A4.3 Acceleration Cross-Spectral Density Magnitude of Accelerometers A_1 and A_2 on Simply-Supported Plate.

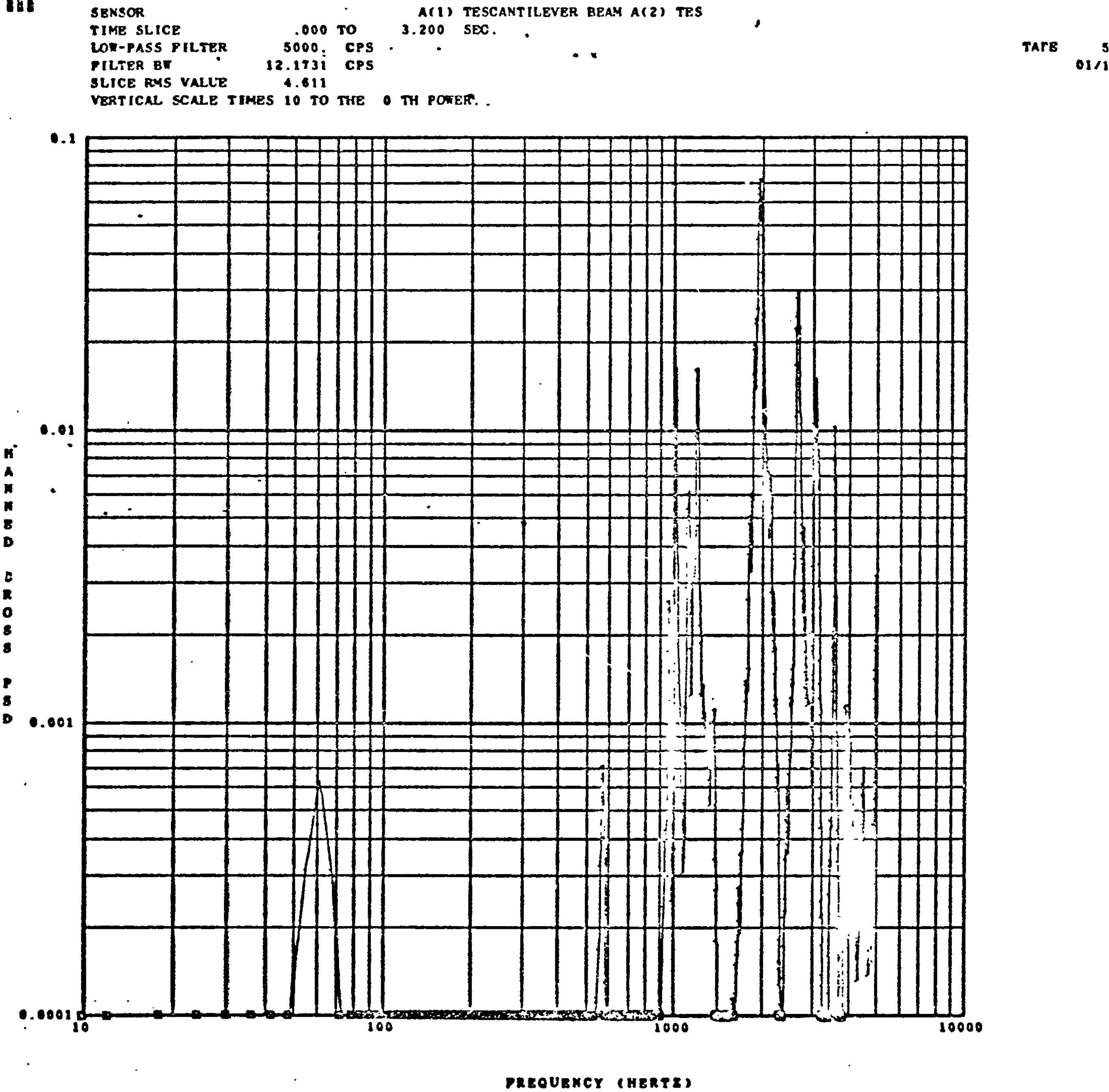

(b) Test 8b

Fig. A4.3 (Continued)

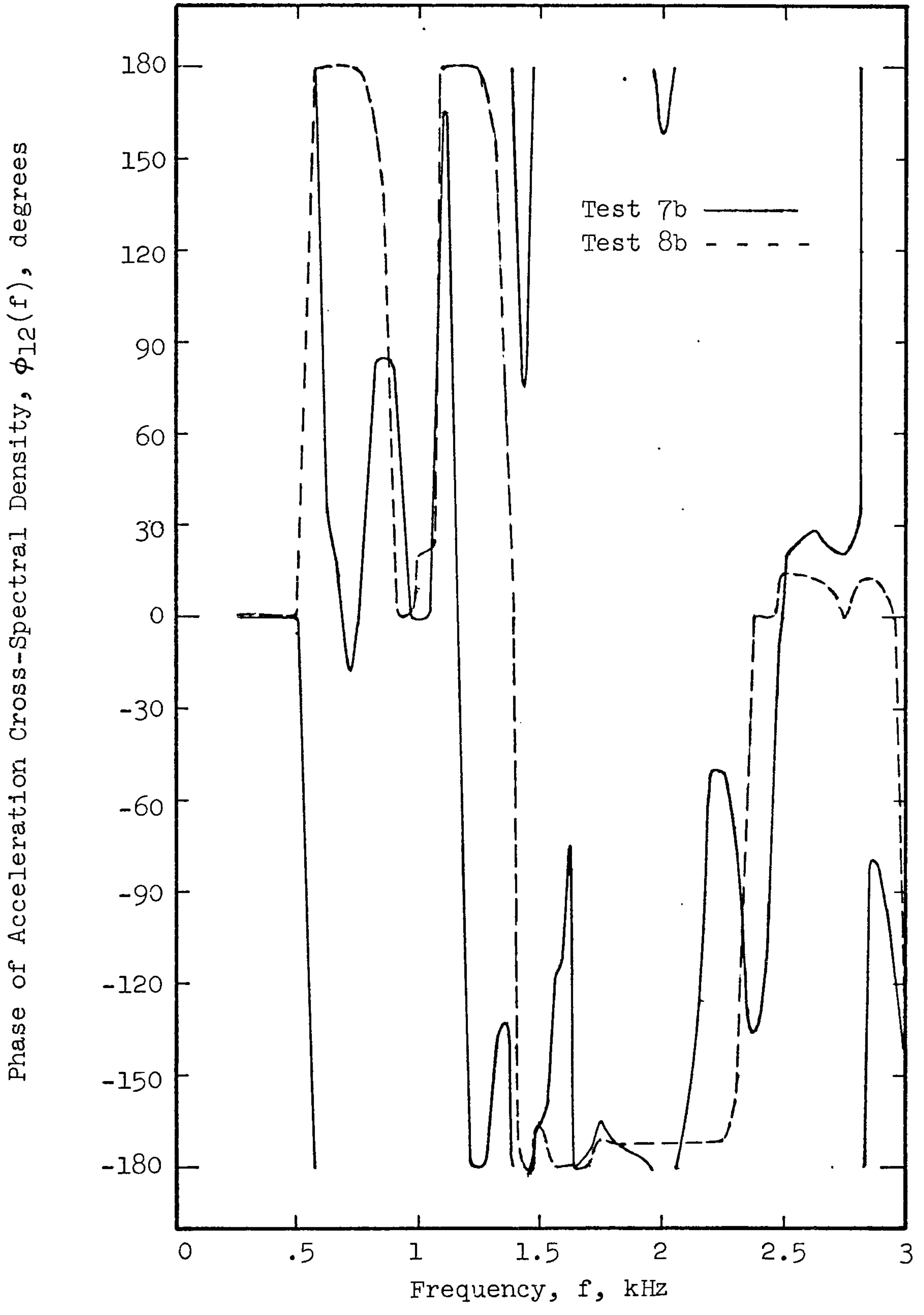

Fig. A4.4 Comparison of Acceleration Cross-Spectral Density Phase of Accelerometers A_1 and A_2 for Complex Excitation Test 7b and Simulation Test 8b on Simply-Supported Plate

SENSOR . P TEST 7B RUN 1 REQ DJ 468
TIME SLICE .000 TO 3.200 SEC.
LOW-PASS FILTER 5000. CPS
FILTER BW 12.1769 CPS
SLICE RMS VALUE .002
VERTICAL SCALE TIMES 10 TO THE 6 TH POWER.

TAPE 56863
01/19/70

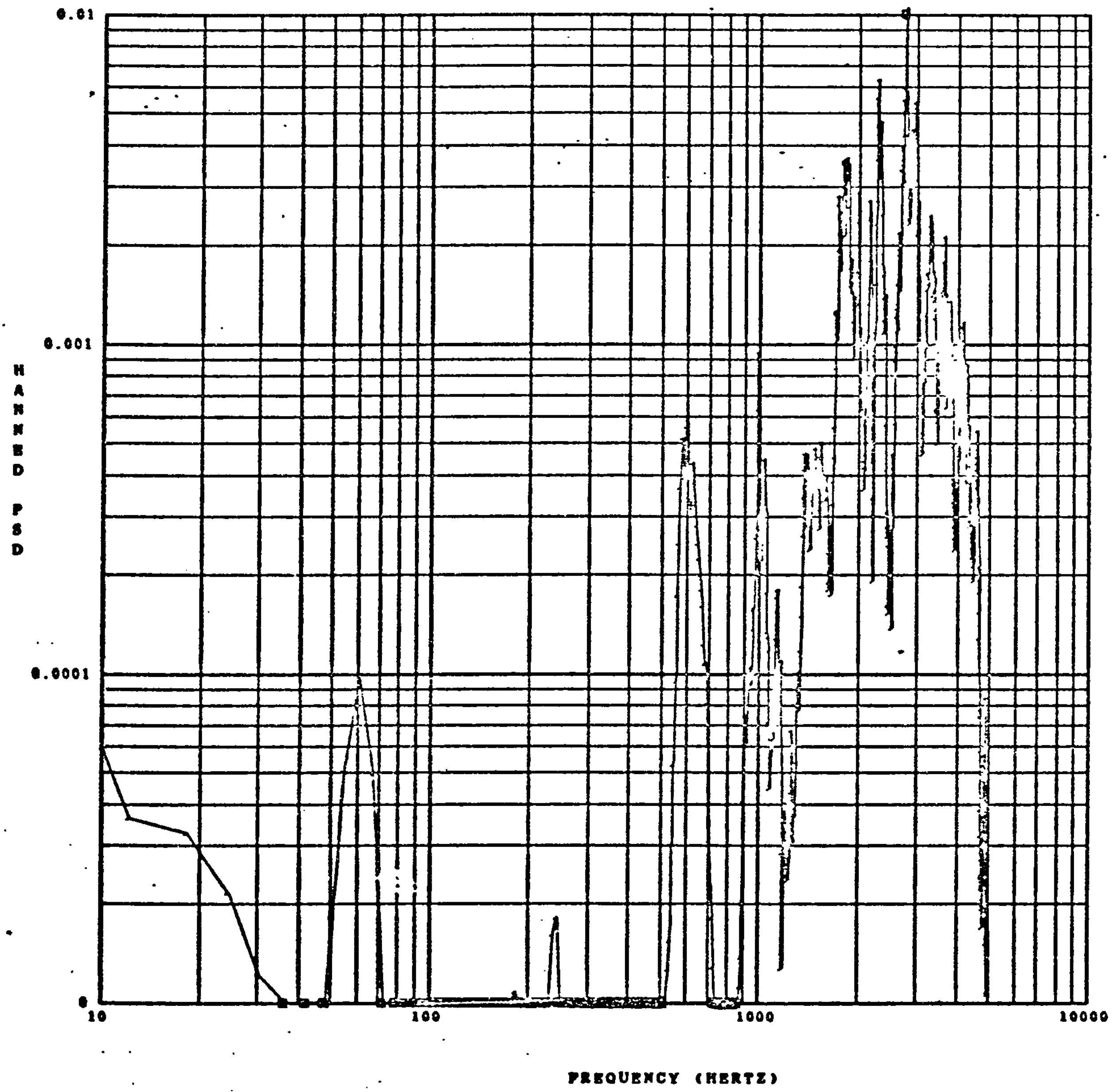

PAGE 9.

(a) Pressure Spectral Density

Fig. A4.5 Complex Excitation of Test 7b

SENSOR F(A) TEST 7B RUN 1 REQ DJ 468
TIME SLICE .000 TO 3.200 SEC.
LOW-PASS FILTER 5000. CPS
FILTER BW 12.1769 CPS
SLICE RMS VALUE .093
VERTICAL SCALE TIMES 10 TO THE 3 TH POWER.

TAPE 56863
01/19/70

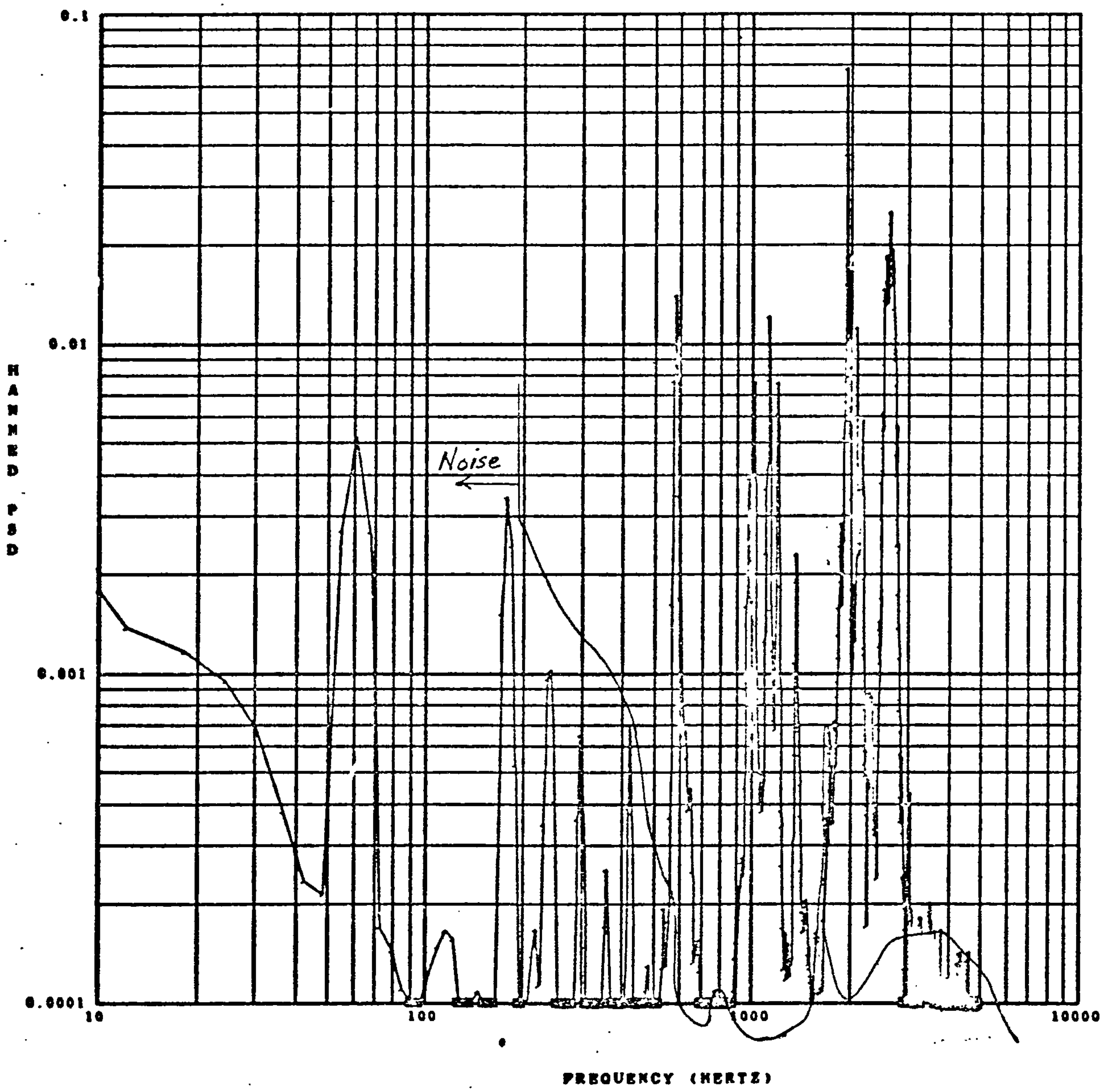

PAGE 8.

(b) Force Spectral Density

Fig. A4.5 (Continued)

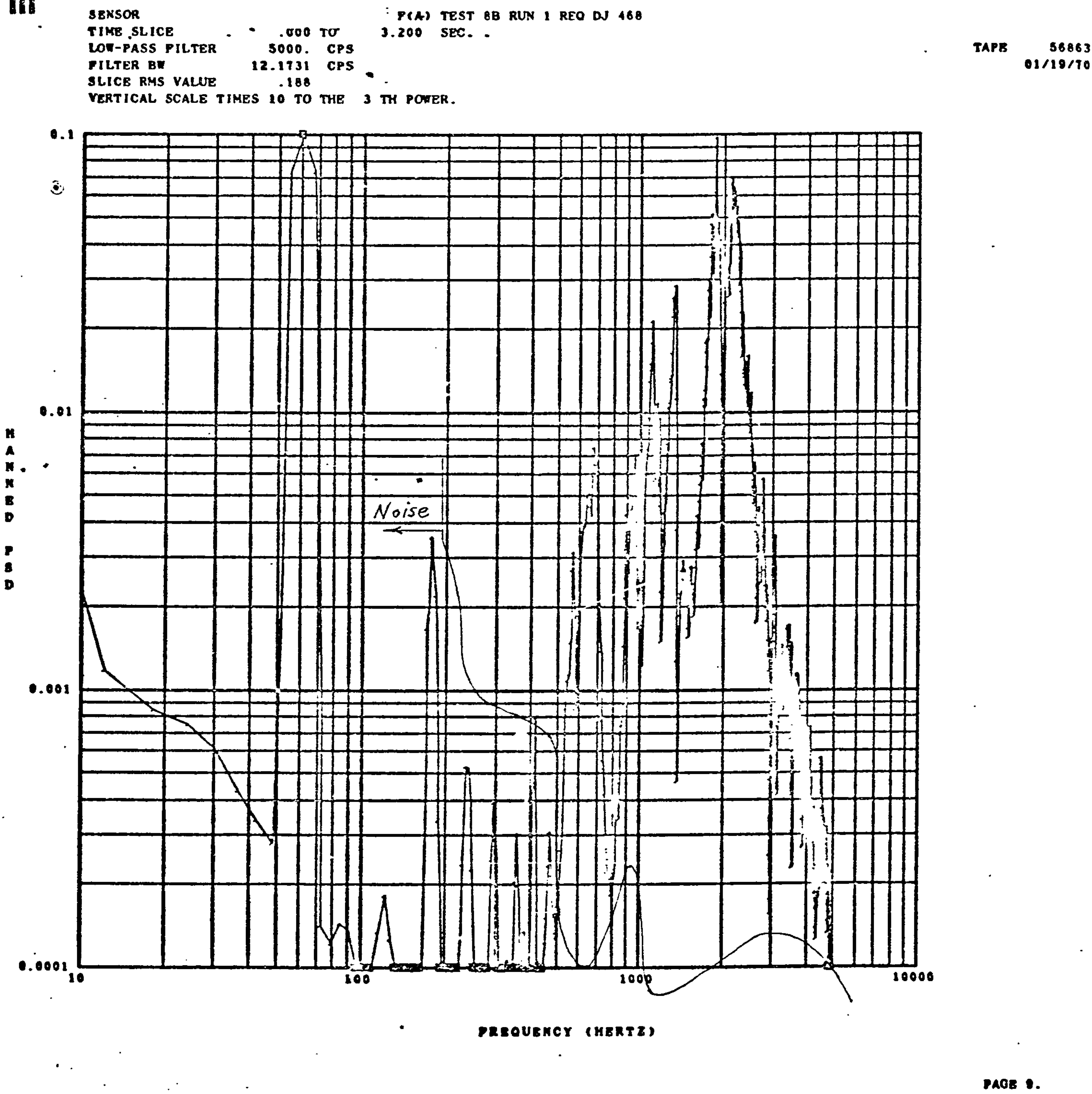

Fig. A4.6 Simulation Force Spectral Density for Test 8b.

Appendix 5

CANTILEVER BEAM TESTS 3a, 4a, 3b AND 4b

Presented in this appendix are the data from Complex Excitation Tests 3a and 3b and their respective Simulation Tests 4a and 4b for the cantilever beam. These tests were conducted in the manner of Tests 3d, 4d, 3e, and 4e of Chapter 3, except that the shakers were mounted on a 3/8-inch steel shaker support structure, as shown in Fig. 3.2a, page 34. This shaker support was found to respond significantly to excitation in the 2400-2700 Hz range when both shakers were attached to the beam. This tended to affect beam response in the vicinity of the third resonance, as shown in the following figures. The spectrum shaping filters had bandwidths which were too wide to simulate the response of this resonance. Therefore, the support structure of 1-inch steel was constructed for use in the tests reported in Chapters 3 and 4.

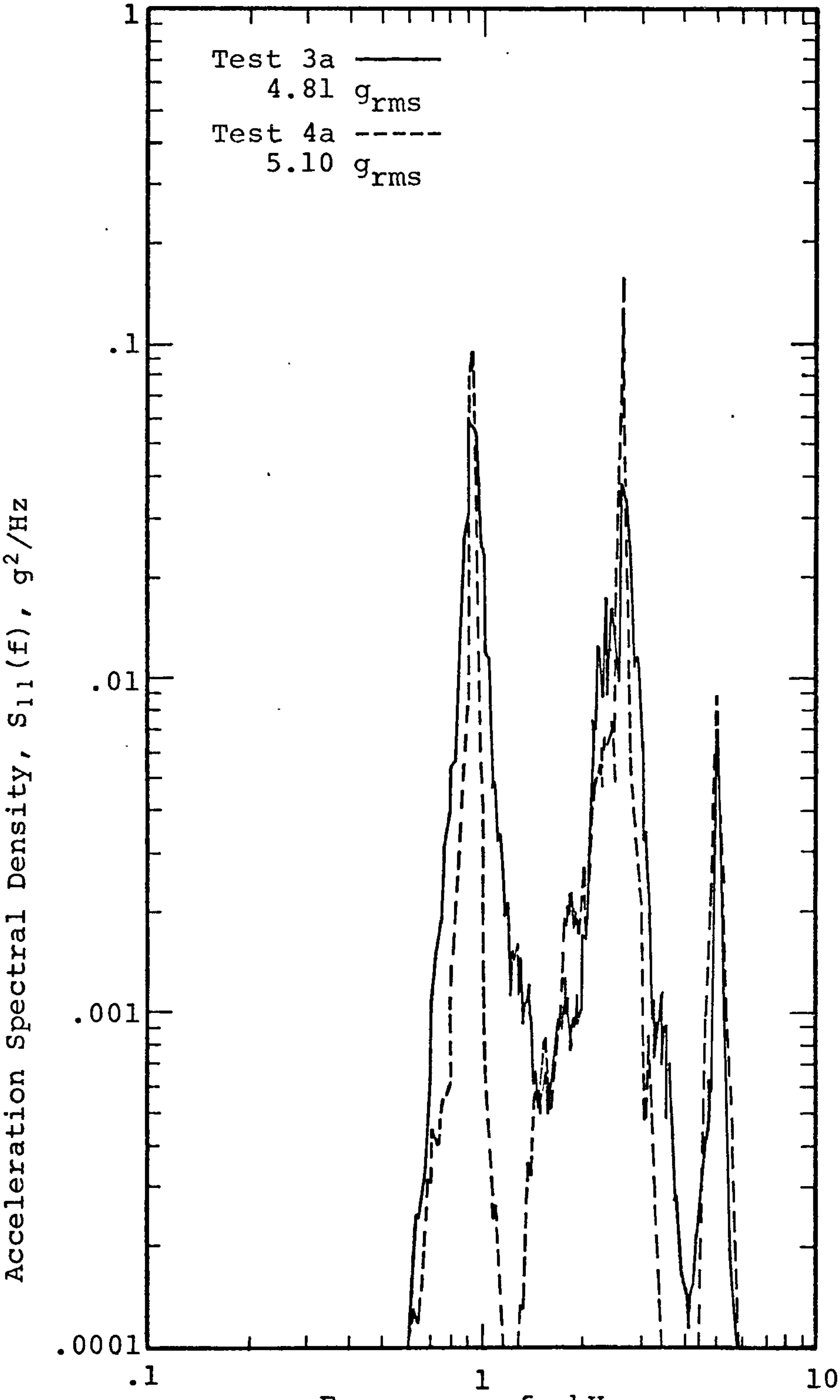

(a) Acceleration Spectral Density for Tip Accelerometer A_1

Fig. A5.1 Comparison of Complex Excitation Test 3a and Simulation Test 4a for Cantilever Beam (3/8-inch Shaker Support)

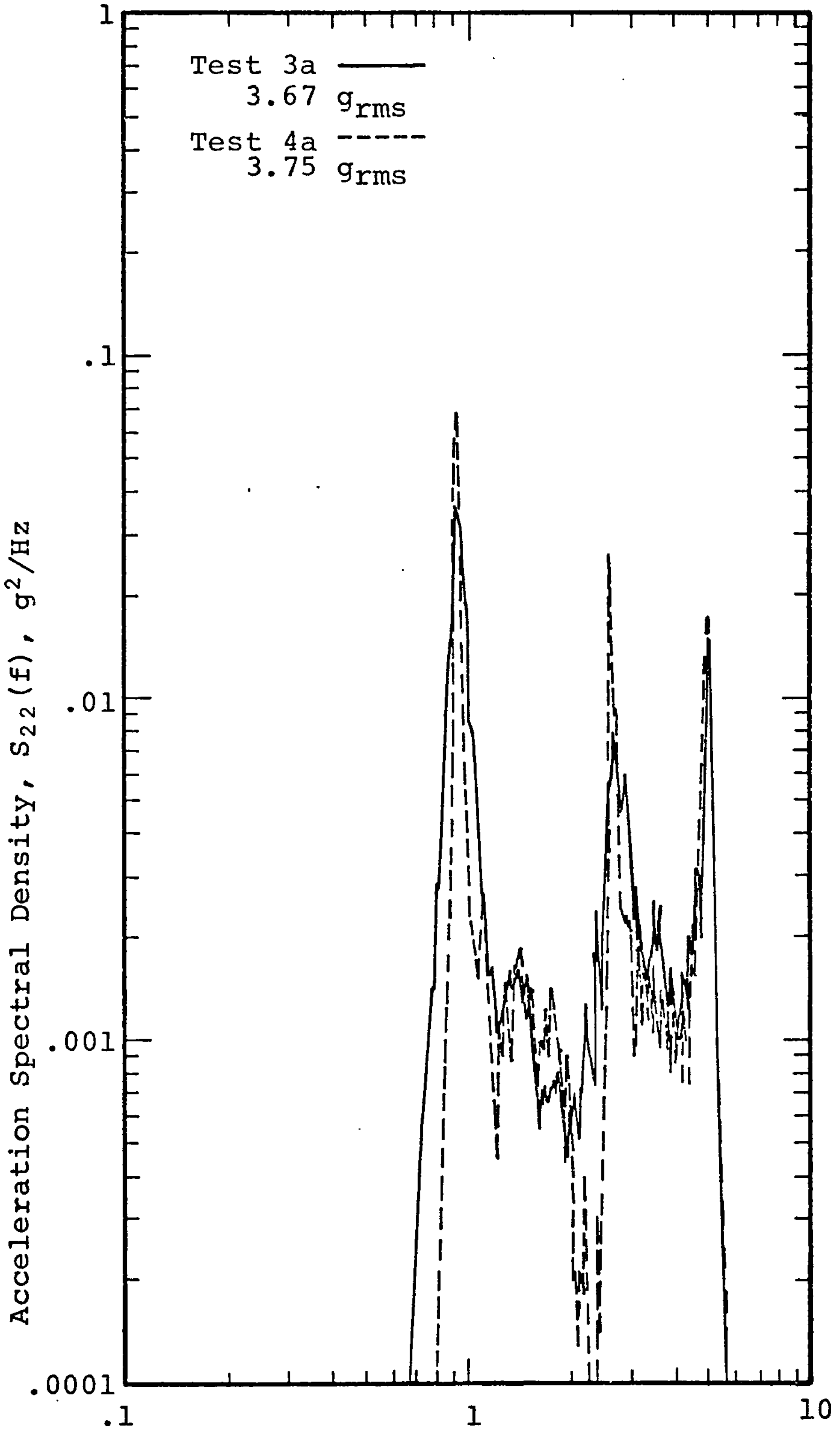

(b) Acceleration Spectral Density for Mid-length Accelerometer A_2

Fig. A5.1 (Continued)

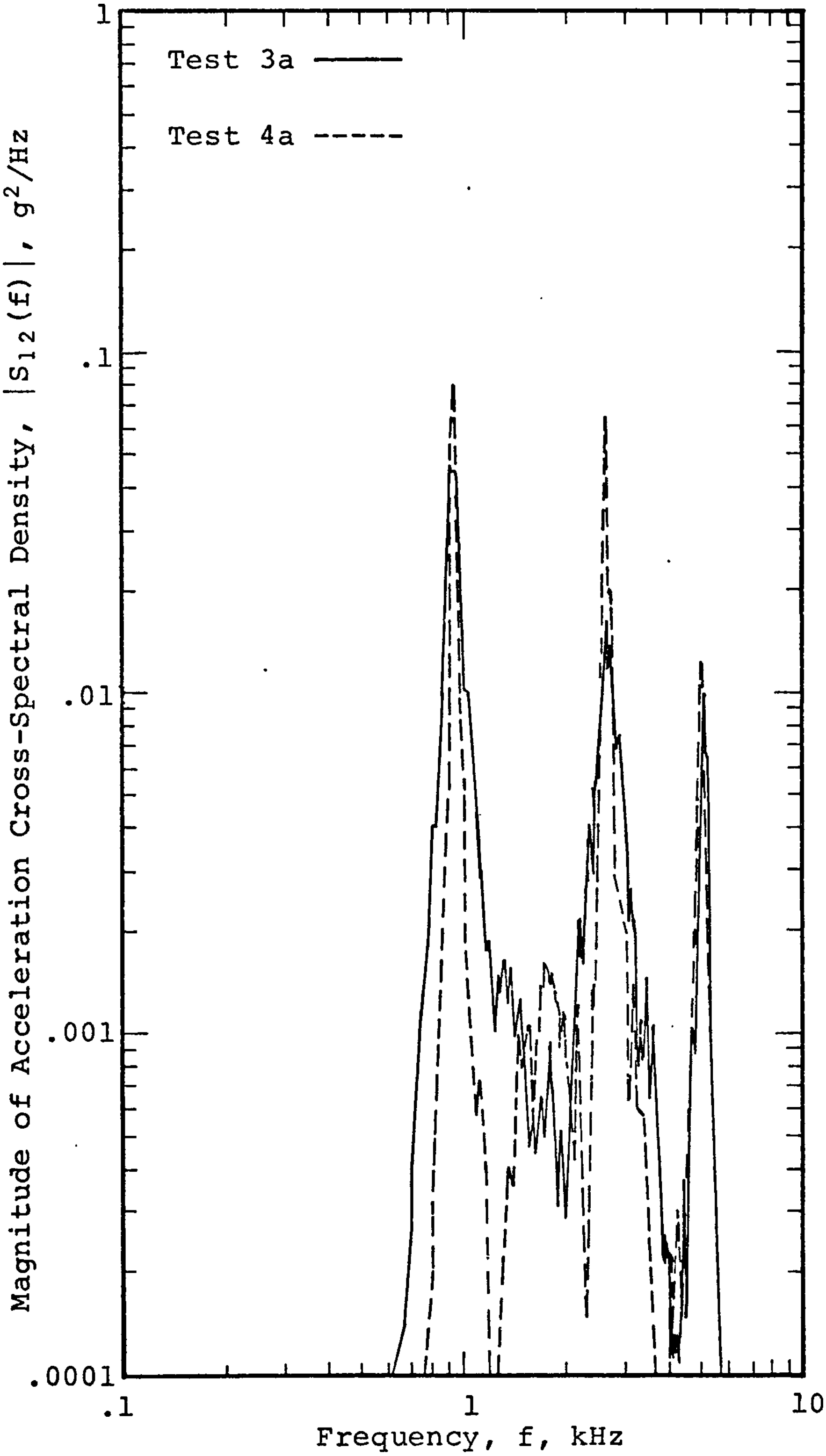

(c) Acceleration Cross-Spectral Density Magnitude for Accelerometers A_1 and A_2

Fig. A5.1 (Continued)

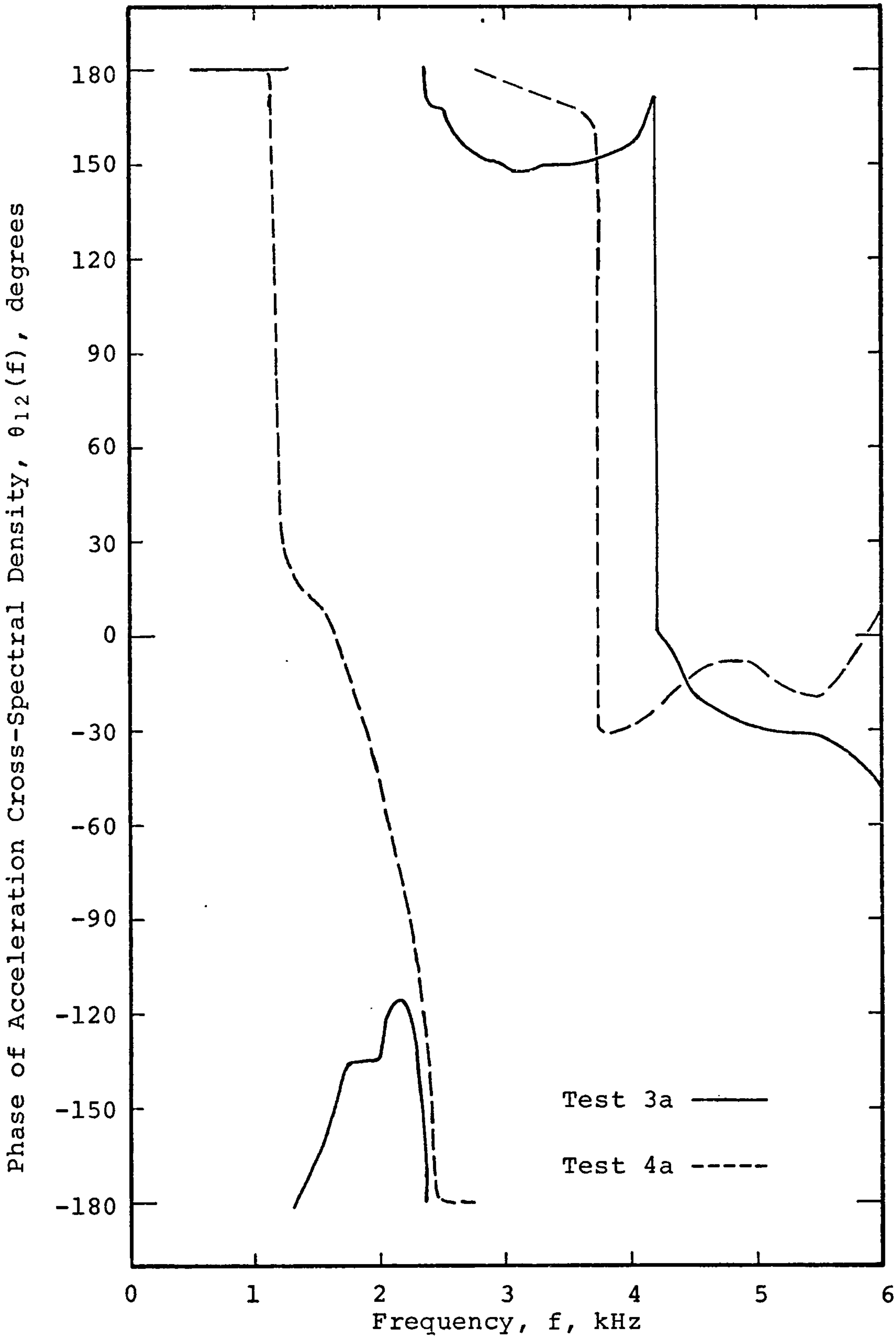

(d) Acceleration Cross-Spectral Density Phase for Accelerometers A_1 and A_2

Fig. A5.1 (Continued)

SENSOR F(A) TEST 3A RUN 2
TIME SLICE .008 TO 1.600 SEC.
LOW-PASS FILTER 6000. CPS
FILTER BW 24.4072 CPS
SLICE RMS VALUE .257
VERTICAL SCALE TIMES 1000.0

TAPE 5
10/1

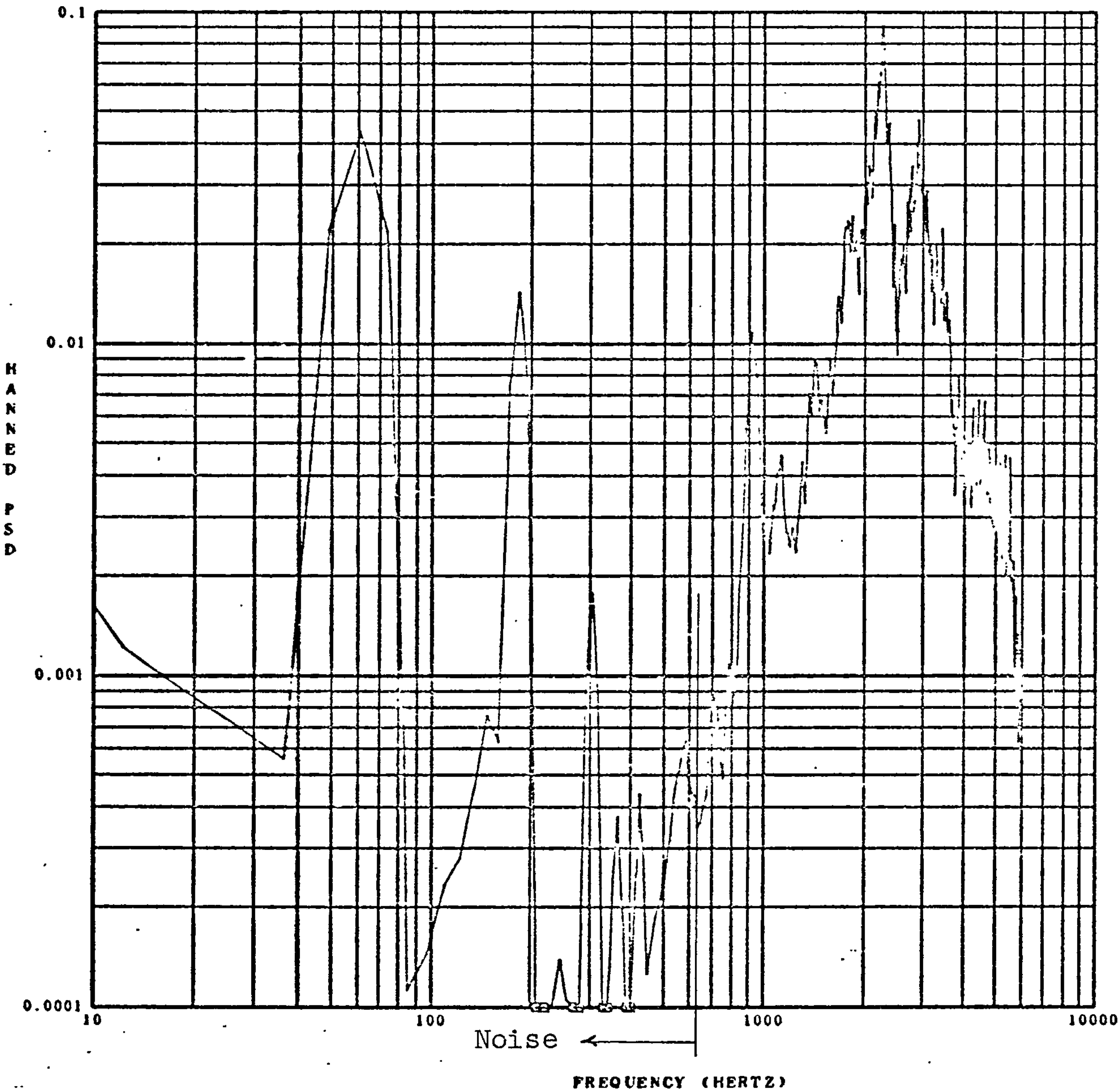

(a) F_A Force Spectral Density

PAGE 7.

Fig. A5.2 Complex Excitation of Test 3a

SENSOR F(B) TEST 3A RUN 2
TIME SLICE .008 TO 1.600 SEC.
LOW-PASS FILTER 6000. CPS
FILTER BW 24.4072 CPS
SLICE RMS VALUE .343
VERTICAL SCALE TIMES 1000.0

TAPE 546[illegible]
10/16/6[illegible]

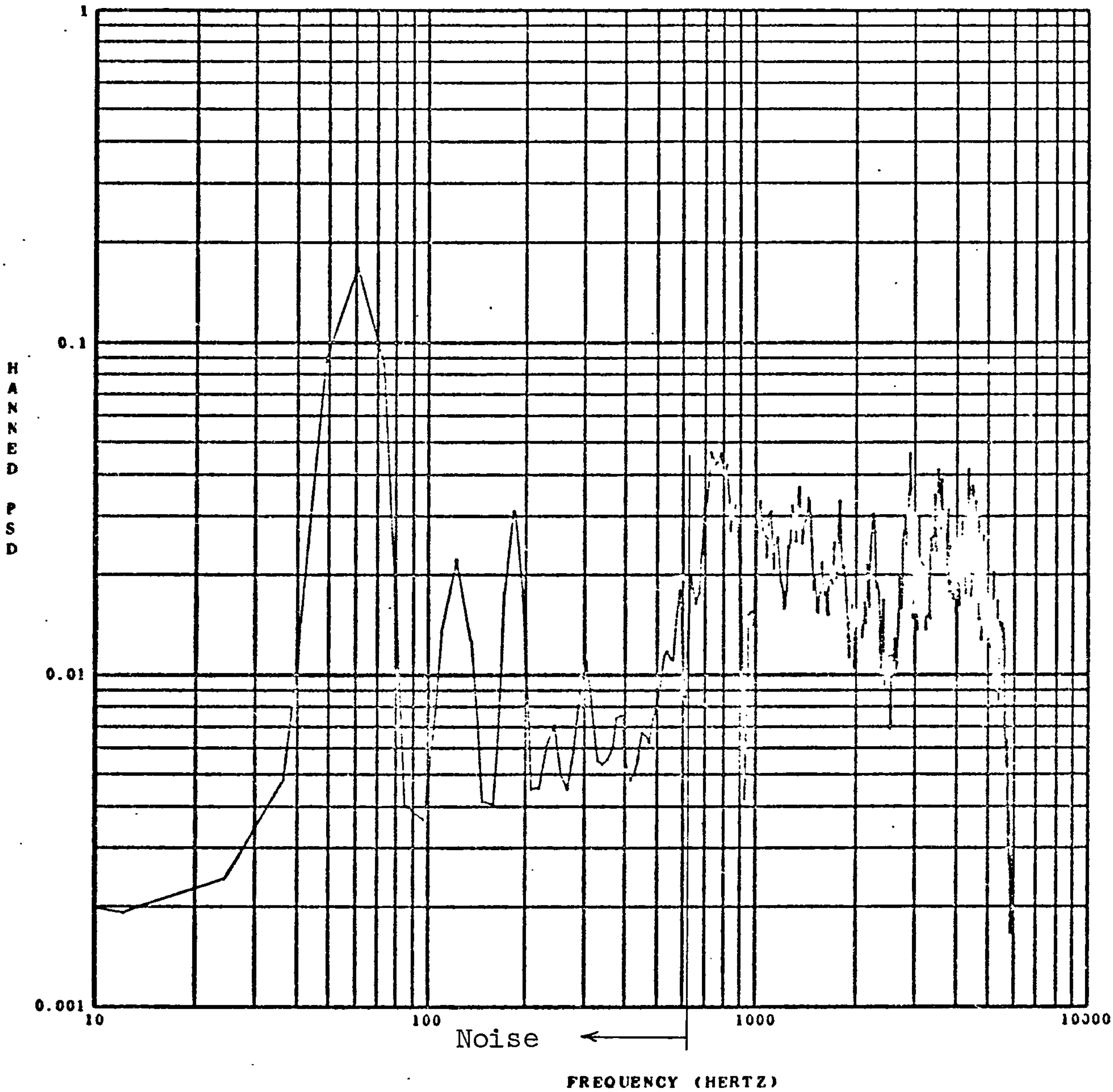

(b) F_B Force Spectral Density

PAGE 7.

Fig. A5.2 (Continued)

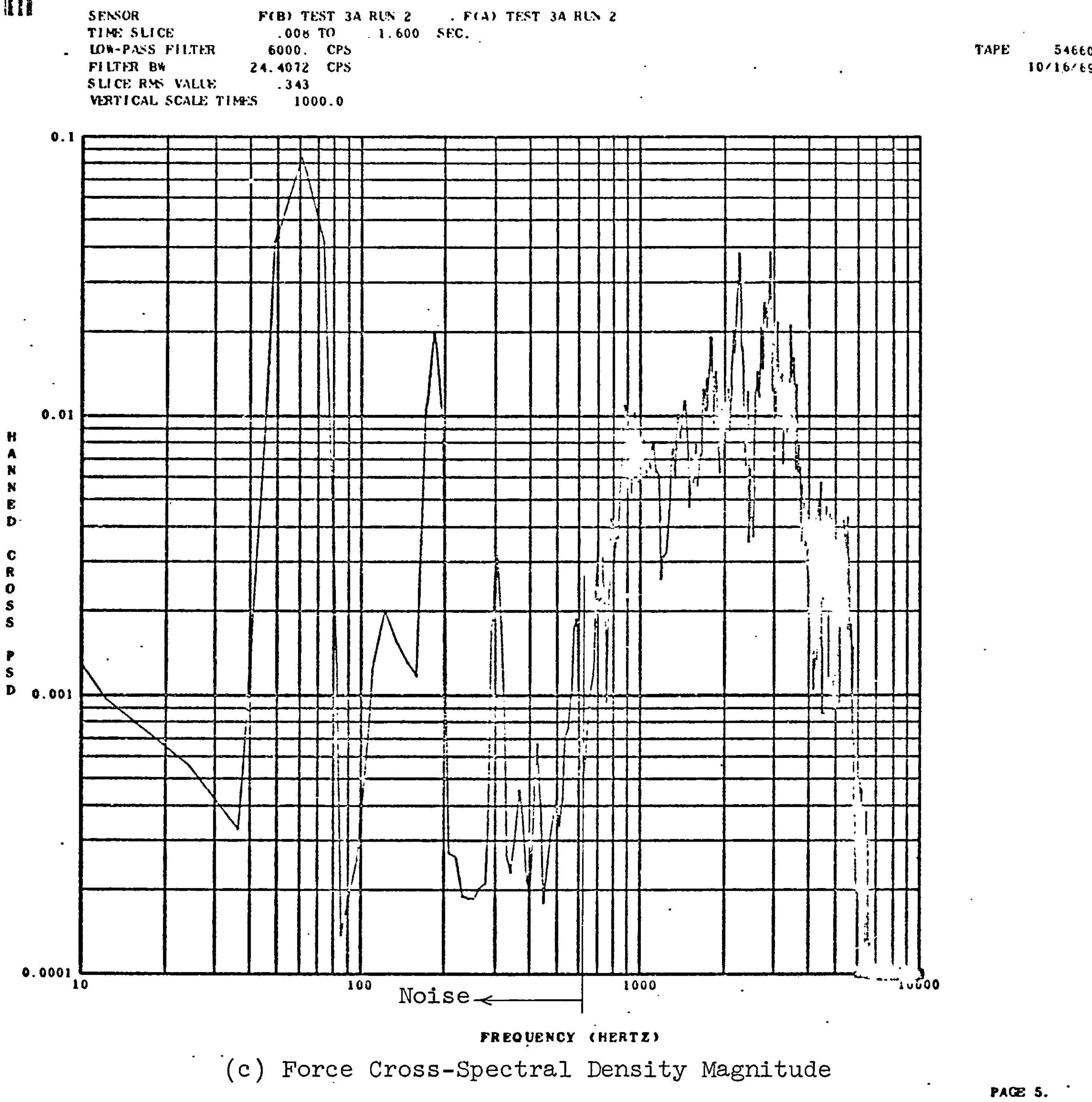

(c) Force Cross-Spectral Density Magnitude

Fig. A5.2 (Continued)

SENSOR F(B) TEST 3A RUN 2 F(A) TEST 3A RUN 2
TIME SLICE .008 TO 1.600 SEC.
LOW-PASS FILTER 6000. CPS
FILTER BW 24.4072 CPS
SLICE RMS VALUE .343

TAPE 54660
10/16/69

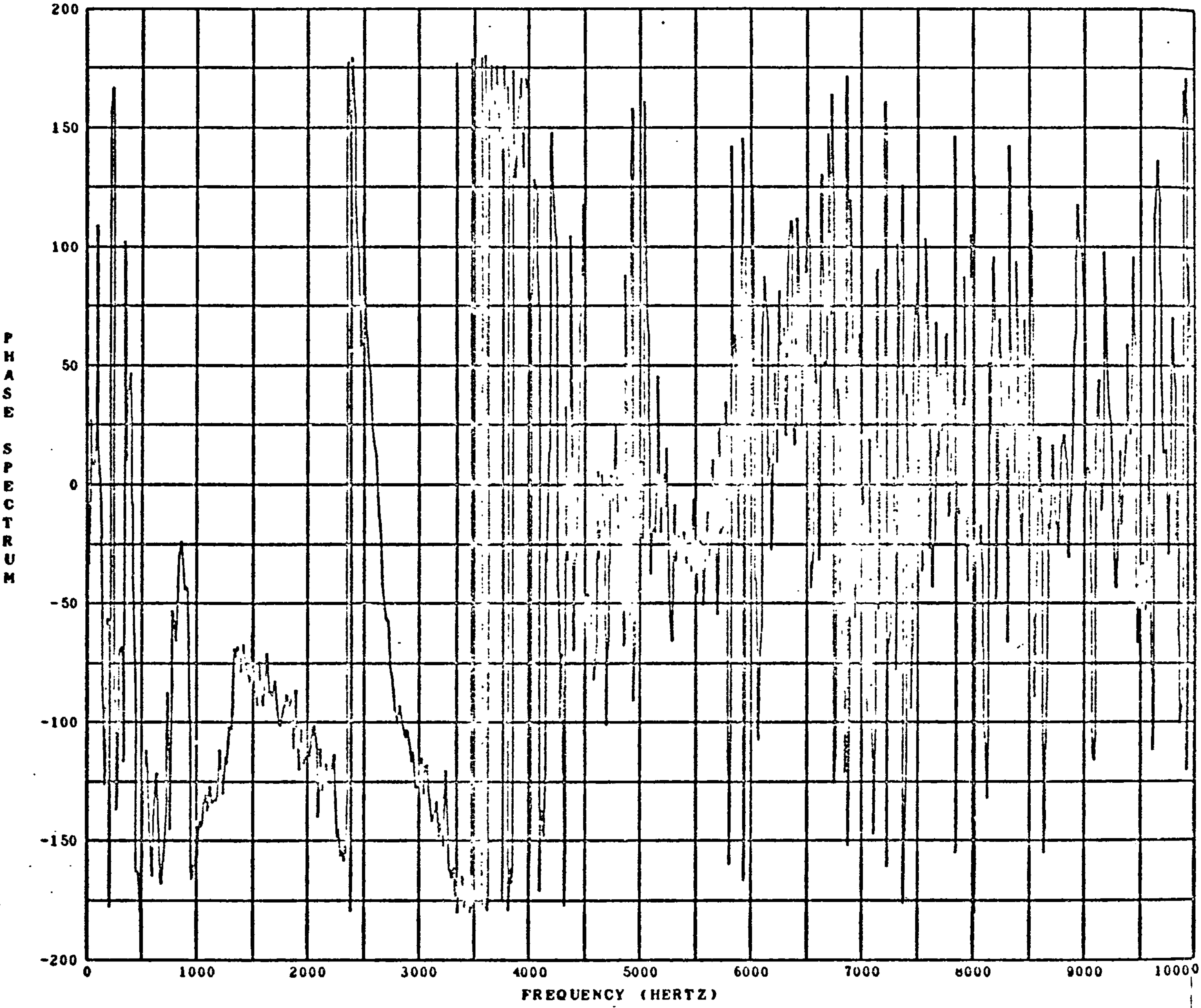

(d) Force Cross-Spectral Density Phase

Fig. A5.2 (Continued)

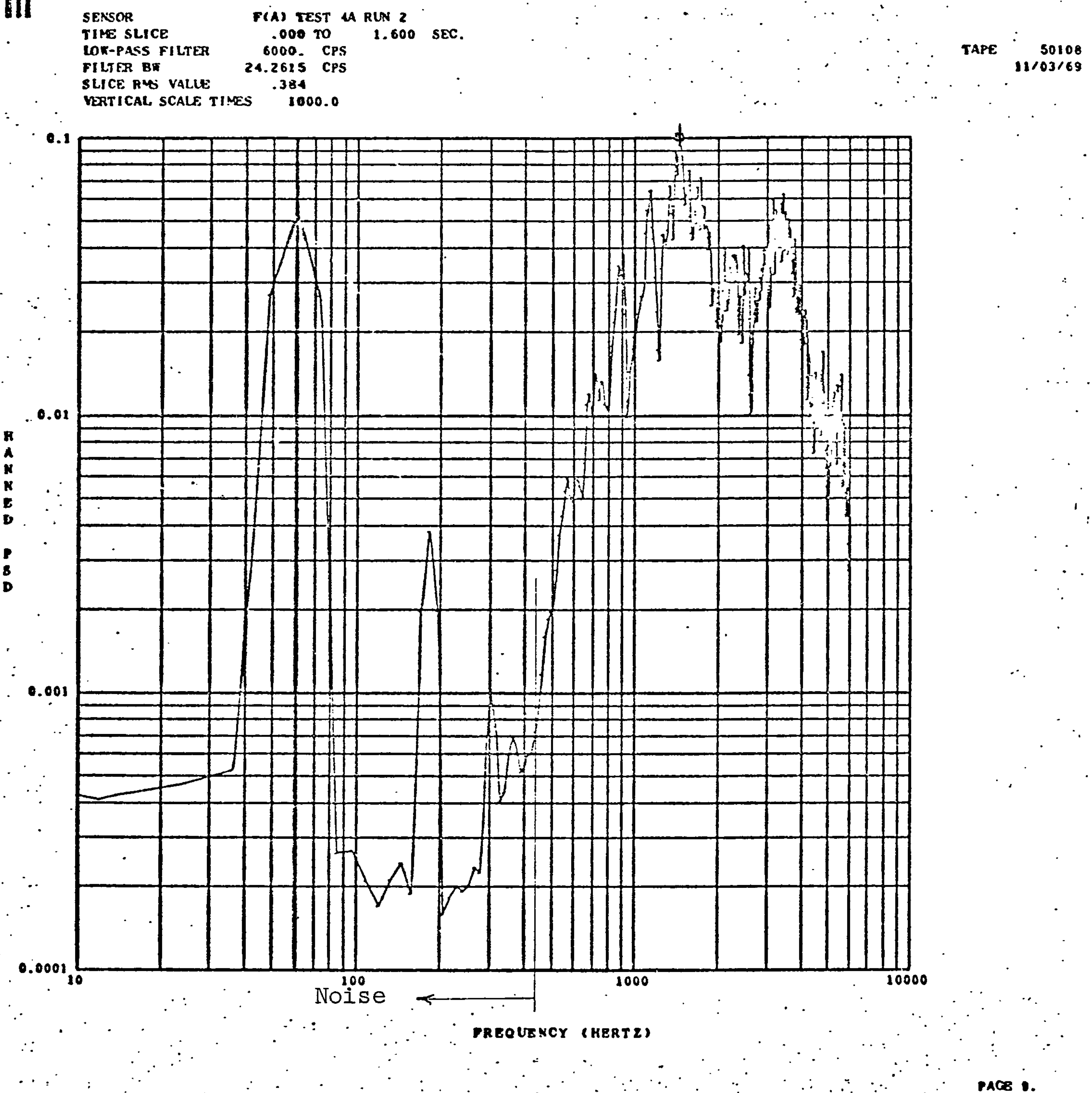

Fig. A5.3 Simulation Force Spectral Density for Test 4a

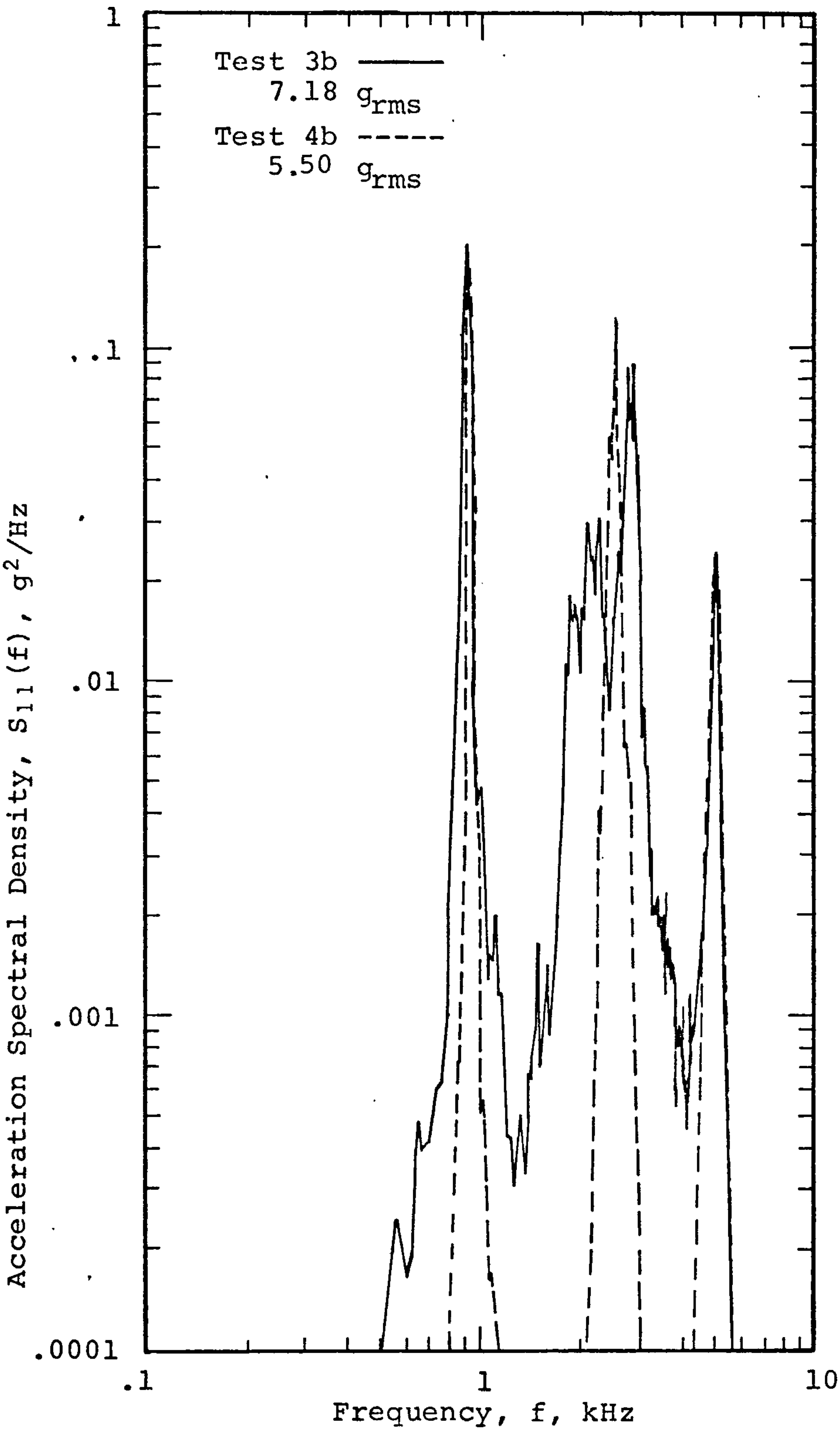

(a) Acceleration Spectral Density for Tip Accelerometer A_1

Fig. A5.4 Comparison of Complex Excitation Test 3b and Simulation Test 4b for Cantilever Beam (3/8-inch Shaker Support)

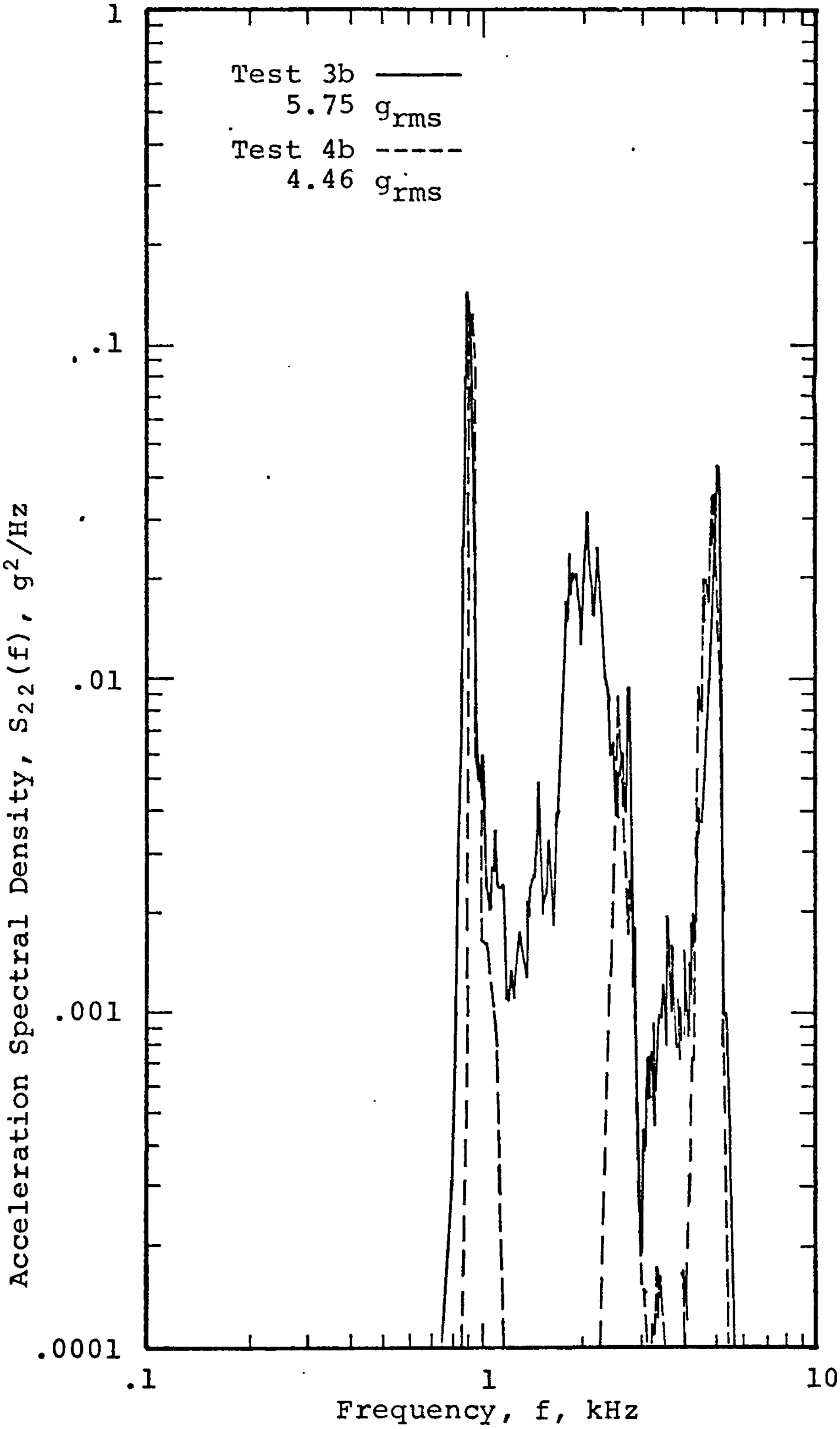

(b) Acceleration Spectral Density for Mid-length Accelerometer A_2

Fig. A5.4 (Continued)

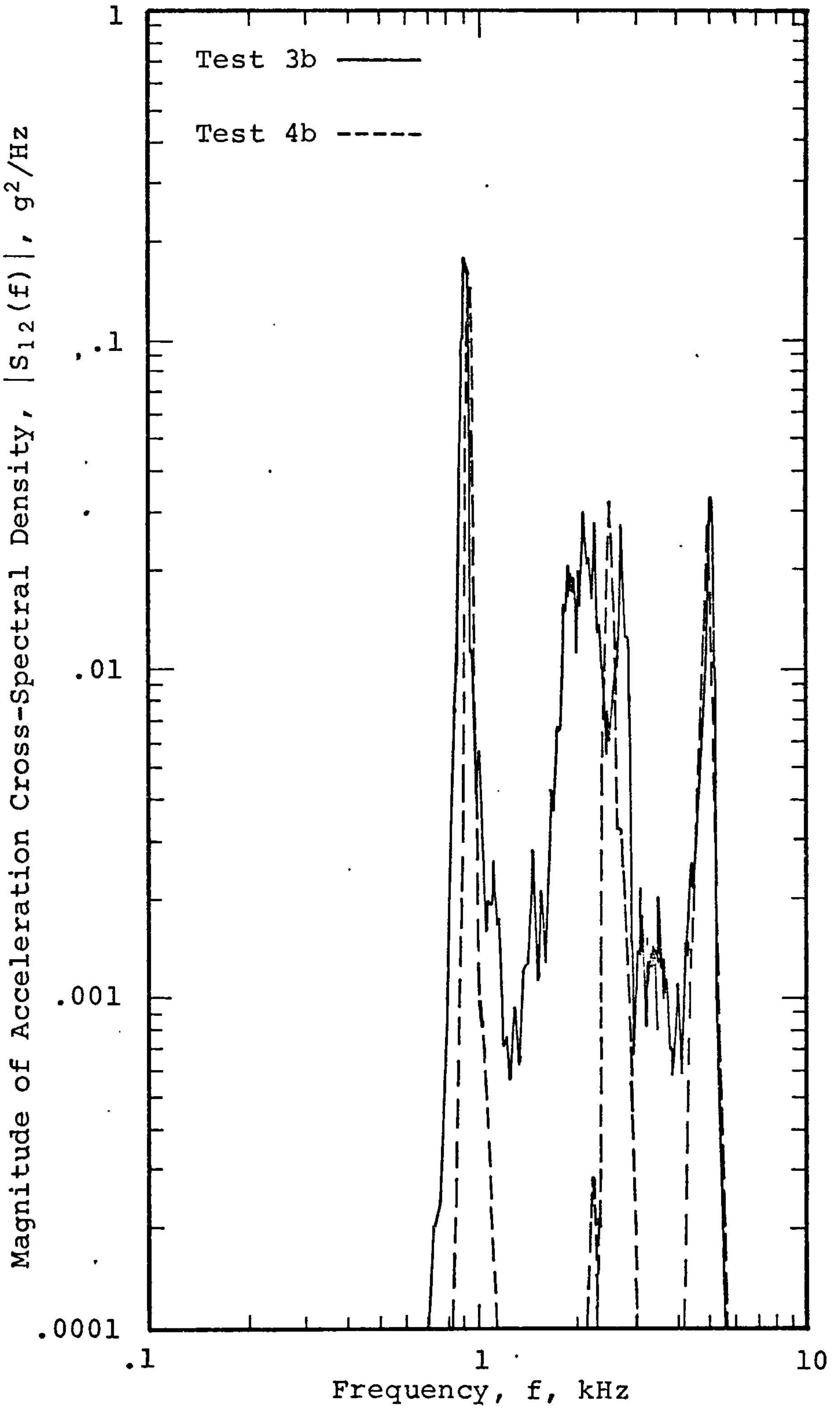

(c) Acceleration Cross-Spectral Density Magnitude for Accelerometers A_1 and A_2

Fig. A5.4 (Continued)

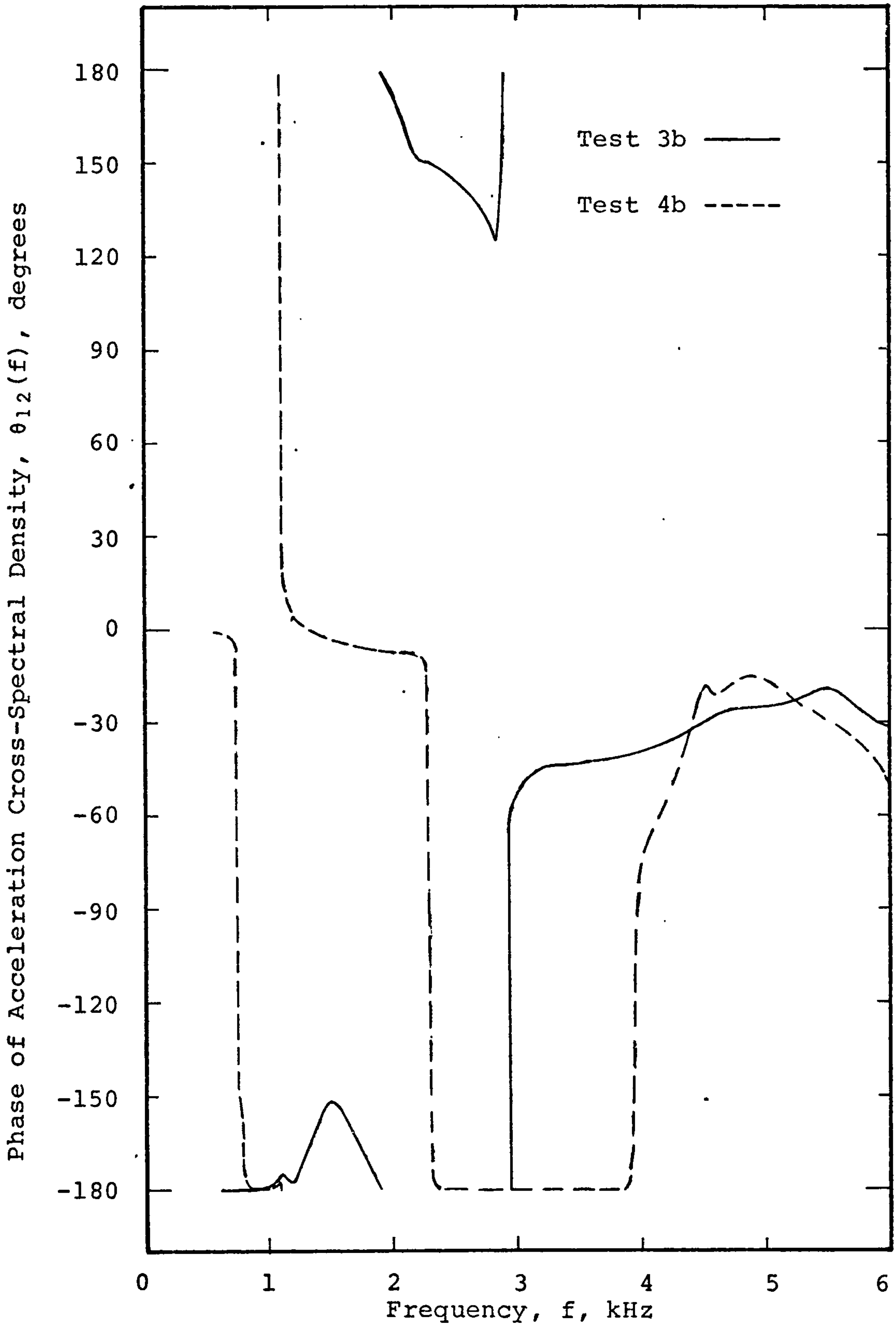

(d) Acceleration Cross-Spectral Density Phase for Accelerometers A_1 and A_2

Fig. A5.4 (Continued)

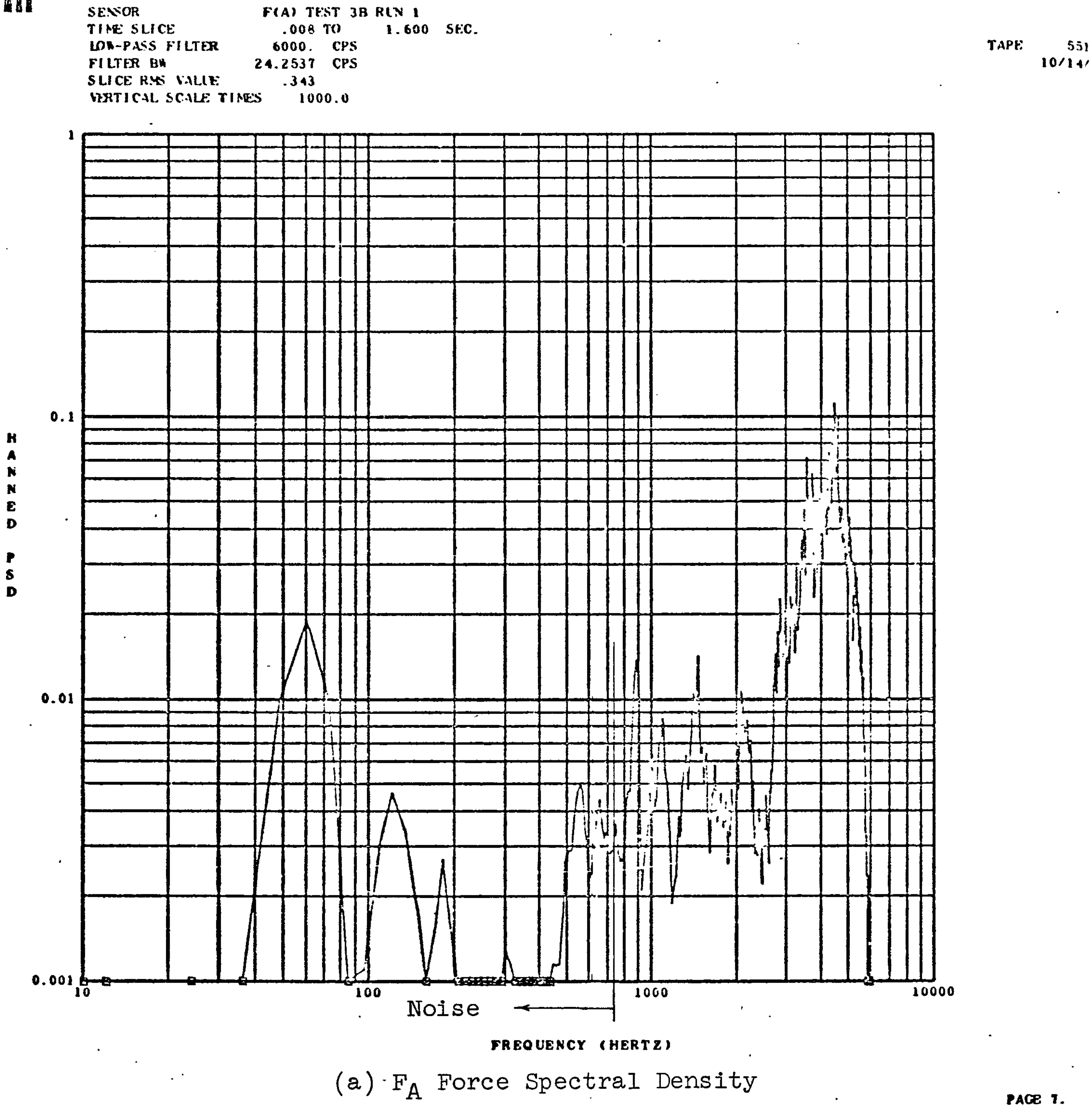

(a) F_A Force Spectral Density

Fig. A5.5 Complex Excitation of Test 3b

SENSOR F(B) TEST 3B RUN 1
TIME SLICE .008 TO 1.600 SEC.
LOW-PASS FILTER 6000. CPS
FILTER BW 24.2537 CPS
SLICE RMS VALUE .635
VERTICAL SCALE TIMES 1000.0

TAPE 55104
10/14/69

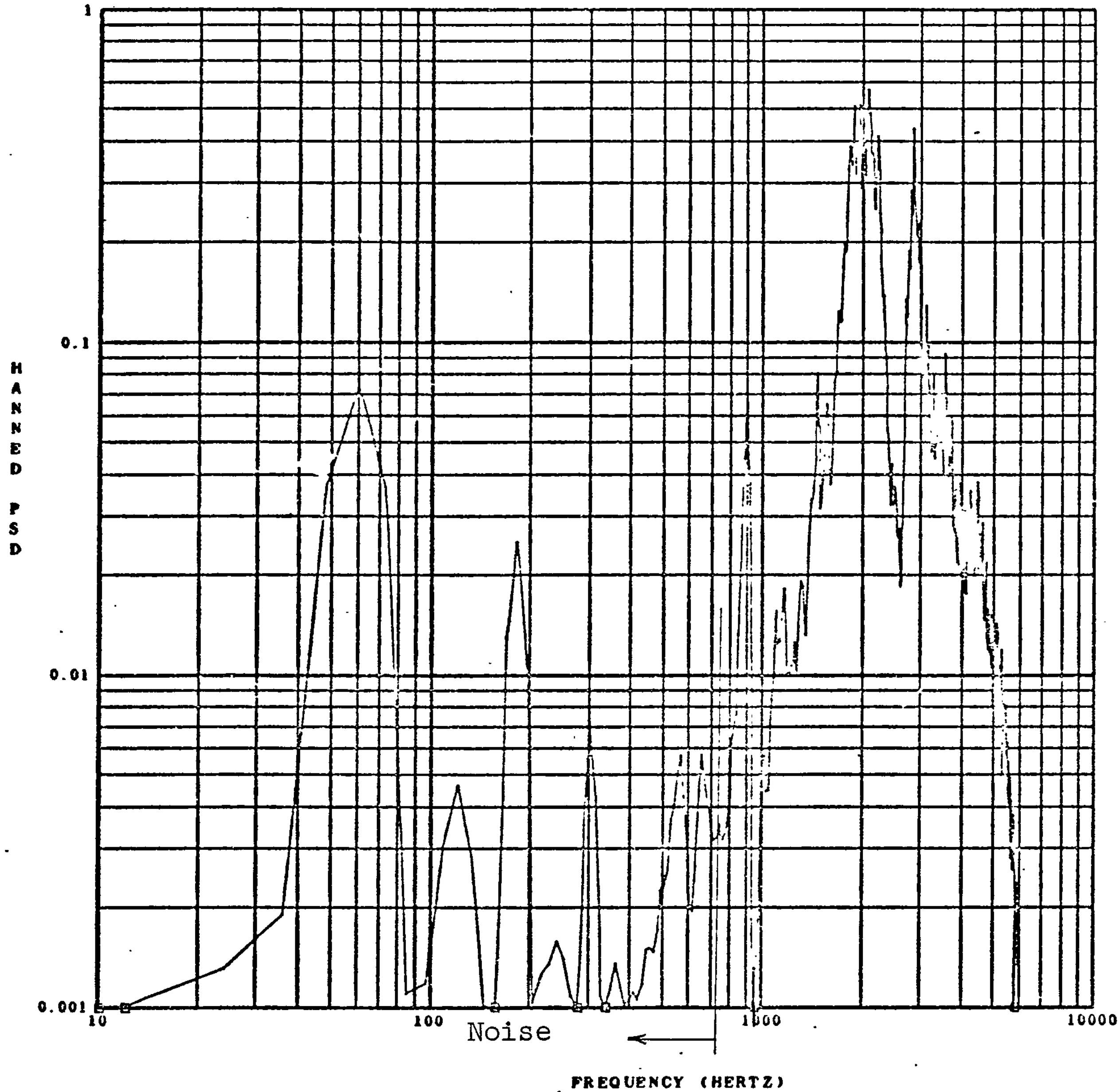

(b) F_B Force Spectral Density

Fig. A5.5 (Continued)

SENSOR F(A) TEST 3B RUN 1 F(B) TEST 3B RUN 1
TIME SLICE .008 TO 1.600 SEC.
LOW-PASS FILTER 6000. CPS
FILTER BW 24.2537 CPS
SLICE RMS VALUE .343
VERTICAL SCALE TIMES 1000.0

TAPE 551
10/14/

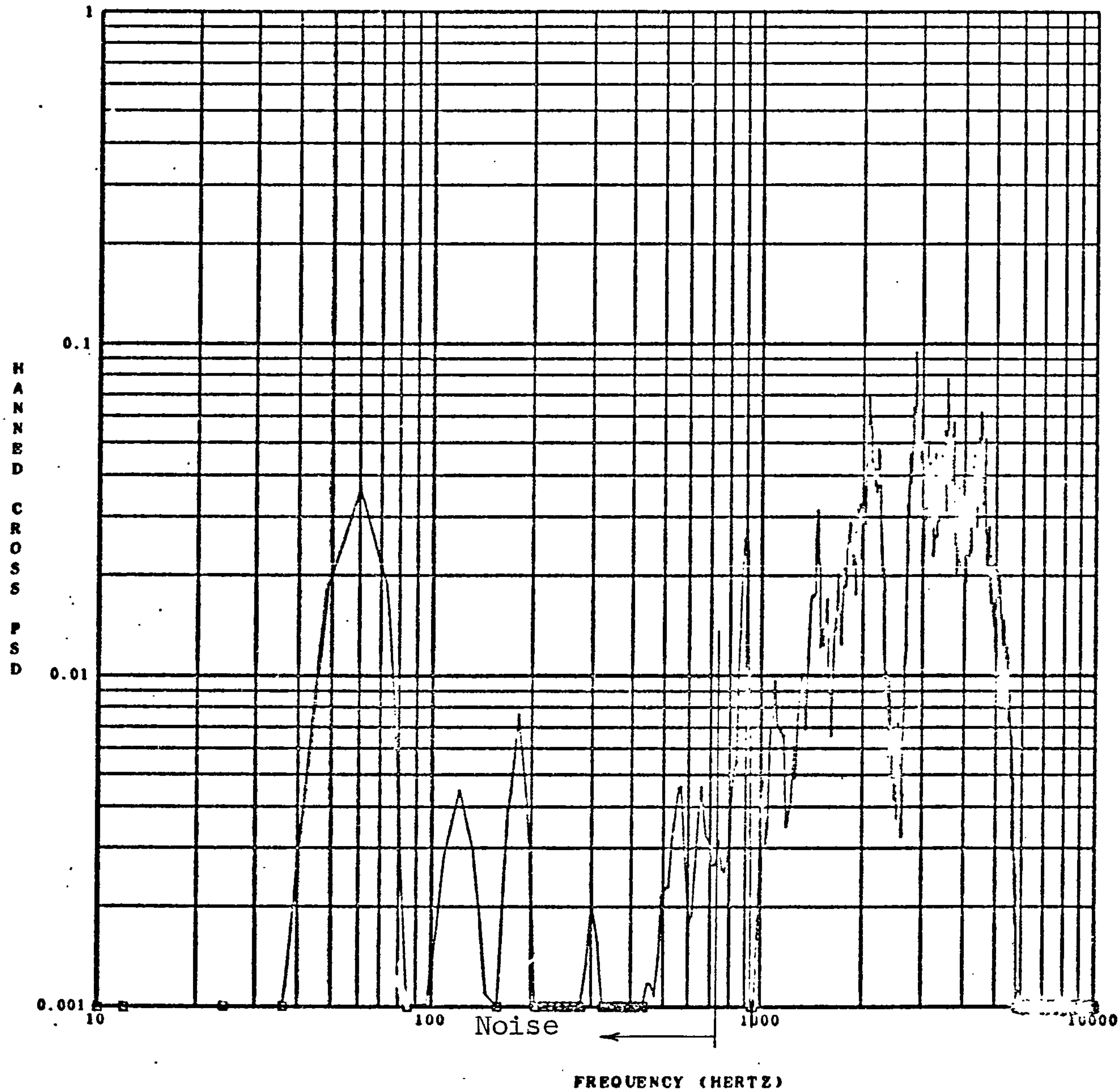

(c) Force Cross-Spectral Density Magnitude

Fig. A5.5 (Continued)

SENSOR F(A) TEST 3B RUN 1 F(B) TEST 3B RUN 1
TIME SLICE .008 TO 1.600 SEC.
LOW-PASS FILTER 6000. CPS
FILTER BW 24.2537 CPS
SLICE RMS VALUE .343

TAPE 55104
10/14/69

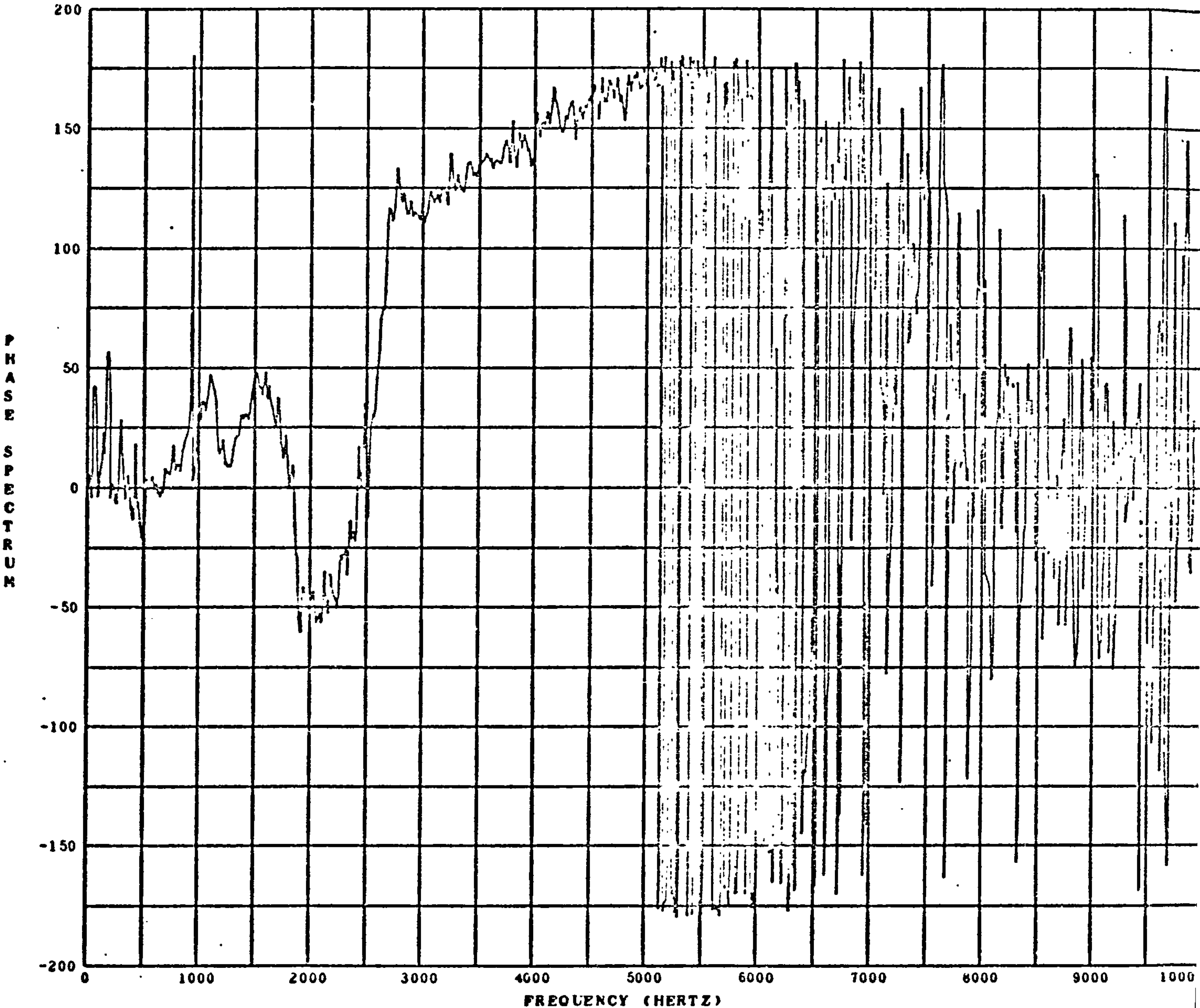

PAGE 19.

(d) Force Cross-Spectral Density Phase

Fig. A5.5 (Continued)

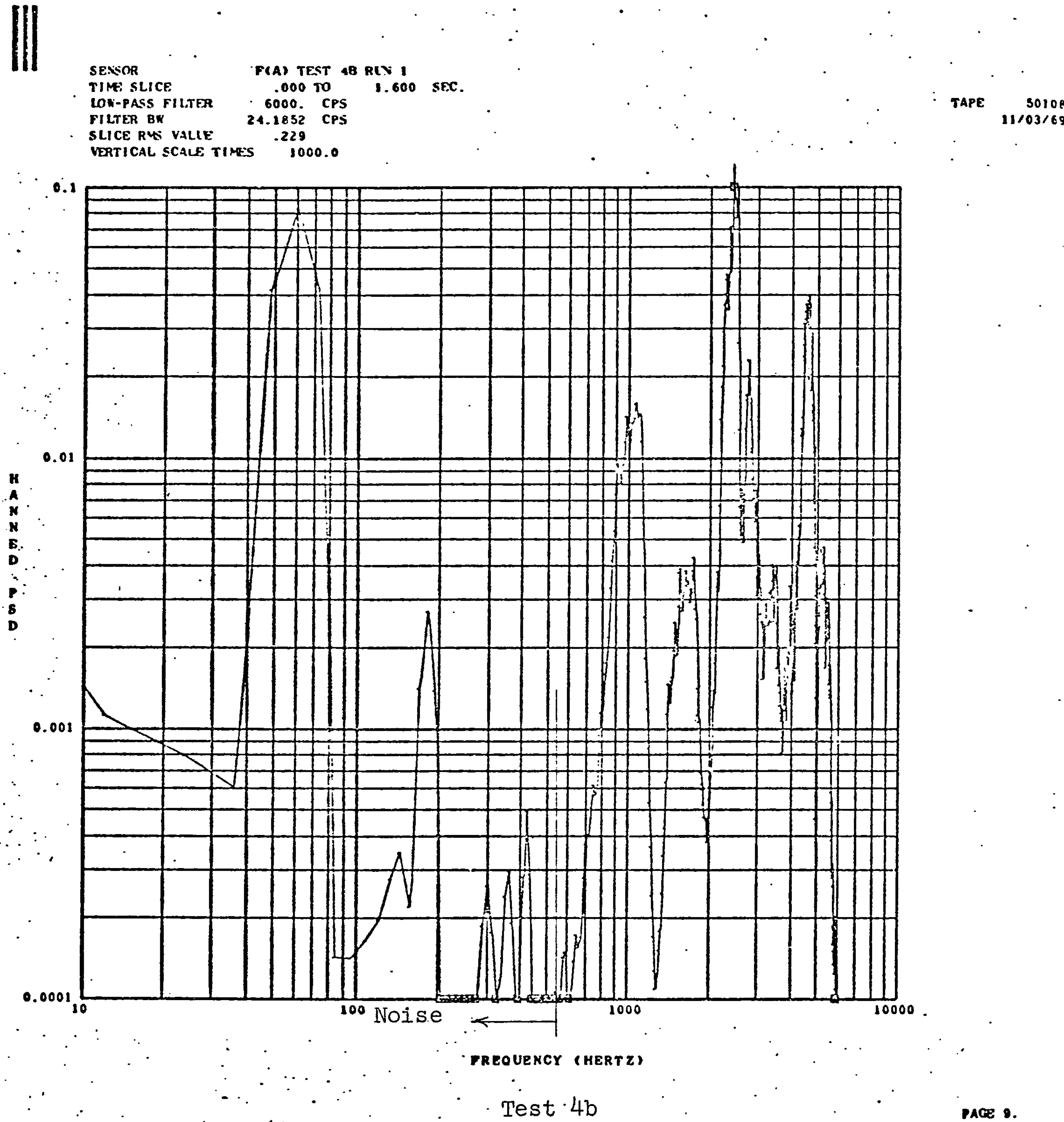

Test 4b

Fig. A5.6 Simulation Force Spectral Density for Test 4b

BIBLIOGRAPHY

1. R. H. Lyon, Random Noise and Vibration in Space Vehicles, Shock and Vibration Information Center, U.S.D.OD., 1967.

2. R. V. Doggett, Jr., "Comparison of Full-Scale and Model Buffet Response of Apollo Boilerplate Service Module," NASA TMX-1202 (1966).

3. K. McK. Eldred, "Vibroacoustic Environmental Simulation for Aerospace Vehicles," Sh. and Vibr. Bull., 37, 5, 1-11 (1968)

4. R. J. Wren, W. D. Dorland, J. D. Johnston, Jr., and K. McK. Eldred, "Concept, Design, and Performance of the Spacecraft Acoustic Laboratory," Sh. and Vibr. Bull., 37, 5, 25-54 (1968)

5. W. D. Dorland, R. J. Wren, and K. McK. Eldred, "Development of Acoustic Test Conditions for Apollo Lunar Module Flight Certification," Sh. and Vibr. Bull., 37, 5, 139-52 (1968).

6. Comments by T. D. Scharton on "Acoustically Induced Vibration Testing of Spacecraft Components," R. W. Peverly, Sh. and Vibr. Bull., 36, 3, 39-46 (1967).

7. W. E. Noonan, "Vibration Methods for Multiple Random Excitation," Sh. and Vibr. Bull., 37, 3, 89-97 (1968).

8. M. Trubert, "Structural and Electromechanical Interaction in the Multiple-Exciter Technique for Random Vibration Testing," J. Acoust. Soc. Amer., 41, 1185-92 (1967).

9. T. Usher, Jr., "Average Control for Sinusoidal- and Random-Vibration Testing," J. Acoust. Soc. Amer., 41, 840-49. (1967)

10. A. J. Curtis, H. T. Abstein, and R. J. Varga, "On the Use of Multiple (Multi-Point) Random Excitation with Application to Surveyor Spacecraft Tests," Sh. and Vibr. Bull., 35, 2, 49-74 (1966).

11. J. D. Newton, "Methods of Control of Multiple Shaker Testing System," Sh. and Vibr. Bull., 35, 2, 85-96 (1966).

12. H. R. Berkman, "Control Point Averaging for Large Specimen Vibration Tests," Sh. and Vibr. Bull., 37, 3, 75-88 (1968).

13. D. Scholz, "An Alternate Method of Exciter System Equalization," Sh., Vibr., and Asso. Environ. Bull., 33, III 109-12 (1964).

14. W. C. Beecher, "Pitfalls in Random Simulation," Sh. and Vibr. Bull., 34, 5, 1-14 (1965).

15. A. J. Curtis, J. G. Herrera, and R. F. Witters, "Combined Broadband and Stepped Narrowband Random Vibration," Sh. and Vibr. Bull., 36, 2, 33-47 (1967).

16. J. V. Otts and N. F. Hunter, "Reproduction of Complex and Random Waveforms at Various Points on a Test Item," Sh. and Vibr. Bull., 36, 3, 47-54 (1967).

17. D. U. Noiseux, "Simulation of Reverberant Acoustic Testing by a Vibration Shaker," Sh., Vibr., and Asso. Environ. Bull., 33, III, 125-36 (1964).

18. J. H. Putukian, "Simulating Missile-Firing Acoustical Environment by Equivalent Mechanical Vibration," Sh. and Vibr. Bull., 34, 5, 83-91 (1965).

19. P. A. Franken, T. D. Scharton, and T. H. Mack, "Comparison of Mariner Assembly-Level and Spacecraft-Level Vibration Tests," Sh. and Vibr. Bull., 36, 3, 27-38 (1967).

20. J. D. Robson, An Introduction to Random Vibration, Elsevier Publishing Company, New York, 1964.

21. J. D. Robson and J. W. Roberts, "A Theoretical Basis for the Practical Simulation of Random Motions," J. Mech. Engrg. Sci., 7, 3, 246-51 (1965).

22. L. S. Jacobsen and R. S. Ayre, Engineering Vibrations, McGraw-Hill Book Co., Inc., New York, 1958.

23. W. T. Thomson, Vibration Theory and Applications, Prentice-Hall, Inc., Englewood Cliffs, N.J., 1965.

24. S. Timoshenko, Vibration Problems in Engineering, D. Van Nostrand Co., Inc., New York, 1937.

25. C. M. Harris and C. E. Crede, Shock and Vibration Handbook, McGraw-Hill Book Co., New York, 1961.

26. Y. Chen, Vibrations: Theoretical Methods, Addison-Wesley Publ. Co., Inc., Reading, Mass., 1966.

27. W. C. Hurty and M. F. Rubinstein, Dynamics of Structures, Prentice-Hall, Inc., Englewood Cliffs, N.J., 1964.

28. D. Young and R. P. Felgar, "Table of Characteristic Functions Representing Normal Modes of Vibration of a Beam," Engr. Res. Ser. 44, No. 4913-13 (University of Texas, 1949).

29. R. Plunkett, "Measurement of Damping," Structural Damping, ed. J. E. Ruzicka, Proceedings of A.S.M.E. Colloquim, December, 1959, pp. 117-32.

30. J. S. Bendat and A. G. Piersol, Measurement and Analysis of Random Data, John Wiley & Sons, Inc., New York, 1966.

31. S. H. Crandall and W. D. Mark, Random Vibration in Mechanical Systems, Academic Press, New York, 1963.

32. J. McBryde, "MSC Statistical and Wave Analysis Program (VIBAN 3)," Lockheed Electronics Co., Program Documentation, Program No. Q467, Project No. 4587 (1969).